論文 / 著書情報
Article / Book Information

題目(和文)	カザフ共和国北部コクチェタフ変成帯の変成進化過程
Title(English)	Metamorphic evolution of the Kokchetav massif, northern Kazakhstan
著者(和文)	眞砂英樹
Author(English)	
出典(和文)	学位:博士(理学), 学位授与機関:東京工業大学, 報告番号:甲第5301号, 授与年月日:2003年3月26日, 学位の種別:課程博士, 審査員:
Citation(English)	Degree:Doctor (Science), Conferring organization: Tokyo Institute of Technology, Report number:甲第5301号, Conferred date:2003/3/26, Degree Type:Course doctor, Examiner:
学位種別(和文)	博士論文
Type(English)	Doctoral Thesis

Metamorphic Evolution of the Kokchetav Massif, Northern Kazakhstan

Hideki Masago

Ph D. thesis Mar. 2003

Division of Earth and Planetary Sciences
Graduate School of Science and Engineering
Tokyo Institute of Technology

Contents

Ackowledgements

Field investigations of the Kokchetav massif were carried out by the Tokyo Institute of Technology – Waseda University – Stanford University – Geophysical Laboratory collaborate research team conducted by Profs. S. Maruyama, Y. Ogasawara and J. G. Liou during 1997–1999, involving the following staffs: Drs. Y. Kaneko, M. Terabayashi, H. Yamamoto, T. Ota, R. Anma, M. Ishikawa, C. D. Parkinson, R. Y. Zhang, D. Rumble III, I. Katayama, Y. Nakajima, J. Yamamoto and K. Yamauchi. This research project was financially supported by the International project on the whole Earth Dynamics of the Science and Technology Ministry of Japan.

Doctor S. Omori made a great help in thermodynamic calculation performed in Chaps. II & III. These chapters would have not completed without his help. Doctor S. Itoh provided a technical comment on a discussion about diffusion effect in garnet (Chap. III). In the oxygen isotope analysis (Appendix B), Dr. D. Rumble III at Geophysical Laboratory allowed me to use his facilities and helped me in many ways. The field investigation of the top and bottom boundaries of Sanbagawa Belt (Appendix C) was carried out with Drs. K. Okamoto, M. Terabayashi and I. Katayama.

All staffs and colleagues in the department, especially Prof. S. Maruyama gave many technical advices, discussions and comments, and encouragements all the time. I thank all the people listed above.

Some studies in this thesis were performed using a research grant from the Japan Society for the Promotion of Science for Young Scientist (No. 05232).

Overview

Orogeny is the term which means a geological phenomenon occurring at the convergent plate margins including magmatism, metamorphism and major reconstruction of geological structures. In terms of the plate tectonic paradigm, the Phanerozoic history of the Earth is regarded as a repetition of active orogenic period and less active inter-orogenic period. One of the most remarkable findings of the early plate tectonic studies in 1970–1980s, is to figure out the two different types of orogeny throughout the Earth's history: collision-type and Pacific-type. The former is formed by the collision of two continents. The type localities of this type of orogeny are Alps and Himalaya. The latter, which is also termed as Cordirrelan-type orogeny, occurs at the convergent plate margins under which an oceanic plate subducts. The type localities of this type of orogeny are the circum-Pacific regions as its name represents. Representative structures of these two types of orogens are shown in Fig. 0–1. Himalaya and SW-Japan are chosen as type localities of collision- (Fig. 0–1a) and Pacific-type (Fig. 0–1b) orogens, respectively. Table 0–1 summarises the comparison about their dimensions, components, large-scale structures....*etc*. Their similarities and dissmilarities are described as below. The most important similarity is their large-scale structure. Both types of orogens have subhorizontal structure, which is asymmetric with ocean-ward vergency. The most remarkable difference is the dimensions. The total width of the Pacific-type orogen is a few to tens of kilometre, whereas the collision-type is about ten times as large as that. In terms of component of the orogen, the largest difference is the presence of huge batholith belts as wide as 300 km in the Pacific-type orogens. These batholith belts are composed of granitoids characteristically of tornalite–trogjemite–granodiorite (TTG) compositions. The collision-type is associated only with a small amount of granitic intrusions often refers as leucogranite. Hence, the Pacific-type orogeny contributes to the continental growth, whereas the collision-type only reconstructs the distribution of continents and makes no contribution to their growth. Both the collision- and Pacific-type orogens have regional metamorphic belt in their core parts called as orogenic roots. Although its dimension is very different by the orogen type, regional metamorphic belt occurs as a flat-lying thin sheet in both types of orogens. The formation and the exhumation of the regional metamorphic belt is the

most essential event in orogenic processes. Therefore, to clarify the nature of metamorphism is of first importance to understand the orogeny.

This gave an oppotunity to the metamorphic petrologists to make contributions to geodynamics. In late 1970s to 1980s, studies of metamorphic petrology combined to orogenic tectonics were in fashion, and numbers of important contributions were accumulated. The first important theorem of orogeny is that there is a close relationship between the orogenic type and the baric type of metamorphism — collision-type has medium-*P* type (kyanite–sillimanite series alminosilicates, no blueschist) metamorphic facies series, whereas Pacific-type has high-*P* type (jadeite-, glaucophane-bearing) metamophic facies series. Hence, metamorphic pressure does not exceed 12–13 kbar in collsion-type orogeny, which means continental crust does not subduct deeper than the Moho depth.

A micro-scale analysis of mineral compositions of zoned minerals enabled by the spread of electron probe (EPMA) revealed a metamorphic pressure–temperature–time (*P–T–t*) path. Estimated *P–T–t* path for individual rocks are clockwise curves in most metamorphic belts. Metamorphic geotherm defined as a sequence of peak metamorphic conditions of each individual rock, which does not coincide with *P–T–t* path of individual rocks in general (Fig. 0–2).

Another finding is an ‘inverted metamorphism’ in collisional metamorphic belts. As geothermal gradient has a positive slope, lower structural level has higher temperature (and pressure, of course) in a normal region. Nevertheless, higher grade rocks are situated at structurally higher part in some collisonal orogens. Therefore, geothermal gradient is inverted in a certain domain in the collsional metamorphism (Gansser, 1964).

Based on these contributions, theory of orogenic process began to be formulated in middle 1980s, and is summarised in the orogenic model of England & Thompson (1984). They proposed a simple crustal duplication model for continental collision, and calculated the thermal evolution of metamorphic belt after collision (Fig. 0–3). This model well explains the clockwise *P–T–t* path, medium-*P* type metamorphic facies series, and the discordance of individual *P–T–t* path and metamorphic geotherm.

Discovery of the ultrahigh-pressure metamorphic (UHPM) rocks caused a catastrophe to the established theory of orogeny. Definition of UHPM is based on the existence of metamorphic coesite and/or diamond in the supracrustal rocks. The first

discovery of metamorphic coesite from the Dora Maira (Western Alps) by Chopin (1984) and from the Western Gneiss Region (Norwegian Caledonide) by Smith (1984) cast a doubt to this theory of orogeny. Both localities are collision-type orogens. Stability of coesite under a reasonable geothermal gradient is *ca*. > 100 km in depth, which is far beyond the traditionally believed pressure limit of collision metamorphism. Further, metamorphic diamond was also found from gneiss in the Kokchetav massif, northern Kazakhstan (Sobolev & Shatsky, 1990), which means much higher pressure condition than coesite-bearing rocks. These high pressures cannot be explained by the above-mentioned crustal duplication model. Since then, there has been a long debate about the origin of the UHPM rocks: *in situ* or boulder. In most UHPM terranes, the occurrence of UHPM rock is very rare or even limited to one outcrop or hand specimen in some terranes. Furthermore, in many cases, its occurrences is limited to the certain lithology (mostly eclogite) enclosed in country rocks of lower-*P* assemblage. For these reasons, UHPM was first recognised as an olistostrome or tectonic block in a mélange unit, and the rest of the terrane is still regarded as medium-*P* type with maximum depth of < 30 km. However, following after the discovery by Chopin (1984) and Smith (1984), new occurrence of UHPM has been reported from many regions of the world, and now 17 localities are recognised as UHPM terranes including Europe, Asia, Africa, South America and Antarctica. It is unreasonable to assume all of these UHPMs as olistostrome or tectonic block.

To give a clear answer to this problem, an extensive project was carried out by the research group led by Tokyo Institute of Technology since 1997. Our tactics was 1) detailed field mapping and a systematic sample collection, 2) inclusion mineralogy as relict of peak or prograde assemblages, 3) metamorphic petrology with discriminating the late-stage effect, and 4) confirmation by experimental petrology.

We have done a field mapping and sample collection for total 3 months by 30 members in the Kokchetav during 1997–1999, and made a protolith based geological map of 1/5,000 scale. The result of mapping was compiled by Kaneko *et al*. (2000). Major contributions of this work are as follows: 1) the Kokchetav massif has a flat-lying structure composed of several fault-bound lithotectonic units, 2) occurrences of eclogite and other high-*P* rocks are restricted to the structurally intermediate part of the HP–UHPM unit, and *P*–*T* conditions decrease towards both the top and the bottom boundaries of the unit, and 3) the overlying and underlying geological units are feebly

to non-metamorphosed sedimentary, and low-*P* type metasedimentary rocks, respectively, both of which are bounded to the HP–UHPM unit by subhorizontal faults. Detailed structural analyses of interior of the HP–UHPM unit by Yamamoto *et al*. (2000, 2002) have revealed that the meso- to micro-scale subvertical structures which predominates throughout the Kokchetav massif are resulted from later-stage intra-layer folding and the large-scale structure is rather subhorizontal. Relative motion of the top and the bottom boundary faults are determined based on the shear sense indicators by Ishikawa *et al*. (2000) and Yamamoto *et al*. (2002) as normal and reverse faults, respectively. This infers a selective denudation of the HP–UHPM unit bounded by the paired faults.

The second important contribution is an extensive inclusion mineralogy in zircon by Katayama *et al*. (2000). They had extracted zircons from about 200 samples and identified inclusion species by laser-raman spectrometry, then two important results were obtained. The first, UHP minerals were found not only from eclogite but also from metasedimentary rocks and orthogneiss whose matrices have low- to medium-*P* mineral assemblages. This means that the country rocks also had undergone the HP–UHP metamorphism, but almost completely lost the HP–UHP mineralogy due to retrograde hydration recrystallisation. Secondly, the increased number of localities of coesite and diamond enabled to define a regional extent of these minerals as zones. Further, these localities are restricted to the eclogitiferous unit (Unit II of Kaneko *et al*., 2000). This fact clearly rules out the possibility of UHPM as neither a tectonic block nor an olistostrome.

Masago (2000; Chap. I), Ota *et al*. (2000) and Okamoto *et al*. (2000) have described the metabasites of various grades to reveal the nature of metamorphism of the whole massif. Masago (2000; Chap. I) have described the metabasites of the westernmost Barchi-Kol and the easternmost Borovoye areas to make metamorphic zonation and defined a metamorphic facies series of the massif and mineral reactions between each mineral zone. Ota *et al*. (2000) has made a detailed thermal profile along the direction perpendicular to the lithotectonic boundaries in Kulet–Saldat-Kol areas. The obtained thermal profile was consistent to the geologic profile.

There are also new findings in a field of mineralogy. Okamoto *et al*. (2000) has described solubility of K into omphacitic clinopyroxene in Kumdy-Kol eclogites. This is unique to the Kumdy-Kol eclogites, and not observed in eclogites of other areas of

the Kokchetav massif. Okamoto *et al*. (2000) further mentioned that the solubility of K into clinopyroxene has a positive correlation with pressure, and is potentially used as geobarometer, based on his experiments by multi-anvil apparatus. Katayama *et al*. (2001) described the presence of unusual Ca-Eskola component in omphacitic clinopyroxene in Kumdy-Kol eclogites. Katayama & Nakashima (2003) detected a small amount (~ 1000 ppm order) of water in nominally anhydrous minerals particularly in clinopyroxene. Although the water content is too low compared to the hydrous minerals, they suggested that the modally abundant clinopyroxene in a subducted slab could be a major carrier of water to the deep mantle.

Determination of *P–T–t* conditions is one of the fundamental works to the understanding of metamorphism. Parkinson (2000) first reported the prograde mineralogical records in a compositionally zoned garnet porphyroblast in whiteschists in the Kokchetav massif. He found a zoned distribution of SiO_2 polymorph inclusions: monocrystalline quartz in the spessartine-rich core domain, and coesite and its pseudomorphs in the mantle domain. Masago (Chap. III) has further extended this work, which gave quantitative constraints of the prograde *P–T* conditions by thermobarometry involving Ti-phase inclusions, and has drawn a prograde *P–T–t* path. Thermodynamic forward modeling of garnet growth is qualitatively consistent with this estimated *P–T–t* path, which gives a theoretical assurance for this path. The estimated prograde *P–T–t* path is counter-clockwise and exactly coincides with the metamorphic geotherm of the terrane. These features are highly contradictory to the classically drawn *P–T–t* paths in many collisional metamorphic belts.

Katayama *et al*. (2001) gave age contributions to this *P–T–t* path by SHRIMP chronology. They discriminated three growth stages in zircons by cathode luminescence observations combined with zonal distribution of inclusion minerals, and determined the ages of each domain. The obtained ages clustered in three groups. The core ages are variable but all in the Middle Proterozoic. On the other hand, the mantle ages are clustered around 537 ± 9 Ma, and rim ages are around 507 ± 8 Ma. Some have another thin domain at the outermost part of the grain yielding 456–461 Ma, which corresponds to the age of the Devonian plutonism. This excellent work has enabled the quantitative argument of the exhumation rate of the metamorphic belt at first. In the previous studies, exhumation rates of the HP–UHP terranes are very fast (a few m.y. to the surface). Contrary, this work has proven the exhumation time from the coesite stable depth to the

surface is about 30 m.y., that is one order of magnitude slower than the previous studies.

There are also important contributions in the branch of geochemistry. Yamamoto *et al.* (2002) analysed the whole rock chemistry of the Kokchetav matabasites of amphibolite through quartz-eclogite, coesite-eclogite to diamond-eclogite grade, and discussed about the change of bulk chemistry with metamorphic grade. The major conclusions of this study are 1) the protolith of the Kokchetav metabasites are MORB-like affinity, and 2) eclogites are more depleted in K and REE than the lower grade equivalents due to metasomatism mainly related to the breakdown of amphiboles at amphibolite/eclogite transition.

Stable isotope studies are another contributions of geochemical study. Masago *et al*. (2003) made a systematic analysis of oxygen isotopes of the silicate minerals, and found extremely low $\delta^{18}O$ in some eclogites. As there is no systematic difference between fresh and amphibolitised eclogites, this feature is not originated from retrograde hydration. They concluded that these low $\delta^{18}O$ compositions are pre-subduction (protolith) remnants, which was formed at rift environment where meteoric water circulated probably during the 'Snowball Earth' period. Ota *et al*. (2002) analysed carbon and oxygen isotope compositions of carbonate rocks, concluding the similar interpretation.

Experimental petrology by Okamoto & Maruyama (1998) supports the petrological and mineralogical findings of the natural UHPM rocks. Based on the re-equilibrium experiments in the system of MORB + H_2O, they have proposed a subdivision of the eclogite facies as lawsonite-eclogite, amphibole-eclogite, zoisite-eclogite and dry-eclogite facies.

With synthesizing the above mentioned contributions involving field mapping, structural geology, metamorphic petrology, mineralogy, chronology and geochemistry, a new formulation of the collision orogeny has begun. Maruyama & Parkinson (2002) proposed a tectonic model, which systematically explains the tectonic evolution of the Kokchetav massif from its protolith formation, metamorphism, exhumation, to post-orogenic magmatism.

Accumulation of new data produced some important remarks. Based on the compilation of the *P–T* conditions of the various regions of the Kokchetav massif, Maruyama & Parkinson (2000) pointed out a kink of geotherm of the metamorphic belt around 700 °C, 12–15 kbar. The initiation of the UHPM is another interesting aspect of

UHPM study. No UHPM is found in the period older than the latest Proterozoic (> 630 Ma), and most UHPM are reported from the Phanerozoic orogens. Maruyama *et al*. (1997) compiled the *P–T* conditions of the regional metamorphic belts of the world, and pointed out the gradual cooling of metamorphic geotherm through the history of the Earth.

This thesis focuses to the Kokchetav metamorphism. It consists of four chapters and appendixes. The thesis first describes the outline of metamorphism of the Kokchetav massif from a systematic analysis of metabasites from low- to high-grade in Chapter I. In this chapter, basic metamorphic natures of the massif such as metamorphic zonation, metamorphic facies series, phase relations….*etc*. are revealed. Chapter II describes about the retrograde hydration. In every regional metamorphic belt, regardless to its type (Pacific- or collision-type), high-grade metamorphic rocks underwent retrograde hydration during their exhumation to the surface. Its effect, however, has been further underestimated through the history of metamorphic petrology. Occurrence of UHPM suggests that most of the country rocks have undergone nearly complete recrystallisation during the exhumation process at mid-crustal depth. In this chapter, the texture and mineralogy of the retrograde hydration are described, and provides a possible estimation of the amount of infiltrated water. In Chapter III, prograde *P–T–t* path is estimated using the distribution of mineral inclusions in compositionally zoned garnet in whiteschist samples. The deduced prograde *P–T–t* path for whiteschist is counter-clockwise, and coincides the metamorphic field *P–T–t* gradient deduced from matabasites in the previous chapters. In the last chapter (Chap. IV), a possible tectonic model of the Kokchetav massif is provided. As mentioned above, the classical model of collision orogeny is no more applicable to UHP terranes. A new tectonic model deduced from the geological, structural, metamorphic and chronological constraints is proposed.

Appendix is three-fold. Appendix A is geological outline of the Kokchetav massif. This will give readers a general background about the geology of the Kokchetav massif. Appendix B is a description about the oxygen isotope geochemistry of the Kokchetav silicates. This is the second report of unusually low $\delta^{18}O$ eclogtes after Chinese UHP terranes. Appendix C is a structural analyses of the top and the bottom boundaries of the Sanbagawa Belt, which I have worked. The Sanbagawa Belt is one of the representative Pacific-type orogens, and is a good example for comparison with the collision-type Kokchetav massif.

Abbreviations for minerals and components used in this thesis are basically after Kretz (1983) in the following exceptions: Brs: barroisite; Coe: coesite; Daph; daphnite; Dia: diamond; Gr: graphite; Gei: geikelite; Na-Aug: sodic-augite; Phn: phengite; Pph: pyrophanite.

REFERENCES

Chopin, C., 1984. Coesite and pure pyrope in high-grade pelitic blueschists of the Western Alps: A first record and some sequences. *Contributions to Mineralogy and Petrology,* **86,** 107–118.

England, P. C. & Thompson, A. B., 1984. Pressure–Temperature–time paths of regional metamorphism. I. Heat transfer during regions of thickened continental crust. *Journal of Petrology,* **25,** 894–928.

Gansser, A., 1964. Geology of the Himalayas. *Interscience*, pp. 289, London.

Ishikawa, M., Kaneko, Y., Anma, R. & Yamamoto, H., 2000. Subhorizontal boundary between ultrahigh-pressure and low-pressure metamorphic units in the Sulu–Tjube area of the Kokchetav Massif, Kazakhstan. *The Island Arc*, **9,** 317–327.

Kaneko, Y., Maruyama, S., Terabayashi, M., Yamamoto, H., Ishikawa, M., Anma, R., Parkinson, C. D., Ota, T., Nakajima, Y., Katayama, I., Yamamoto, J. & Yamauchi, K., 2000. Geology of the Kokchetav UHP–HP massif, Kazakhstan, central Asia. *The Island Arc*, **9,** 264–283.

Katayama, I., Zayachkovsky, A. A. & Maruyama, S., 2000. Prograde pressure–temperature records from inclusion in zircons from ultrahigh-pressure–high-pressure rocks of the Kokchetav Massif, northern Kazakhstan. *The Island Arc*, **9,** 417–427.

Katayama, I., Maruyama, S., Parkinson, C. D., Terada, K. & Sano, Y., 2001. Ion micro-probe U–Pb zircon geochemistry of peak and retrograde stages of ultrahigh-pressure metamorphic rocks from the Kokchetav massif, northern Kazakhstan. *Earth and Planetary Science Letters*, **188,** 185–195.

Katayama, I. & Nakashima, S., 2003. Hydroxyl in clinopyroxene from the deep subducted crust: Evidence for H_2O transport into the mantle. *American Mineralogist*, **88,** 229–234.

Kretz, R., 1983. Symbols for rock-forming minerals. *American Mineralogist*, **68,** 277–279.

Maruyama, S., Liou, J. G. & Terabayashi, M., 1996. Blueschists and eclogites of the world and their exhumation. *International Geology Review*, **38,** 485–594.

Maruyama, S. & Parkinson, C. D., 2000. Overview of the geology, petrology and tectonic framework of the high-pressure–ultrahigh-pressure metamorphic belt of the Kokchetav Massif, Kazakhstan. *Island Arc*, **9,** 439–455.

Masago, H., 2000. Metamorphic petrology of the Barchi-Kol metabasites, western Kokchetav ultrahigh-pressure–high-pressure massif, northern Kazakhstan. *The Island Arc*, **9,** 358–378.

Masago, H., Rumble, D. III, Ernst, W. G., Parkinson, C. D. & Maruyama, S., 2003. Low $\delta^{18}O$ eclogites from the Kokchetav massif, northern Kazakhstan. *Journal of Metamorphic Geology (in press)*.

Okamoto, K. & Maruyama, S., 1998. The high pressure stability limits of lawsonite in the MORB + H_2O system. *American Mineralogist*, **84,** 362–373.

Okamoto, K., Liou, J. G. & Ogasawara, Y., 2000. Petrology of the diamond-grade eclogite in the Kokchetav Massif, northern Kazakhstan. *The Island Arc*, **9,** 379–399.

Ota, T., Terabayashi, M., Parkinson, C. D. & Masago, H., 2000. Thermobaric structure of the Kokchetav ultrahigh-pressure–high-pressure massif deduced from a north–south transect in the Kulet and Saldat-Kol regions, northern Kazakhstan. *The Island Arc*, **9,** 328–357.

Parkinson, C. D., 2000. Coesite inclusions and prograde compositional zonation of garnets in whiteschist of the Kokchetav UHP–HP massif, Kazakhstan: a record of progressive UHP metamorphism. *Lithos*, **52,** 215–233.

Smith, D. C., 1984. Coesite in clinopyroxene in the Caledonides and its implications for geodynamics. *Nature*, **310,** 641–614.

Sobolev, N. V. & Shatsky, V. S., 1990. Diamond inclusions in garnets from metamorphic rocks. *Nature*, **343,** 742–746.

Yamamoto, H., Ishikawa, M., Anma, R. & Kaneko, Y., 2000. Subhorizontal boundary between ultrahigh-pressure and low-pressure metamorphic units in the Sulu-Tjube area of the Kokchetav massif, Kazakhstan. *The Island Arc*, **9,** 304–316.

Yamamoto, H., Ishikawa, M., Anma, R. & Kaneko, Y., 2002. Subhorizontal structure and kinematic evolution of HP–UHP metamorphic rocks in the central Kokchetav massif. In: Parkinson, C. D., Katayama, I., Liou, J. G. & Marruyama, S. (Eds.), *The Diamond-Bearing Kokchetav Massif, Kazkahstan*. 71–89. Universal Academy Press, Tokyo.

Yamamoto, J., Maruyama, S., Parkinson, C. D. & Katayama, I., 2002. Geochemical characteristics of metabasites from the Kokchetav massif: Subduction zone metasomatism along an intermediate geotherm. In: Parkinson, C. D., Katayama, I., Liou, J. G. & Marruyama, S. (Eds.), *The Diamond-Bearing Kokchetav Massif, Kazkahstan*. 71–89. Universal Academy Press, Tokyo.

Table 0–1. Comparison of the specifications of collision-type and pacific-type orogens.

	collision-type	Pacific-type
Dimension	Width: a few 10 km Length: a few 1000 km Thickness: a few km	Width: a few km Length: a few 100 km Thickness: a few 100 m
Protolith	Platform sediments, granite, bimodal vocanics (basalt and dacite)	Deep sea sediments (chert, mudstone), trench-fill turbibite, MORB-type basalt
Metamorphic facies series	medium-*P* type	high-*P* type
Granitic batholith	rare or absent	huge
Orogenic peridotite	Grt-, Sp-peridotite	Sp-, Pl-peridotite

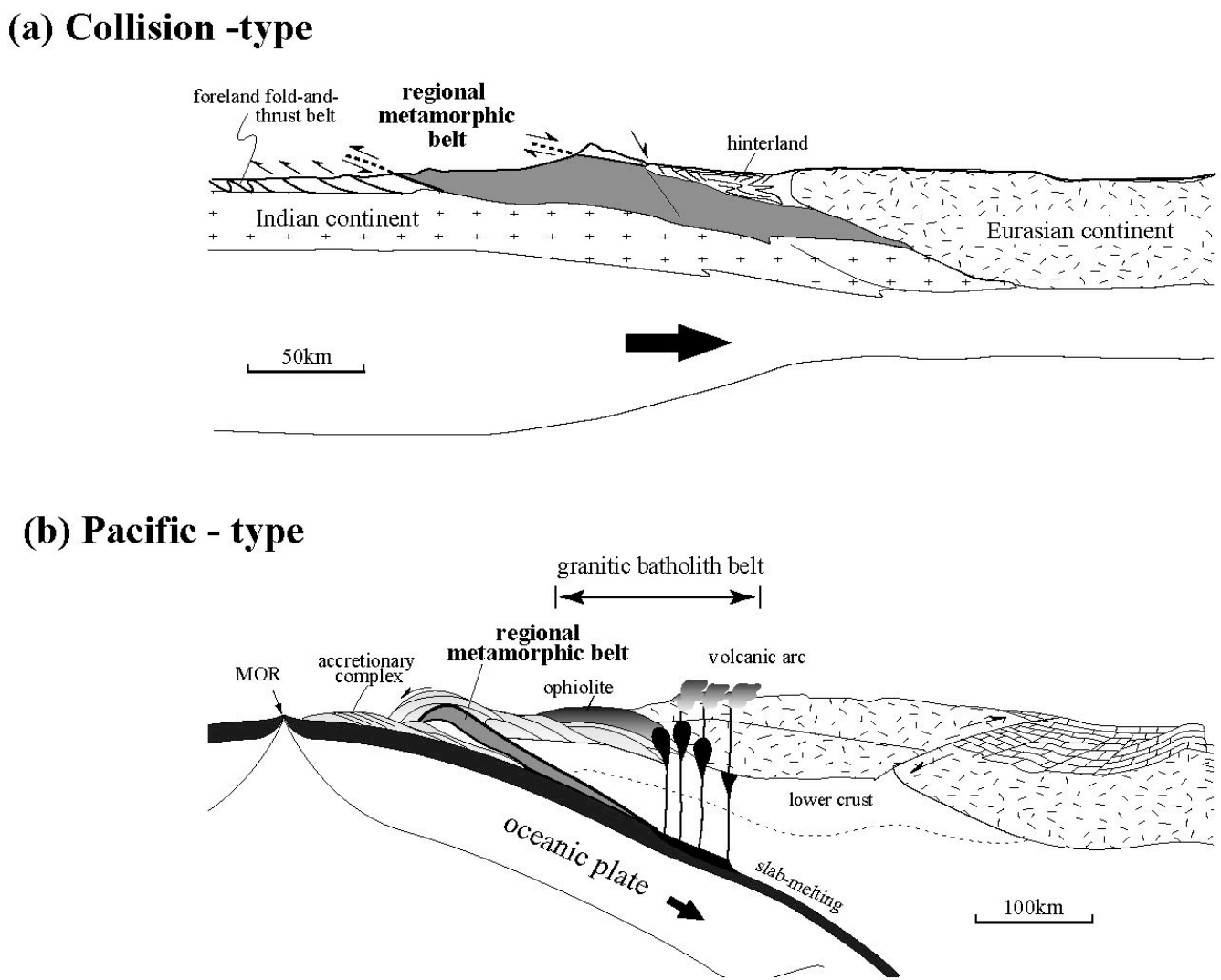

Fig. 0–1 Large-scale structure of two types of orogeny. a) Collision-type orogen. Type locality of this type of orogen is Himalaya. b) Pacific-type orogen. Type locality of this orogen is SW-Japan. MOR: mid-oceanic ridge.

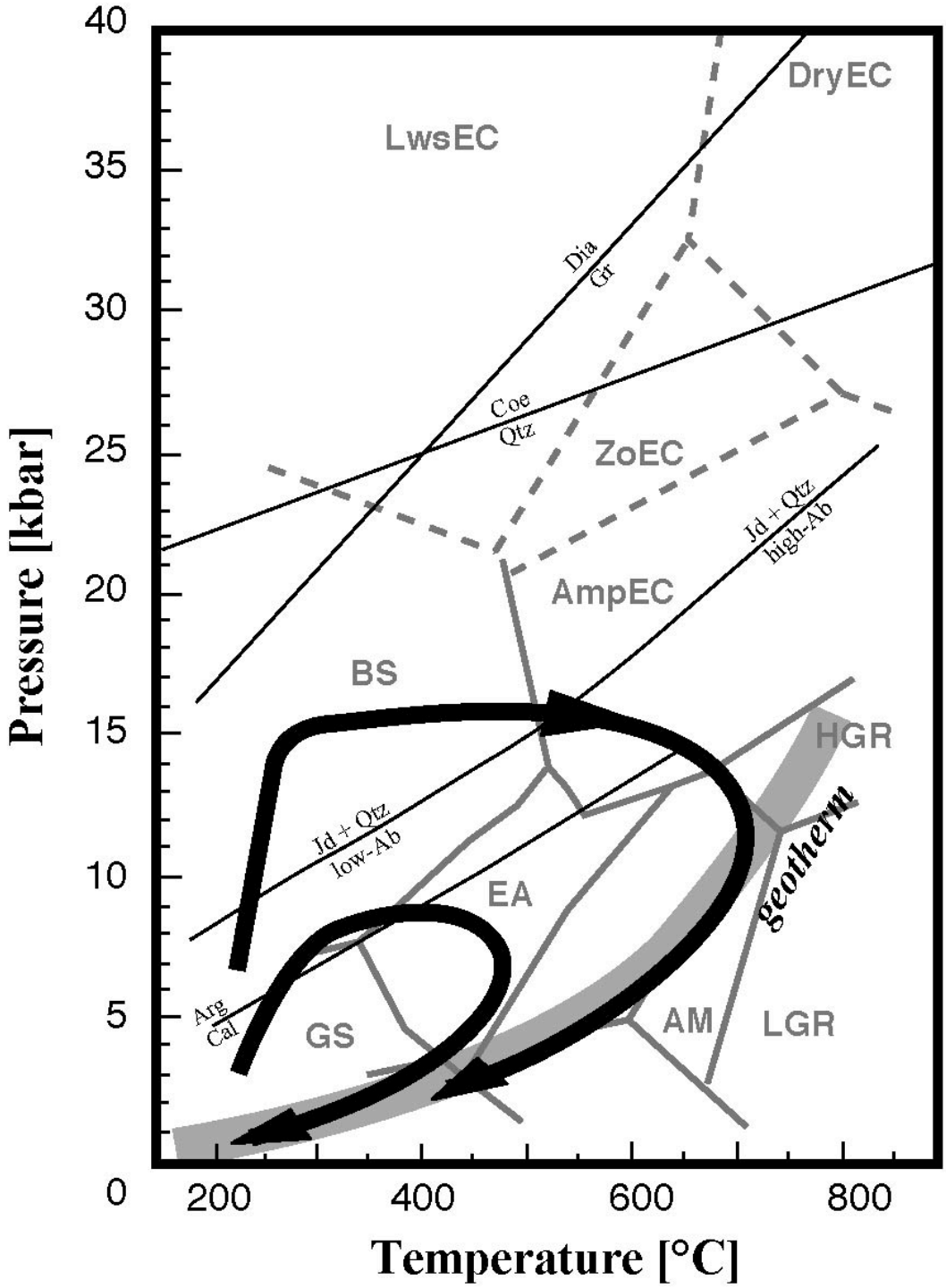

Fig. 0–2 Relationships between metamorphic *P–T* paths of individual rocks and geothermal gradient of the collisional metamorphic belt in traditional metamorphic petrology (England & Thompson, 1984). *P–T* paths of individual rocks (shown as solid lines) draw clockwise curve. Geothermal gradient of the metamorphic belt is defined as a series of *P–T* conditions of the individual rocks at their thermal peak stages, which do not coincide with individual *P–T* path in general.

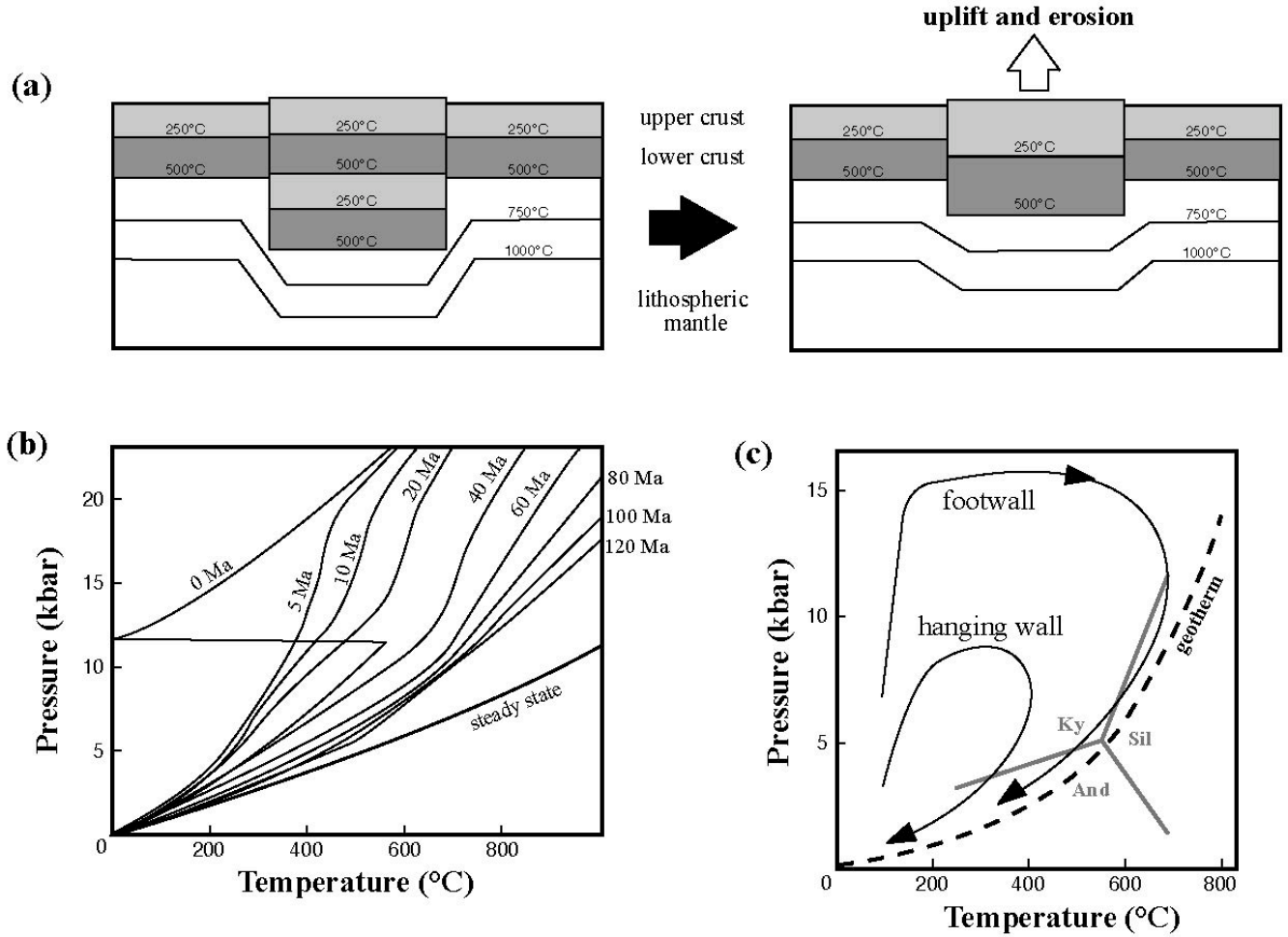

Fig. 0–3 Classical model for continetal collision orogeny of England & Thompson (1984) and Thompson & England (1984). a) Schematic cross-sections of the collisional orogen showing the crustal thickening by collision (left) and the sebsequent uplift and erosion (right). b) Thermal profiles along depth of the collision zone at various time after collision. Discontinuous thermal profile formed by doubly-thickened crusts (0 Ma) changes to recover the steady state geotherm with time. c) *P–T* paths for the hanging wall and the footwall of the orogen.

CHAPTER I

Metamorphic Petrology of the Kokchetav Metabasites

ABSTRACT

Basic features of metamorphism such as pressure–temperature (*P–T*) structure, metamorphic facies series and mineral reactions of the Kokchetav massif are revealed from a systematic study of metabasites from low- to high-grade. Two regions were chosen for this purpose: the Barchi-Kol and the Borovoye regions. In both regions, metabasites of relatively wide *P–T* range are widely distributed, which is appropriate for this study.

In the Barchi-Kol region, located at the westernmost part of the Kokchetav massif, metabasites from the epidote-amphibolite (EA) facies to the coesite-eclogite (CEC) facies are exposed. Based on the equilibrium mineral assemblages, the Barchi-Kol region is divided into four zones: BK–A to BK–D. Zone BK–A is characterized by the assemblage: Ep + Hbl + Pl + Qtz, with minor garnet. Zone BK–B is characterized by the assemblage: Grt + Hbl + Pl + Qtz + Czo. Zone BK–C is defined by the appearance of sodic-augite, with typical assemblages: Grt + Na-Aug + Ts–Prg +Qtz ± Pl ± Ep/Czo. Zone BK–D is characterized by the typical eclogite assemblage: Grt + Omp + Qtz + Rt, with minor phengite and zoisite. Inclusions of quartz pseudomorph after coesite were identified in several samples of zone BK–D. Chemical compositions of rock-forming minerals of each zone were analysed and reactions between each zone were estimated. Metamorphic *P–T* conditions of each zone were estimated using several geothermobarometers as 8.6 ± 0.5 kbar, 500 ± 30 °C for zone BK–A, 11.7 ± 0.5 kbar, 700 ± 30 °C for zone BK–B, 12–14 kbar, 700–815 °C for zone BK–C, and 27–40 kbar, 700–825 °C for zone BK–D.

Boroboye region is located at the eastern end of the Kokchetav massif. Metamorphic rocks of the HP–UHP unit of wide *P–T* range and an overlying low-grade unit are widely exposed in this region. Various kinds of metabasites occur in this area including greenschist, amphibolite and eclogite. Based on the distribution of their mineral assemblages, five mineral zones are defined in this area. Zone BV–A has greenschist facies mineral paragenesis: Ep + Chl + Pl (Ab) + Qtz + Ttn. Distribution of zone BV–A is restricted in the Unit V (lithological definition after Kaneko *et al*., 2000), an overlying unit of the HP–UHP unit. Zone BV–B is characterized by epidote-amphibolite facies assemblage: Ep + Hbl + Pl (Ab~Olg) + Qtz ± Ilm/Ttn. Zone BV–C is characterized by amphibolite facies assemblage: Hbl–Prg + Pl (Olg) + Qtz ± Ilm/Rt.

Zone BV–D is defined by the appearance of garnet in amphibolite, which has an assemblage of Grt + Prg + Pl + Qtz ± Ilm/Rt. Eclogite sporadically occurs in this zone with mineral assemblage: Grt + Na-Aug + Qtz + Rt ± Prg. Zone E is characterized by eclogite mineal assemblage: Grt + Omp + Qtz + Rt ± Phn. Metamorphic *P*–*T* conditions were estimated as 36.5 ± 0.4 kbar, 730–810 °C for zone E eclogites. Estimated temperatures for zones BV–B to BV–D amphibolites are partly overlapping in the range of 500–710 °C. However, distribution coefficient between coexisting Ca-amphibole and plagioclase ($K_{D\ Amp–Pl}$) shows a relative increase of temperature from zone BV–B to zone BV–D, which shows a clear correspondence with geological structure.

Metamorphic field gradient obtained from both regions kinks at around 700 °C, 12–15 kbar, and higher-grade part than this clipping point has steeper d*P*/d*T*. This infers a traditionally defined baric type of the metamorphic facies series such as low-*P*, medium-*P* and high-*P* types are no more applicable to characterise the metamorphic belts.

INTRODUCTION

Metamorphic coesite was first discovered in 1984 in the Western Alps (Chopin, 1984) and Norwegian Caledonides (Smith, 1984). Since then, several other UHPM belts have been recognised, such as the Bohemian massif (Scmädicke *et al*., 1992; O'Brien, 1993), and the Qingling–Dabie–Sulu terranes of central China (Wang *et al*., 1989). The Kokchetav massif is a unique UHPM terrane where both metamorphic microdiamond (Sobolev & Shatsky, 1990; Shatsky *et al*., 1995) and coesite (Zhang *et al*., 1997) have been reported. The peak pressures are estimated to be over 60 kbar (Okamoto *et al*., 2000) in the Kumdy-Kol region, and the massif is considered to consist of the most deeply subducted materials exposed nowhere. These orogenic belts usually consist not only of UHP metamorphic units but also of low-*P* and medium-*P* metamorphic units (*e.g.* Tabata *et al*., 1998). However, most previous studies of HP–UHPM terranes, have only focused on the highest grade parts of the terranes such as the coesite- and/or diamond-bearing rocks, with little attention to the adjacent lower grade rocks. For understanding of the tectonics of HP–UHP rocks and their relation to subduction processes, a systematic petrological study of all rock types is essential.

The Barchi-Kol and the Borovoye regions, located at the western and eastern margin of the Kokchetav HP–UHP massif, respectively, are best to delineate the nature of the metamorphism. There, rocks of wide range of metamorphic grade are distributed. In this chapter, systematic changes of mineral parageneses, mineral chemistry and *P–T* conditions of the Barchi-Kol and the Borovoye metabasites are described in detail, and some implications for metamorphic phase relations and exhumation tectonics are presented.

GEOLOGICAL OUTLINE

The Kokchetav HP–UHPM unit is subdivided into four lithotectonic units named as Unit I to IV from the structural bottom to the top (Kaneko *et al*., 2000; *see* detail in Appendix A). *P–T* conditions of the HP–UHP unit is highest in the structural intermediate Unit II, and decrease towards both the top and bottom boundaries.

In the Barchi-Kol area, Units I, II and IV crop out. Unit I occupies the northern

part of the area and consists of acidic gneiss (leptite) interlayered with amphibolite and minor eclogite (Fig. I–1). The lithological boundary trends NE–SW and is subvertical. The dominant foliation is concordant with the lithological boundary. In the northernmost part of the study area, a post-orogenic 200 x 160 m^2 massive gabbroic body is intruded into unit I rocks and truncates the primary structures. Unit II overlies Unit I and is characterized by alternating pelitic/psammitic gneisses intercalated with several thin layers of orthogneiss and lenticular eclogite bodies. The general trend of the foliation of unit II is concordant with that of unit I. Eclogite bodies are elongated subparallel to the foliation of the country rocks. Most eclogite bodies are amphibolitised along their margins. Some relatively small eclogite blocks are completely amphibolitised to the core of the body, however peak eclogite assemblages are usually preserved in the cores of relatively large bodies. Amphibolitisation is also observed along cracks which truncate the eclogite foliation at high angles. Unit II is in fault contact with unit IV to the south. Unit IV is predominantly composed of massive to foliated quartzite. To the south of Karly-Kol (a lake *ca*. 9 km southeast from Barchi-Kol), minor mafic schists occurs as block incorporated within the quartzite. A thin ultramafic slice occurs within a fault zone between Units II and IV to the south of the Barchi-Kol lake. It is composed of variably serpentinized peridotite and pyroxenite. Similar ultramafic rocks are also observed as small blocks just to the north of the fault zone.

The Borovoye area is located at the eastern end of the Kokchetav massif. The HP–UHPM unit is widely exposed *ca*. 10 km x 10 km area to the north of the Bolishoe Chebachye Lake. The Unit II, III and IV are exposed from south to north basically in this order with some minor repetitions (Fig. I–2). Foliations generally have ENE–WSW strike and moderately to steeply dip to either north or south, suggesting to ubiquitous occurrence of close folds with metre to decimetre scale. Boundaries of each unit are generally parallel to the mega-scopic internal structure, dipping gently to moderately to the north. They indicate top-to-the south sense of movement and apparently seem to be reverse faults in the lower half, but does the *vice versa* in the upper half. Unit II is composed of abundant eclogite blocks of a few metre to several decimetre size (long axis), enveloped by pelitic and partly whiteschist-like metasedimentary schists. Eclogite bodies are amphibolitised at various degree along margins and fractures. Unit III is predominated by orthogneiss with minor lenses of fine-grained acidic gneiss (leptite).

At the central part of Unit III, amphibolite-rich layer is exposed along an ENE–WSW trend antiformal axis. A few eclogite bodies and amphibolite bodies of eclogite-origin are distributed sporadically. Unit IV mainly consisits of quartzite and silicious schists with minor amount of epidote amphibolite. To the north of the whole HP–UHP units, low-grade metamorphosed Unit V is widely distributed. It consists mainly of slate, shale, quartzite, sandstone, marble/limestone and conglomerates. Very minor amount of greenschist occurs closely to the boundary to Unit IV. Asymmetric textures such as porphyroclast systems, preferred orientation of quartz aggregates, drag folds and shear bands, all indicate a top-to-the south sense of movement (*See* Appendix A).

The southern margin of the HP–UHPM units is uncomformably covered by shoshonite and its volcanoclastic sediments. Shoshonite occurs as either massive or lava flow, brecciated to ash-flow sediments. To the south of shoshonite distribution, the Devonian granite is intruded throughout all of other lithlogies.

PETROGRAPHY AND METAMORPHIC ZONATION

Metabasites are distributed sporadically but widespread throughout both the Barchi-Kol and the Borovoye regions. Approximately 150 and 500 metabasite samples were collected the Barchi-Kol and the Borovoye region, respectively, which were petrologically investigated. For the purpose of this study, heavily retrograded samples were excluded; peak assemblages were obtained based on the petrographic observation. Figures I–3 & I–4 shows an areal distribution of the observed mineral assemblages in the Barchi-Kol and the Borovoye region, respectively. In both regions, mineral assemblage in metabasites shows a systematic regional change, which enables to define several mineral zones. Petrography of each zone metabasite is described below.

Barchi-Kol Region

In the Barchi-Kol region, four mineral zones are defined as zone BK–A to BK–D (BK stands for ‘Barchi-Kol’). The equilibrium assemblages of each zone are listed in Fig. I–5. Zone BK–A is characterized by the assemblage: Ep + Hbl + Pl + Qtz, and is restricted to unit IV. Zone BK–B is characterized by the assemblage: Hbl + Grt + Pl +

Qtz + Czo. Zone C to the south of zone BK–B, is defined by the occurrence of Na-Ca clinopyroxene (sodic-augite or omphacite), and mineral assemblage: Grt + Na-Aug (or Omp) + Ts–Prg + Rt + Qtz ± Pl. Both zone BK–B and BK–C assemblages are distributed in Unit I. Zone BK–D is characterized by the typical eclogite mineral assemblage: Grt + Omp + Rt + Qtz/Coe + Phn, and by the absence of both primary plagioclase and amphibole distinguishes this zone from zone BK–C. Zone BK–D is located to the south of zone BK–C. Several eclogite samples contain quartz pseudomorphs after coesite as inclusions in omphacite (Fig. I–6). The occurrence of coesite pseudomorph is restricted to two eclogite blocks both of which are located in the centre of zone BK–D. Petrological features are described for each zone metabasite in the following section.

Zone BK–A

Zone BK–A metabasites contain Hbl + Ep/Czo + Qtz + Pl ± Cal ± Rt or Ttn. Garnet and apatite were also observed in a few samples. Foliation and lineation are well developed and defined by preferred orientation of amphibole and clinozoisite (Fig. I–7a). Amphiboles contain inclusions of epidote and rare composite grains of rutile, ilmenite and titanite. Epidote has inclusions of quartz and amphibole. Some amphibole grains are rimmed by Ep + Pl symplectites. Minor primary plagioclase crystals are in equilibrium contact with other constituent, whereas secondary one has an irregular grain boundary. Garnet occurs in two samples (N463, N464) as subhedral crystals with embayed rims; some are fragmented and fractured and filled with chlorite. Some grains are rimmed by kelyphites of Pl + Kfs + sericite, rarely with augite.

Zone BK–B

Metabasites in this zone are generally coarse-grained and well-foliated. Representative mineral assemblage is Hbl + Grt + Pl + Qtz ± Czo ± Rt ± Ttn (Fig. I–7b). Epidote is present in haematite-bearing metabasites. In a few samples, assemblage: Cum + Hbl + Grt was also observed. Subhedral hornblende and zoisite grains define the foliation. Euhedral garnet occasionally contains inclusions of quartz, zoisite and rutile. Plagioclase occurs as anhedral, is equlibrium with other constituent minerals and constitutes very low modal proportion. Actinolite rims hornblende, and rutile is rimmed by titanite aggregates. In epidote-rich samples, tiny actinolite agregates are overgrown

around epidote.

Zone BK–C

This zone is defined by the first occurence of clinopyroxene. The typical mineral assemblage of metabasites in this zone is: Grt + Na-Ca Cpx (Na-Aug or Omp) + Ts–Prg + Rt + Qtz ± Zo ± Pl, suggesting upper amphibolite/eclogite transitional condition. Biotite was also observed in one sample (K432). Samples of this zone typically display coarse-grained granoblastic texture (Fig. I–7c). Garnet, clinopyroxene, amphibole and rutile are all euhedral with sharp grain boundaries. Plagioclase is modally low. It occurs as anhedral but shows a sharp contact with the other constituent minerals. Zoisite is also very minor and is as anhedral. Garnet contains many tiny inclusions of quartz, rutile and epidote.

Zone BK–D

All metabasites in this zone are eclogites and occur as elongated blocks within gneiss in unit II. The main constituent minerals are Grt, Omp, Qtz, Rt, ±Zo, ±Phn. Eclogites texturally vary from granoblastic to inequigranular-elongated sample. Foliation is defined by the preferred orientation of omphacite and phengite (Fig. I–7d).

Phengite is a rather common in Barchi-Kol eclogites, whereas zoisite-bearing eclogite is not common, and contains very minor zoisite. Retrograde amphibole appears as large porphyroblasts up to 5 mm in addition to the above listed assemblages, and overgrown the primary foliation defined by omphacite and phengite. These amphiboles are poikiloblastic with many inclusions of garnet, omphacite, rutile and quartz. Excluding such a secondary amphibole, the following mineral assemblages are observed in eclogite; Grt + Omp, Grt + Omp + Phn, and Grt + Omp + Zo in addition to quartz/coesite and rutile. Their regional distribution shows no systematic variation, and all three assemblages are found even in a single eclogite block of ca. 240 m x 100 m (Fig. I–3); such variation seems to reflect the local difference of the bulk composition. Inclusions of polycrystalline quartz with radial fractures (presumably pseudomorph after coesite) was identified in omphacite from four samples (Fig. I–6) derived from two eclogite bodies, both of which are located at the central part of zone BK–D (Fig. I–3). The mineral assemblages of these coesite-bearing eclogites are Grt + Omp, and Grt + Omp + Phn in addition to coesite and rutile. It is noted that these samples contain no

zoisite.

Most eclogites have undergone retrograde metamorphism. Symplectite of Ca-Amp + Pl is common along the grain boundary of omphacite and garnet. In several samples, Aug + Pl symplectites are developed instead. In many cases, symplectite has developped only on the omphacite side, whereas garnet preserves a straight grain boundary. In many samples, cleavages truncate the eclogite foliation and are filled with Ca-Amp + Pl, or calcite. Another retrograde texture is Bt + Pl symplectite around phengite. Details about retrograde metamorphism are described in the next chapter.

Borovoye Region

In the Borovoye region, the following five zones are defined based on the mineral assemblage: 1) Ep + Chl + Pl + Qtz + Ttn, 2) Amp (Hbl) + Ep + Pl + Qtz ± Ilm ± Ttn, 3) Amp (Hbl–Prg) + Pl + Qtz ± Rt ± Ilm, 4) Grt + Amp (Hbl–Prg) + Pl + Qtz ± Rt ± Ilm, and 5) Grt + Omp + Rt + Qtz ± Phn. Their areal distribution is shown in Fig. 3. It has a regional trend from north to south, and five mineral zones (zone BV–A to zone BV–E) can be defined based on their distribution (Figs. I–4 & I–8). Petrological features are described for each zone metabasite in the following sections.

Zone BV–A

Zone BV–A metabasites are greenschist with strong schitosity defined by preferred orientation of chlorite. Mineral lineation is also developed, being defined by epidote and quartz. (Fig. I–9a). Matrix is mostly composed of chlorite of strong greenish colour and flaky shape. Albite and epidote appear as porphyroblasts. Epidote is yellow-greenish in colour. Albite and quartz have low modal proportion and have anhedral grain shape.

Zone BV–B

Metabasites in this zone is characterized by mineral assemblage of Hbl + Ep/Czo + Pl (Ab~Olg) + Qtz (Fig. I–9b). Ilmenite and/or titanite appear as accessory phases, probably replacing igneous iron oxides. Hornblende is elongated and is pale-greenish in colour. Clinozoisite is almost colourless. Planer and linear fabrics are not strongly developed.

Zone BV–C

This zone is differed from the previous zone by the disappearance of clinozoisite. Metabasites in this zone is generally coarser-grained than those of zone BV–B and almost massive. Representative mineralogy and texture is shown in Fig. I–9c. Typical mineral assemblage is: Amp (Hbl–Prg) + Pl + Qtz ± Ilm/Rt. Amphiboles are coarser-grained than those of zone BV–B ~ 1 mm (long axis), and are brownish in z-axis colour. Some amphiboles have optical zonation with brownish cores mantled by pale-green rims.

Zone BV–D

This zone is defined by the appearance of almandine-rich garnet in amphibolite of ordinary bulk composition. Very minor amount of eclogite samples are also distributed sporadically among amphibolites. Amphibolite in this zone is massive and coarse-grained (Fig. I–9d). Garnet is generally coarse-grained and nearly euhedral. However, the outermost rims are rounded by late-stage hydration alteration. Kelyphite rims are observed in some grains. Most garnets have diagonal cracks filled by epidote and/or chlorite, and some are completely fragmented and chloritised. Eclogite in this zone is massive and coarser-grained than those of zone BV–E described below (Fig. I–9e). Some amphibolites contain augitic clinopyroxene. These clinopyroxenes contain many plagioclase exolutions (Fig. I–10) and are considered to be retrograded from eclogitic omphacite.

Zone BV–E

All metabasites in this zone are eclogite. Their distribution is restricted to a narrow zone to the north of the Bolishoe Chebachye Lake. These eclogites have simple mineral assemblages: Grt + Omp + Rt + Qtz ± Phn. Neither coesite nor its pseudomorph has not yet been observed. Eclogites are massive and have equigranular texture of mostly composed of garnet and omphacite of same dimension (Fig. I–9f). Retrograde symplectite of Hbl + Pl and/or Cpx (augitic) + Pl have developed at various degree along grain boundaries. Another retrograde mineral is a large hornblende porphyroblast. It is brownish in colour, has distinctive paired cleavages, and overgrows on the eclogitic minerals. Chlorite is another common retrograde hydrous mineral. It most frequently appears as a crack-filling mineral of garnet. A large flaky chlorite also appears in T533.

ROCK-FORMING MINERALOGY

Major element analysis of consituent minerals in metabasites was performed using JEOL JXA8800 electron probe microanalyser (EPMA) in the Department of Earth and Planetary Science, Tokyo Institute of Technology. Operating conditions were 15 kV accelating voltage and 12 nA current. Beam is focused to be < 4 μm. Data were reduced using a ZAF matrix correction method. Representative mineral compositions of the Barchi-Kol and the Borovoye regions are listed in Tables I–1 & I–2, respectively.

Garnet

Garnet occurs in all zones in the Barchi-Kol region, and zone BV–D and BV–E in the Borovoye region. Garnet compositions in the studied samples are expressed as $(Fe^{2+}, Mg, Ca, Mn)_3Al_2Si_3O_{12}$. Substituting for Al site, a small amount of Fe^{3+} can be incorporated, however, it is generally very small or even zero in all analysed samples.

Analysed garnets are generally rich in almandine component. In the Barchi-Kol samples, pyrope component (X_{Prp} = Mg/(Fe^{2+}+Mg+Mn+Ca)) ranges from 0.10 in zone BK–A to 0.34 in zone BK–D (Fig. I–11). Grossular component varies from 0.15 to 0.34, and systematically higher in zone BK–D than in zones BK–A to BK–C, although they are partly overlapping. Compared among zone BK–D garnets, garnet in zoisite-bearing eclogites has higher grossular component than that in zoisite-free ones. Several garnets in coesite pseudomorph-bearing samples of zone BK–D have Na_2O contents up to 0.12 wt%. Such garnets are also rich in Si, which commonly exceeds 3.00 and reaches up to 3.1 for 12 oxygens.

Similar compositional variations by metamorphic zone and mineral assemblage were observed also in the Borovoye samples (Fig. I–12). In zone BV–D samples, garnet in eclogites is richer in pyrope and grossular componemts ($Alm_{37–41}Prp_{26–31}Grs_{28–36}Sps_1$) than that in amphibolites ($Alm_{50–57}Prp_{18–23}Grs_{22–27}Sps_{1–2}$). Garnet in clinopyroxene-bearing amphibolites has slightly higher pyrope and lower almandine components ($Alm_{46–53}Prp_{22–25}Grs_{22–28}Sps_1$) than that in clinopyroxene-free ones. Zone BV–E garnet has a wide compositional range of $Alm_{43–64}Prp_{14–28}Grs_{18–38}Sps_{0–2}$, which overlaps with that in clinopyroxene-bearing amphibolites in zone BV–D. However, they have a wider

range toward grossular-rich side, which is comparable to those in zone BV–D eclogites (Fig. I–12).

Barchi-Kol garnets are classified into three types in terms of compositional zoning. Type I garnet is concentrically zoned with increasing pyrope component from core to rim with a concomitant decrease of almandine component (Fig. I–13a). Spessartine component also shows normal zoning although its content is generally low. Type II is sector zoning characterized mainly by the difference of Fe/Mg ratio (Fig. I–14). Type III is unzoned, chemically homogeneous type with or without a slight decrease of pyrope and/or grossular components at the very thin part of the outermost rim (Fig. I–13b). Types I and II garnets are common in zones BK–B and BK–C metabasites although the latter shows less variable change of composition. In contrast, type III garnet is dominant in zone BK–D eclogites. Borovoye garnets are essentially homogeneous, which correspond to type III of the Barchi-Kol garnet.

Plagioclase

Plagioclase appears as a common matrix phase in metabasites of both regions. In the Barchi-Kol region, plagioclase occurs in zones BK–A, BK–B and some samples of zone BK–C, although their modal constitutions are generally small. Plagioclase in zone BK–A is oligoclase with X_{An} = 0.17–0.21, whereas that in zone BK–B varies sample by sample from oligoclase to andesine with X_{An}= 0.13–0.40. In zone BK–C, plagioclase is again oligoclase with X_{An} = 0.12–0.20.

In the Borovoye samples, plagioclase occurs as one of the major matrix minerals. Some plagioclase show compositional zonation with anorthite-rich core and albite-rich rim, probably due to later-stage re-equilibrium. Orthoclase component is negligibly small in every sample. In zone BV–A, plagioclase is albite with X_{An} = 0.01–0.03. In zones BV–B to BV–D sample, plagioclase composition varies from albite to andesine. Generally, anorthite component increases from zone BV–B to zone BV–D (Fig. I–15), although there are some exceptions such as K813 and Y1000. The former sample is located close to the fault zone and highly sheared. Thus, the plagioclase composition might have been modified during deformational recrystallisation at the latest stage. The latter sample partly preserves igneous texture. Plagioclase with unconformably high anorthite content in this sample might be a relict of the igneous precursor.

Also in eclogite, plagioclase is present as a symplectite mineral. The composition

of such plagioclase ranges from albite to labradorite, and is wider than that of the matrix phase.

Amphiboles

Amphiboles are one of the commonest minerals in metabasites in both regions, which appear as major matrix minerals in zones BK–A to BK–D in the Barchi-Kol region, and in zone BV–B to BV–D in the Borovoye region.

Amphiboles were texturally classified into three types (Fig. I–16). The first type occurs as subhedral grain in matrix which is comparable in size with other matrix minerals. This type of amphibole generally defines foliation and lineation. The second type occurs as coarse-grained porphyroblast in eclogite, which is randomly oriented with respect to the dominant foliation. This type of amphibole generally has many inclusions of eclogitic minerals such as garnet and clinopyroxene. The third type occurs as symplectite of Amp + Pl. Each type occurs in the both regions.

Ferric iron content is calculated based on the so called '13CNK' method (*e.g.* Spear, 1993): to satisfy the stoichiometry as Si + Al + Ti + Mg + Fe^{2+} + Fe^{3+} + Mn = 13 for 23 oxygens. Amphibole nomenclature follows Leake *et al*. (1997).

The matrix amphiboles from different zones have different compositions (Figs. I–17 & 18). Most amphiboles from zones BK–A and BK–B plot in the hornblende field. Some grains are significantly zoned; cores contain more Na in M4 site than the rims. In zone BK–C, matrix amphibole has higher Al^{IV} and A site occupancy and plots in the tschermakite to pargasite field. The Borovoye amphiboles show similar compositional trend. In the Borovoye region, amphiboles occur as a matrix phase from zone BV–B to zone BV–D. Amphiboles change their compositions from hornblende to pargasite from zone B to zone D along exchange vector of $(Na + K)\square^{-1}$ (edenite substitution) : $Al(IV)Si^{-1}$ (tschermak substituion) = 1.4 : 1 (Fig. III–9). Prograde actinolite is not observed. The first appeared amphibole in zone BV–B is hornblende without coexisting actinolite. This suggests a tectonic gap existing between zones BV–A and BV–B.

Compositional zonation between core and rim are recognised in some amphiboles, particularly in zone BV–B amphiboles, which have hornblende core and actinolite rim (Fig. I–18). Some amphiboles have more irregular zonation patterns suggesting break up and subsequent heeling of a grain, probably during the retrograde stage.

Porphyroblastic and symplectic amphiboles have wider compositional ranges; most

of porphyroblastic amphiboles have slightly higher Na in M4 site. The composition of symplectic amphibole scatters over a very wide range from actinolite to tschermakite as well as barroisite fields (Fig. I–19).

Clinopyroxene

Clinopyroxene commonly occurs as a matrix phase in zones BK–C and BK–D in Barchi-Kol, and zones BV–D and BV–E in Borovoye. As clinopyroxene has a complex solid solution at high-*P*, calculation of Fe^{3+} needs to be done carefully. The most problematic factor is existence of Ca-Eskola component, which contains molecular vacancy. However, the cation total of the analysed clinopyroxenes is almost identical to 4.000 for six oxygens, suggesting Ca-Eskola component is negligibly small. Thus, Fe^{3+} is calculated to balance the charge for six oxygens following the method of Ryburn *et al*. (1976).

Clinopyroxene shows a systematic compositional variation by zones. Clinopyroxene in zone BK–C falls in the sodic-augite to omphacite field with X_{Jd}, defined as: Jd/(Jd + Di + Hd + Acm + Ca-Ts + Ca-Es), ranging from 0.10 to 0.34. Ca-tschermak component is less than 0.05. Acmite component is < 0.14 and slightly higher than that in clinopyroxene of zone D described later. Clinopyroxenes in zone BK–C are more or less zoned with jadeite component decrease at the rim. Clinopyroxenes in zone BK–D samples are omphacite with X_{Jd} ranging from 0.21 to 0.43, X_{Acm} < 0.18, and Ca-tschermak component < 0.05. They are chemically homogeneous in general except for a slight decrease in jadeite component at the outermost rim as well as a slight increase of Fe^{2+}/Mg. No compositional discontinuity was observed between augite and omphacite (Fig. I–20). Clinopyroxene is known to contain appreciable K_2O at pressures > 5 GPa (Okamoto & Maruyama, 1998). However, K_2O content of clinopyroxenes in the Barchi-Kol metabasites is below the detection limit (< 0.05 wt%).

In Borovoye metabasites, similar distinctive compositional variation was observed between zones BV–D and BV–E clinopyroxenes, in terms of jadeite component. Zone BV–E clinopyroxene is omphacite with X_{Jd} = 0.27–0.38. It contains < 0.04 of Ca-Tschermak component. Acmite component is negligible. Clinopyroxene in zone D ecogite has jadeite component ranging from 0.09 to 0.16, and is classified into sodic-augite after the nomenclature of Essene & Fyfe (1967). Calcium-Tschermak component ranges from 0.09 to 0.14, suggesting a feature of high-*T*/low-*P* type clinopyroxene.

Fe^{2+}/Mg ratio is slightly higher than that in zone BV–E eclogite. Clinopyroxene in zone BV–D amphibolite has virtually no jadeite component (< 0.03) and higher Fe^{2+}/Mg ratio, and is classified into augite (Fig. I–21). It is known that there is a miscibility gap between augite and omphacite at temperature below 700 °C (*e.g*. Carpenter, 1980). This gap was not observed from analysed clinopyroxenes, which suggests their formation temperatures are higher than the gap closure temperature

Clinopyroxene also occurs in symplectite along the rim of matrix omphacite in eclogites. This type of clinopyroxene is augite with higher Fe^{2+}/Mg ratio and Ca-tschermak component (up to 0.13) than that of matrix omphacite.

Epidote group minerals

Epidote group minerals are common in metabasites of relatively lower-grade in both regions. In the Barchi-Kol region, epidote group minerals occur in zones BK–A and BK–B as common matrix minerals, and are also present in several eclogite samples of zones BK–C and BK–D. Epidote and rarely clinozoisite occur in zone BK–A metabasites. In zone BK–B, clinozoisite is common and epidote occurs only in a haematite-bearing sample. Secondary epidote replaces garnet or forms aggregates with plagioclase at the rims of amphibole in some zone BK–A rocks.

In some samples, concentric zonal textures marked by differences in the pistacite component are observed. However, some clinozoisite grains display hourglass textures. The pistacite component ($X_{Ps} = Fe^{3+}/(Fe^{3+} + Al)$) in the hourglass textured clinozoisite is small as 0.02–0.04. For the concentrically zoned grains, pistacite component decreases from 0.03–0.06 at the core to 0.02–0.04 at the rim.

Epidote is a major constituent mineral in zone BV–A of the Borovoye metabasites. In zone BV–B, epidote presents but modally minor, and clinozoisite occurs more commonly instead. Epidote is also present as a secondary mineral in zones BV–B, BV–C and BV–D. Primary epidote in zone BV–A has a compositional range of X_{Ps} = 0.20–0.35, whereas that in zone BV–B ranges from 0.10 to 0.25, which is indicating a progressive compositional change (Fig. I–22). Secondary epidote occurs as a vein and/or is replacing rim of other minerals such as amphiboles and garnet. These secondary epidote generally has higher pistacite component than the primary ones.

Phengite

Phengite is observed in some eclogite samples in zones BK–D and BV–E. It occurs as a matrix phase with a comparable size to garnet and omphacite and generally defines foliations with omphacite.

The Si value ranges from 3.25 to 3.52 (for 11 oxygens) for the Barchi-Kol phengite and from 3.39 to 3.49 for the Borovoye ones. And the core generally has higher Si contents than the rim. The margarite component is negligibly small (< 0.01). Paragonite component is also low, which is as small as < 0.1 and is systematically higher in the rims than in the core. Magnesium number [= Mg/(Fe+Mg)] is *ca*. 0.8 and shows little variation except for a slight decrease in the rim in some samples.

Chlorite

Chlorite occurs as a major matrix phase in zones BV–A and BV–B, or as a secondary phase in the higher-grade zones of the Borovoye metabasites. Primary chlorite is flaky in shape, strong greenish in colour, and forming planer and linear fabrics in zone BV–A. Chlorite in zone BV–B is modally smaller, and is less orientated. Secondary chlorite displays various textures. The most frequently observed texture is symplectite or altered rim around amphibole, garnet, clinopyroxene and titanite. Chlorite also occurs as a large patchy porphyroblast, which has overgrown across the former fabrics. Some of these chlorites do not have distinct grain shape and exhibit amoeboid texture. In zones BV–D and BV–E, chlorite is often filling the cracks of garnet porphyroblast, very frequently associated with epidote. All analysed chlorites have Si = 5.6–6.4 regardless to metamorphic grade and texture, which is on the clinoclore–chamosite series substitution vector (Fig. I–23). Chlorite in zone BV–B is richer in Fe than those in zone BV–A. Secondary chlorite has similar compositional range to zone BV–B chlorite. Secondary chlorite filling garnet crack has more Fe-rich composition than other textured secondary chlorite.

Apatite

Apatite is a common accessory mineral occurring all zones in both regions. It appears as an elongated grain of ~ 100 μm in size (long axis), and often aligns on the foliation and mineral lineation. Some apatite exhibit pale purplish colour and are considered to be flourapatite.

Ilmenite

Ilmenite is the most frequently present opaque mineral in the metabasites of both regions. It commonly occurs in zones BK–B and BK–C of the Barchi-Kol region, and in zones BV–B, BV–C and BV–D of the Borovoye region. Metamorphic ilmenite often contains certain amount of geikelite (Mg end-member) and pyrophanite (Mn end-member) component. The analysed ilmenite solid-solutions generally contain < 0.09 of pyrophanite component. Difference among mineral zones is not certain. Geikelite component is negligibly small (< 0.01) for all analysed samples.

THERMOBAROMETRY

Metamorphic *P–T* conditions were estimated using several cation-exchange thermobarometers. To obtain the peak *P–T* conditions, peak mineral compositions of zoned minerals should be chosen carefully. For the application of geothermobarometers, equilibrium compositions were selected as follows. When the relevant minerals have no distinctive compositional zonation, their rim compositions were assumed to record the peak–*T* conditions. Some amphiboles have distinctive core–rim compositional zonation with pargasitic core rimmed by actinolitic amphibole. In these cases, the latter is considered to be clearly a late-stage product, thus the core composition was utilised to estimate the peak *P–T* conditions. In a case of plagioclase, anorthite content is higher in core than in rim, which suggests retrograde modification for rim part. Therefore, core compositions were used for peak *P–T* estimation. For garnet and clinopyroxene, if the grains have normal zoning (rim-ward Fe^{2+}/Mg decrease for garnet, and rim-ward Fe^{2+}/Mg increase for clinopyroxene), rim compositions were used. And otherwise core compositions were used. Silicon content in phengite is critical for the pressure estimation. In general, Si in phengite increases with increasing pressure. Hence the highest Si analysis in each grain was regarded to represent the peak composition. Although the estimated temperatures and/or pressures do not necessarily represent the peak ones, this choice will give the minimum *P–T* conditions for each sample.

Eclogite

For eclogite thermometry, Fe^{2+}–Mg exchange Grt–Cpx thermometers of Ellis & Green (1979), Krogh Ravna (2000a), Powell (1985) were applied. For barometry, a Grt–Cpx–Phn geobarometer of Waters & Martin (1993) was applied to the phengite-bearing samples. In addition, a Grt–Amp–Pl–Qtz barometer of Kohn & Spear (1990) and a semi-quantitative amphibole geothermobarometer of Ernst & Liu (1998) were also applied to the amphibole-bearing eclogites of zone BK–C. Results are listed in Table I–3.

The results of the Grt–Cpx–Phn barometry are consistent with the presence/absence of coesite pseudomorph for the Barchi-Kol eclogites, except for one sample (H299). Based on the results of barometry, temperatures of phengite-free eclogites were calculated at arbitrary pressures of 35 and 30 kbar for coesite pseudomorph-bearing and free samples, respectively. In general, thermometers of Ellis & Green (1979), Powell (1985) and Krogh Ravna (2000a) yielded higher temparature in this order. These differences reach up to 45 °C and are usually about 30 °C. For the reasons mentioned above, Krogh Ravna (2000a)'s thermometer is used in the following discussion as giving a minimum temperature condition. The thermometric result was also plotted on the map (Fig. I–24). All calculated temperatures are within 700–825 °C and show no systematic variation on the map. It is noted that the rather wide temperature range exists even in the same eclogite block. This is more clearly presented in the cases of relatively large blocks. For instance, F483, F484, F488, F494 and F495 were all collected from the same block, whereas the calculated temperature ranges from 740 to 825°C. Even if the peak mineral compositions were carefully selected based on the zoning patterns of the relevant minerals, compositional modification during post-peak metamorphism in a local cm scale may have affect the temperature estimation. Estimated *P*–*T* conditions for zone BK–C using Grt–Cpx thermometer of Krogh Ravna (2000a) and Grt–Amp–Pl–Qtz barometer of Kohn & Spear (1990) are 700–815 °C, 12–14 kbar. The semi-quantitative amphibole geothermobarometer of Ernst & Liu (1998) yields much wider range for pressure of 9.1–15.1 kbar but more restricted range for temperature of 700–760 °C.

As estimated pressure by phengite barometer for the phengite-bearing sample (J336) was 36.5 ± 0.4 kbar, temperature calculations of other phengite-free eclogites were arbitrary performed at 36.5 GPa for the Borovoye ecogites. There was a slight

difference between estimated temperatures by different thermometers. Thermometer of Ellis & Green (1979) generally yielded the highest temperature, whereas Krogh Ravna (2000a)'s yielded the lowest, as is the case with the Barchi-Kol eclogites. Their differences are usually less than 30 °C and 95 °C at maximum. Estimated temperatures for zone BV–E eclogites range from 731 to 807 °C by thermometer of Krogh Ravna (2000a), and have a regional variation. Three samples collected from northwestern coast of the Bolishoe Chebachie Lake (T507, T527 & T533) show rather uniform temperature, whereas the sample taken from northeastern coast of the Bolishoe Chebachie Lake has about 80 °C higher temperature than those of former three samples. Two eclogite samples of zone BV–D have distinctively higher temperature than those of zone BV–E eclogites: 1003 and 914 °C by Krogh Ravna (2000a)'s.

Amphibolite

Thermobarometry of amphibolite is difficult. There are not many good thermobarometers for amphibolite compared to eclogite and granulite. The applicable thermometers are Amp–Pl thermometer of Blundy & Holland (1990), Grt–Amp thermometer of Krogh Ravna (2000b) and Graham & Powell (1984), and Grt–Amp–Pl barometer of Kohn & Spear (1990).

For zones BK–A and BK–B samples of the Barchi-Kol region, the Grt–Amp–Pl–Qtz geothermometer of Graham & Powell (1984) and the Grt–Amp geothermobarometer of Kohn & Spear (1990) were employed. Results of thermobarometry are shown in Fig. I–25. Uncertainties of thermobarometers are quoted from the referred literatures. Estimated *P*–*T* values by using Kohn & Spear (1990)'s thermobarometer are 8.6 ± 0.5 kbar, 400 °C for zone BK–A, and 11.7 ± 0.5 kbar, 720–730 °C for zone BK–B, respectively. On the other hand, estimated temperatures by Graham & Powell (1984) are 500 ± 30 °C and 700 ± 30 °C for zones BK–A and BK–B, respectively.

Temperatures estimation for the Boroboye amphibolites by Blundy & Holland (1990)'s thermometer are 582–710 °C for zone BV–B, 503–687 °C for zone BV–C and 620–689 °C for zone BV–D. For the application of this thermometer, pressure is needed to be given independently. For garnet-bearing zone BV–D samples, temperatures are calculated at the pressure estimated by Kohn & Spear (1990)'s geobarometer as mentioned below. For zones BV–B & BV–C samples, temperatures are calculated at the

arbitrary fixed pressure at 7 and 10 kbar, respectively. There is no systematic difference in temperature in different zones, and temperature distribution within each zone also seems to be random. Further, for zone BV–D samples, temperatures estimated by different thermometer are quite inconsistent for one another. These problems are partly due to difficulty in constructing thermodynamic cation mixing model for both amphibole and plagioclase. Because both hornblende and plagioclase have complicated and highly non-ideal mixing, thermometers involving these minerals are empirical. Pressure estimation for garnet-bearing samples of zone BV–D resulted in 12.3–15.2 kbar.

DISCUSSION

Phase Relations

The characteristic minerals in the Barchi-Kol metabasites include Grt, Na-Ca Cpx (Omp or Na-Aug), Amp (Hbl or Ts–Prg), Phn, Ep, Czo, Rt, Ttn, Pl, Ap, Coe and Qtz. These minerals can be described compositionally by 12 components: SiO_2, TiO_2, Al_2O_3, Fe_2O_3, FeO, MnO, MgO, CaO, Na_2O, K_2O, P_2O_5 and H_2O.

In order to simplify the system for chemographic analysis, the following assumptions have been made:

1. Each of K_2O, TiO_2 and P_2O_5 is minor component, and is restricted to one phase (phengite, rutile or titanite, and apatite, respectively) and can be treatd as an accessory inert component.
2. SiO_2 is present as quartz or coesite and treated as excess component.
3. H_2O is an aqueous fluid which is externally buffered.
4. MnO is a minor constituent. And when exist, it tends to concentrate to garnet core which is not in equilibrium with other matrix phases.
5. Fe_2O_3 is regarded as minor and thus ignored.
6. FeO and MgO should be treated as different components. However, to simplify the model system, the FeO/(FeO+MgO) ratio is fixed. This makes the freedom of the system reduced. (Nakajima *et al.*, 1977).

For example, K-bearing phase includes amphibole and rare biotite in zones BK–A to BK–C, is phengite in zone BK–D. Therefore, the change of mineral assemblage from

zone BK–C to BK–D cannot be explained without regarding to the effect of K_2O. However K_2O content is low in basaltic bulk composition that is assumed insignificant in the effect on the phase analysis. The similar assumption is true for TiO_2. As titanite is the only Ti-bearing phase in zone BK–A and rutile in other zones. The transformation of Ti-phase from titanite to rutile adds more Ca to the system. This effect may be explained as other Ca-phases (most probably, plagioclase) become richer in Ca by the addition of the Ca from titanite. In this section, phase relations of studied metabasites with various metamorphic grades are described in the following system:

$N = Na_2O$

$A = Al_2O_3 + Fe_2O_3$

$C = CaO$

$F = (Fe, Mg)\ O$.

Zone BK–A to zone BK–B

The change of mineral parageneses from zone BK–A to BK–B can be explained by the continuous NACF reaction in which the four-phase assemblage: Ep + Hbl + Pl + Grt shifts towards the more calcic side because zone BK–B plagioclase has higher anorthite content than that of zone A. This is a well-known reaction to explain the gradual disappearance of epidote from basaltic bulk compositions (Spear, 1993). Although Spear (1993) considers a shift of the four-phase paragenesis Ep + Hbl + Pl + Chl, garnet often appears instead of chlorite in relatively Fe-rich bulk composition and/or higher pressure condition and the reaction occurs in the same manner. The mineralogical change from zone BV–B to BV–C in the Borovoye region is also explained by this reaction.

Zone BK–B to zone BK– C

The change in mineral assemblage from zone BK–B to zone BK–C can be explained by the following pierced plane reaction on the NACF diagram (Fig. I–26a);

$$42\ Na_{0.45}Ca_{1.7}(Fe, Mg)_{4.1}Al_{2.2}Si_{6.7}O_{23}(OH)_2 + 2\ Ca_2Al_3Si_3O_{12}(OH) + 13\ Na_{0.65}Ca_{0.35}Al_{1.3}Si_{2.7}O_8$$

Hbl Zo Pl

$$= 48\ Ca_{0.7}(Fe, Mg)_{2.3}Al_2Si_3O_{12} + 78\ Na_{0.35}Ca_{0.6}(Fe, Mg)_{0.8}Al_{0.25}Si_2O_6 + 23\ SiO_2 + 43H_2O$$

Grt Na-Aug Qtz

The representative analyses of the minerals of each zone were used as chemical

compositions of the relavant minerals of this reaction. The $Mg/(Fe^{2+}+Mg)$ ratio was fixed within 0.75–0.85 for hornblende. As the consequence, the typical assemblage of garnet amphibolite is unstable in this model system, and the following four-phase assemblages appear; (1) Grt–Na-Aug–Hbl–Zo (Fig. I–26b); (2) Grt–Na-Aug–Hbl–Pl (Fig. I–26c); and (3) Grt–Na-Aug–Zo–Pl (Fig. I–26d). The first listed assembalge lacks plagioclase and is a typical assemblage of EC facies whereas plagioclase is stable in the latter two assemblages of the upper-AM facies. However, three assemblages can appear at the same *P–T* condition if the appropriate bulk compositions are chosen. In relatively Na-poor, Al-poor bulk composition, assemblage (1) appears whereas in Na-rich, Al-poor bulk, assemblage (2) appears, and in Al-rich, Ca-rich bulk, assemblage (3) still presents. The last one was not observed in the studied samples due to inappropriate bulk composition. With increasing pressure, it is expected that clinopyroxene changes its composition to more sodic one along Aug–Jd tie-line, as omphacite is a typical clinopyroxene in eclogite. Concomitantly, the modal contents of plagioclase decreases and finally disappears in the EC facies. This expands the stability field of eclogite assemblage towards Na-richer side, and finally whole of typical basaltic bulk composition is emcompassed in this field. In contrast, the other two assemblages occur in the more restricted bulk compositions. Several analysed samples of zone BK–C lack plagioclase, and clinopyroxene in such samples becomes more sodic up to $Jd_{30}Aug_{70}$ (acmite component is generally low), as to be classfied into the omphacite field. This nature is well explained by the above mentioned phase relationship of the gradual expansion of the EC field and concomitant shrinking of the highpressure-AM assemblage fields.

Metamorphic Facies Series of the Kokchetav Massif

Metamorphic facies series, defined as a series of the *P–T* condition of each mineral zone, has traditionally been used as a basic classification of the metamorphic belt. Metamorphic petrology traditionally has classified the metamorphic belt into three types in terms of metamorphic facies series: low-*P* type, medium-*P* type and high-*P* type. Low-*P* type is characterized by the series from lower-AM to pyroxene-hornfels and sanidinite facies. This type is also characterized by the andalusite–sillimanite series alnimosilicates. Medium-*P* type metamorphic facies series is characterized by the AM–GR facies series, and kyanite–sillimanite series alminosilicates. High-*P* type is

characterized by the BS facies, and characteristically contains jadeite and glaucophane-bearing metabasites. Furthermore, metamorphic petrologists have correlated these baric type classification to the tectonic settings of the metamorphic belt in plate tectonic paradigm. High-*P* and medium-*P* type metamorphism are peculiar to the two different types of subduction: Pacific-type and collision-type, respectively. Low-*P* type is restricted to contact metamorphism. This classification has been used as a basic law to correlate metamorphic petrology to tectonics for a long time.

The metamorphic facies series of the Kokchetav massif has turned this over completely. Results of thermobarometry of the Barchi-Kol and the Borovoye metabasites are summarised in the *P–T* space, as well as *P–T* conditions of other regions of the Kokchetav massif (Fig. I–27a). Metamorphic facies series of the Kokchetav massif starts from EA in the Unit IV of the Barchi-Kol and the Borovoye regions, through AM, Qtz-EC, Coe-EC and reaches to Dia-EC facies in the Kumdy-Kol region. It steeply kinks at around 10–12 kbar, 700 °C, which corresponds to the conditions of Moho depth. Metamorphic facies series has been virtually regarded as a paleogeotherm of the subduction zone. The Kokchetav massif shows that the geothermal gradient of the subduction zone is not uniform as it has been believed, but changes with depth. Therefore, the baric type classification such as high-*P* type or medium-*P* type no more makes any sense, because it changes in a single metamorphic belt.

This is contradictory to the general understanding of the traditional metamorphic petrology, but is consistent with the prediction from the numerically simulated geotherm of the subduction zone. Figure I–27b illustrates the calculated geotherms along Benioff plane of subduction zone of various plate age (Peacock, 1996). The calculated getherms show variation with age of the subducting slab. The older slab has the lower temperature at the same depth. Although their gradients are different, they commonly have kink around the Moho depth. This feature is the consistent with the obserbed metamorphic geotherm in the Kokchetav massif. This is simply predicted from geophysics because geothermal gradient is exponentially decreases with depth. Nevertheless, traditional metamorphic petrology has assumed the near-linear geothermal gradient for metamorphic belt. One of the main reasons for that is the misunderstanding of the peak metamorphic conditions largely obscured by the retrograde metamorphism. This problem will be discussed in detail in the next chapter.

Tectonic Implications

The compiled *P–T* conditions of the Kokchetav massif are not continuous. A large *P–T* break (chiefly pressure) exists between 15 and 22 kbar (Fig. I–27a). This corresponds to between Units I & III and Unit II. Another large break exists between 42 and 52 kbar. This is within Unit II. Does it mean the metamorphism in the Kokchetav massif is discontinuous? The answer to this question is given by the *P–T–t* path deduced from garnet zoning, described and discussed in detail in Chap. III. Compositionally zoned garnet in the Kulet whiteschist has a continuous growth records from low to peak metamorphic conditions (Chap. III). This denies the possibility of discontinuous metamorphism in the Kokchetav massif. Hence the *P–T* discontinuity present in the massif must has been formed during the exhumation stage.

Large pressure gap exists even within a single zone. For example, zone BK–D has a pressure range of about 13 kbar in a narrow zone. For the whole massif, about 50 kbar of pressure range which corresponds to the 150 km of crustal thickness exists within only a 2 km thick sheet. This cannot be explained without considering the reconstruction with ‘thinning out’ of the thermobaric struture during exhumation. Boundaries between each two lithotectonic unit are fault. Therefore, it is no wonder that a certain part of the massif between two units had been missing during the reconstruction. In the case of intra-unit pressure break, another tectonic model is needed. There is no distinctive layer-parallel fault within each unit. Hence, intra-unit reconstruction of *P–T* structure occurred in a ductile manner.

The maximum pressure of the Barchi-Kol eclogites is below diamond-stability field. On the other hand, diamond is reported from the country gneiss in the Barchi-Kol region (Lavrova *et al*., 1996). This means the country gneiss are derived from deeper part of the subduction zone than eclogite. This relationship favours the following tectonic model. Eclogite and the country gneiss are assumed to be rigid body and viscous fluid in this model, respectively. In a exhumation process, heavy eclogite bodies have down-going movement relative to the matrix gneiss. However, the net buoyancy of the eclogite plus gneiss is larger, and consequently the whole massif has exhumed as a coherent body. Each eclogite block has different velocity according to its dimension. As a consequence, mixing of the eclogite blocks of different depth origin in the enveloping gneiss is expected to occur in this process.

Similar mixing of metabasite blocks and consequent disturbance of *P–T* structure

might have occurred in the lower-grade parts of the massif. However, it is noted that such a mixing does not occur among different lithotectonic units. Figure I–28a shows a regional variation of partition coefficient (K_D) between amphibole and plagioclase in amphibolites in the Borovoye region. Definition of $K_{D\ (Amp–Pl)}$ is followed after Blundy & Holland (1990) as $K_{D\ (Amp–Pl)} = ((Si - 4)/(8 - Si))_{Amp} \cdot X_{Ab}$. It shows a remarkable difference between zones BV–B & BV–C and BV–D. As in the former two zones, K_D value ranges from 1.80 to 1.14, whereas in the latter zone K_D is less than 1 for most samples. Figure I–28b shows a geological cross-section along A–A' in Fig. I–30, and regional variation of K_D value projected onto this line. The thermal discontinuity corresponds to the geological boundary. However, K_D has no systematic regional variation within each zone. This result further supports the model proposed for the thermobaric structure in the Barchi-Kol region.

REFERENCES

Berman, R. G., Aranovich, L. Y. & Pattison, D. R. M., 1995. Reasessment of garnet-clinopyroxene Fe-Mg exchange thermometer: II. Thermodynamic analysis. *Contributions to Mineralogy and Petrology*, **119,** 30–42.

Blundy, J. D. & Holland, J. B., 1990. Calcic amphibole equilibria and a new amphibole–plagioclase geothermometer. *Contributions to Mineralogy and Petrology*, **104,** 208–224.

Bohlen, S. R. & Boettcher, A. L., 1982. The quartz–coesite transformation: A pressure determination and the effect of other components. *Journal of Geophysical Research*, **87,** 7073–7038.

Bundy, F. P., 1980. The P, T phase and reaction diagram for elemental carbon. *Journal of Geophysical Research*, **85**, 6930–6936.

Carlson, W. D., 1983. The polymorphs of $CaCO_3$ and the argonite–calcite transformation. *Reviews in mineralogy*, **11,** 191–225.

Carpenter, M. A., 1980. Mechanism of exsolution in sodic pyroxene. *Contributions to*

Mineralogy and Petrology, **71,** 289–330.

Chopin, C., 1984. Coesite and pure pyrope in high-grade pelitic blueschists of the Western Alps: A first record and some sequences. *Contributions to Mineralogy and Petrology*, **86,** 107–118.

Ernst, W. G. & Liu, J., 1998. Experimental phase-eqilibrium study of Al- and Ti-contents of calcic amphibole in MORB —A semiquantitative thermobarometer. *American Mineralogist*, **83**, 952–969.

Ellis, D. J. & Green, D. H., 1979. An experimental study of the effect of Ca upon garnet–clinopyroxene Fe–Mg exchange equilibria. *Contributions to Mineralogy and Petrology*, **71,** 13–22.

Essene, E. J. & Fyfe, W. S., 1967. Omphacite in Californian metamorphic rocks. *Contributions to Mineralogy and Petrology*, **15,** 1–23.

Graham, C. & Powell, R., 1984. A garnet–hornblende geothermometer: calibration, testing, and application to the Peloa Schist, Southern California. *Journal of Metamorphic Geology*, ***2,*** 13–31.

Holland, T. J. B., 1980. The reaction albite = jadeite + quartz determined experimentaly in the range 600–1200 °C. *American Mineralogist*, **65,** 125–134.

Kaneko, Y., Maruyama, S., Terabayashi, M., Yamamoto, H., Ishikawa, M., Anma, R., Parkinson, C. D., Ota, T., Nakajima, Y., Katayama, I., Yamamoto, J. & Yamauchi, K., 2000. Geology of the Kokchetav UHP–HP massif, Kazakhstan, central Asia. *The Island Arc*, **9,** 264–283.

Kohn, M. J. & Spear, F. S., 1990. Two new geobarometers for garnet amphibolites, with application to southeastern Vermont. *American Mineralogist*, **75,** 89–96.

Krogh Ravna, E., 2000a. The garnet–clinopyroxene Fe^{2+}–Mg geothermometer: an updated calibration. *Journal of Metamorphic Geology*, **18,** 211–219.

Krogh Ravna, E., 2000b. Distribution of Fe^{2+} and Mg between coexisting garnet and hornblende in synthetic and natural systems: an empirical calibration of the garnet–hornblende Fe–Mg geothermometer. *Lithos*, **53,** 265–277.

Lavrova, L. D., Pechinikov, V. A., Petrova, M. A. & Zayachkovsky, A. A., 1996. Geology of Barchi-Kol diamondiferous area. *Otechestvennaia Geologia*, **12,** 20–27 *(in Russian).*

Leake, B. E., Wolley, A. R., Arps, C. E. S., Birch, W. D., Gilbert, M. C., Grice, J. D., Hawthorne, F. C., Kato, A., Kisch, H. J., Krivovichev, V. G., Linthout, K., Laird, J., Mandarino, J. A., Maresch, W. V., Nickel, E. H., Rock, N. M. S., Schumacher, J. C., Smith, D. C., Stephanson, N. C. N., Ungaretti, L., Whittaker, E. J. W. & Youzhi, G., 1997. Nomenclature of amphiboles: Report of the subcomittee on amphiboles of the International Mineralogical Association, commission on new minerals and mineral names. *American Mineralogist*, **82,** 1019–1037.

Nakajima, T., Banno, S. & Suzuki, T., 1977. Reactions leading to the disappearance of pumpellyite in low-grade metamorphic rocks of the Sanbagawa metamorphic belt in central Shikoku, Japan. *Journal of Petrology,* **18**, 263–284.

Newton, R. C. & Smith, J. V., 1967. Investigations concerning breakedown of albite at depth in the earth. *Journal of Geology,* **45,** 268–286.

O'Brien, P. J., 1993. Partially retrograded eclogites of the Münchberg Massif, Germany: Record of a multi-stage Variscan uplift history in the Bohemian Massif. *Journal of Metamorphic Geology,* **11,** 241–260.

Oh, C. W. & Liou, J. G., 1998. A petrogenetic grid for eclogite and related facies under high-pressure metamorphism. *The Island Arc*, **7,** 36–51.

Okamoto, K. & Maruyama, S., 1998. The high pressure stability limits of lawsonite in the MORB + H_2O system. *American Mineralogist*, **84,** 362–373.

Okamoto, K., Liou, J. G. & Ogasawara, Y., 2000. Petrology of the diamond-grade eclogite in the Kokchetav Massif, northern Kazakhstan. *The Island Arc*, **9,**

Ota, T., Terabayashi, M., Parkinson, C. D. & Masago, H., 2000. Thermobaric structure of the Kokchetav ultrahigh-pressure–high-pressure massif deduced from a north–south transect in the Kulet and Saldat-Kol regions, northern Kazakhstan. *The Island Arc*, **9,** 328–357.

Peacock, S. M., 1996. Thermal and petrologic structure of subduction zone. In: Bebout, G. E., Scholl, D.W., Kirby, S. H. & Platt, J. P. (Eds.), *Subduction: Top to Bottom*, Geophysical Monograph, **96,** 119–133. American Geophysical Union. Washington D. C.

Powell, R., 1985. Regression diagnostics and robust regression in geothermometer/geobarometer calibration: the garnet–clinopyroxene geothermometer revisited. *Journal of Metamorphic Geology,* **3,** 231–243.

Ryburn, R. J., Råheim, A. & Greeen, D. H., 1976. Determination of the *P, T* paths of natural eclogites during metamorphism —record of subduction: A correction to a paper by Råheim & Green (1975). *Lithos*, **9,** 161–164.

Schmedicke, E., 1991. Quartz pseudomorphs after coesite in eclogites from the Saxonian Erzgebirge. *European Journal of Mineralogy,* **1,** 231–238.

Shatsky, V. S., Sobolev, N. V. & Vavilov, M. A., 1995. Diamond-bearing metamorphic rocks of the Kokchetav massif (northern Kazakhstan). In: Coleman, R. G. & Wang, X. (Eds.), *Ultrahigh-pressure Metamorphism*. 427–455. Cambridge University Press, London.

Smith, D. C., 1984. Coesite in clinopyroxene in the Caledonides and its implications for geodynamics. *Nature*, **310**, 641–644.

Sobolev, N. V. & Shatzky, V. S., 1990. Diamond inclusion in garnets from metamorphic rocks: a new environment for diamond formation. *Nature*, **343,** 742–746.

Spear, F. S., 1993. *Metamorphic phase equlibria and pressure-temperature-time paths*, pp. 411–415, 606–607. Mineralogical Society of America Monograph, Washington D. C.

Tabata, H., Maruyama, S. & Shi, Z., 1998. Metamorphic zoning and thermal structure of the Dabie ultrahigh pressure–high pressure terrane, central China. *The Island Arc*, **7,** 142–158.

Wang, X., Liou, J. G. & Mao, H. K., 1989. Coesite-bearing eclogite from Dabie mountains, central China. *Geology,* **17,** 1085–1088.

Waters, D. J. & Martin, H. N., 1993, Geobarometry in phengite-bearing eclogites. *Terra Abstracts*, **5**, 410–401.

Zhang, R. Y., Liou, J. G., Ernst, W. G., Coleman, R. G., Sobolev, N. V. & Shatsky, V. S., 1997. Metamorphic evolution of diamond-bearing and associated rocks from the Kokchetav Massif, northern Kazakhstan. *Journal of Metamorphic Geology*, **15,** 479–496.

Table I–1. Representative mineral compositions in the Barchi-Kol metabasites.

Garnet	zone A	zone B	zone C	zone D	
				Cps-free	Cps-bearing
wt%					
SiO_2	37.55	37.56	38.41	39.32	39.18
TiO_2	0.17	0.03	0.10	0.04	0.24
Al_2O_3	21.13	21.92	21.11	21.86	21.33
Cr_2O_3	0.02	0.00	0.00	0.00	0.00
FeO*	25.93	26.36	27.43	22.62	22.23
MnO	3.77	0.76	0.52	0.44	0.49
MgO	2.43	2.77	4.16	5.37	6.00
CaO	8.97	9.95	8.21	10.83	9.90
Na_2O	0.00	0.03	0.03	0.03	0.12
Total	99.97	99.40	99.96	100.50	99.50
Cations (O=12)					
Si	2.983	2.976	3.018	3.020	3.031
Ti	0.010	0.002	0.006	0.002	0.014
Al	1.979	1.955	1.978	1.945	1.945
Cr	0.001	0.000	0.000	0.000	0.000
Fe^{3+}	0.035	0.000	0.000	0.000	0.000
Fe^{2+}	1.688	1.747	1.803	1.452	1.438
Mn	0.254	0.051	0.035	0.028	0.032
Mg	0.288	0.328	0.487	0.615	0.692
Ca	0.763	0.845	0.691	0.891	0.820
Na	0.000	0.005	0.004	0.004	0.018
Total	8.000	8.001	7.996	7.991	7.991
X_{Alm}	0.564	0.588	0.598	0.486	0.482
X_{Prp}	0.096	0.110	0.162	0.206	0.232
X_{Sps}	0.085	0.017	0.011	0.010	0.011
X_{Grs}	0.255	0.284	0.229	0.298	0.275

Cps: coesite pseudomorph

Table I–1. *Continued.*

Clinopyroxene	zone C	zone D	
		Cps-free	Cps-bearing
wt%			
SiO_2	53.36	56.43	55.63
TiO_2	0.25	0.12	0.09
Al_2O_3	8.24	10.36	8.79
Cr_2O_3	0.02	0.03	0.02
Fe*O	9.61	4.60	4.69
MnO	0.05	0.01	0.02
MgO	7.84	8.39	9.84
CaO	15.14	14.67	15.78
Na_2O	4.72	6.01	5.06
K_2O	0.00	0.00	0.01
Total	99.23	100.61	99.90
Cations (O=6)			
Si	1.973	2.000	1.994
Ti	0.007	0.003	0.002
Al(IV)	0.027	0.000	0.008
Al(VI)	0.332	0.433	0.364
Cr	0.000	0.001	0.001
Fe^{3+}	0.033	0.000	0.004
Fe^{2+}	0.264	0.136	0.137
Mn	0.002	0.000	0.001
Mg	0.432	0.443	0.526
Ca	0.600	0.557	0.606
Na	0.338	0.413	0.352
K	0.000	0.000	0.000
Total	4.009	3.986	3.994
X_{Jd}	0.287	0.428	0.345
X_{Ac}	0.032	0.000	0.004
X_{Aug}	0.681	0.572	0.651

Cps: coesite peudomorph

Table I–1. *Continued.*

Phengite	zone D	
	Cps-free	Cps-bearing
wt%		
SiO_2	52.31	53.40
TiO_2	0.85	0.86
Al_2O_3	26.64	25.03
Cr_2O_3	0.02	0.00
Fe*O	2.11	1.90
MnO	0.01	0.00
MgO	3.72	4.29
CaO	0.04	0.00
Na_2O	0.49	0.19
K_2O	10.40	10.45
Total	96.60	96.13
Cations (O=11)		
Si	3.435	3.514
Ti	0.042	0.042
Al(IV)	0.565	0.486
Al(VI)	1.497	1.455
Cr	0.001	0.000
Fe	0.116	0.104
Mn	0.001	0.000
Mg	0.364	0.421
Ca	0.003	0.000
Na	0.063	0.025
K	0.872	0.877
Total	9.020	8.865

All iron in phengite is calculated as Fe^{2+}. Cps: coesite pseudomorph.

Table I–1. *Continued.*

Amphibole	Type I			Type II	Type III
	zone A	zone B	zone C		
	Hbl	Hbl	Ts	Brs	Prg
wt%					
SiO_2	47.34	47.44	42.92	46.36	37.77
TiO_2	0.40	0.45	1.44	0.59	0.00
Al_2O_3	11.68	11.67	12.11	14.96	20.11
FeO*	13.09	9.11	16.10	10.70	18.71
MnO	0.22	0.10	0.03	0.06	0.31
MgO	12.43	14.69	10.13	11.11	5.56
CaO	9.58	11.02	9.77	8.23	11.93
Na_2O	2.05	1.40	2.48	3.94	1.57
K_2O	0.28	0.20	0.65	0.37	1.37
Total	97.15	96.09	95.62	96.37	97.34
Cations (O=23)					
Si	6.758	6.767	6.423	6.697	5.732
Al(IV)	1.242	1.233	1.577	1.303	2.268
Al(VI)	0.723	0.729	0.559	1.244	1.328
Ti	0.043	0.049	0.162	0.065	0.000
Fe^{3+}	0.906	0.585	0.552	0.000	0.193
Fe^{2+}	0.656	0.502	1.463	1.292	2.182
Mn	0.027	0.012	0.004	0.008	0.039
Mg	2.645	3.124	2.261	2.391	1.258
Ca	1.464	1.683	1.567	1.273	1.940
Na(M4)	0.536	0.317	0.433	0.727	0.060
Na(A)	0.031	0.069	0.288	0.378	0.403
K	0.052	0.037	0.123	0.069	0.266
Total	15.082	15.106	15.411	15.447	15.669

Table I–1. *Continued.*

	Epidote			**Zoisite**	
	zone A	zone B	zone C	zone B	zone D
wt%					
SiO_2	37.93	37.44	38.49	38.69	39.06
TiO_2	0.10	0.04	0.01	0.02	0.25
Al_2O_3	26.15	19.45	22.73	31.74	29.68
Cr_2O_3	0.01	0.03	0.00	0.01	0.02
Fe*O	8.26	18.82	15.16	1.85	4.75
MnO	0.12	0.08	0.12	0.00	0.17
MgO	0.06	0.01	0.07	0.03	0.00
CaO	23.57	22.69	22.82	23.88	23.90
Na_2O	0.00	0.01	0.01	0.00	0.00
Total	96.27	98.63	99.42	96.24	97.84
Cations (O=12)					
Si	3.020	3.020	3.026	2.999	3.012
Ti	0.006	0.003	0.001	0.001	0.015
Al	2.454	1.849	2.107	2.900	2.698
Cr	0.000	0.002	0.000	0.001	0.001
Fe^{3+}	0.495	1.142	0.897	0.108	0.276
Mn	0.008	0.005	0.008	0.000	0.011
Mg	0.007	0.001	0.009	0.003	0.000
Ca	2.010	1.961	1.923	1.984	1.975
Na	0.000	0.002	0.001	0.000	0.000
Total	8.001	7.985	7.972	7.997	7.988
Ps	16.8	38.2	29.9	3.6	9.3

Table I–1. *Continued.*

Plagioclase	zone A	zone B	zone C
wt%			
SiO_2	62.08	59.17	64.43
TiO_2	0.00	0.04	0.00
Al_2O_3	24.22	25.79	21.76
Fe_2O_3	0.61	0.03	0.17
MnO	0.05	0.00	0.00
MgO	0.01	0.02	0.00
CaO	5.47	7.96	3.01
Na_2O	8.16	6.90	9.43
K_2O	0.07	0.07	0.57
Total	100.67	99.99	99.37
Cations (O=8)			
Si	2.736	2.640	2.860
Ti	0.000	0.001	0.000
Al	1.258	1.356	1.138
Fe^{3+}	0.020	0.001	0.006
Mn	0.002	0.000	0.000
Mg	0.001	0.002	0.000
Ca	0.258	0.381	0.143
Na	0.697	0.597	0.812
K	0.004	0.004	0.032
Total	4.976	4.981	4.991
An	27.0	38.9	15.0

All iron is calculated as Fe_2O_3.

Table I–2. Representative mineral analyses in the Borovoye metabasites.

Garnet

zone/lithology	D am	D ec	E ec
sample	T707	J696	J336
SiO_2	38.62	39.29	38.76
TiO_2	0.02	0.08	0.15
Al_2O_3	21.48	22.27	21.73
Cr_2O_3	0.00	0.00	0.05
FeO*	25.62	19.21	21.26
MnO	0.64	0.35	0.47
MgO	4.67	8.07	6.43
CaO	8.72	10.80	10.67
Na_2O	0.00	0.02	0.01
K_2O	0.01	0.03	0.00
P_2O_5	0.01	0.01	0.04
Total	99.79	100.11	99.56
(O = 12)			
Si	3.019	2.976	2.989
Ti	0.001	0.004	0.009
Al	1.978	1.988	1.975
Cr	0.000	0.000	0.003
Fe^{3+}	0.000	0.051	0.027
Fe^{2+}	1.675	1.166	1.345
Mn	0.042	0.022	0.030
Mg	0.544	0.911	0.740
Ca	0.730	0.876	0.881
Na	0.000	0.003	0.002
K	0.001	0.002	0.000
P	0.001	0.001	0.003
Total	7.991	8.001	8.003
X_{Alm}	0.560	0.392	0.449
X_{Prp}	0.182	0.306	0.247
X_{Sps}	0.014	0.008	0.010
X_{Grs}	0.244	0.295	0.294

am: amphibolite; ec: eclogite.

Table I–2. *Continued.*

Plagioclase	matrix				symp	Grt kely
zone	A	B	C	D	D	D
sample	K989	Y998	K834	T714	T585	J413
SiO_2	68.01	67.01	64.56	59.02	58.54	57.05
TiO_2	0.03	0.00	0.00	0.06	0.04	0.00
Al_2O_3	20.34	20.58	22.37	25.18	26.04	27.69
Cr_2O_3	0.00	0.00	0.00	0.00	0.00	0.00
Fe_2O_3	0.07	0.00	0.16	0.32	0.46	0.68
MnO	0.02	0.05	0.00	0.00	0.00	0.02
MgO	0.03	0.01	0.00	0.00	0.02	0.00
CaO	0.44	1.27	3.26	7.20	8.55	9.82
Na_2O	10.99	10.98	9.75	7.59	6.37	5.70
K_2O	0.30	0.12	0.11	0.15	0.07	0.06
P_2O_5	0.00	0.00	0.00	0.00	0.00	0.00
Total	100.24	100.04	100.22	99.51	100.08	101.00
(O = 8)						
Si	2.965	2.937	2.840	2.650	2.614	2.537
Ti	0.001	0.000	0.000	0.002	0.001	0.000
Al	1.045	1.063	1.160	1.333	1.370	1.451
Cr	0.000	0.000	0.000	0.000	0.000	0.000
Fe^{3+}	0.003	0.000	0.005	0.011	0.017	0.023
Mn	0.001	0.002	0.000	0.000	0.000	0.001
Mg	0.002	0.001	0.000	0.000	0.002	0.000
Ca	0.021	0.059	0.154	0.346	0.409	0.468
Na	0.929	0.933	0.832	0.660	0.551	0.491
K	0.017	0.007	0.006	0.009	0.004	0.003
P	0.000	0.000	0.000	0.000	0.000	0.000
Total	4.983	5.002	4.996	5.011	4.969	4.974
An	2.1	6.0	15.5	34.1	42.4	48.6

symp: symplectite; Grt kely: kelyphite of garnet.

Table I–2. *Continued.*

Epidote	matrix		vein
zone	A	B	E
sample	K989	Y1000	T507
SiO_2	37.67	38.80	38.26
TiO_2	0.00	0.00	0.21
Al_2O_3	21.67	27.94	23.41
Cr_2O_3	0.05	0.04	0.02
Fe_2O_3	15.81	7.59	13.03
MnO	0.33	0.14	0.05
MgO	0.01	0.03	0.07
CaO	23.22	24.04	23.47
Na_2O	0.00	0.00	0.01
K_2O	0.01	0.02	0.01
P_2O_5	0.03	0.08	0.18
Total	98.79	98.69	98.72
(O = 12)			
Si	3.005	3.003	3.022
Ti	0.000	0.000	0.013
Al	2.038	2.549	2.180
Cr	0.003	0.003	0.001
Fe^{3+}	0.949	0.442	0.774
Mn	0.022	0.009	0.004
Mg	0.001	0.004	0.008
Ca	1.985	1.994	1.987
Na	0.000	0.000	0.001
K	0.001	0.002	0.001
P	0.002	0.005	0.013
Total	8.004	8.005	7.990
Ps	31.8	14.8	26.2

Table I–2. *Continued.*

Clinopyroxene	matrix			symplectite
zone/lithology	D am	D ec	E	E
sample	T711	J696	T507	T527
SiO_2	48.23	50.32	55.99	54.28
TiO_2	0.45	0.67	0.10	0.08
Al_2O_3	7.53	9.57	8.60	2.29
Cr_2O_3	0.00	0.12	0.03	0.01
FeO*	12.70	7.48	4.14	9.31
MnO	0.32	0.06	0.00	0.07
MgO	9.41	10.90	10.17	11.94
CaO	19.83	19.33	16.09	20.75
Na_2O	1.10	1.84	4.75	1.16
K_2O	0.06	0.03	0.01	0.06
P_2O_5	0.07	0.04	0.05	0.01
Total	99.69	100.36	99.92	99.95
(O = 6)				
Si	1.833	1.843	2.000	2.013
Ti	0.013	0.018	0.003	0.002
Al (IV)	0.167	0.157	0.000	0.000
Al (VI)	0.171	0.256	0.362	0.100
Cr	0.000	0.003	0.001	0.000
Fe^{3+}	0.077	0.032	0.000	0.000
Fe^{2+}	0.326	0.197	0.124	0.289
Mn	0.010	0.002	0.000	0.002
Mg	0.533	0.595	0.542	0.660
Ca	0.808	0.758	0.616	0.824
Na	0.081	0.131	0.329	0.083
K	0.003	0.001	0.001	0.003
P	0.002	0.001	0.002	0.000
Total	4.024	3.995	3.978	3.977
X_{Cats}	0.151	0.146	0.000	0.000
X_{Jd}	0.003	0.091	0.352	0.096
X_{Di}	0.481	0.551	0.527	0.629
X_{Hd}	0.295	0.182	0.121	0.275
X_{Ac}	0.070	0.030	0.000	0.000

Table I–2. *Continued.*

Amphibole	matrix				porphyroblast	symplectite
zone/lithology	B	C	D am	D ec	E	E
sample	Y983	K813	T707	J696	T507	J336
SiO_2	47.64	43.03	40.08	42.13	48.79	47.41
TiO_2	0.24	1.32	2.08	2.00	0.40	0.09
Al_2O_3	8.47	10.55	13.82	13.32	12.12	10.69
Cr_2O_3	0.00	0.04	0.00	0.07	0.06	0.03
FeO*	19.60	19.95	18.08	13.11	10.08	13.91
MnO	0.31	0.21	0.04	0.02	0.06	0.05
MgO	9.33	9.03	8.72	12.21	14.07	11.77
CaO	11.73	11.37	10.76	11.41	9.29	12.35
Na_2O	0.73	1.52	1.97	2.20	2.59	1.04
K_2O	0.62	1.08	1.74	1.24	0.76	0.40
Total	98.65	98.11	97.34	97.71	98.24	97.79
(O = 23)						
Si	7.008	6.447	6.052	6.187	6.832	6.902
Ti	0.027	0.148	0.236	0.221	0.042	0.010
Al (IV)	0.992	1.553	1.948	1.813	1.168	1.098
Al (VI)	0.476	0.309	0.511	0.492	0.833	0.736
Cr						
Fe^{3+}	0.442	0.649	0.571	0.429	0.624	0.121
Fe^{2+}	1.970	1.850	1.712	1.181	0.556	1.572
Mn	0.039	0.027	0.006	0.002	0.007	0.007
Mg	2.047	2.016	1.964	2.674	2.938	2.555
Ca	1.849	1.825	1.741	1.796	1.394	1.927
Na (M4)	0.151	0.175	0.259	0.204	0.606	0.073
Na (A)	0.055	0.267	0.318	0.421	0.097	0.220
K	0.116	0.205	0.334	0.233	0.136	0.075
Total	15.171	15.473	15.652	15.654	15.233	15.295

Table I–2. *Continued.*

Chlorite	matrix			Grt alt	porphyroblast
zone	A	B	C	D	E
sample	K989	Y983	Y834	J419	T533
SiO_2	28.50	27.47	26.55	26.07	27.71
TiO_2	0.11	0.10	0.04	0.05	0.03
Al_2O_3	18.31	20.46	21.05	19.41	18.17
FeO	21.39	27.01	23.92	29.66	27.97
MnO	2.04	0.34	0.34	0.34	0.37
MgO	18.22	12.79	15.98	11.39	14.62
CaO	0.20	0.06	0.05	0.06	0.00
Na_2O	0.00	0.01	0.03	0.05	0.04
K_2O	0.04	0.05	0.07	0.04	0.01
Total	89.00	88.33	88.12	87.17	88.94
(O = 28)					
Si	6.057	6.337	5.760	5.904	6.046
Ti	0.017	0.029	0.007	0.009	0.004
Al(IV)	1.926	1.634	2.234	2.087	1.950
Al(VI)	2.661	3.367	3.147	3.094	2.721
Al	4.587	5.001	5.381	5.181	4.671
Fe	3.803	4.625	4.340	5.616	5.102
Mn	0.367	0.024	0.063	0.065	0.069
Mg	5.772	4.169	5.169	3.846	4.756
Ca	0.045	0.031	0.011	0.015	0.001
Na	0.000	0.016	0.011	0.022	0.016
K	0.011	0.037	0.020	0.012	0.002
Total	20.659	20.269	20.762	20.670	20.668

Grt alt: altered from garnet.

Table I–2. *Continued.*

Phengite		**Ilmenite**			
zone	E	zone	B	C	D
sample	J336	sample	Y1000	K813	J419
SiO_2	54.09	SiO_2	0.03	0.03	0.04
TiO_2	0.74	TiO_2	53.94	52.68	54.19
Al_2O_3	26.58	Al_2O_3	0.01	0.00	0.01
Cr_2O_3	0.06	Cr_2O_3	0.06	0.00	0.00
FeO*	1.30	FeO*	42.31	43.26	44.12
MnO	0.00	MnO	3.11	3.47	1.95
MgO	4.46	MgO	0.18	0.17	0.09
CaO	0.02	CaO	0.00	0.00	0.04
Na_2O	0.49	Na_2O	0.00	0.00	0.00
K_2O	10.40	K_2O	0.04	0.05	0.03
Total	98.14	P_2O_5	0.04	0.00	0.00
		Total	99.73	99.67	100.46
(O = 11)		(O = 3)			
Si	3.475	Si	0.001	0.001	0.001
Ti	0.036	Ti	1.017	1.002	1.016
Al (IV)	0.525	Al	0.000	0.000	0.000
Al (VI)	1.487	Cr	0.001	0.000	0.000
Cr	0.003	Fe^{3+}	0.000	0.000	0.000
Fe*	0.070	Fe^{2+}	0.887	0.914	0.920
Mn	0.000	Mn	0.066	0.074	0.041
Mg	0.427	Mg	0.007	0.007	0.003
Ca	0.002	Ca	0.000	0.000	0.001
Na	0.061	Na	0.000	0.000	0.000
K	0.852	K	0.001	0.002	0.001
Total	8.951	P	0.001	0.000	0.000
		Total	1.981	1.999	1.984
		$X_{Fe\text{-}Ilm}$	0.924	0.919	0.954
		X_{Pph}	0.069	0.075	0.043
		X_{Gei}	0.007	0.007	0.004

Table I–3. Average and standard diviation (1s) of the *P–T* calculation of the Barchi-Kol eclogites using several geothermobarometers. Pressures marked by * are estimated by phengite barometer of Waters & Martin (1993), whereas others are arbitrary fixed at 35 and 30 kbar for coesite pseudomorph-bearing/free samples, respectively.

	EG		KR		PW		BM		
sample	Ave.	SD	Ave.	SD	Ave.	SD	Ave.	SD	P (kbar)
F446	800	6	770	7	779	6	686	26	40*
F431	815	13	788	14	795	13	647	13	35*
H299	761	16	725	19	739	17	621	18	33*
F467	748	20	703	28	725	21	606	11	28*
F477	753	32	720	35	732	33	654	19	28*
H317	812	12	781	17	791	13	646	6	30*
F413	858	51	825	58	837	52	863	12	35
F430	797	19	767	21	777	19	635	6	35
H303	756	27	720	33	735	28	573	29	30
F457	742	12	705	14	720	13	582	3	30
F483	857	18	825	20	837	19	860	16	30
F484	846	26	814	29	826	27	869	20	30
F488	779	31	740	35	757	32	855	8	30
F494	821	13	778	21	799	14	838	15	30
F495	850	14	815	15	830	14	879	10	30
F442	769	28	736	31	749	29	620	20	30
K369	745	35	708	40	723	36	626	35	30

EG: Ellis & Green (1979); KR: Krogh Ravna (2000a); PW: Powell (1985); BM: Berman *et al.*(1995). Ave.: average; SD: standard diviation (1s).

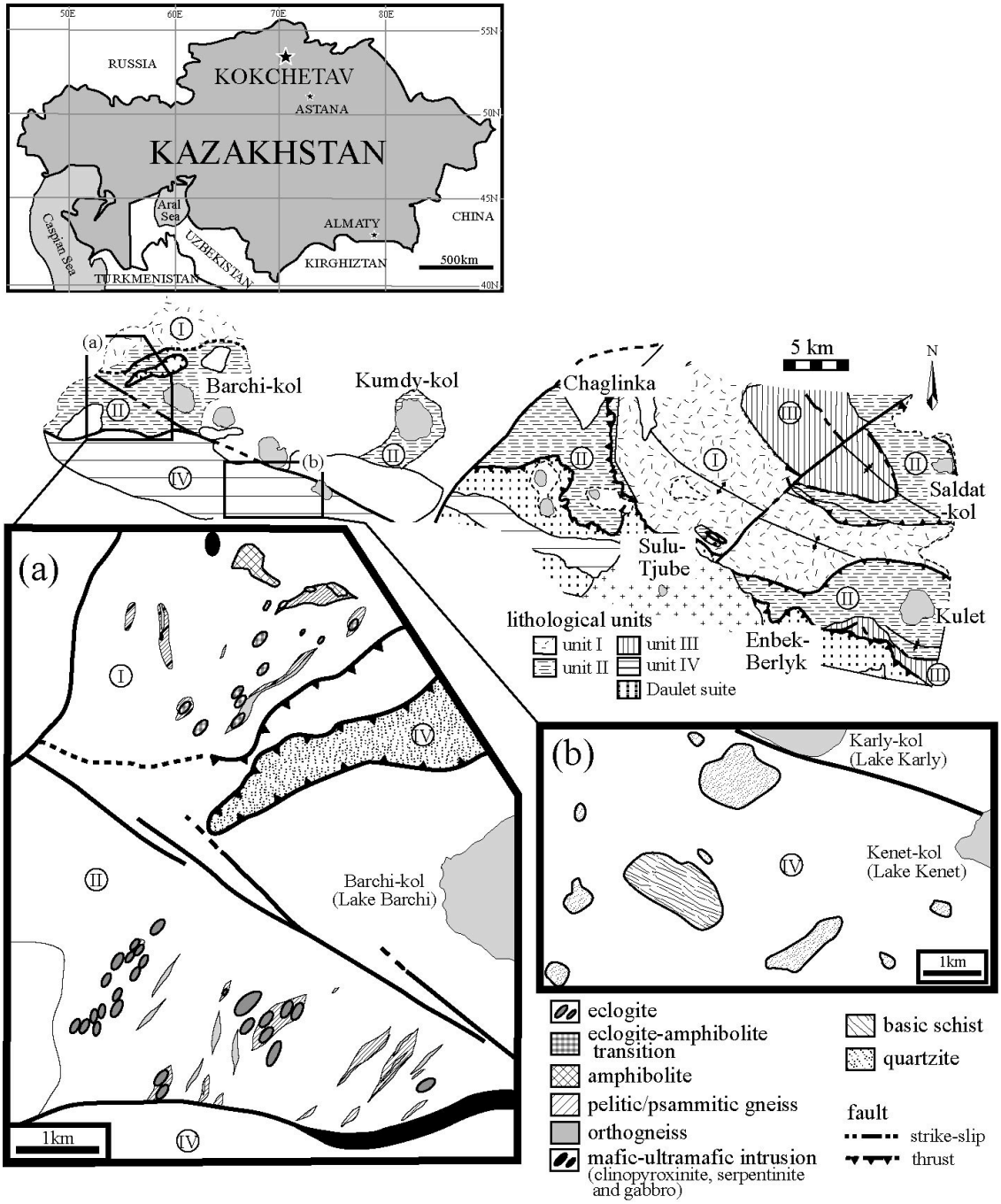

Fig. I–1 Simplified geological map of the Kokchetav metamorphic belt (after Kaneko *et al.* 2000) and close up of the Barchi-Kol region. Numbers I–IV in the map are litholoical units defined by Kaneko *et al.* (2000).

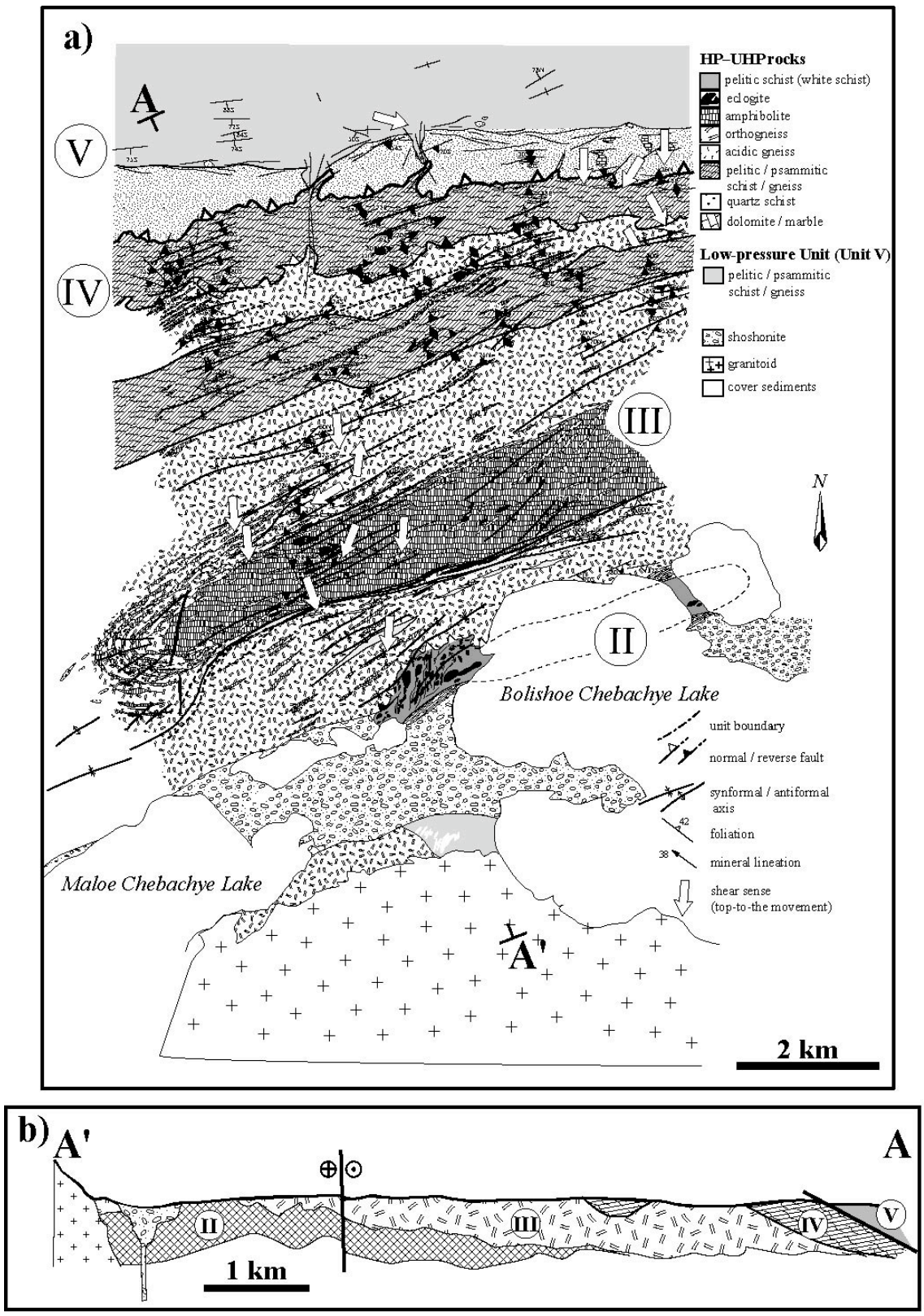

Fig. I–2 Geological map and cross-section of the Borovoye region (modified after Kaneko *et al.*, 2000). a) Geological map; b) Geological cross-section along A–A' shown in (a).

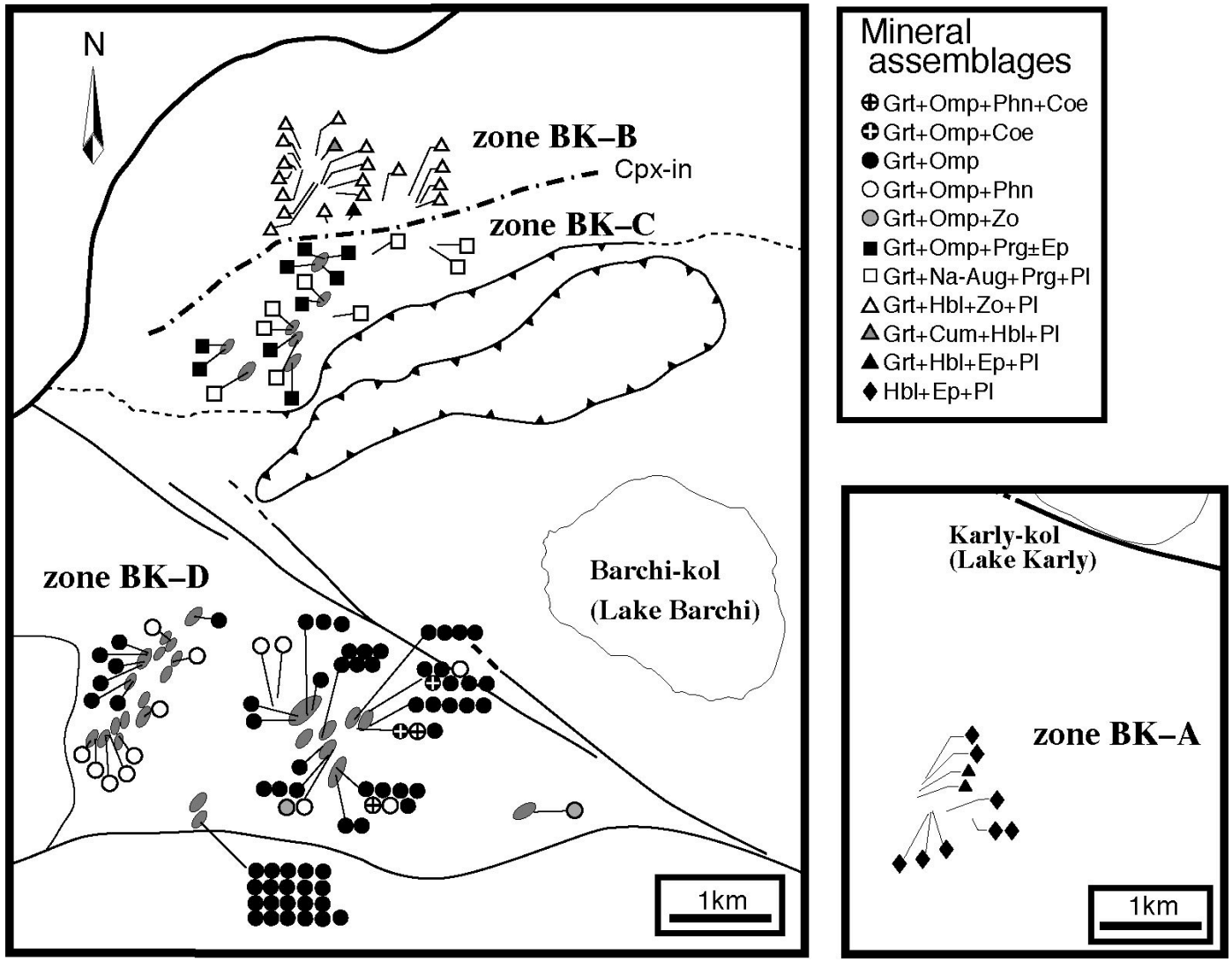

Fig. I–3 Regional distribution of metamorphic mineral assemblages in the Barchi-Kol metabasites.

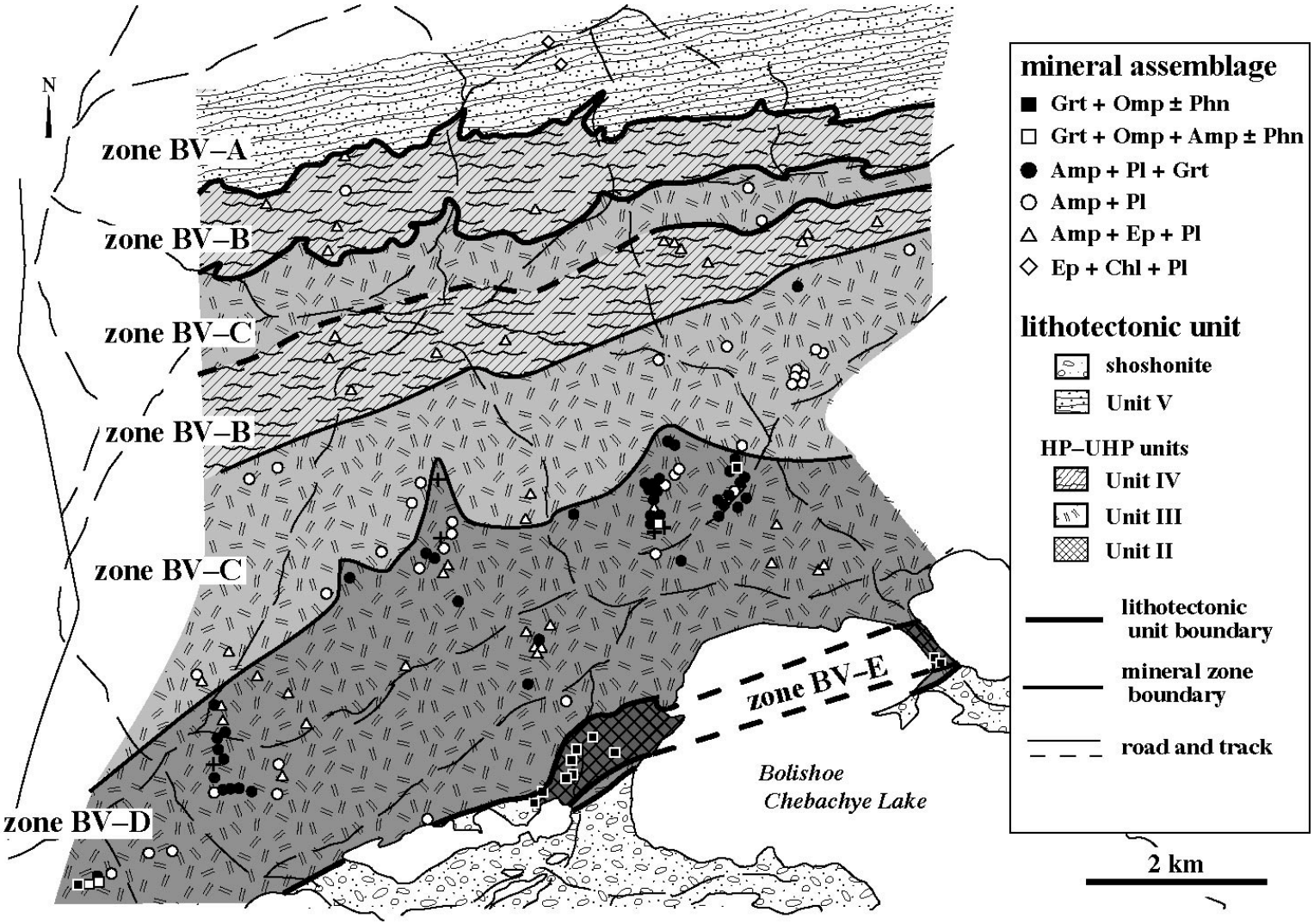

Fig. I–4 Regional distribution of the metamorphic mineral assemblages in the Borovoye metabasites.

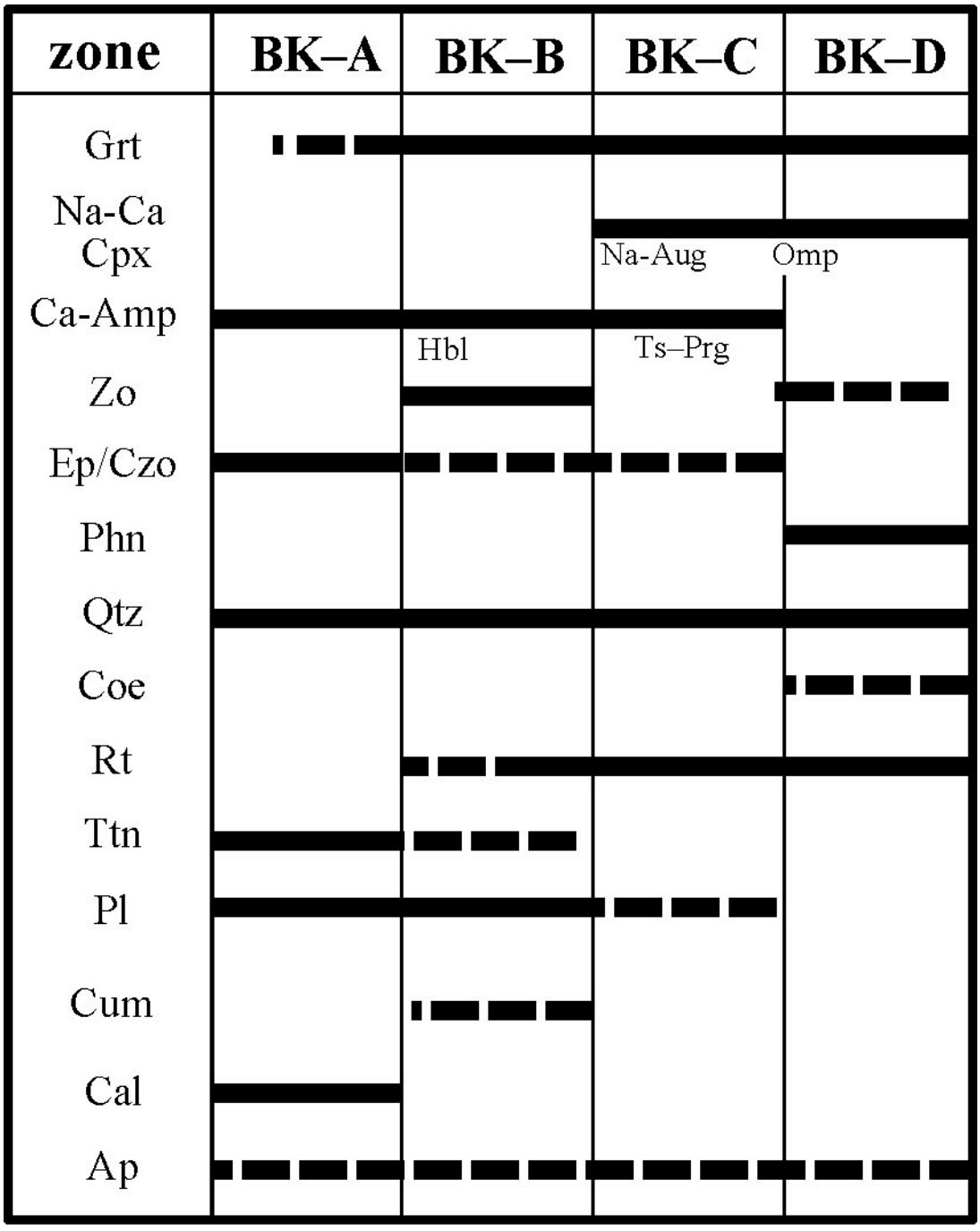

Fig. I–5 Generalised mineral parageneses of metabasites in the Barchi-Kol area.

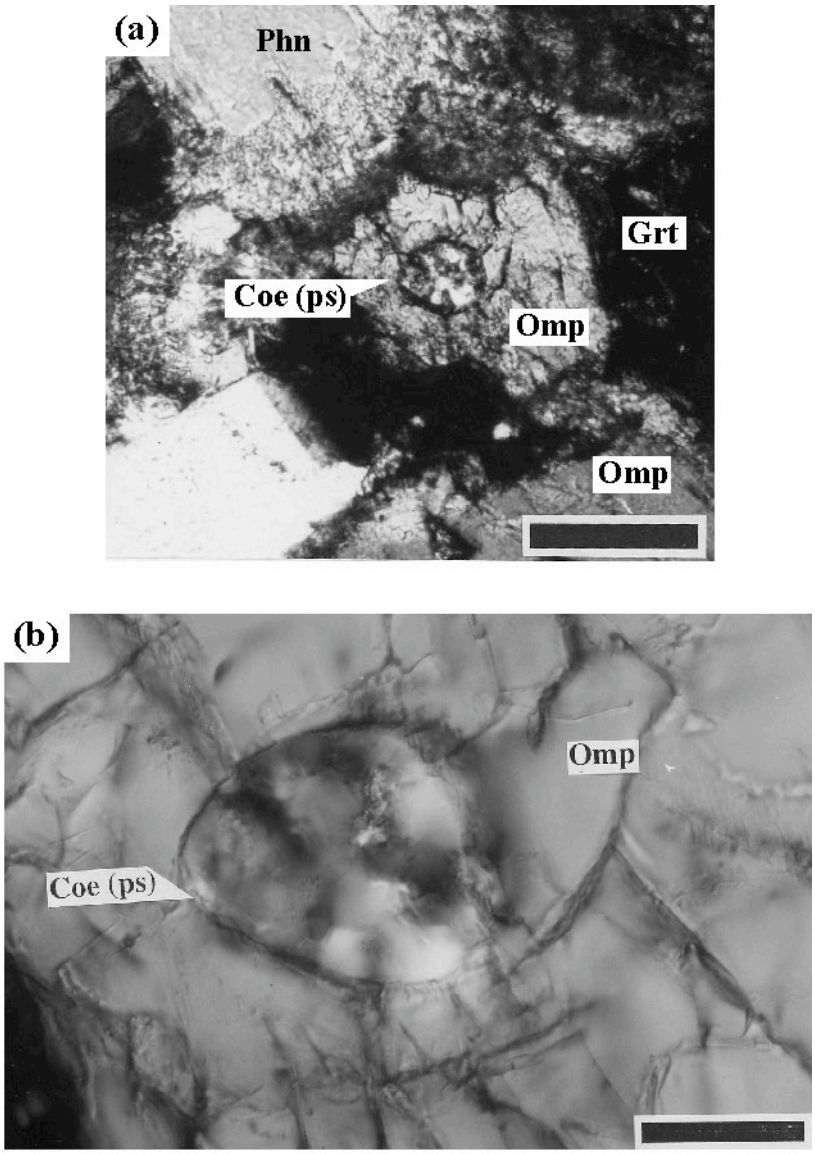

Fig. I–6 Photomicrographs showing polycrystalline quartz pseudomorph after coesite included in omphacite from phengite-bearing eclogite in the Barchi-Kol region. Scale bar indicates (a) 0.1 mm; (b) 0.02 mm. Crossed polarised light.

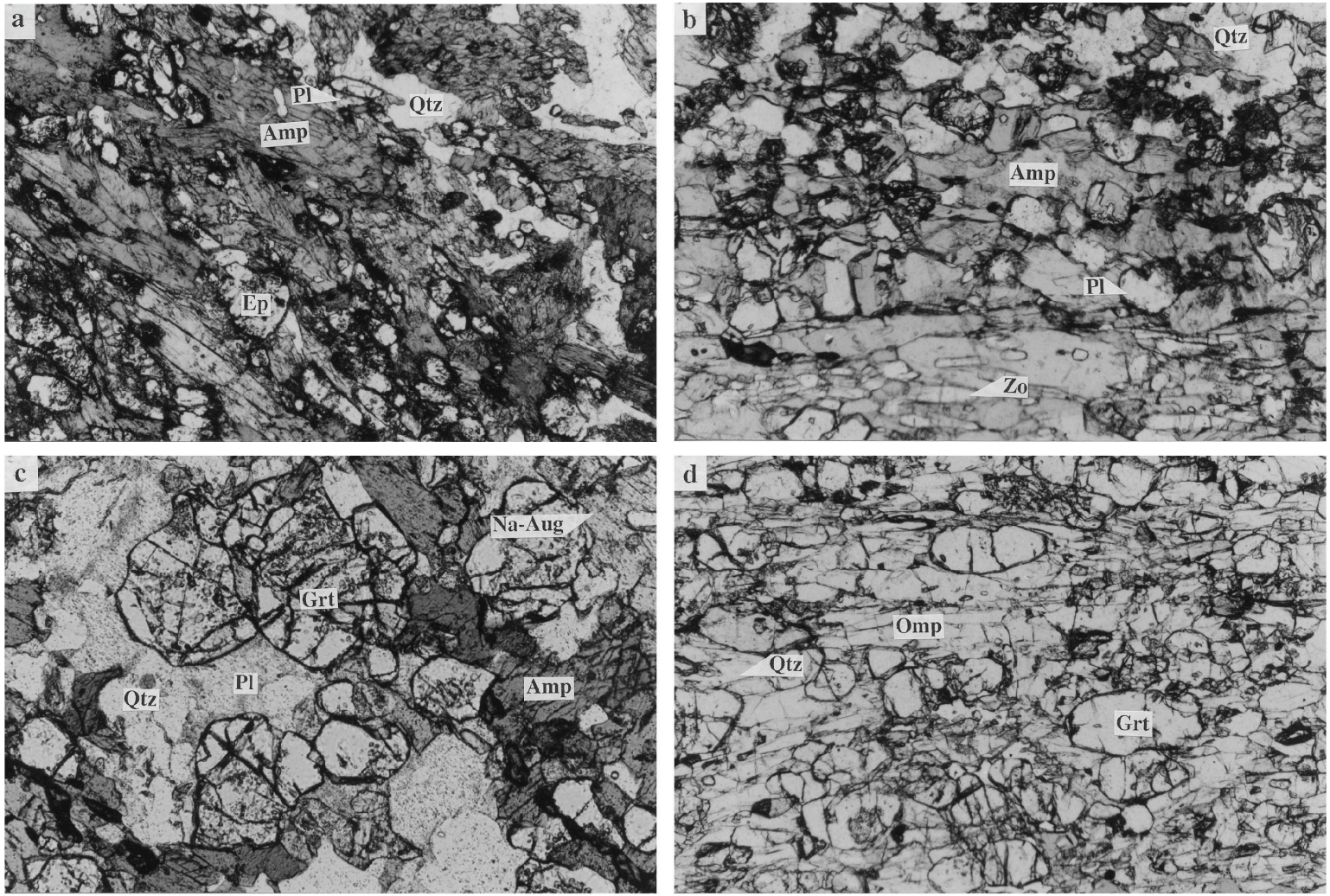

Fig. I–7 Photomicrographs showing typical texture of the Barchi-Kol metabasite of each zone. (a) zone BK–A; (b) zone BK–B; (c) zone BK–C; (d) zone BK–D. The width of the field of view is about 2 mm for (a) and (b), and 4 mm for (c) and (d). Plane-polarised light.

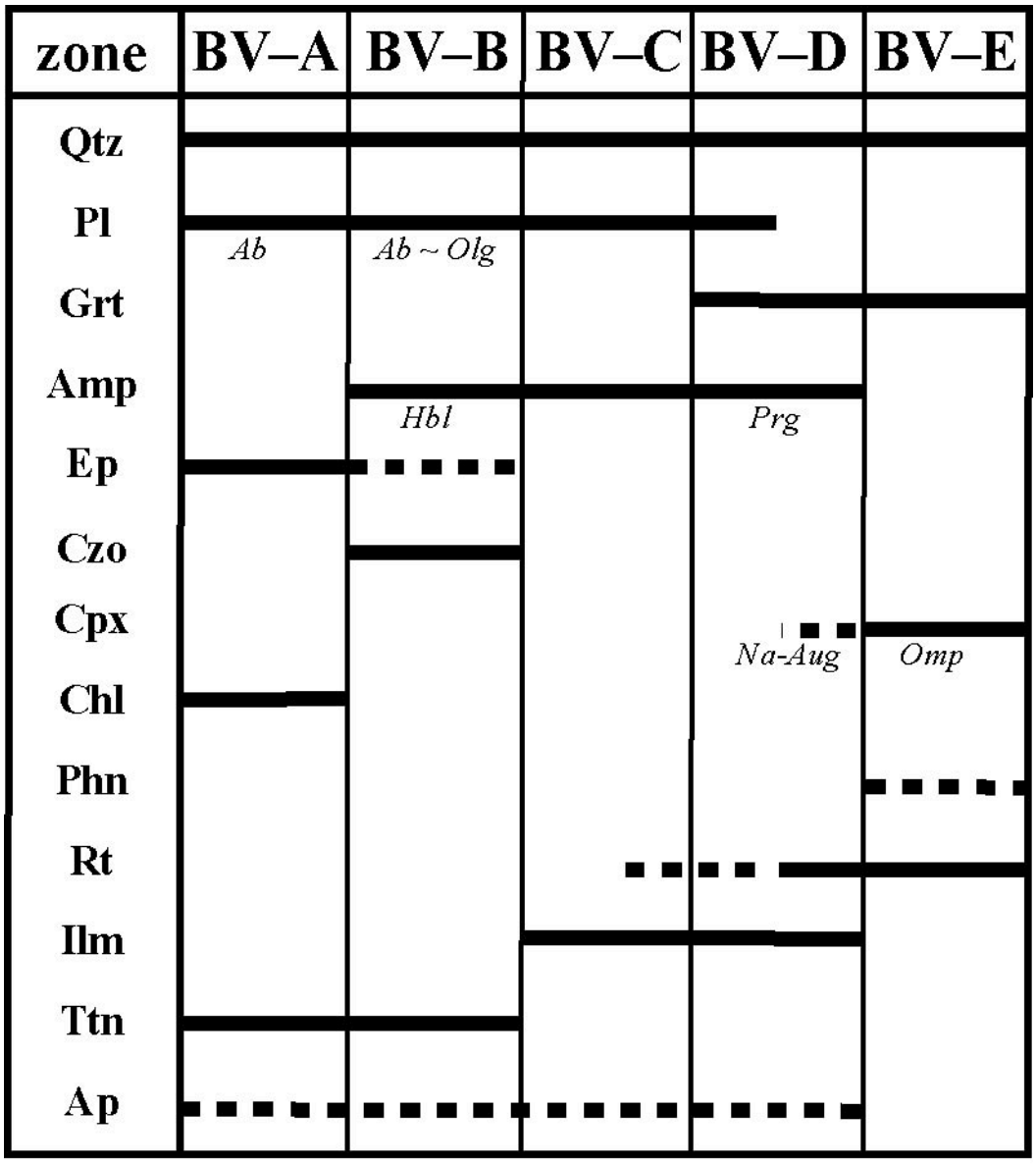

Fig. I–8 Generalised mineral parageneses in the Borovoye metabasites.

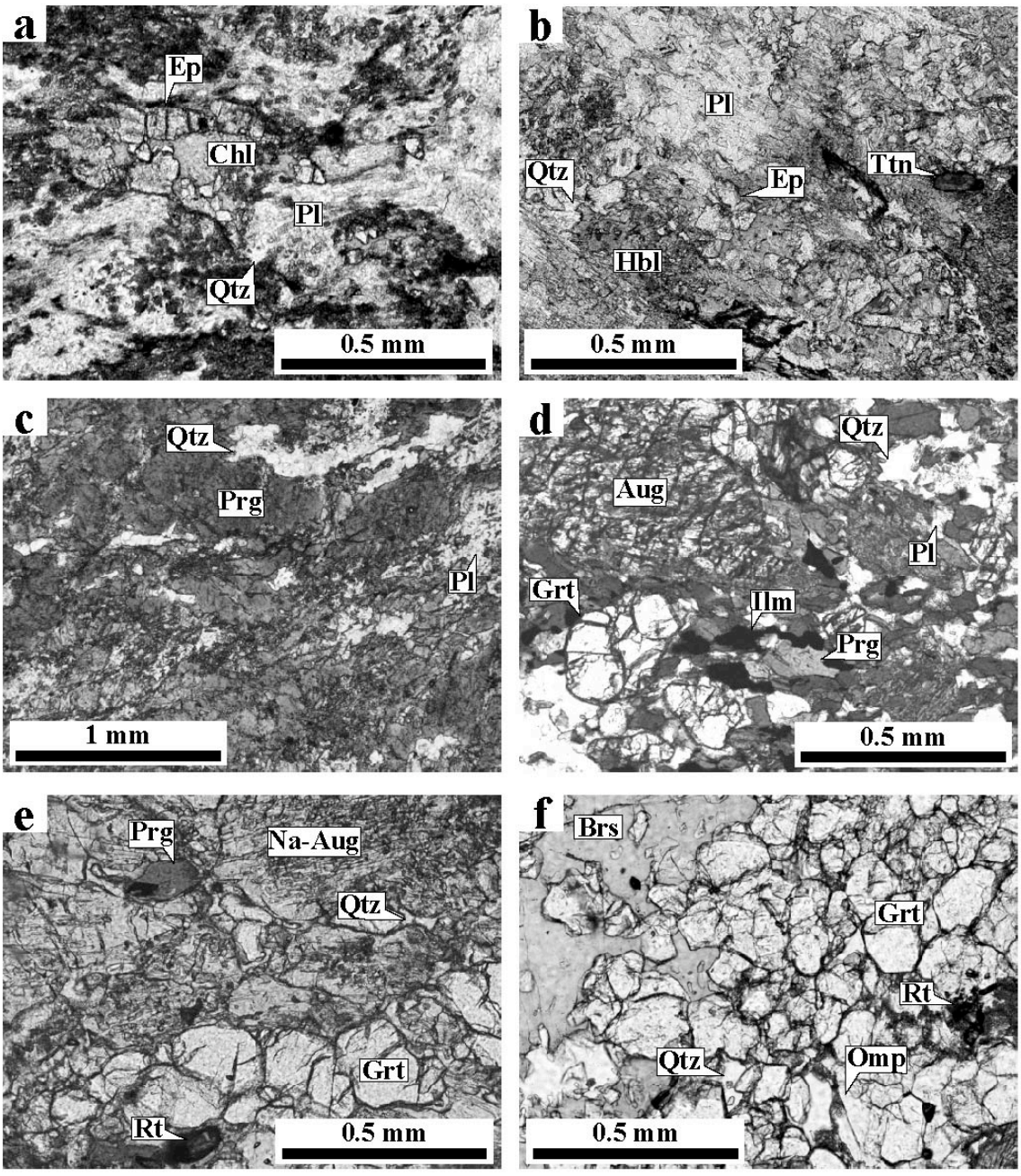

Fig. I–9 Photomicrographs showing typical minerals and textures in metabasite of each mineral zone in the Borovoye region. a) zone BV–A; b) zone BV–B; c) zone BV–C; d) zone BV–D amphibolite; e) zone BV–D eclogite; f) zone BV–E.

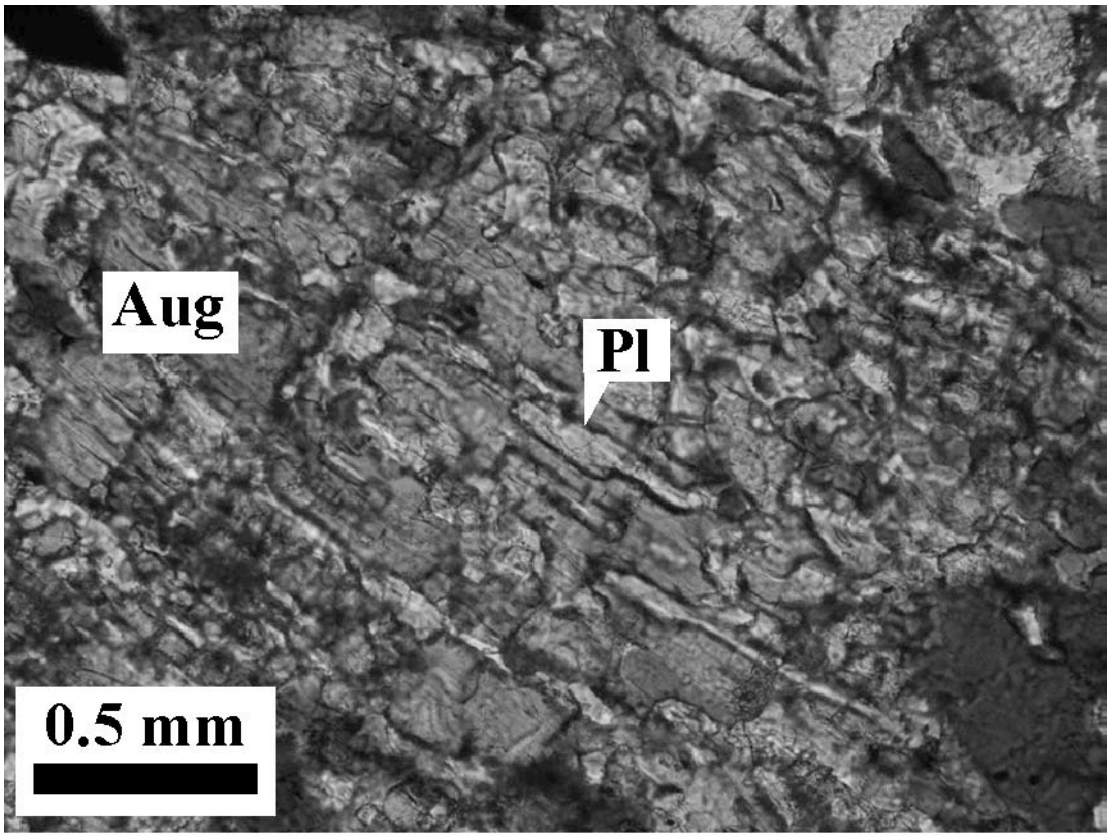

Fig. I–10 Plagioclase exsolution lamelae in augite in zone BV–D amphibolite in the Borovoye region. Exsoluted plagioclase has topotaxial relationship with host augite. Plain polarised light .

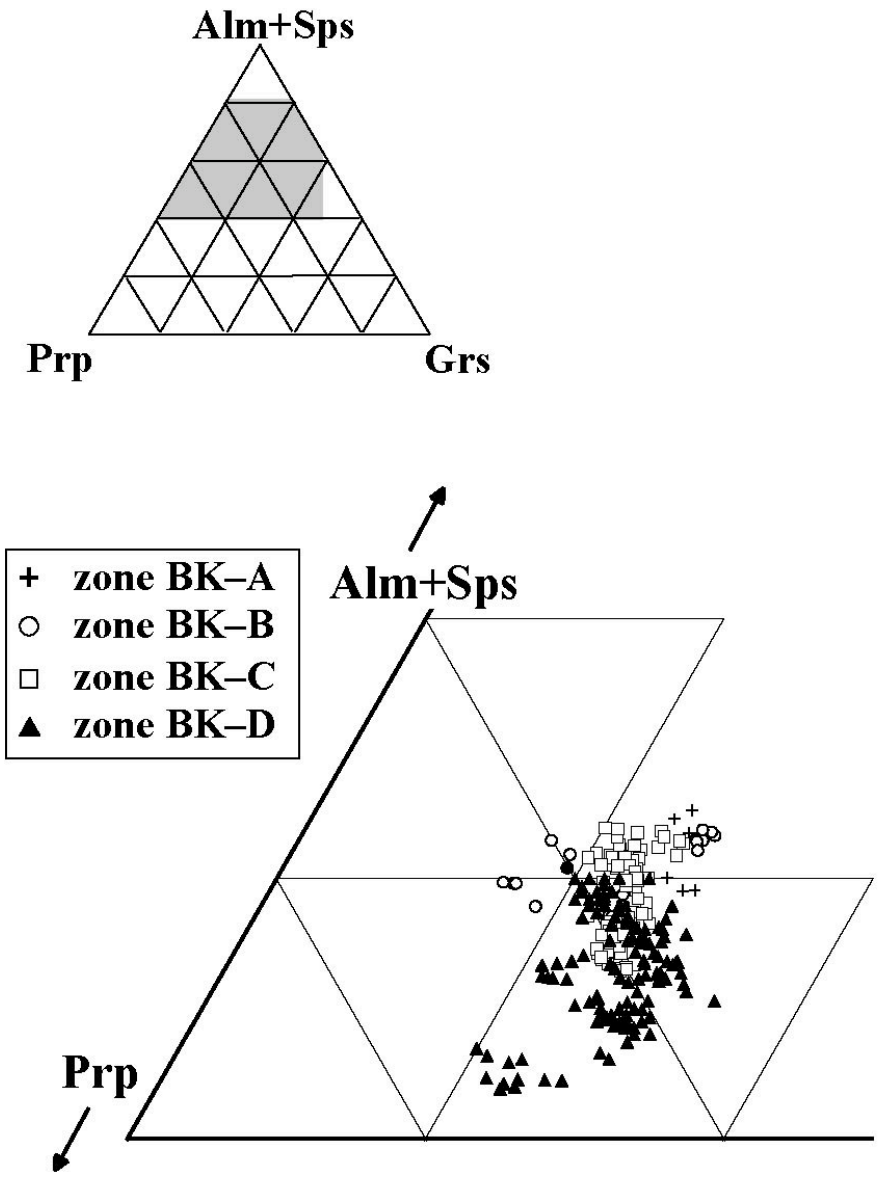

Fig. I–11 Compositions of analysed garnets from each zone of the Barchi-Kol region.

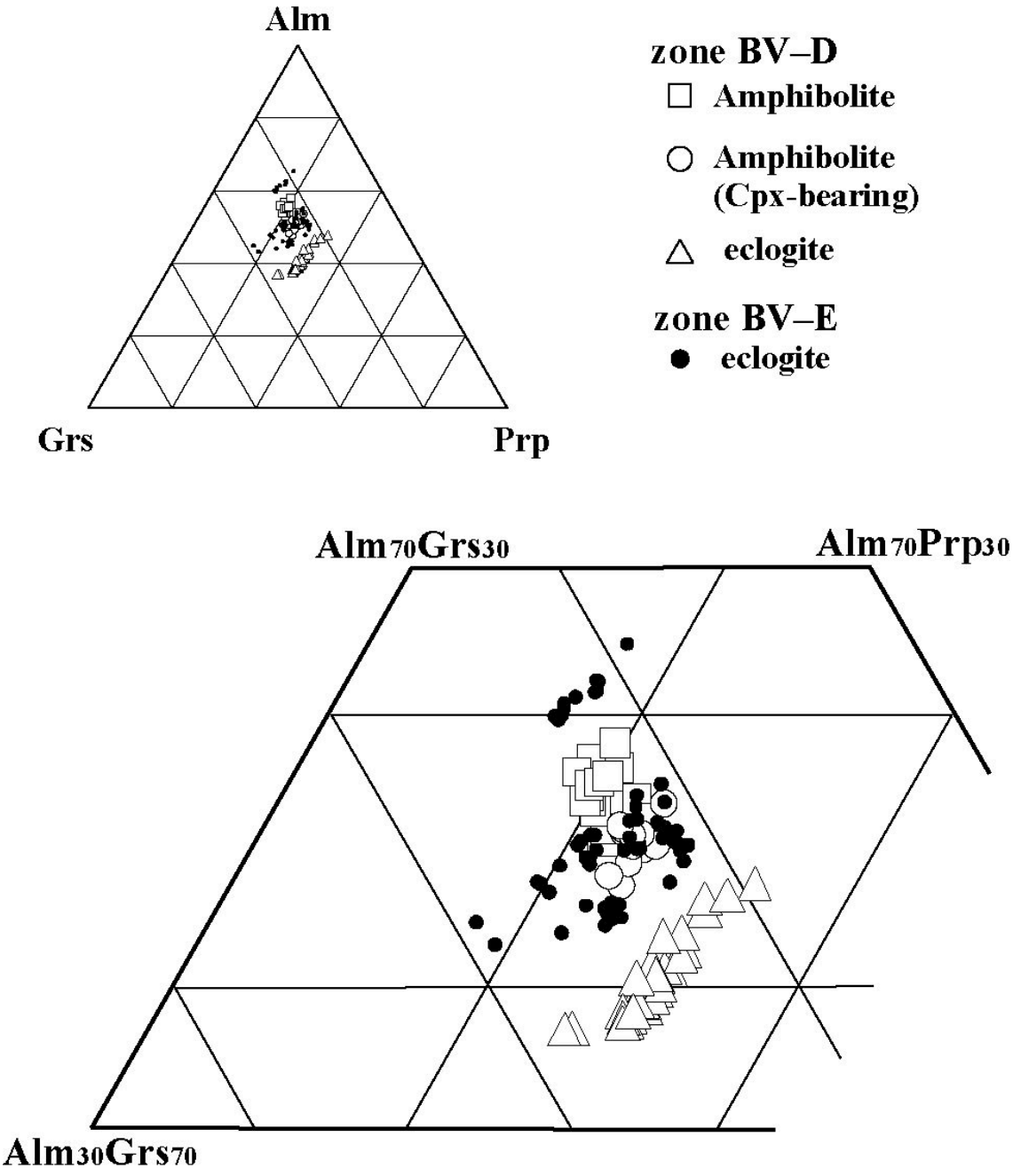

Fig. I–12 Compositional variation of garnets of various grades and lithologies in the Borovoye region.

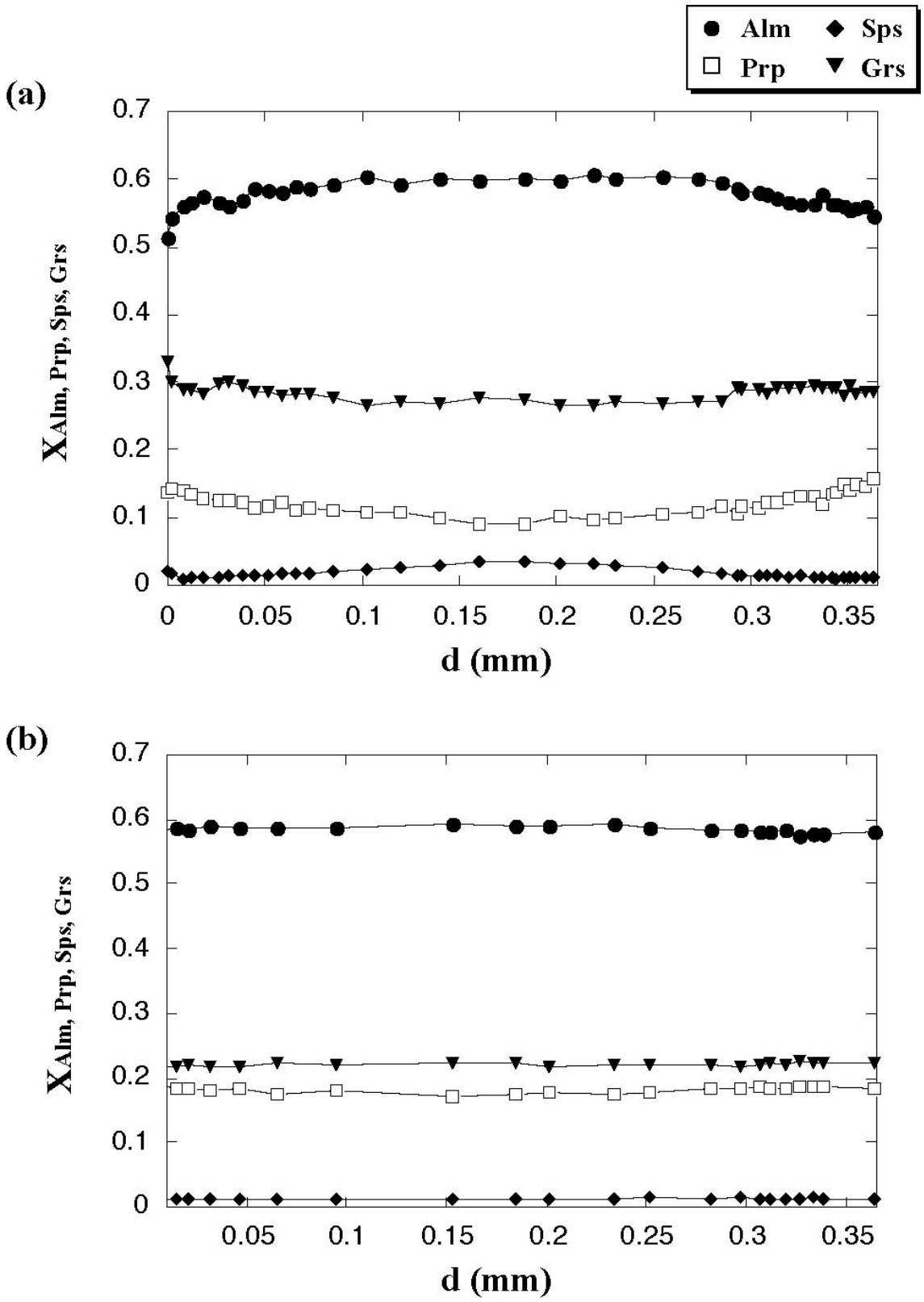

Fig. I–13 Compositional line profiles of garnet of type I & III zoning observed in the Barchi-Kol metabasites. a) Type I zoned garnet. Zone BK–B, Unit I.b) Type III zoned garnet. Zone BK–D, Unit II.

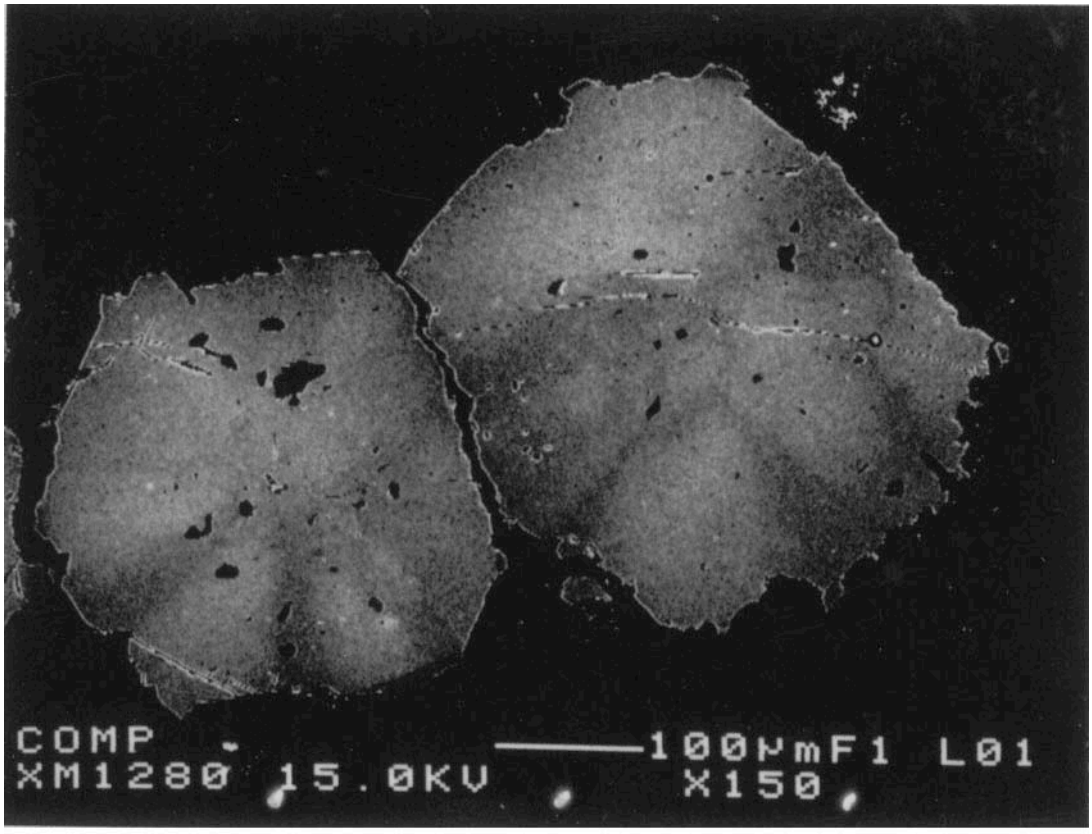

Fig. I–14 Back-scattered electron imagery of type II (sector-zoned) garnets observed in zone BK–B in the Barchi-Kol region.

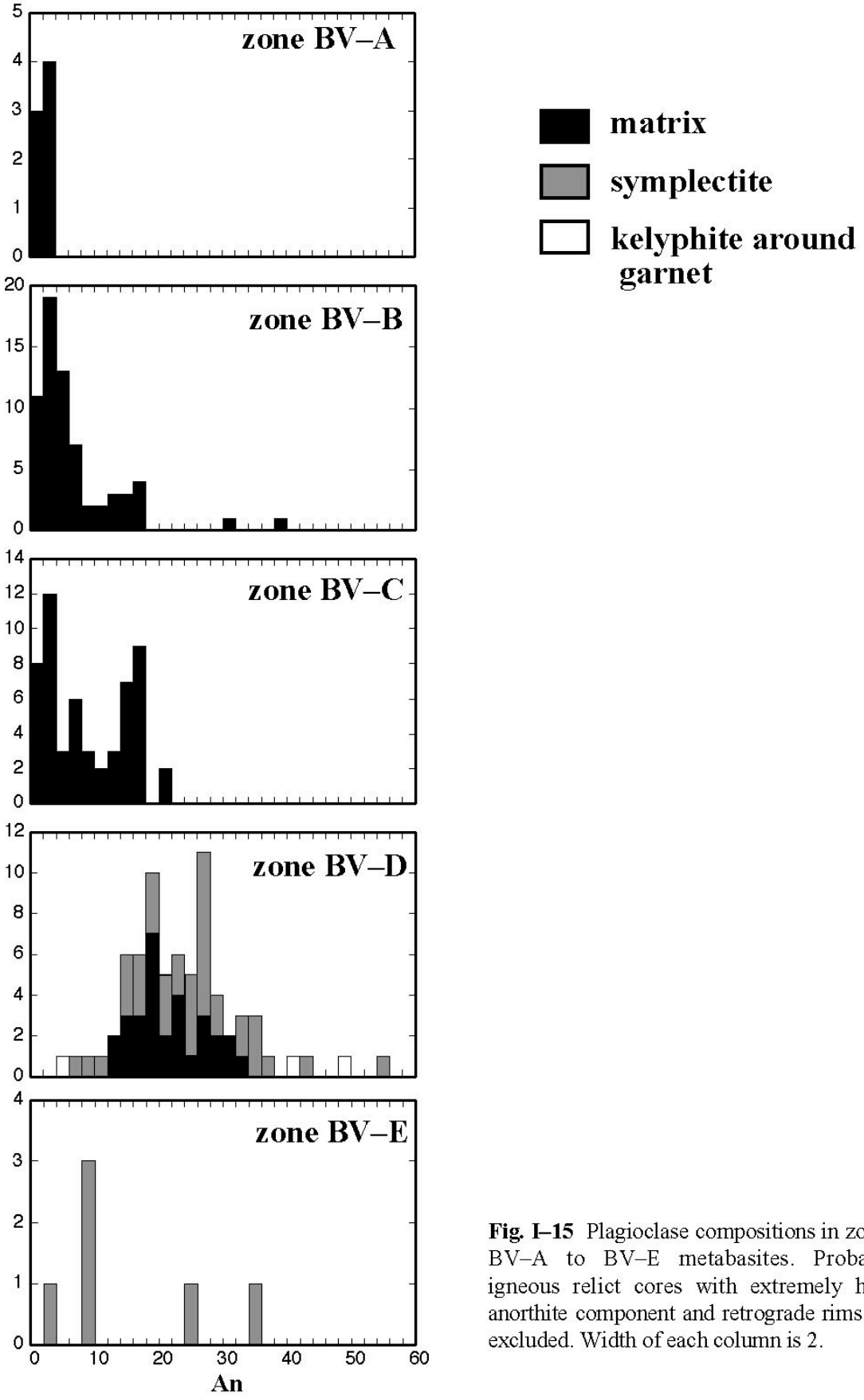

Fig. I–15 Plagioclase compositions in zones BV–A to BV–E metabasites. Probable igneous relict cores with extremely high anorthite component and retrograde rims are excluded. Width of each column is 2.

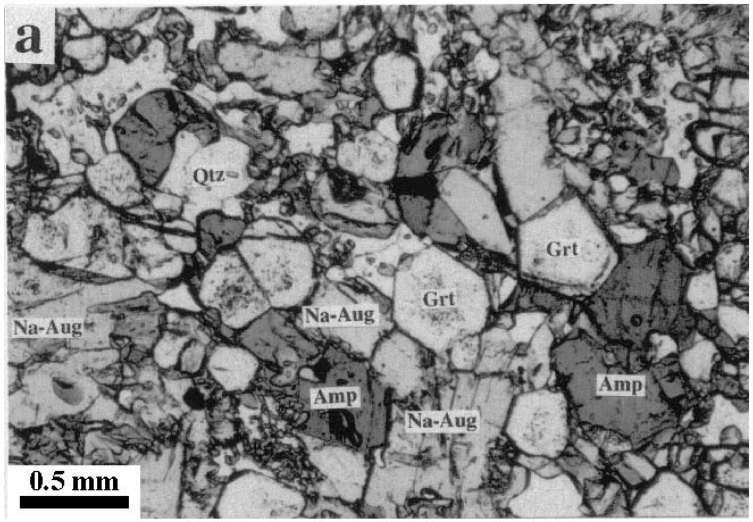

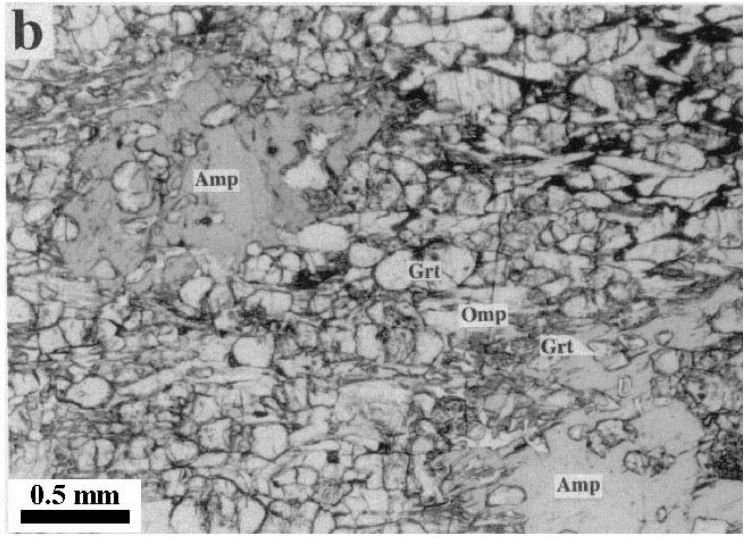

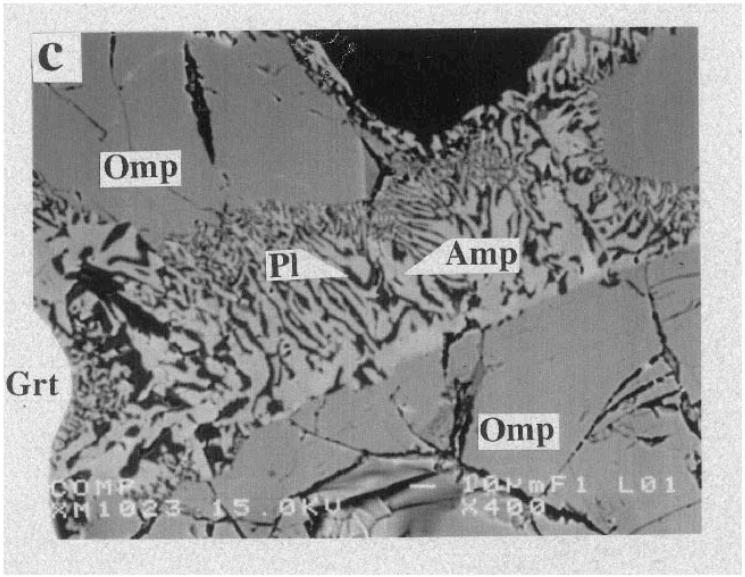

Fig. I–16 Photomicrographs (a & b) and back-scattered electron imagery (c) showing amphiboles of three different textures. a) Amphibole occurs as a matrix phase with mutual contacts with garnet and clinopyroxene. Amphibolite from zone BK–C; b) Large porphyroblastic amphibole overgrown over the eclogitic minerals and textures. Eclogite from zone BK–D; c) Symplectic amphibole grown along the grain boundary between garnet and omphacite. Eclogite from zone BK–D.

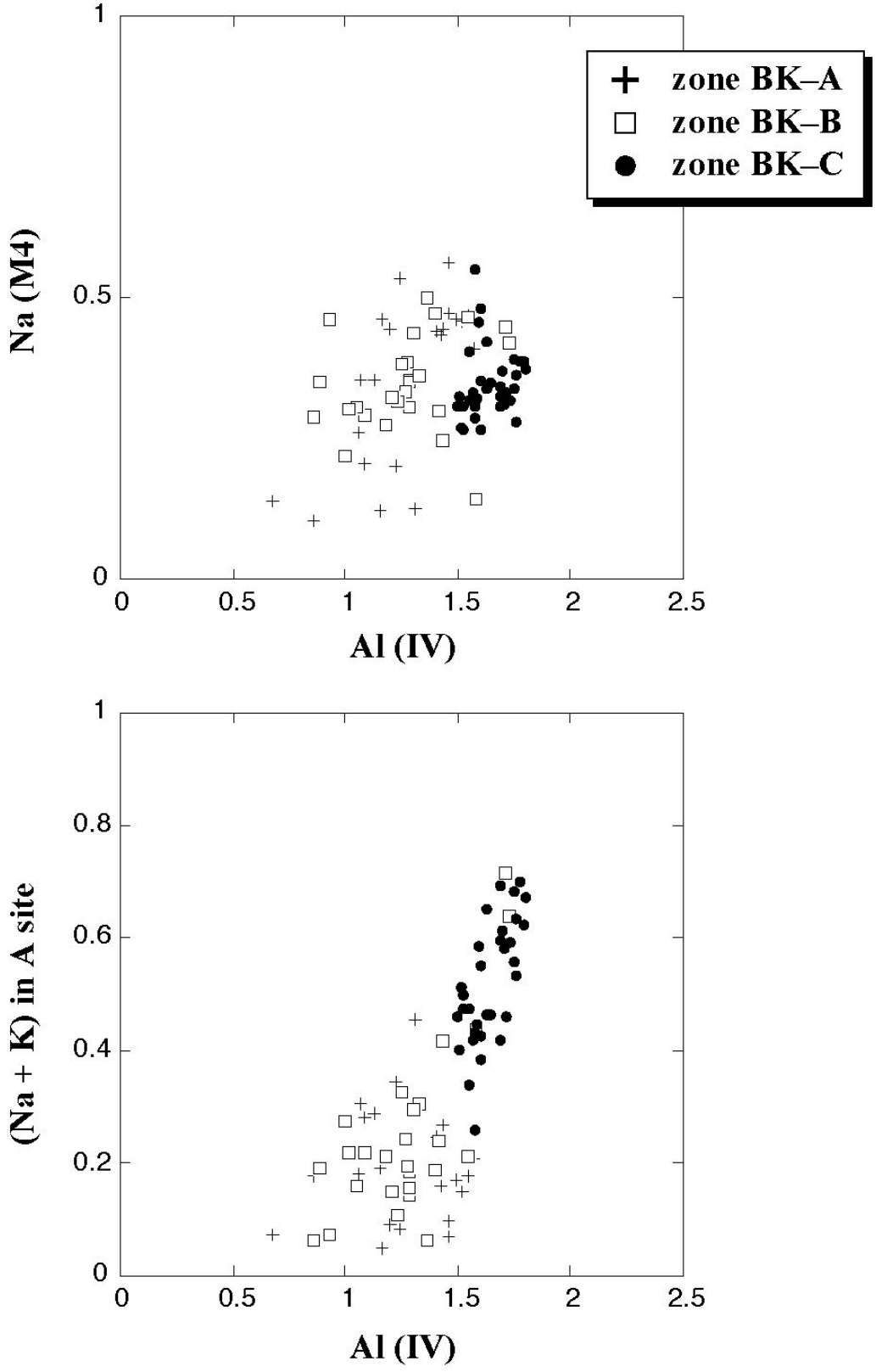

Fig. I–17 Compositions of primary amphiboles of each zone in the Barchi-Kol region. (a) Al (IV) *vs* Na (M4) ; (b) Al (IV) *vs* (Na + K) in A site (A site occupancy). Cations are calculated on the basis of 23 oxygens. Amphibole nomenclature is after Leake *et al*. (1997).

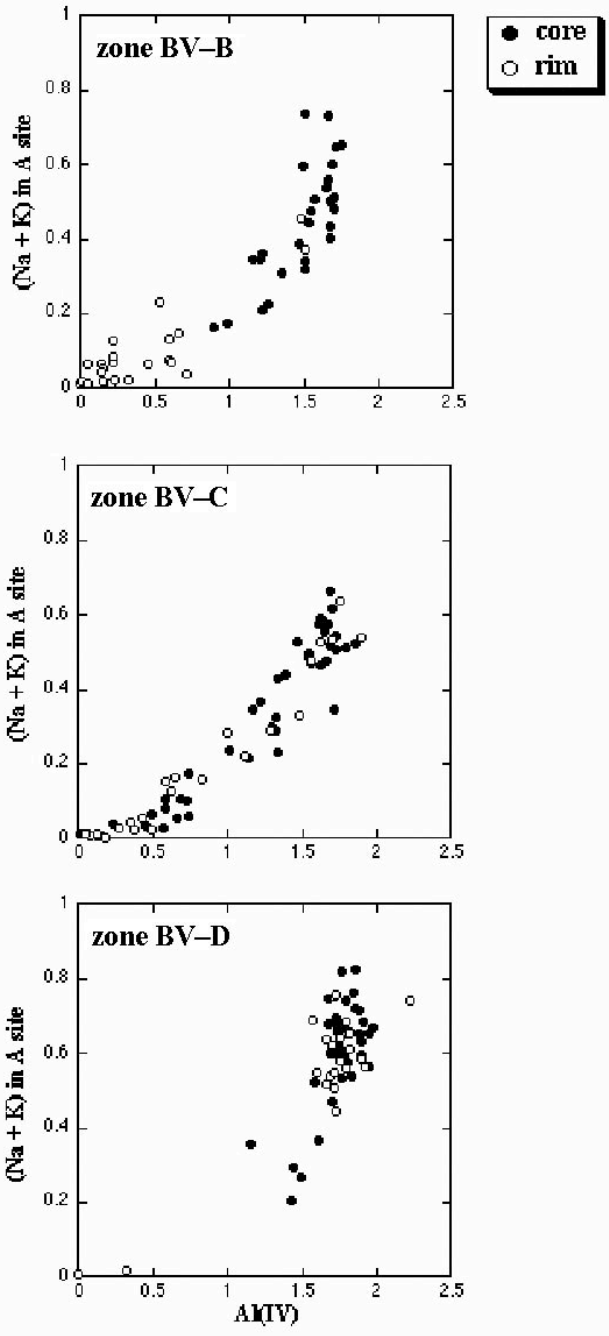

Fig. I–18 Compositional variation of matrix amphiboles of various zones in the Borovoye region.

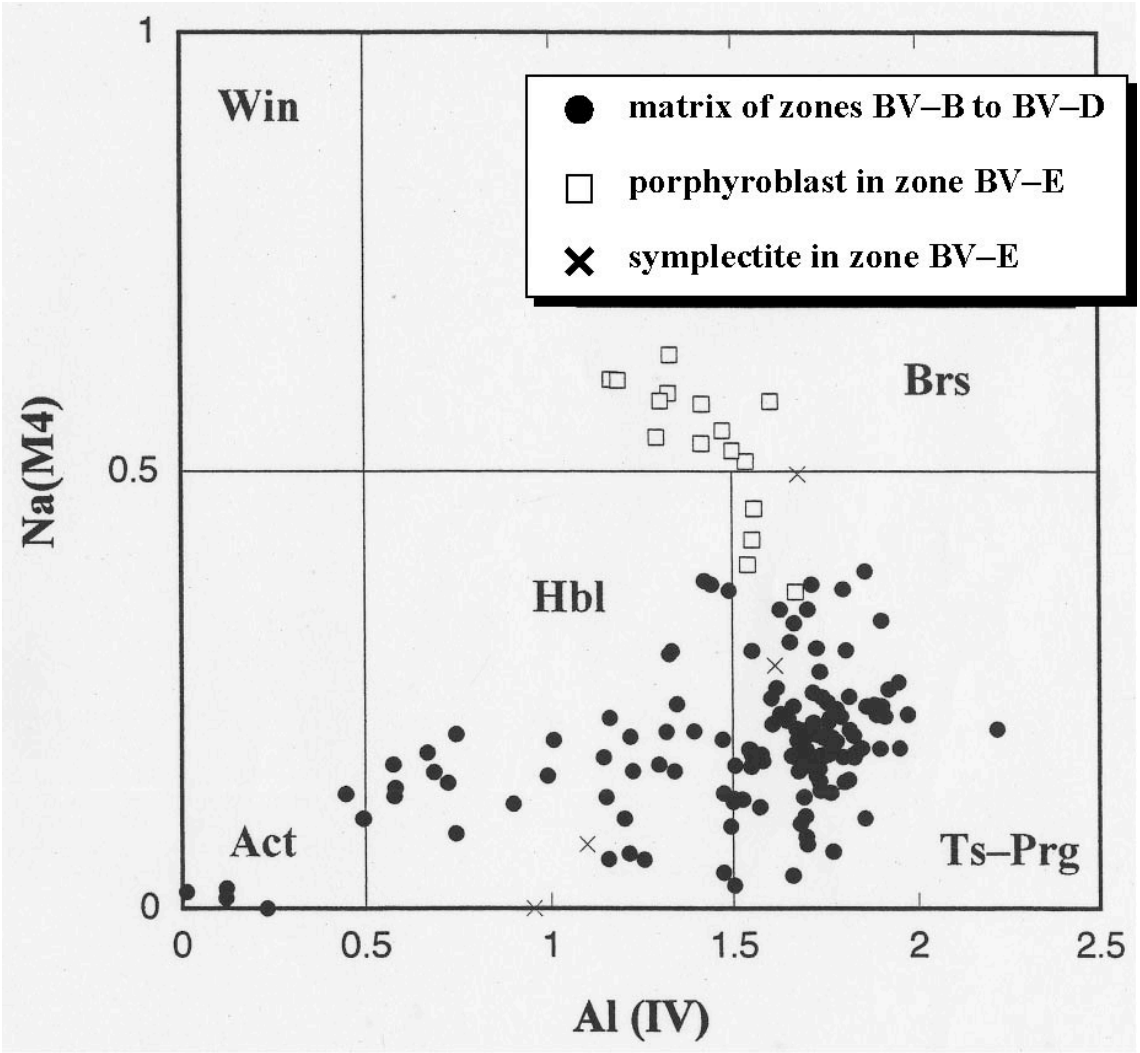

Fig. I–19 Amphibole compositions of various textures in the Borovoye metabasites.

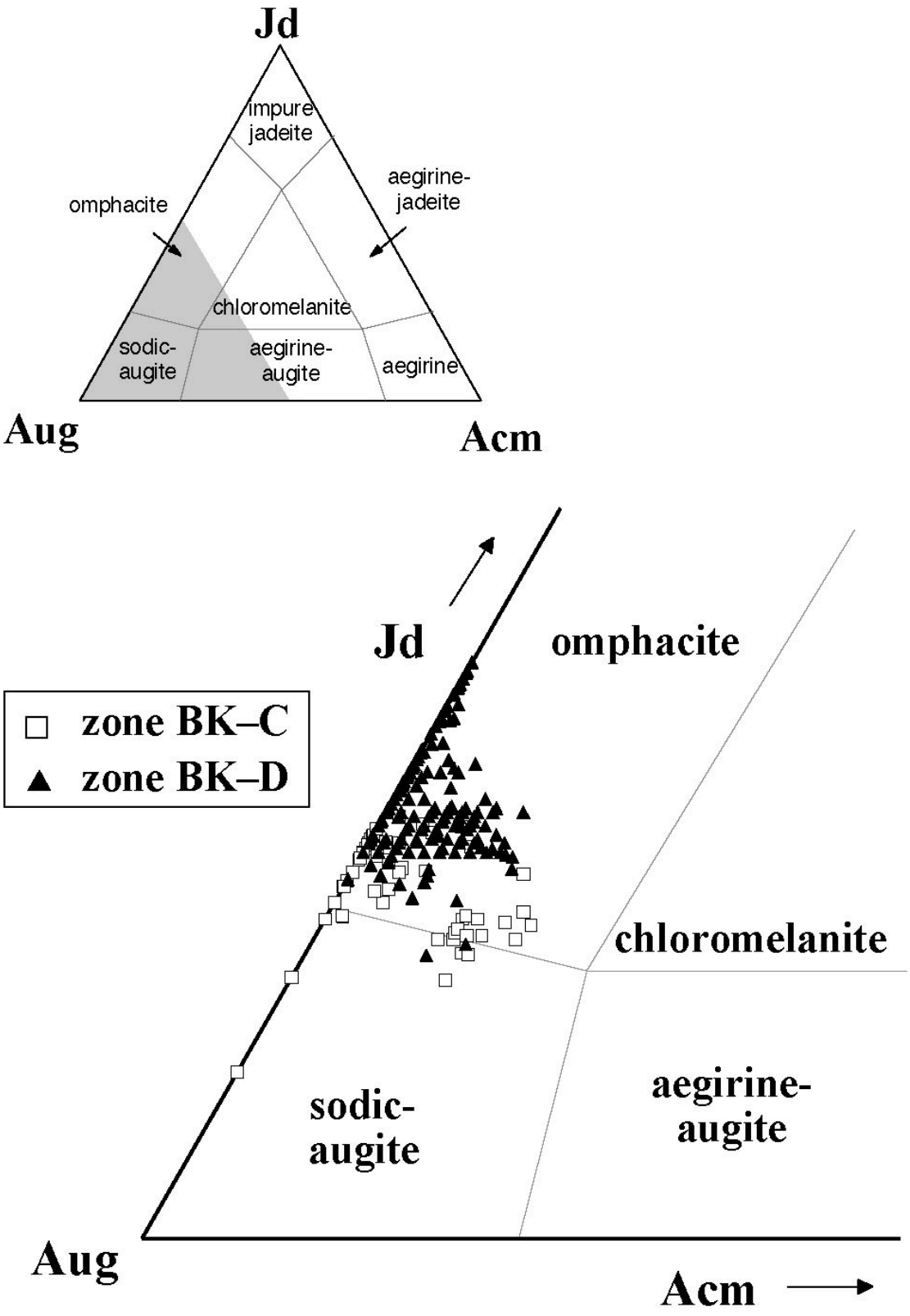

Fig. I–20 Compositions of analysed clinopyroxenes from each zone in the Barchi-Kol. Clinopyroxene nomenclature is after Essene & Fyfe (1967).

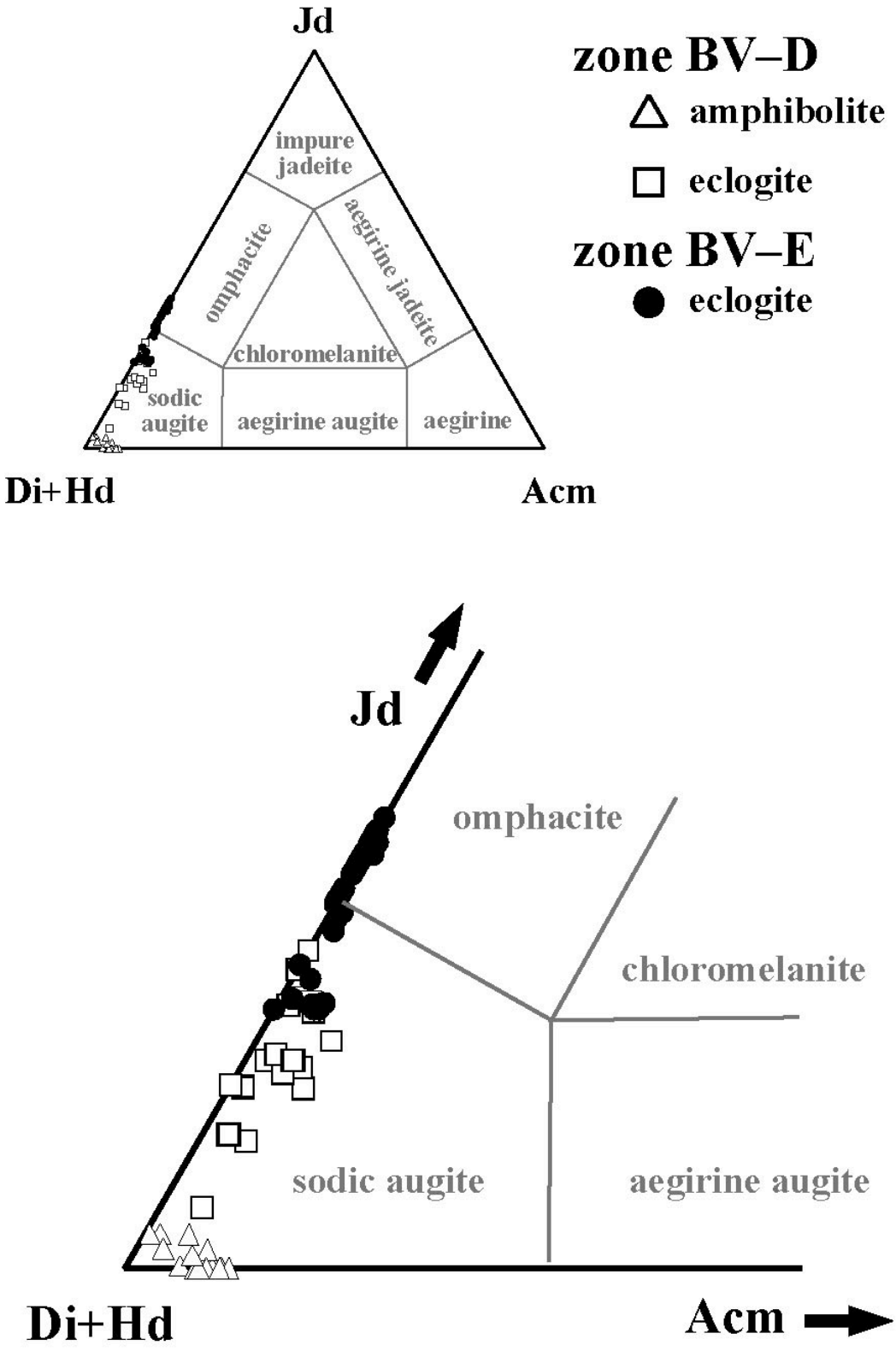

Fig. I–21 Clinopyroxene compositions of various zones and lithologies in the Borovoye region. Clinopyroxene nomenclatute is followed after Essen & Fyfe (1967).

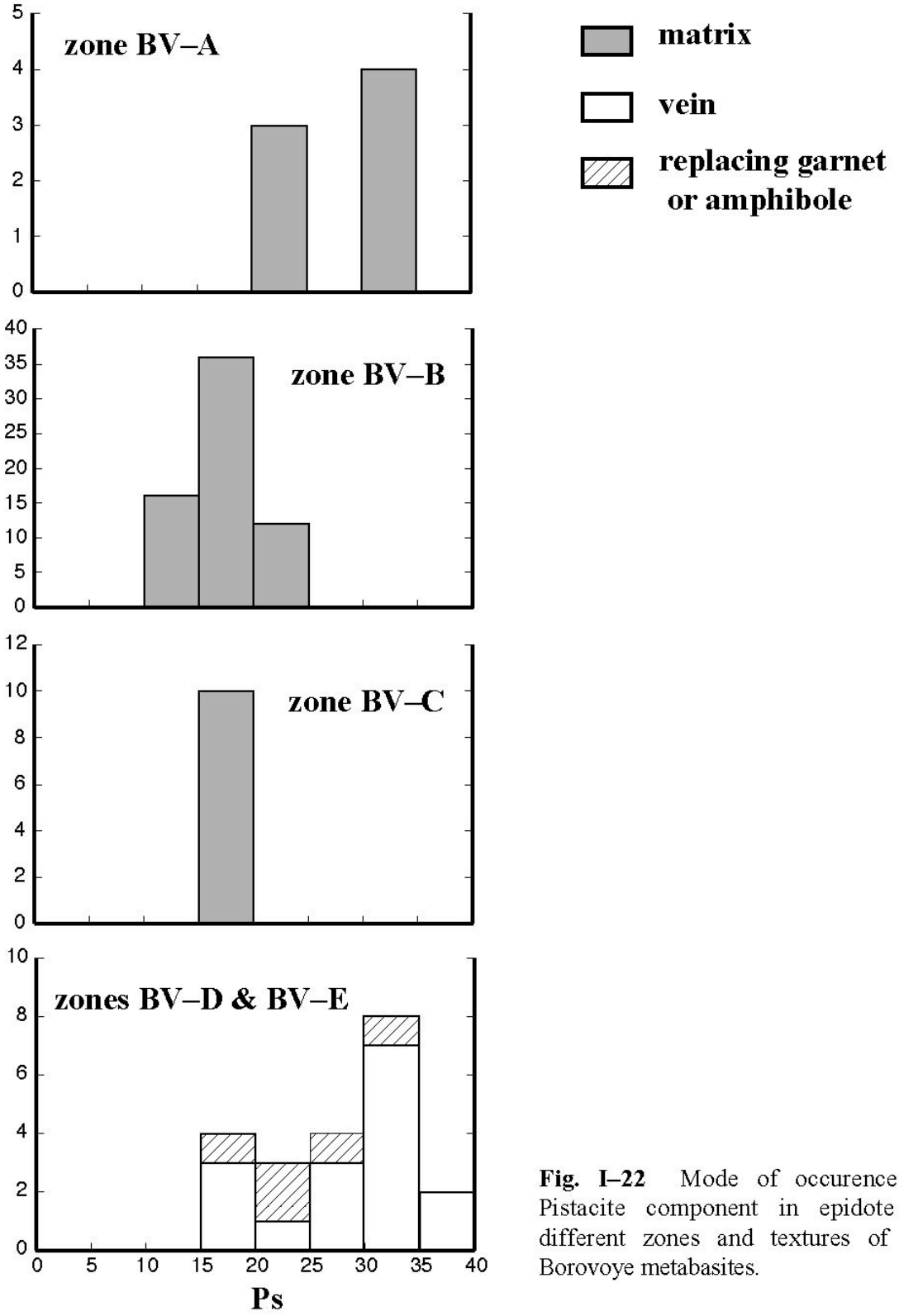

Fig. I–22 Mode of occurence of Pistacite component in epidote of different zones and textures of the Borovoye metabasites.

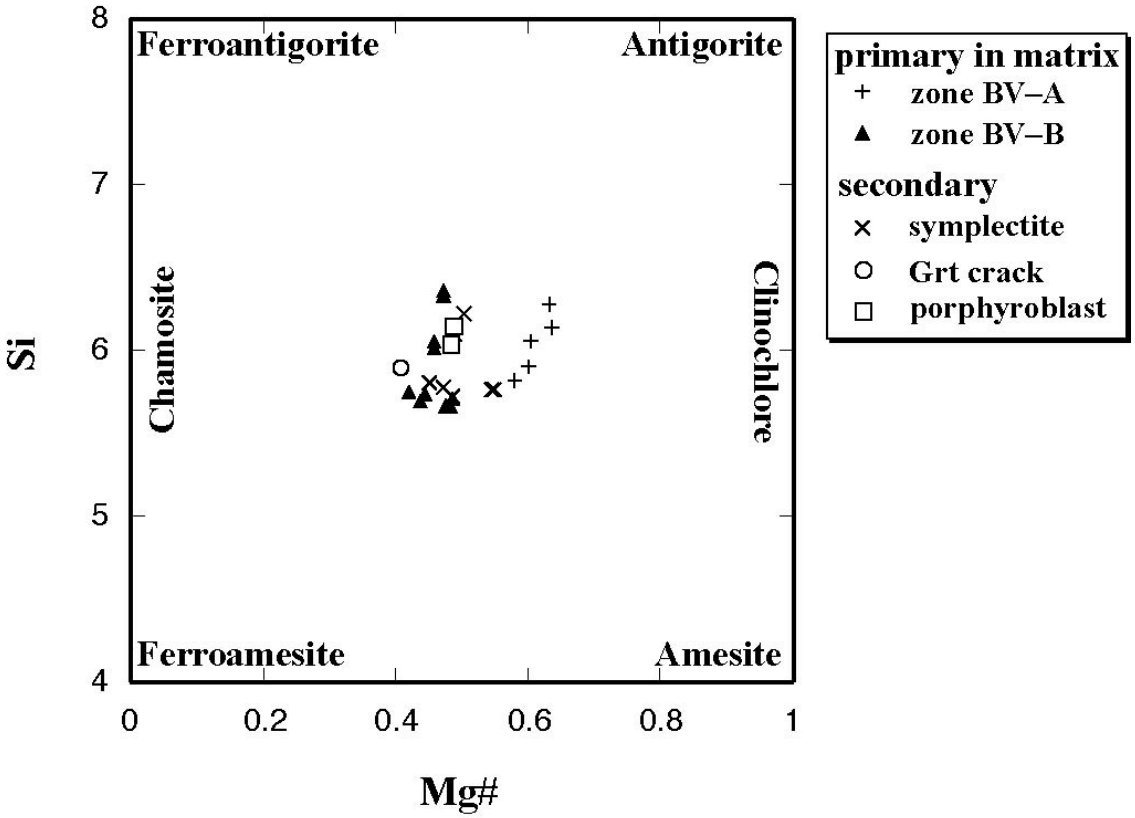

Fig. I–23 Compositional variation of chlorite by mineral zones and textures in the Borovoye metabasites.

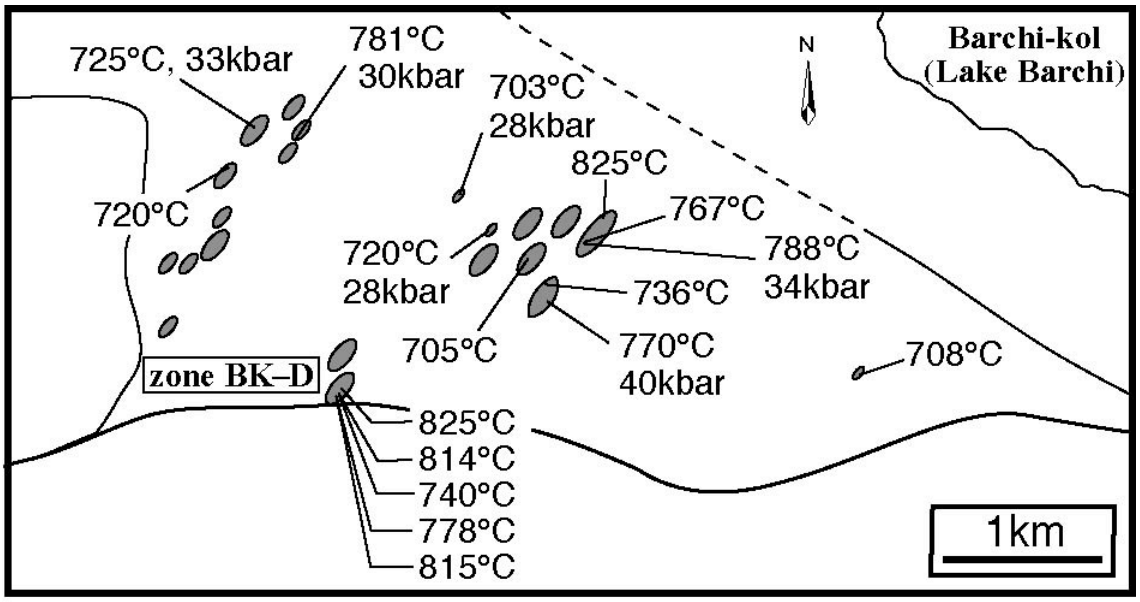

Fig. I–24 Spatial variation of metamorphic *P–T* conditions of eclogites in the Barchi-Kol region. Temperatures and presures are determined using a garnet–clinopyroxene geothermometer of Krogh Ravna (2000a) and a phengite geobarometer of Waters & Martin (1993).

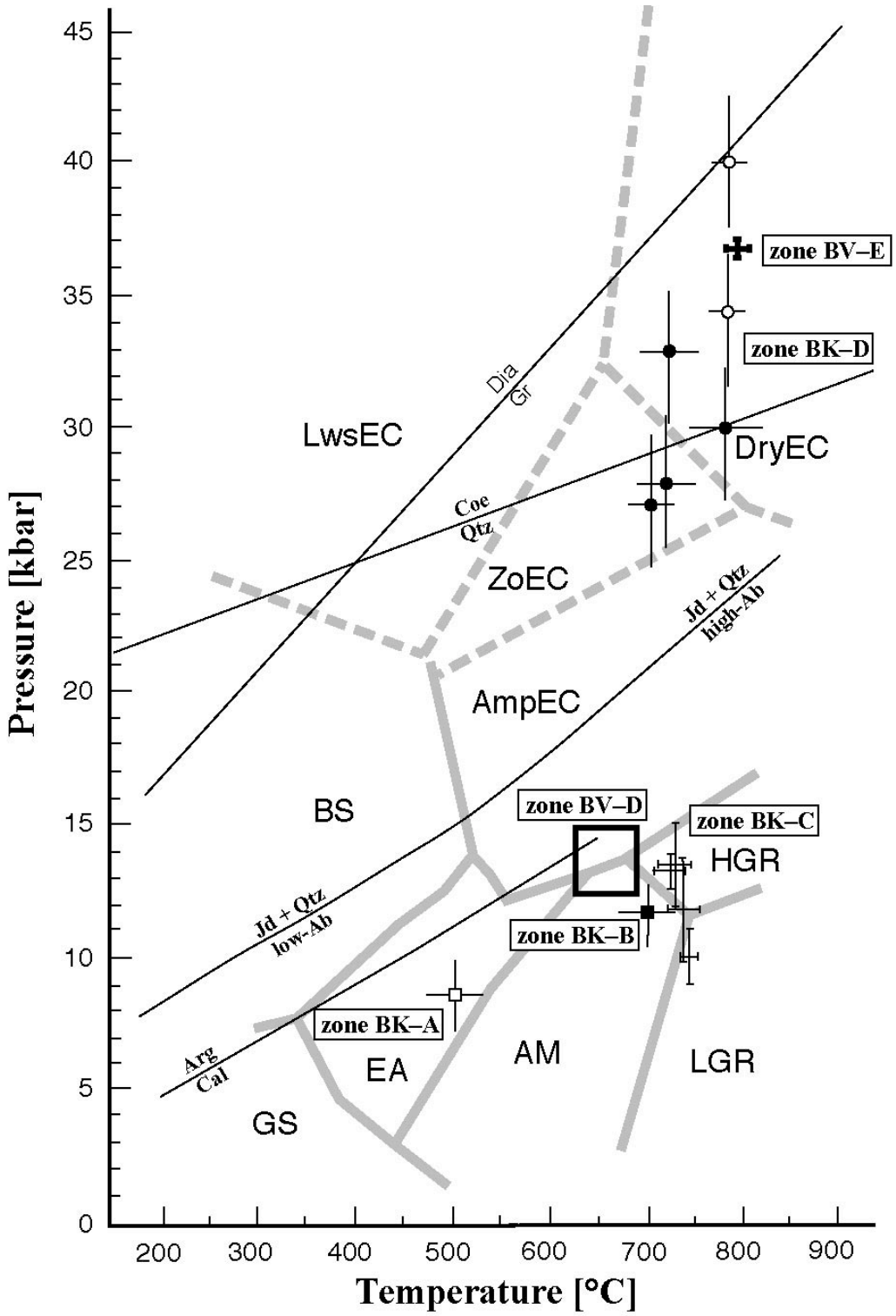

Fig. I–25 *P–T* estimates of each mineral zone by geothermobarometers. Open and solid circle symbols in zone BK–D represent coesite pseudomorph-bearing and absent samples, respectively. The *P–T* regimes are after the petrogenetic grid of Oh & Liou (1998) and Okamoto & Maruyama (1997) together with the experimenatally determined stability fields for diamond/graphite (Bundy 1980), coesite/quartz (Bohlen & Boettcher, 1982), jadeite + quartz = high albite (Holland, 1980), jadeite + quartz = low albite (Newton & Smith, 1967) and aragonite/calcite (Carlson, 1983).

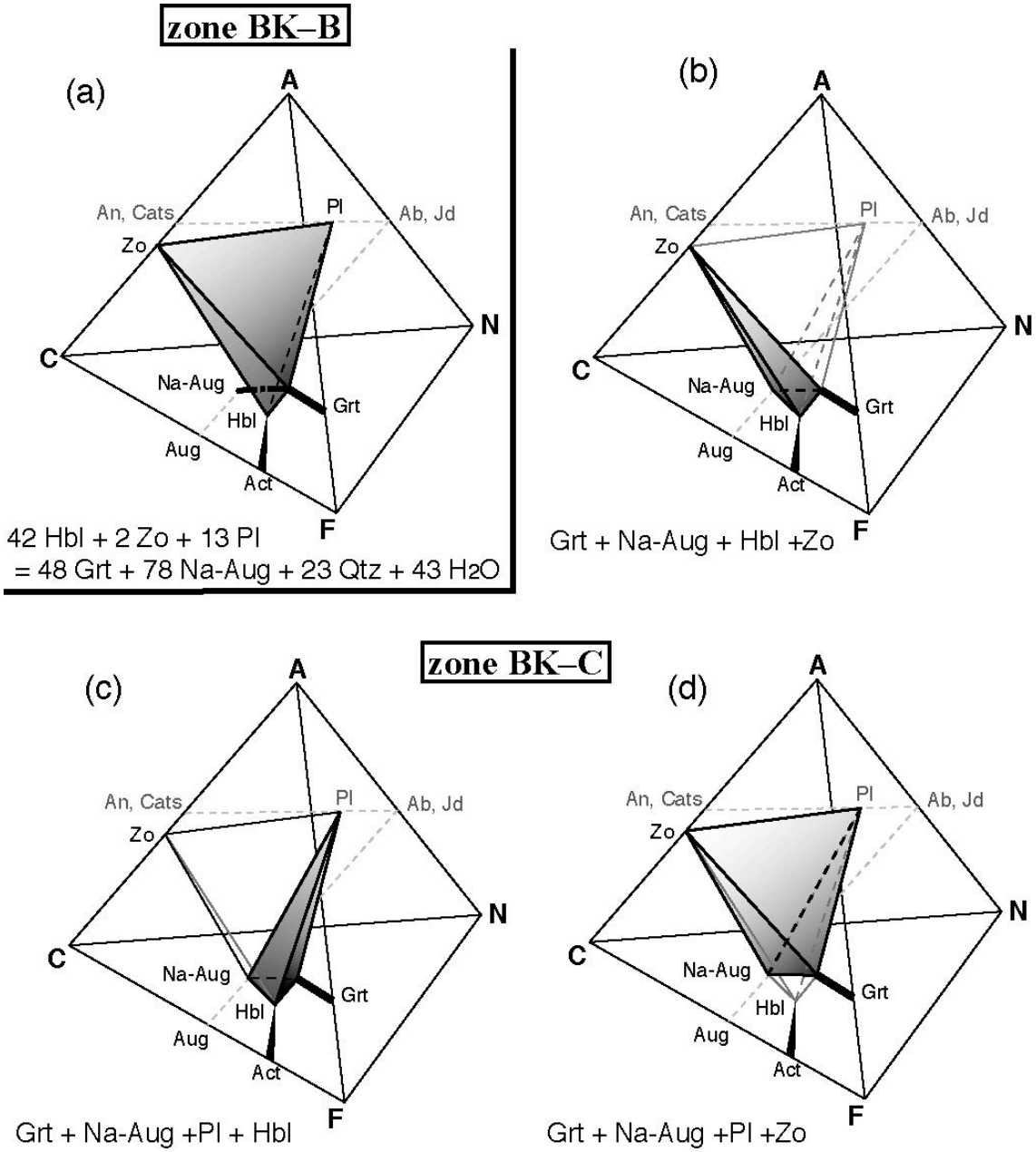

Fig. I–26 NACF tetrahedral phase diagram showing (a) change of mineral parageneses from zone BK–B to zone BK–C and (b)–(d) three possible parageneses in zone BK–C. Mineral parageneses shown in (d) does not actually occur in zone BK–C.

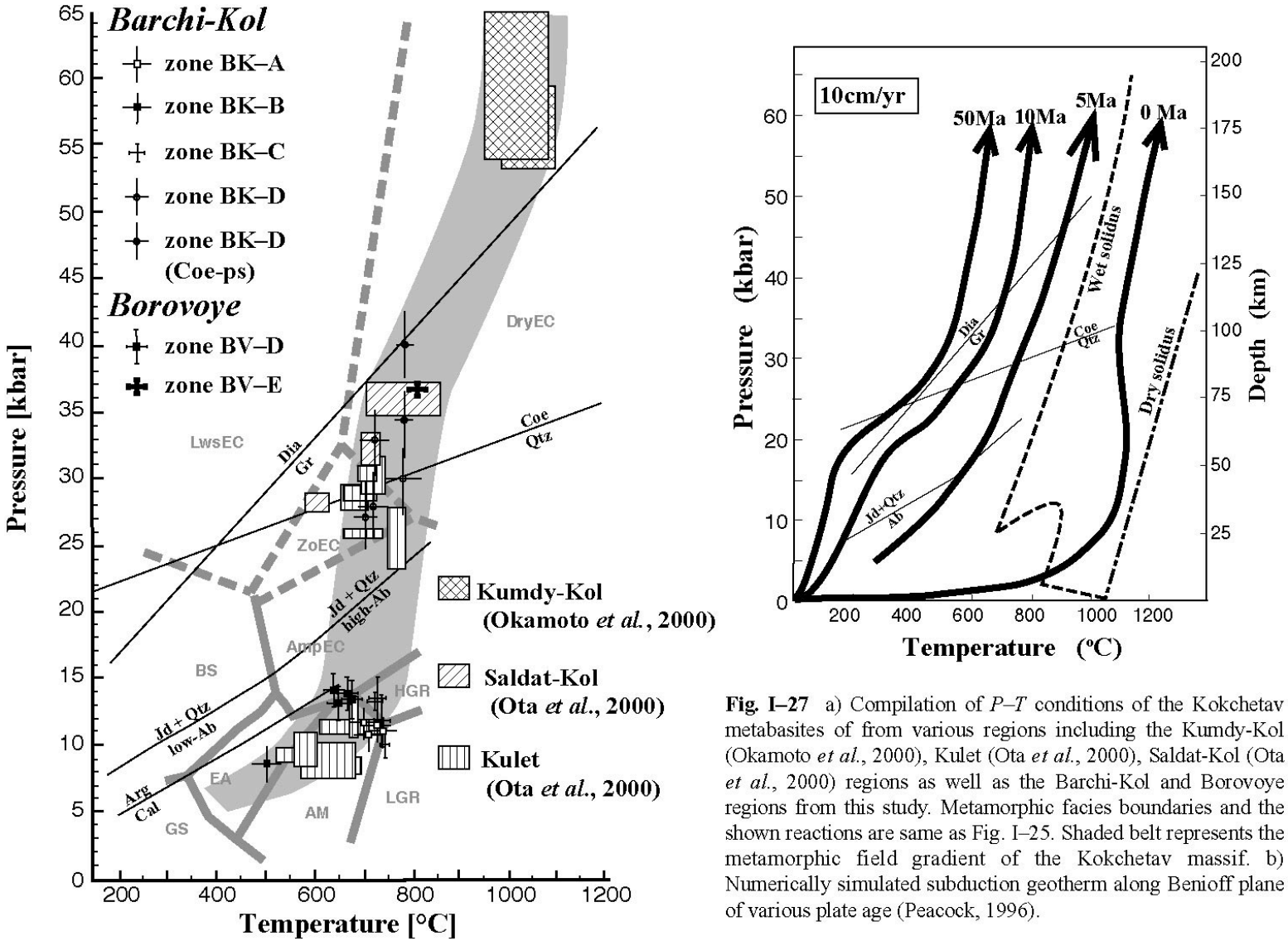

Fig. I–27 a) Compilation of *P–T* conditions of the Kokchetav metabasites of from various regions including the Kumdy-Kol (Okamoto *et al.*, 2000), Kulet (Ota *et al.*, 2000), Saldat-Kol (Ota *et al.*, 2000) regions as well as the Barchi-Kol and Borovoye regions from this study. Metamorphic facies boundaries and the shown reactions are same as Fig. I–25. Shaded belt represents the metamorphic field gradient of the Kokchetav massif. b) Numerically simulated subduction geotherm along Benioff plane of various plate age (Peacock, 1996).

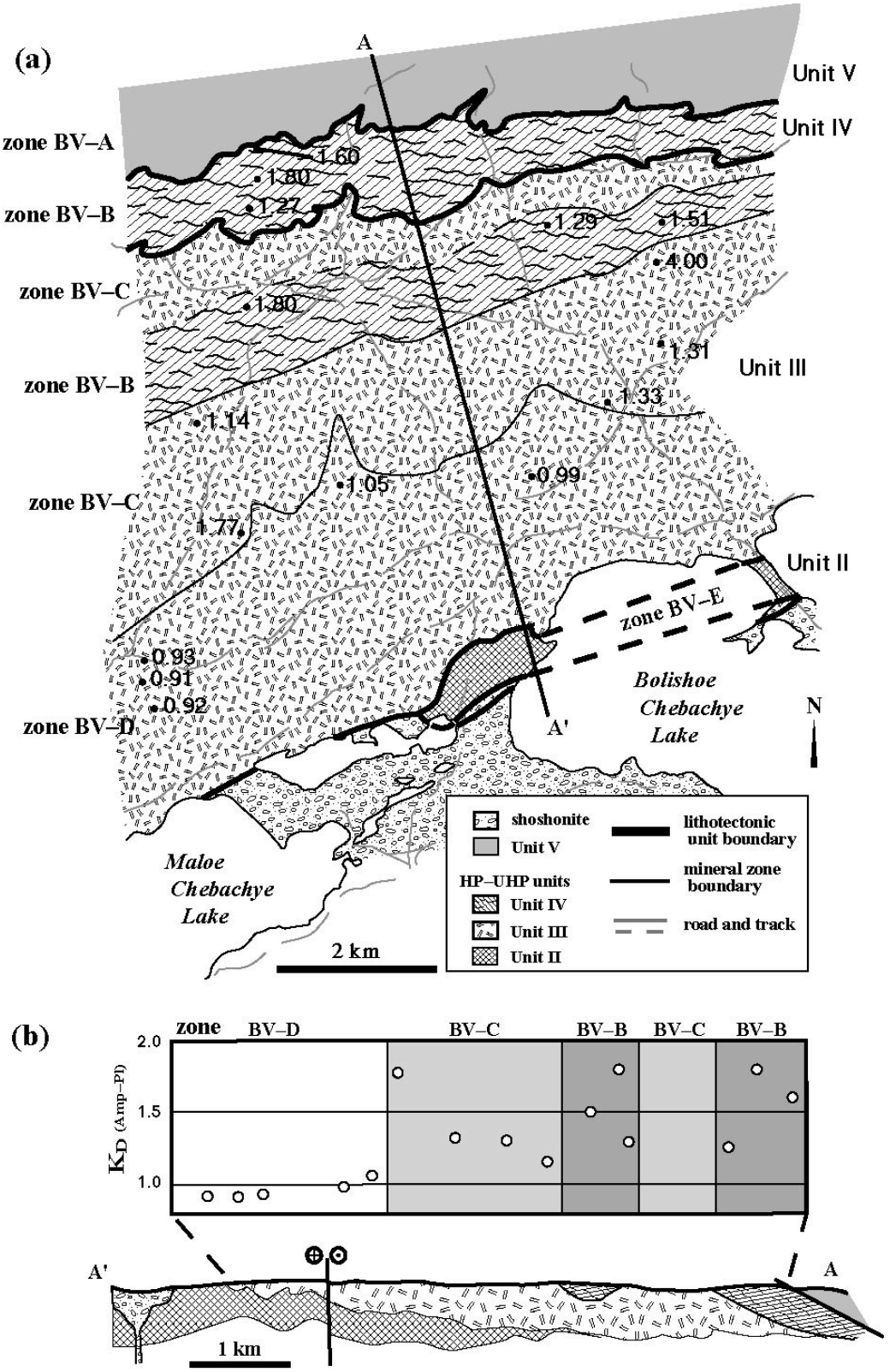

Fig. I–28 a) Regional distribution of distribution coefficient (K_D) between coexisting amphibole and plagioclase in the Borovoye amphibolites. Definition of K_D is followed after that used in Blundy & Holland (1990). b) Geologic cross-section along A–A' shown in (a), and K_D projected onto the line.

CHAPTER II

Reevaluation of Hydration Effect during Retrograde Metamorphism

ABSTRACT

Metamorphic rocks generally have undergone extensive hydration during their exhumation process, which associates with a major recrystallisation of the metamorphic minerals. This hydration effect, however, has long been further underestimated in most metamorphic belts. This recrystallisation occurs so extensively which obliterates the former mineralogy almost completely. For this reason, mineral assemblages equilibrated during the retrograde hydration have long been misunderstood as peak ones in many previous studies of metamorphism.

The Kokchetav massif is a rare example where retrograde hydration effect can be examined. Because both peak and retrograde mineralogy can be distinguished in some rocks in the Kokchetav massif. These samples give opportunity for a quantitative evaluation of the retrograde hydration effect.

In this chapter, retrograde mineralogy and texture of each lithology are described. Metabasite displays a localised hydration textures such as at the rims of rock body and cracks. On the other hand, hydration effect in rocks with strong fabric (*e.g.* gneisses and schists) is much more pervasive as it causes nearly complete recrystallisation of the matrix minerals.

The volume of infiltrated water during the retrograde hydration was calculated based on the peak and the present mineralogy. Eclogite, which is assumed virtually to be dry at its peak stage, takes about 1.0 wt % of water during amphibolitisation. For metapelite and orthogneiss, the peak mineral assemblages and mineral modes are thermodynamically estimated. And the infiltrated water amount is calculated as a difference from the present water content. The calculation yielded 0.6 wt % of water infiltration for metapelite. On the other hand, the orthogneiss yielded no water infiltration during the retrograde recrystallisation. Based on the above estimation and the volume ratio of each lithology in the massif, the volume of the infiltrated water to the Kokchetav HP–UHP unit was calculated as 14.8 km^3, which is equal to 493 cm^3 per square centimetre of minimum flux.

The most possible source of retrograde water is the Daulet Suite, an underlying metasedimentary unit beneath the HP–UHP unit. The estimated water infiltration into the HP–UHP unit is comparable to the released water from the Daulet Suite in the order of magnitude.

INTRODUCTION

It has long been recognised about the importance of aqueous fluid in the metamorphic reactions. However, it is difficult to estimate its activity because of its high mobility. There has been an assumption about the activity of fluid, which has been applied almost *a priori* in the studies of metamorphic petrology. It assumes nearly water-saturated conditions on the down-going path, and water-undersaturated conditions on the exhumation path. Most prograde metamorphic reactions are dehydration reaction. Once water is released by the breakdown of hydrous minerals, it is removed from the system and never returns. Therefore, water is monotonously removed from the system on the prograde path of the metamorphic rocks. On the contrary, most of retrograde reactions are hydration reaction. Once rocks lost their water on their prograde paths, there is no sufficient water to cause the back reactions. For this reason, back reactions occur only at limited extent after once rocks reached at peak metamorphic conditions. This has been applied for the explanation for metamorphic rocks can preserve near-peak mineralogy and compositions to the surface. This assumption seems to be plausible, but is too opportunistic for metamorphic petrologists.

Discovery of the UHPM threw a question to this assumption. After the first discovery of UHPM by Chopin (1984) and Smith (1984), UHPM was found from many metamorphic belts, all of which are of collision-type. Before the discovery of UHPM, these metamorphic belts are regarded as 'medium-*P*' type whose pressure does not exceed 12 kbar. This type of metamorphism is also referred as Barrovian-type metamorphism, and has been regarded to be typical to the collision-type metamorphism. The type localities of Barrovian-type metamorphism are Dalradian and Appalachia. The Barrovian-type metamorphism is characterized by the series of mineral isograds in a pelitic system such as chlorite-, biotite-, garnet-, staurolite-, kyanite- and sillimanite-isograd from low to high-grade. UHPM is completely inconsistent with the Barrovian metamorphic facies series. The required pressure for UHPM is *ca*. 30 kbar at minimum under the realistic geothermal gradient. This is completely inconsistent with the *P–T* conditions of the surrounding rocks. In the early days of the UHPM study, UHPM was regarded to be a tectonic block or an olistostrome, and the rest of the metamorphic belt was still believed to have medium-*P* type metamorphic facies series. Nevertheless, as new UHPM localities are reported one after another, this explanation became to be

inappropriate. Tectonic block and olistostorome should not observed so commonly in orogenic belts. Furthermore, as Katayama *et al*. (2000) demonstrated the regional extent of UHPM, the mélange or olistostrome model were denied, at least in the Kokchetav massif. This clearly suggests that the most parts of the massif had experienced HP–UHPM conditions, which now have converted to medium-*P* type mineral assemblages rocks. There is no more a reason to believe the above mentioned assumption about the water activity. The example of the Kokchetav massif infers that hydration during exhumation occurs much more extensively than we have expected. As back reactions obliterated the former mineralogy at the peak stage almost completely, metamorphic petrologists have taken it for the primary ones. That was nearly a 'perfect crime'.

However, it was actually not perfect. A discovery of tiny coesite inclusions from nominally 'medium-*P*' type metamorphic belt requires a reevaluation of the Barrovian metamorphism, which has been believed to be typical to the collision related metamorphism. It is now obvious to have been formed during the retrograde hydration. For the beginning, we need to discriminate the retrograde minerals from the primary ones based on the textures and the inclusion mineralogy. The origin and the amount of the water are also important problems. If the majority of the rocks were nearly dry at their peak metamorphic conditions, a certain amount of water must have been infiltrated from the outside of the system. We need to propose and the possible source of water, and inspect whether it is sufficient to account for this volume. Another important problem is the mode of hydration. It is expected there are several different modes of hydration for different rock types.

The Kokchetav massif is the best example to solve this sort of problem. Because it has a large contrast between the peak and the retrograde stages of the metamorphism. Reevaluation of the Barrovian metamorphism in the Kokchetav massif will be the new standard of the collision related metamorphism of the world.

DESCRIPTION OF HYDRATION TEXTURES

Metabasites

Degree and textures of hydration in metbasites are various. Metabasites occur as

blocks or layers in other lithologies such as ortho- and paragneisses, leptite (fine-grained acidic gneiss) and schists. They are distributed sporadically throughout the massif, and their metamorphic grade ranges from epidote-amphibolite through amphibolite, quartz-ecogite, coesite-eclogite to diamond-eclogite facies (*see* Appendix I). Metabasite bodies are frequently hydrated from their margins. Eclogite often displays a clear relationship of core–rim structure consists of relatively fresh eclogite part and variously amphibolitised part as a result of retrograde hydration (Fig. II–1). Some of relatively small bodies are completely amphibolitised. Hydration also takes place along fractures (Fig. II–2a). Metabasites often have a set of diagonal fractures which intersect the planar and linear structures in metabasites with high angle. Veins are also common in every type of metabasites. The vein-forming minerals are various and have a correlation with metamorphic grade. Quartz is one of the commonest vein mineral from low- to high-grade. Epidote and/or clinozoisite are also common in the rocks of higher than epidote-amphibolite. Vein epidote are yellow-greenish in colour, and has generally higher pistasite component than that in the matrix (Fig. I–22). Amphibole vein is rather common in eclogite. It is sometimes associated by plagioclase and forms amphibolite vein. In some lower-grade rocks, acicular actinolitic amphibole veins are observed. Calcite vein is often observed in relatively lower-grade metabasites. Another common texture of hydration in eclogite is a large porphyroblastic amphibole. It has grown inconsistently larger than the other matrix eclogitic minerals and is often observed as a dark patch of a few millimetre by naked eye in the outcrop (Fig II–2c).

Representative microscopic hydration textures are symplectite mainly around omphacitic clinopyroxene, corona texture around garnet, and chloritisation and/or actinolitisation around amphibole of hornblende–pargasitic compositions. Most symplectite around omphacitic clinopyroxene is composed of hornblende + plagioclase (Fig. II–3a). However, there is also symplectite composed of augite + plagioclase (Fig. II–3b), suggesting a relatively dry metamorphic condition. Garnet is very often fragmented by diagonal fractures which is filled by epidote ± chlorite (Fig. II–3c). Some garnet have corona composed of epidote and/or chlorite.

In any scale, hydration effect in metabasite is localised. Hydrocracking might have worked as an important mode of hydration.

Metapelites

Exposure of pelitic schist/gneiss is not much. Because of their vulnerability to weathering, outcrops of these lithologies are limited. However, numerous marmot holes are helpful as a natural drilling, which tell the wide distribution of these rocks underneath the grasslands and farms. Metapelites have virtually no evidence of HP metamorphism in their matrix assemblages represented as: Qtz + Pl + Ms (with various degrees of celadonite component) + Bt ± Grt ± Ky ± Sil ± And ± St (Fig. II–4a). Apatite, rutile, zircon and tourmaline occur as common accessory minerals. Some metapelites lack muscovite and contain K-feldspar instead, and often migmatitic (Fig. II–4b). Metapelites commonly have strong planar and linear fabrics defined by preferred orientation of sheet silicates (muscovite and biotite), and elongated quartz, plagioclase and sillimanite, respectively. These mineral assemblages suggest medium pressure condition. However, inclusions of HP–UHP minerals in zircon in Unit II schist and gneiss (Katayama *et al*., 2000) clear evidences of former HP–UHPM conditions. Consequently, it is suggested that the retrograde hydration is more pervasive than in the metabasites, which causes nearly complete recrystallisation of the matrix minerals. Garnet and kyanite may be the relicts of HP metamorphism. Garnet generally have strong prograde compositional zonation characterized by decreasing spessartine component from core to rim, except for the diamond-grade Kumdy-Kol samples (*See* Chap. III).

Orthogneiss

Orthogneiss occupies the major part of the massif, especially in Unit III. Mineral assemblages of orthogneiss are quite simple: Qtz + Pl + Kfs + Ms + Bt. Rutile, apatite, tourmaline are commonly contained as accessory phases. No indication of HP–UHPM is reported from orthogneiss.

Acidic Gneiss

Mineral assemblages in acidic gneiss are basically same as those in orthogneiss. The only difference is the acidic gneiss is much finer-grained than orthogneiss.

Metacarbonates

Distribution of metacarbonate is not much. It is mostly restricted to the Kumdy-

Kol area. Hydration effect in this rock type is scarce. Mineral assemblages of metacarbonates are: Cal + Dol ± Di ± Grt (grossular-rich) ± Ttn.

P–T ESTIMATION OF THE RETROGRADE METAMORPHISM

P–T conditions of the retrograde metamorphism were estimated from the mineral parageneses and conventional thermobarometry. The matrix mineral assemblage of Grt + St + Bt observed in some metapelites has rather narrow temperature range as 550–625 °C.

Meabasites generally have several stages of retrograde minerals. Some metabasites have textures showing a key to the retrograde *P–T* path. They are summarised as follows: 1) Hbl + Pl and/or Aug + Pl symplectite around eclogitic omphacite and/or garnet, 2) patchy hornblende porphyroblast in eclogite, 3) amphibolitisation of eclogite, 4) plagioclase exsolution in sodic-augite in the Borovoye eclogite, 5) epidote and/or chlorite formation along cracks in garnet in amphibolite, 6) actinolitic rim around amphiboles of hornblende to pargasitic composition in amphibolite, 7) decrease in X_{An} in plagioclase rim and 8) epidote vein in amphibolite. Estimated retrograde *P–T* path from these mineralogical and textural relationships is shown in Fig. II–5.

A Borovoye eclogite sample T507 has symplectite of Aug + Hbl + Pl, an upper amphibolite facies assemblage. Application of Jd + Qtz = Ab geobarometer (Holland, 1983), and Hbl–Pl geothermometer (Blundy & Holland, 1990) resulted in 10.7 kbar and 680 °C for formation condition of this assemblage. Pressure–temperature conditions for patchy hornblende porphyroblast in eclogite are difficult to estimate. These amphiboles are generally have high Na content in M4 site, which have a positive correlation with pressure, and some of them are classified into barroisite. This infers that these amphiboles are formed at higher pressure conditions than prograde amphiboles in amphibolite in Units I, III & IV. In more advanced stage of retrograde metamorphism, eclogite is almost completely transformed into amphibolite. Although highly amphibolitised, fragmented garnet clots remain together with tiny lath of omphacite as relics of former eclogite stage. Hornblende–plagioclase thermometry yielded 632 °C at pressure of 11 kbar for the latest stage. Hornblende–garnet–plagioclase barometery on the assumption that garnet was in equilibrium with amphibolite matrix minerals, yielded

13.3 kbar. This is too high compared to the above-mentioned *P–T* conditions.

Above-mentioned textures (5) to (8) all suggest greenschist facies conditions at the latest stage. As metamorphic conditions of Unit V, the hangingwall of HP–UHP units, are of greenschist facies, these textures are considered to be formed at the time of juxtaposition of HP–UHP nappe to the depth of mid-crustal level.

VOLUME ESTIMATION OF INFILTRATED WATER

Based on the compositions and the modes of retrograde hydrous minerals, the amount of infiltrated water is calculated. The calculation method is: 1) to estimate the modes of retrograde hydrous minerals in each rock type, then 2) multiply the volume ratio of each rock type in the massif. First of all, it is essential to assume the mineral species and their modes at the peak metamorphic stage. Eclogite is simply assumed to be dry at the peak stage. Indeed, some eclogites contain primary hydrous minerals such as amphibole, zoisite and phengite. However, their modes are generally low, hence this assumption is virtually applicable. Modal abundance of the constituent minerals in retrograde amphibolite (ex-eclogite) is: Hbl (40 %) + Grt (30 %) + Pl (20 %) + Qtz (10 %). The bulk water content calculated from this mineral assemblage is 1.0 wt %. Therefore, amphibolitisation of eclogite associates 1.0 wt % water absorption.

For metapelite, estimation of water content at peak metamorphic stage is not so simple because it contains a certain amount of phengitic mica even at the peak condition. Peak mineral assemblage and modal abundances are calculated in a K_2O–Na_2O–FeO–MgO–Al_2O_3–SiO_2–H_2O system using a UniEQ computer program of Omori & Ogasawara (1998) with thermodynamic datasets of Berman & Arranovich (1996). The estimated peak metamorphic mineral assemblage is given as Coe (30 %) + Phn (35 %) + Grt (25 %) + Jd (8 %). The present mineralogy of metapelite is Qtz (37 %) + Pl (13 %) + Kfs (8 %) + Bt (34 %) + Grt (8 %). Accordingly, 0.6 wt% of water has infiltrated to metapelite during the retrograde hydration.

Peak mineral assemblage and modal abundances of orthogneiss were estimated in the same manner. However, orthogneiss does not its mineralogy greatly except for containing coesite and jadeite instead of quartz and plagioclase as well as a little amount of garnet. In these mineralogical changes are accompanied no hydration nor dehydration,

and no excess water was calculated at the peak condition. This means that the orthogneiss does not work as an accepter of the retrograde water. This is also the case with the leptite, because it has almost same granitic bulk composition.

The estimated retrograde water volume for each lithology is summarised in Table II–1. The percentage of the occupied area of each lithology on the geologic map is orthogneiss (15 %), metapelite (31 %), leptite (14 %), eclogite (4 %), amphibolite (18 %) and others (18 %). Quartzite, metacarbonate and silicious schist are included in the other lithologies. The water absorption to these rocks are so limited which can be ignored in the calculation. Based on the detailed field mapping in the Chaglinka region (Fig. II–1), 65 % of eclogite are amphibolitised due to retrograde hydration. These area ratio are converted to volume ratio as orthogneiss (12 %), metapelite (39 %), leptite (12 %), eclogite (2 %), amphibolite (12 %) and others (17 %).

The volume of infiltrated water into the HP–UHPM unit calculated from the above mentioned estimation is 14.8 km^3, if the dimension of the massif is assumed to be 150 x 20 x 2 km^3. Its detail is 0.8 km^3 to eclogite and 14.0 km^3 to metapelite. It is noted that the most of the infiltrated water is absorbed to metapelite. Although amphibolitisation of eclogite also absorbs a certain amount of water, the volumetric proportion of eclogite in the massif is so low, it makes little contribution in the retrograde hydration.

DISCUSSION

Origin Of The Retrograde Fluid

As demonstrated in the previous section, large amount of aqueous fluid has infiltrated from the outside of the HP–UHPM unit. The next problem is the origin of this voluminous water. The most plausible candidate for that is the Daulet Suite, an underlying metamorphic unit beneath the HP–UHPM unit. The Daulet Suite consists mainly of pelitic schist, which is in fault contact with the HP–UHPM unit at the southern margin of the Kulet, Sulu-Tjube and Barchi-Kol areas (*see* detail in Appendix I). Metamorphic grade of the Daulet Suite is generally low except for the narrow zone close to the boundary fault with HP–UHPM unit. Terabayashi *et al*. (2002) revealed the increasing metamorphic grade in the Daulet Suite towards the boundary fault, and concluded that it was a contact metamorphism by the exhumed high temperature

HP–UHPM unit. They demonstrated that the water content in the pelitic schist shows a continuous decrease with increasing metamorphic grade towards the boundary. This infers that the water released from the Daulet Suite was absorbed into the overlying HP–UHPM unit at the timing of their juxtaposition at mid-crustal depth. Terabayashi *et al*. (2002) estimated the released water from the Daulet Suite as 0.67 litre per square centimetre. On the other hand, infiltrated water into the overlying HP–UHP unit is calculated as 0.49 litre per square centimetre. This is slightly lower than the released water from the Daulet Suite, but is consistent in the order of magnitude. There are several uncertainties and approximations in the estimation. One of the largest factor which is ignored in the above estimation is the hydration effect on garnet-amphibolite. Similar to eclogite, retrograde recrystallisation from garnet-amphibolite to epidote-amphibolite is accompanied by some hydration reactions. However, its extent is not quantitatively figure out, indeed it is not so extensive as in eclogite. For these reasons, hydration effect on garnet-amphibolite has not been included in the calculation. Nevertheless, garnet-amphibolite is more abundant lithology than eclogite in the massif. If this modification is incorporated, it will increase the volume of water infiltrated into the HP–UHP unit.

Reevaluation of the Barrovian Metamorphism

The above mentioned calculation has revealed that a certain amount of water is infiltrated during the exhumation stage of the HP–UHP unit. This result clearly shows the traditionally used assumption in metamorphic petrology about fluid activity is wrong. That is assuming a low water activity in a nearly closed system for the retrograde path. Metapelites, which occupies the major part in a collision-type metamorphic belt, have undergone nearly complete recrystallisation due to retrograde hydration. In many metamorphic belts, isograds are defined based on the pelitic mineral paragenenses. Now it is obvious that these isograds deduced from the present mineral parageneses in metapelite reflect the thermobaric structure at the retrograde hydration. Hence, the Barrovian-type metamorphism which has been believed to be typical to the collision-type orogeny is now found out to be not a substance but just an illusion of collision related metamorphism.

However, it should be noted that not all minerals are formed at the retrograde hydration stage. Results of thermodynamic calculation indicate some of currently

observed minerals such as garnet, kyanite and phengite are stable even at the peak metamorphic conditions about 1000 °C, 60 kbar. It is expected that some of these minerals metastably remain after rocks are undergone retrograde hydration. Therefore, we should be careful in recognition of the equilibrium assemblage involving these minerals.

This study has concluded that the matrix mineral assemblage s of metapelite are no use for the analysis of the peak metamorphic conditions. Accordingly, traditional metamorphic analyses based on the matrix mineralogy need to be reevaluated in the light of new sight. Inclusion mineralogy is one of the more reliable methods to delineate the peak or prograde metamorphic conditions. Garnet is the best container of the former stage minerals. An example of the *P–T–t* path analysis from garnet inclusions combined with its compositional zoning will be presented in the next chapter.

REFERENCES

Berman, R. G. & Aranovich, L. Y., 1996. Optimized standard state and solution properties of minerals I. Model calibration for olivine, orthopyroxene, cordierite, garnet and ilmenite in the system $FeO–MgO–CaO–Al_2O_3–TiO_2–SiO_2$. *Contributions to Mineralogy and Petrology,* **126,** 1–24.

Blundy, J. D. & Holland, J. B., 1990. Calcic amphibole equilibria and a new amphibole–plagioclase geothermometer. *Contributions to Mineralogy and Petrology,* **104,** 208–224.

Bohlen, S. R. & Boettcher, A. L., 1982. The quartz–coesite transformation: A pressure determination and the effect of other components. *Journal of Geophysical Research*, **87**, 7073–7078.

Bundy, F. P., 1980. The *P, T* phase and reaction diagram for elemental carbon. *Journal of Geophysical Research*, **85**, 6930–6936.

Carlson, W. D., 1983. The polymorphs of $CaCO_3$ and the argonite–calcite transformation. *Reviews in Mineralogy,* **11,** 191–225.

Chopin, C., 1984. Coesite and pure pyrope in high-grade pelitic blueschists of the Western Alps: A first record and some sequences. *Contributions to Mineralogy and Petrology*, **86,** 107–118.

Holland, T. J. B., 1980. The reaction albite = jadeite + quartz determined experimentally in the range 600–1200°C. *American Mineralogist*, **65**, 125–134.

Holland, T. J. B., 1983. The experimental determination of activities in disordered and short-range ordered jadeitic pyroxenes. *Contributions to Mineralogy and Petrology*, **82,** 214–220.

Katayama, I., Zayachkovsky, A. A. & Maruyama, S., 2000. Prograde pressure–temperature records from inclusion in zircons from ultrahigh-pressure–high-pressure rocks of the Kokchetav Massif, northern Kazakhstan. *The Island Arc*, **9,** 417–427.

Newton, R. C. & Smith, J. V., 1967. Investigations concerning breakedown of albite at depth in the earth. *Journal of Geology*, **45,** 268–286.

Oh, C. W. & Liou, J. G., 1998. A petrogenetic grid for eclogite and related facies under high-pressure metamorphism. *The Island Arc*, **7,** 36–51.

Okamoto, K. & Maruyama, S., 1998. The high pressure stability limits of lawsonite in the MORB + H_2O system. *American Mineralogist*, **84,** 362–373.

Omori, S. & Ogasawara, Y., 1998. “UniEQ”: A computer program package for constructing petrogenetic grids. *EOS transactions, American Geophysical Union*, **79,** F999.

Smith, D. C., 1984. Coesite in clinopyroxene in the Caledonides and its implications for geodynamics. *Nature*, **310**, 641–644.

Terabayashi, M., Ota, T., Yamamoto, H. & Kaneko, Y., 2002. Contact metamorphism of the Daulet Suite by solid-state emplacement of the Kokchetav UHP–HP metamorphic slab. *International Geology Review*, **44,** 819–830.

Table II–1. List of retrograde hydrous minerals, amount of infiltrated retrograde water and volume proportion in the massif of each lithology.

lithology		eclogite	metapelite	orthogneiss	leptite
retrograde (abundant)	mineral	Amp (Hbl~Brs)	Bt		
			Ms (low celadonite)		
retrograde (minor)	mneral	Ep/Czo	Chl	Bt	Bt
		Chl		Ms (low celadonite)	Ms (low celadonite)
		Ttn			
retrograde (wt%)	water	1.0	0.6	0.0	0.0
volume (%)	proportion	2	39	12	12

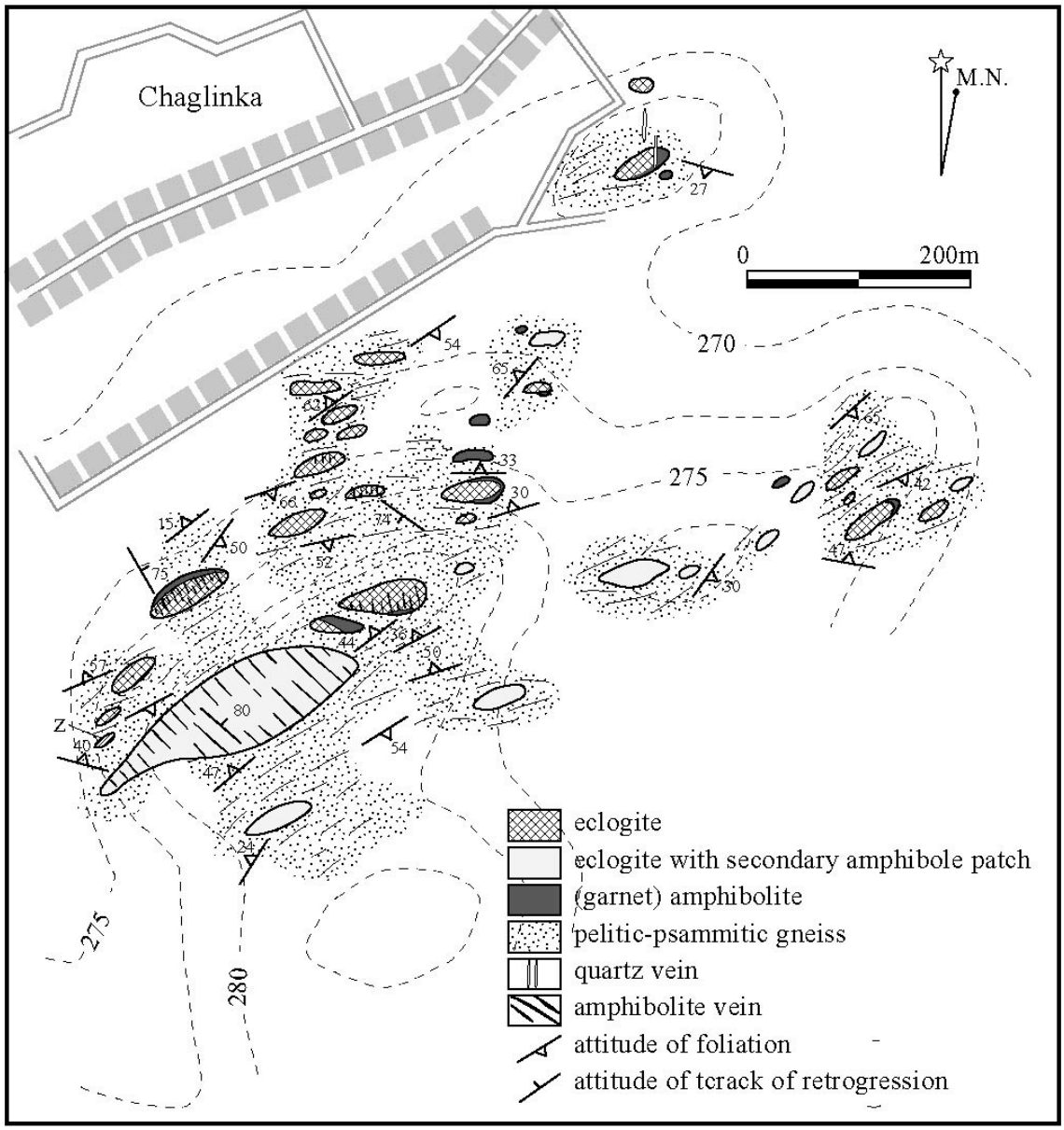

Fig. II–1 Geologic map and of the Chaglinka region indicating the distribution of fresh and amphibolitised eclogite (Kaneko *et al*., 2000).

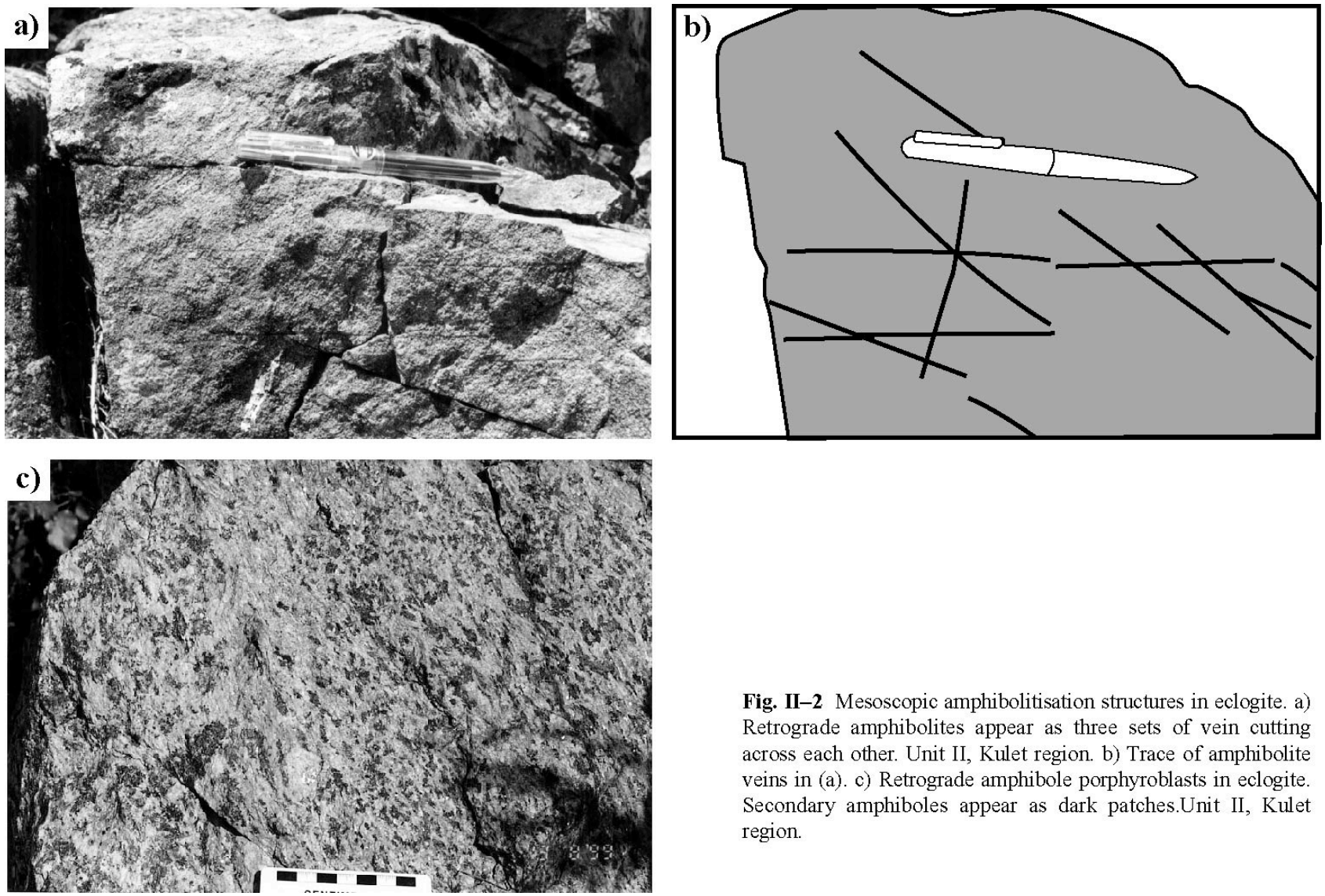

Fig. II–2 Mesoscopic amphibolitisation structures in eclogite. a) Retrograde amphibolites appear as three sets of vein cutting across each other. Unit II, Kulet region. b) Trace of amphibolite veins in (a). c) Retrograde amphibole porphyroblasts in eclogite. Secondary amphiboles appear as dark patches.Unit II, Kulet region.

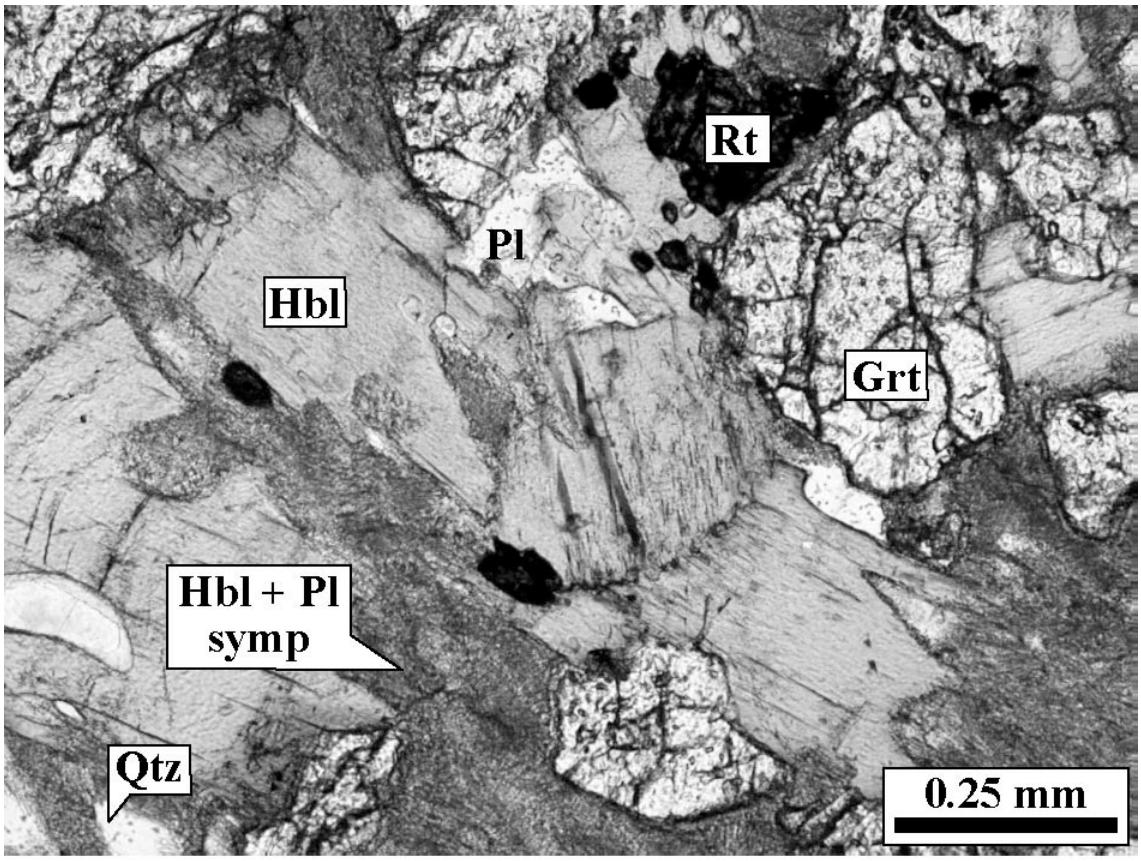

Fig. II–3 Photomicrographs showing the representative minerals and textures of retrograde amphibolite altered from eclogite. symp: symplectite. Plane-polarised light.

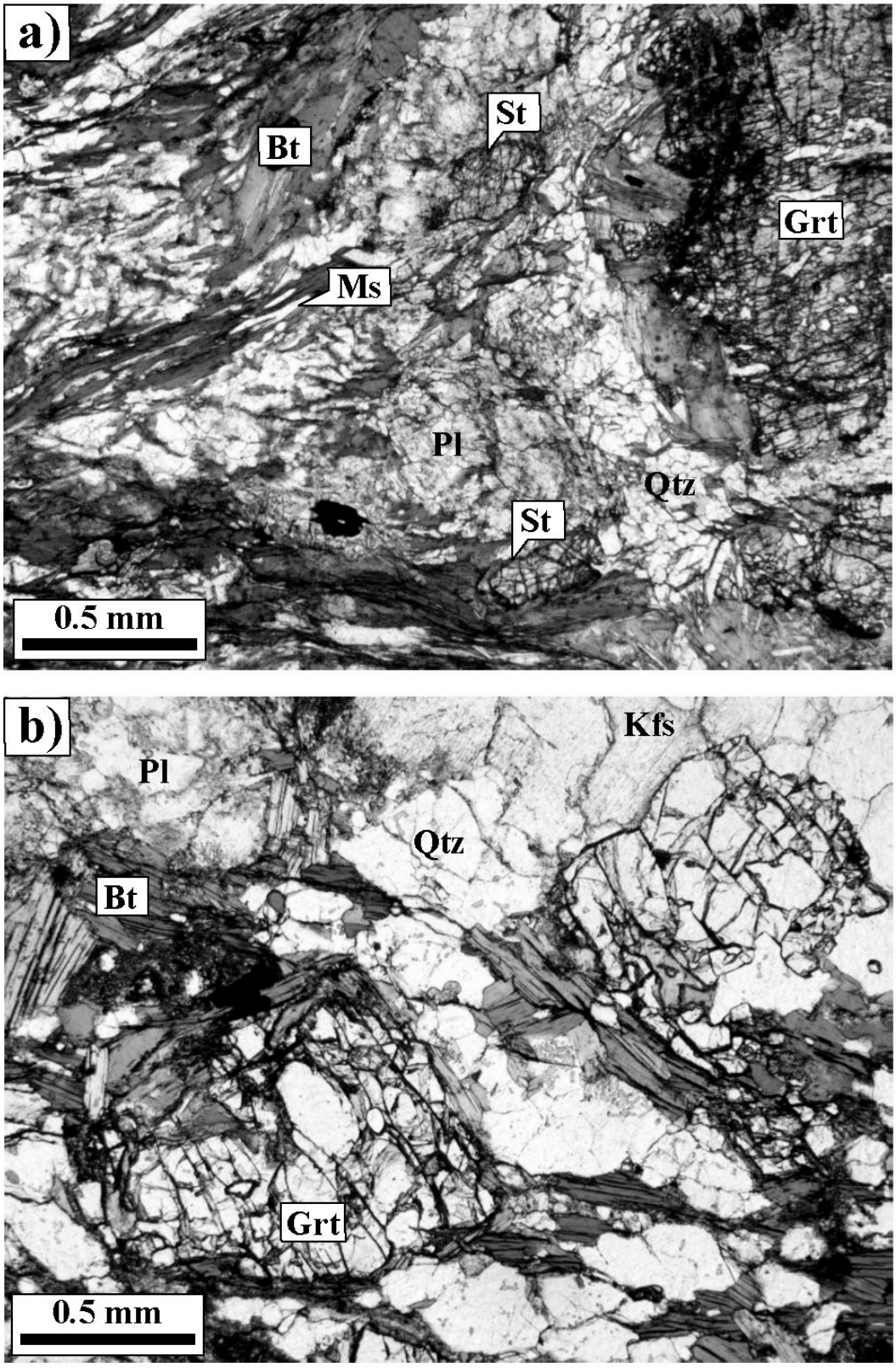

Fig. II–4 Photomicrographs showing the representative minerals and textures of metapelites. a) Grt–St–Bt schist, Chaglinka region; b) Migmatitic gneiss, Kumdy-Kol region. Plane-polarised light.

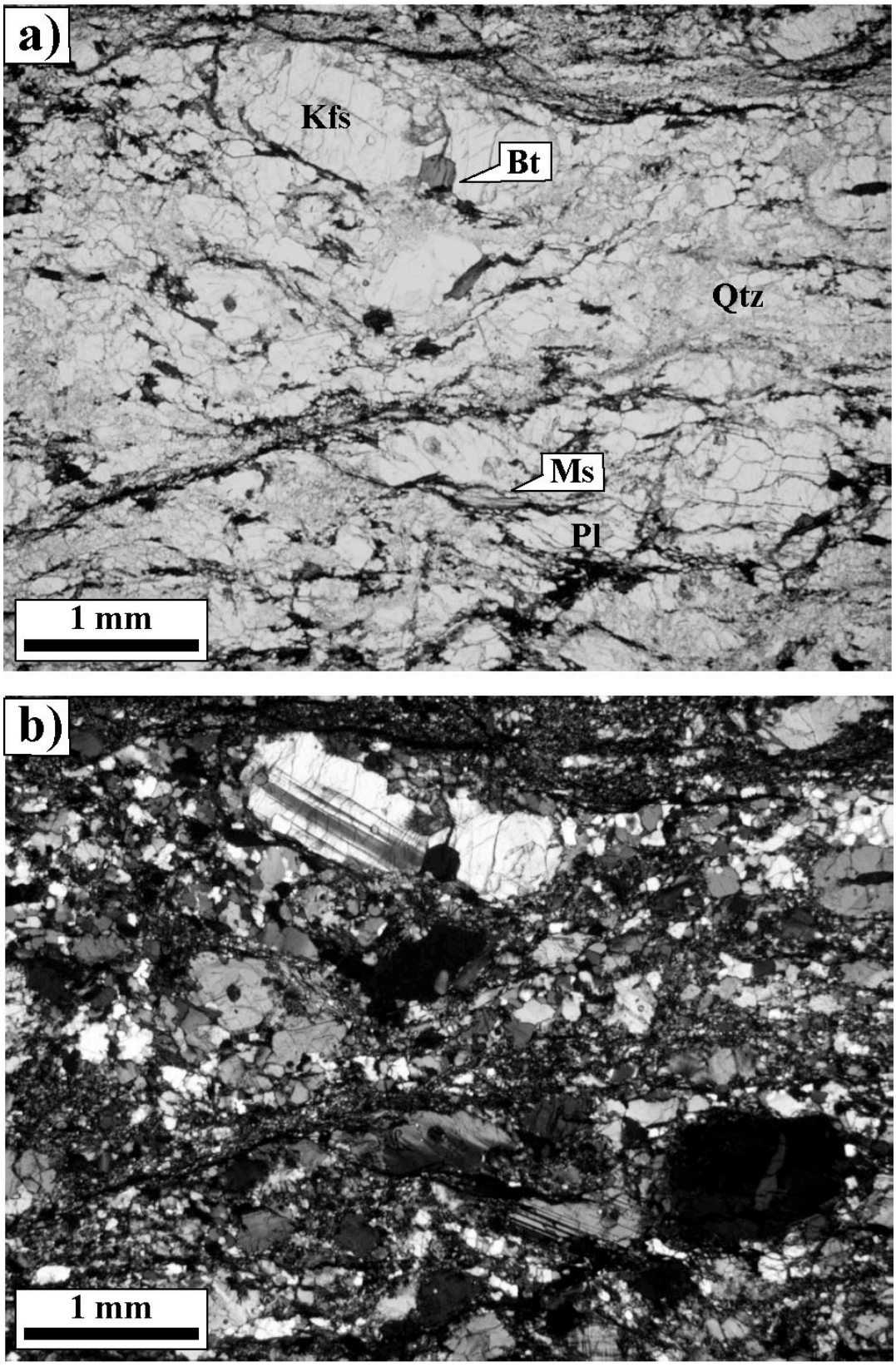

Fig. II–5 Photomicrographs showing the representative minerals and textures of orthogneiss. a) Plane-polarised light; b) Crossed-polarised light.

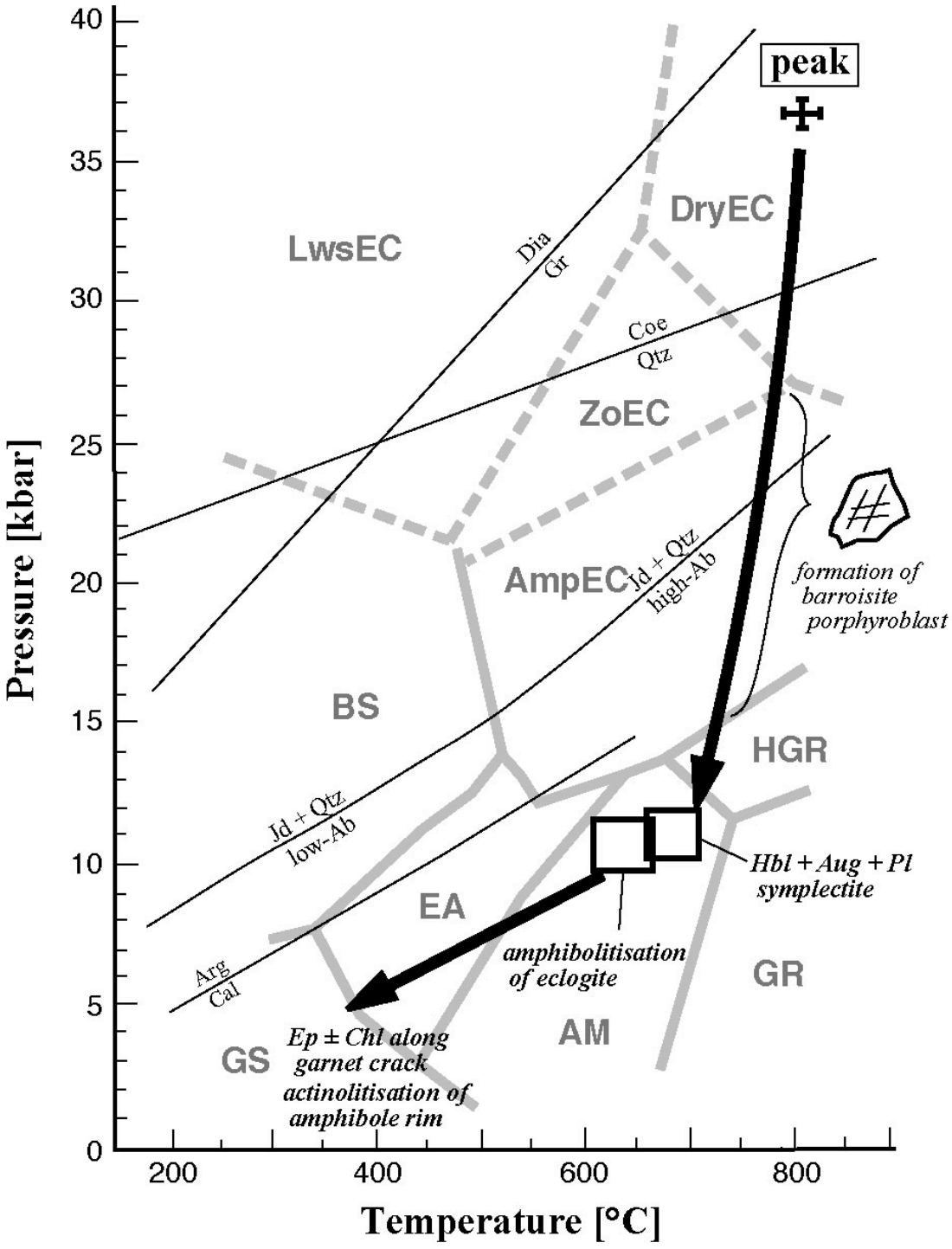

Fig. II–6 Retrograde *P–T* path estimated from the Borovoye eclogites. The *P–T* regimes are after the petrogenetic grid of Oh & Liou (1998) and Okamoto & Maruyama (1998) together with the experimenatally determined stability fields for diamond/graphite (Bundy, 1980), Coe/Qtz (Bohlen & Boettcher, 1982), Jd + Qtz = high-Ab (Holland, 1980), Jd + Qtz = low-Ab (Newton & Smith, 1967) and Arg/Cal (Carlson, 1983).

CHAPTER III

Prograde *P–T* Record Deduced from Inclusion Mineralogy and Compositional Zonation of Pelitic Garnet

ABSTRACT

It has long been a centre of interest of metamorphic petrology to estimate pressure–temperature–time (*P–T–t*) paths for individual rocks. Garnet is a common mineral in metapelites over a wide *P–T* range. Garnet in metapelite generally has a distinctive compositional zonation, and many metamorphic petrologists have drawn *P–T* path using zoned garnet. In this chaper, *P–T–t* path was estimated for whiteschists from the Kulet region using compositional zoning and mineral inclusions in garnet.

The studied whiteschist consists of coarse-grained matrix of quartz, phengite and talc with porphyroblastic garnet and kyanite and minor amount of rutile. The garnet porphyroblast is generally coarse-grained (up to 3 mm) and contains abundant mineral inclusions. The garnet is generally almandine-rich, and has a distinctive compositional zoning. Almandine component shows a rim-ward increase. Pyrope component is generally low and shows a slight increase towards rim. Grossular component shows the most distinctive zoning pattern. It shows a slight rim-ward increase in the core domain, which is followed by large decreases in the mantle and the rim domains. The zoning pattern of spessartine component is more irregular especially in the core domain, but generally decreases towards rim, which characterizes a prograde zoning. These zoning patterns are commonly observed in every analysed garnet.

Mineral inclusions in the garnet are abundant in the core domain, and relatively rare in the mantle and rim domains. The dominant inclusion mineral is SiO_2 polymorph. It displays a clear zonal distribution in garnet porphyroblast. In the core domain, all SiO_2 phase is monomineralic quartz, which occupies the most population of inclusions in the core domain, whereas coesite and its pseudomorph are found in the outermost mantle domain. Next to quartz, Ti-phase inclusions are abundant throughout the core and mantle domains. They also display a zonal distribution. Ilmenite occurs relatively inner part of core domain, and most of which makes a composite inclusion with rutile, whereas monomineralic rutile occurs relatively outer part of core to mantle domains. In the rim region, both of ilmenite and rutile are present, although their population is low. Zircon, apatite, monazite are commonly observed throughout the porphyroblast, and minor kyanite and phengite are observed in the outer-core to mantle domains.

Inclusion thermometry was carried out using ilmenite–garnet thermometer of Pownceby *et al*. (1991). The results range from 500 to 750 °C, and show a systematic

increase from core to rim in each porphyroblast. In the kyanite-bearing domain, the following pressure-sensitive reaction can be used for barometry: 3 Fe-Ilm (in Ilm) + Ky + 2 Qtz = 3 Rt + Alm (in Grt). This barometry yielded pressures of 12–13 kbar for outer-core inclusions at given temperatures.

A petrogenetic grid drawn in K_2O–CaO–FeO–MgO–Al_2O_3–SiO_2–H_2O (KCFMASH) model system using a UniEQ computer program of Omori & Ogasawara (1998) enables forward modeling of the compositional zonation in garnet. The change of grossular component along the model *P–T–t* path expected from the forward modeling is close to the observed grossular profile of outer-core to rim domains. No *P–T* constraint is available from thermobarometry in inner-core domain, however, the forward modeling of garnet zoning makes up for the early stage *P–T–t* path of garnet growth.

The estimated prograde *P–T–t* path is counter-clockwise which bents steeply at around 700 °C, 12–15 kbar. This is similar to the metamorphic field *P–T* gradient of the Kokchetav massif deduced from the metabasites of various grade. This result is highly different from the traditionally drawn clockwise *P–T* path in many metamorphic terranes.

INTRODUCTION

It has long been a centre of interest of metamorphic petrology to clarify the pressure–temperature (*P*–*T*) evolution of the metamorphic rocks. There are several basic assumptions which have been used *a priori* in studies of metamorphic petrology. The first assumption is that the prograde metamorphic reactions occur under chemically nearly equilibrated conditions. The second assumption is that back reactions occur only at limited extent after once rocks reached at peak metamorphic conditions. For these reasons, metamorphic rocks can preserve near-peak mineralogy and compositions. This has been the explanation for that high-grade metamorphic rocks are now present metastably on the surface of the earth. Therefore, metamorphic petrology has been including two self-contradictory assumptions on its basement; assuming equilibrium for prograde stage and disequilibrium for retrograde stage. Based on these assumptions, metamorphic petrology has been established theorems about relationship between subduction tectonics and metamorphism, which culminates in 1980's (*e.g*. England & Thompson, 1984; Ellis, 1987). The important conclusive remarks are, 1) regional metamorphism mainly occurs at plate convergent margins, which are classified into oceanic plate subduction zone (B-type convergent margin) or continental collision zone (A-type convergent margin), 2) there is a close relationship between metamorphic facies series and subduction types; A-type has a medium-*P* (Barrovian) metamorphic belt and B-type has a 'paired metamorphic belt' defined as a pair of high-*P* type and low-*P* type metamorphic belts, 3) prograde *P*–*T* path for each individual rock is clockwise in subduction metamorphism, and 4) metamorphic field *P*–*T* gradient is generally not a similar figure of the *P*–*T* paths for individual rocks.

Discovery of ultrahigh-pressure metamorphic (UHPM) rocks has proved most of these concepts are misunderstandings. In all UHPM localities, UHPM indicators such as coesite and diamond are only found as inclusions of rigid minerals (*e.g.* zircon, garnet), and matrix mineral assemblages of the host rocks are almost completely transformed into low-*P* assemblages (*e.g.* Katayama *et al*., 2000). This fact clearly demonstrates that the assumption about the preservation of peak metamorphic condition is wrong. In other words, what the metamorphic petrologists believed to be peak metamorphic evidence was actually a product of retrograde recrystallisation at the mid-crustal level. This caused a catastrophe to the basic concepts which the metamorphic petrology had been

leaned upon. Consequently, many of above-mentioned theorems need to be reevaluated. For example, most of UHPM rocks were reported from continental collision zones, which are formerly classified as medium-*P* type metamorphic belt. It means that the relationship between metamorphic facies series and subduction type mentioned above is no more true.

Discovery of UHPM caused a destruction of the old regime of the metamorphic petrology, and which now needs to be reconstructed. For this purpose, it is essential to collect reliable datasets for each metamorphic belt, about prograde and retrograde metamorphic paths, metamorphic facies series, rock-forming mineralogy, thermobaric structure and so on. In this chapter, a new estimation of the prograde *P–T–t* path from compositionally zoned garnet is demonstrated.

GEOLOGICAL BACKGROUND AND SAMPLE DESCRIPTION

The studied samples are whiteschist from the Kulet region. The Kulet region contains the largest and most complete exposures of Unit II. Eclogites and associated metasedimentary schists are mainly exposed around Lake Zheltau (Fig. III–1) . As is many other parts of Unit II, the geology of this region is characterized by block-in-matrix relationships involving abundant lensoidal eclogite bodies enclosed in the enveloping metapelite. The elongation direction of the eclogite lenses is roughly NE–SW in the eastern half of the region, and NW–SE in the western half; they are roughly concordant with the strike of the foliation of the enveloping schists. The length of the eclogite bodies (long axis) varies from a few metres to approximately 1 km. Relatively small blocks of eclogite are concentrated in the central part on the south side of the lake. The highest metamorphic grades occur in this central part, where coesite inclusions in garnet of whiteschist are common (Parkinson, 2000). Coesite-bearing rocks are limited to a narrow fault-bounded zone in which adjacent eclogites also yield coesite-grade *P–T* conditions up to 31 kbar, 760 °C (Ota *et al*., 2000). Studied samples were taken from a single outcrop this zone.

Studied whiteschist samples are formerly described petrologically by Parkinson (2000). They commonly have matrix mineral assemblages of: Phn + Tlc + Qtz + Ap + Zrn + Rt + Gr with kyanite and garnet porphyroblasts. Matrix is highly foliated defined

by preferred orientation of phengite and talc. Some garnet and/or kyanite form asymmetric porphyroclast systems with tails consists mainly of phengite (Fig. III–2).

Garnet porphyroblasts are generally subhedral, rounded and equant. Size ranges from 0.2 to 3.0 mm in diameter. However, size distribution of porphyroblast in thin section just reflects an apparent diameter, *i.e.* a diameter of intersection plane of the grain and thin section surface. To overcome this problem, size distribution for mineral separates of garnet porphyroblasts was measured. A hand specimen of whiteschist was carefully crashed and separated by combination of conventional panning, magnet separation and finally hand picking, and 50 garnet porphyroblasts of nearly euhedral shape were randomly collected. Their size distribution exhibits a normal distribution ranging from 1.0 to 3.0 mm (Fig. III–3). These garnet grains were mounted and carefully polished to expose the centre of the grain.

All garnet porphyroblasts contain abundant mineral inclusions especially in their core parts. Over 90 % of inclusions are quartz. However, other minerals also present such as rutile, ilmenite, phengite, kyanite, zircon, apatite, monazite and coesite. Parkinson (2000) also reported margarite, phlogopite, talc, zoisite, graphite and chlorite, but these minerals were not observed in this study. Some mineral species have systematic distribution in the porphyroblast, which is described in detail in the following section.

Kyanite occurs as a large porphyroblast reaching up to 2 cm (long axis), and exhibits a sieve texture with abundant mineral inclusions. Most of inclusions are quartz, and rutile, zircon and garnet are also present.

Garnet rim is generally rounded or irregularly embayed. Thin biotite films are formed in some grain boundaries between garnet and matrix phengite, due to retrograde metamorphism.

CHEMICAL PROFILE OF ZONED GARNET

Element analysis of garnet and other constituent minerals was performed using JEOL JXA8800 electron probe microanalyser in the Department of Earth and Planetary Science, Tokyo Institute of Technology. Operating conditions were 15 kV accelerating voltage and 12 nA current. Beam was focused to be < 4 μm. Data were reduced using a

ZAF matrix correction method. Representative mineral compositions are listed in Table 1.

Garnets are basically almandine-rich. Every analysed garnet grain has very distinctive compositional zonation in terms of almandine, pyrope, spessartine and grossular components (Fig. III–4). Cores are rich in spessartine component up to 0.243, which decreases almost uniformly towards rim, indicating a progressive zoning of garnet. Almandine component shows a simple increase towards rim from 0.625 to 0.899. Grossular component shows a complex up and down pattern. It first shows a slight rim-ward increase from 0.098 to 0.121 in the core region, then it drop to 0.088 and followed by a slight increase to 0.092 in the mantle region, then again drops to 0.044 in the outer rim. Pyrope component is generally low, and shows a simple rim-ward increase from 0.034 to 0.092, except for a distinctive drop at the outermost rim (Fig. III–5).

Some trace elements show characteristic concentration in studied garnets. Some analyses yielded high Na_2O content up to 0.08 wt %. Sodium concentration seems to have no systematic distribution in the grain. Titanium content is generally high around Ti-phase mineral inclusions as high as 0.97 wt% (TiO_2). Even apart from Ti-phase inclusions, TiO_2 reaches 0.10 wt%. Phosphorus shows an characteristic concentration pattern. It is almost below detection limit in most part of the grain, however, is reaching up to 0.15 wt% (P_2O_5) only in the rim part (Fig. III–6).

Smaller garnet porphyroblast lacks Mn-rich core. Figure III–5 compares compositional profiles of larger (N307 Grt3-7) and smaller (N307 Grt2-1) garnet porphyroblasts. The smaller porphyroblast has compositional profiles almost identical to those of mantle to rim parts of the larger one. This suggests that nucleation of the smaller porphyroblast began later stage than the larger one. Thus, the larger grains are expected to have more complete chemical and mineralogical record from early to late stages.

DISTRIBUTION OF MINERAL INCLUSIONS IN GARNET

Figure III–7 shows a distribution of mineral inclusions in garnet porphyroblasts. As Parkinson (2000) described in detail, monocrystalline quartz, polycrystalline quartz (probable former coesite) and monocrystalline coesite show a systematic distribution in

a porphyroblast. Garnet core contains numerous monocrystalline quartz inclusions but neither coesite nor its pseudomorph was found. In contrast, garnet mantle contains the latter two although their amounts are far less than the monocrystalline quartz in the core part. In addition to the SiO_2 polymorphs, Ti-phase minerals also show a systematic distribution in a porphyroblast. Ilmenite occurs relatively inner part of core domain, and most of which makes a composite inclusion with rutile, whereas monomineralic rutile occurs relatively outer part of core to mantle domains. In the rim region, both of ilmenite and rutile are present, although their population is low (Fig. III–7).

Zircon is commonly distributed throughout the porphtroblasts. It is rounded and is very small in size (< 5 μm). Apatite is also a common inclusion mineral and distributed throughout the porphyroblasts. It appears as a rod or elongated ellipsoid with length of < 10 μm. It often makes a composite inclusion with monazite. However, there is no systemtic zonal distribution between these two P-phase minerals. Kyanite and phengite are rare inclusion minerals. They appear in outer-core to mantle domains of garnet porphyroblast.

THERMOBAROMETRY

In order to obtain a *P–T–t* path of the garnet growth, thermobarometry was carried out for each Ti-phase inclusion. For temperature, garnet–ilmenite Fe^{2+}–Mn exchange thermometer of Pownceby *et al*. (1991) was applied in the ilmenite stability field. The results are summarised in Fig. III–8. The obtained temperature shows a systematic rim-ward increase in each garnet porphyroblast, even a ±50 °C of uncertainty originated from the calibration of the thermometer is taken into account.

As mentioned in the previous section, Ti-phase mineral inclusions have zonal distribution in a garnet porphyroblast. It is known both as empirically and experimentaly that rutile has more stability field on the higher pressure side than ilmenite (*e.g*. Bohlen *et al*., 1983). Therefore, their distribution in a garnet porphyroblast qualitatively suggests the rim-ward pressure increase. As kyanite was found around the boundary between outer-core and mantle domain of the garnet porphyroblast, the following relatively pressure-sensitive reaction involving rutile and ilmenite can be applied as a barometer: 3 Fe-Ilm (in Ilm) + alminosilicate + 2 Qtz = Alm (in Grt) + 3 Rt.

A reaction curve for this univariant reaction was calculated in the system of $CaO–FeO–MgO–Al_2O_3–SiO_2–H_2O$ (CFMASH), using a computer program 'UniEQ' (Omori & Ogasawara, 1998). For calculations, an internally consistent thermodynamic datasets for minerals of Berman & Aranovich (1996) were utilised. Garnet was treated as a ternary solid-solution of almandine, pyrope and grossular components with a correction for the effect of spessartine component. Ilmenite was treated as a binary solid-solution of Fe-Ilmenite and geikerite (Mg end-member). For monocrystalline ilmenite and rutile inclusions, the above reaction gives the maximum and minimum pressures of their stability, respectively. Results of thermobarometry are summarised in Table III–2.

FORWARD MODELING OF GARNET ZONATION IN A MODEL SYSTEM

A petrogenetic grid for the analysed whiteschist was constructed in the $K_2O–CaO–FeO–Al_2O_3–SiO_2–H_2O$ (KCFASH) model system up to 40 kbar, 800 °C (Fig. III–9a). All the reaction curves and isopleths were calculated by a computer program 'UniEQ' (Omori & Ogasawara, 1998) with using internally consistent thermodynamic parameters of Berman & Aranovich (1996). Bulk composition of the calculated rock was given as K: Ca : Fe : Al : Si = 4.01 : 0.51 : 7.00 : 24.6 : 62.6 (in molar ratio), in excess of H_2O. Garnet was treated as a binary solid-solution of almandine + pyrope and grossular components. Isopleths represents the grossular component in garnet. Results of inclusion thermobarometry, and the peak *P–T* condition (Parkinson, 2000) are also shown.

As is shown in Fig. III–9a, *P–T* conditions estimated for inclusions in inner-core domain are plotted in the kyanite-free fields. This is a serious contradiction. Because the pressure estimation is based on the kyanite-bearing reaction. Therefore, estimated pressure conditions in kyanite-free fields are invalid (temperature is valid because the reaction used as a thermometer does not include kyanite).

A representative profile of the grossular component in a garnet porphyroblast in shown in Fig. III–9b. The parameter X_{Grs}* on the vertical axis is a normalised grossular component in a almandine–pyrope–grossular ternary system which is defined as X_{Grs}* =

Ca/(Fe + Mg + Ca).

A model *P–T* path along garnet growth is shown in the petrogenetic grid. In the following discussion, validity of this path will be confirmed.

Garnet starts nucleation at the point A. The *P–T* condition of this point is not determined. However, as grossular component increases from the point A until B, garnet nucleation must have occurred somewhere around A in Fig. III–9a. There is no alternative *P–T* path to explain the increase of grossular component from A to B. From the point B to C, grossular component shows a large decrease in a narrow temperature zone. This corresponds to the breakdown of staurolite through: 6 St + 29 Qtz = 4 Alm (in Grt) + 23 Ky + 3 H_2O. An increase of almandine component in garnet in compensation of staurolite causes an apparent decrease of grossular component in garnet from the point B to C. Although this is a continuous reaction, its temperature range is rather narrow as 20–25 °C. Consequently, the change of grossular component in the profile becomes very steep. Staurolite is actually not found as an inclusion in garnet. However, staurolite is a reactant in this reaction, which has been consumed in the higher temperature side of this reaction. It is natural that the reactant phase is hard to remain after the reaction as an inclusion. Therefore the lack of staurolite inclusion does not deny the validity of the estimated path from the point B to C. After the point C, no major garnet involving reaction occurs. The only change is a slight increase of grossular component, as a result of an increase of celadonite component in phengitic mica consuming almandine component as a source of Fe. The grossular component keeps increasing very slightly (~2) until the metamorphic peak. The point D is the metamorphic peak of the whiteschist. Coesite inclusions are found in the outermost mantle region. The peak *P–T* condition is estimated as 34–36 kbar, 720–760 °C (Parkinson, 2000). The garnet also grows during the retrograde stage. The rim part, grown during this stage, has very low grossular component, which is not appear on the *P–T* diagram.

This calculation is performed in a model system, hence the absolute values for grossular component have not much meaning. Nevertheless, it should be noted that the relative change of observed grossular component is very well explained by this forward modeling.

DISCUSSION

Diffusion Effect on the Compositional Zonation in Garnet

Diffusion effect is an unavoidable problem in a discussion of chemical zoning in minerals. In analysed samples, Ca has a very sharp zoning pattern which is rather identical to the euhedral shape of garnet, probably parallel to the crystal growth surface. On the contrary, zoning patterns of other three elements are more vague. Concerning Mn, the maximum content part is not necessarily coincides with morphological centre of the grain. This may reflect the difference of the diffusion rate by each element. Further supportive data to this interpretation is given by a Kumdy-Kol garnet. Garnet in the diamond-bearing metapelite from the Kumdy-Kol region (A12) has virtually homogeneous compositions in terms of Fe, Mg, Mn and even Ca. Only pyrope and grossular show a slight increase and decrease in the outermost rim, respectively (Fig. III–10). As diffusion works more effectively at higher temperatures, explanation by diffusion seems to be appropriate.

Diffusion coefficients at 700 °C are 6.82×10^{-24} for Fe, 1.088×10^{-22} for Mg and 3.44×10^{-24} for Ca (Chakraborty & Ganguly, 1992; Schwandt *et al.*, 1996). It is noted that the diffusion coefficients of Fe and Ca are the same order of magnitude. This means that the difference of zoning pattern between Ca and Fe is not necessarily reflects the difference of diffusion rate. Magnesium has much faster diffusion than Fe and Ca. Diffusion distance for each element was calculated at 700 °C and 750 °C, and at various time after the original growth zoning was formed (Table III–1). Assuming a sharp concentration boundary, and calculated the distance influenced by diffusion is calculated for each element after a certain time. At 700 °C, diffusion distance of Fe becomes 80 μm after 30 m.y., and 104 μm after 50 m.y.. Diffusion distance for Ca is 57 μm and 74 μm for the same time duration, respectively. On the other and, Mg yielded much larger distance as 319 μm and 412 μm for 30 and 50 m.y., respectively. Calculation at 750 °C yielded about twise as large diffusion distance as that at 700 °C for each element. 30–50 m.y. is rather reasonable time compared to the chronological constraints of 30 m.y. for the duration from the peak to the Barrovian metamorphic stages (Katayama *et al.*, 2001). The obtained diffusion distance for each element at 700 °C is almost consistent to those expected from the observed profiles (Fig. III–8).

Calculated diffusion distance at 1000 °C is also listed in Table III–1. This

temperature corresponds to the peak metamorphic temperature of the Kumdy-Kol region. At this temperature, diffusion rates become imcomparably faster than those at 700 °C. The obtained diffusion distances for Fe and Mg are larger than a radius of garnet even after 5 m.y. Although the difference between Ca and other elements becomes larger than at 700 °C, Ca is also homogenised after 30 m.y.

Indeed diffusion effect is one of the possible explanations for the relatively vague zoning patterns of Fe, Mg and Mn, but there is another possibility that zoning patterns of these elements are originally not as sharp as Ca. To test this possibility, a forward modeling of garnet zoning in the system of K_2O–FeO–MgO–Al_2O_3–SiO_2–H_2O (KFMASH) was performed. A petrogenetic grid was calculated in this chemical system up to 40 kbar, 800 °C (Fig. III–11). The program and thermodynamic data were same as those used for the calculation in the KCFASH system. Garnet was treated as a binary solid-solution of almandine–pyrope series, and activity correction for 10 mol% of grossular was made. A model *P*–*T*–*t* path obtained from inclusion thermobarometry and zoning pattern of grossular component is also shown. Pyrope component starts increasing at 550 °C, and continues to increase until around 600 °C. The increase of pyrope component along the model path is almost constant throughout the garnet growth. It is contrasting to the change of grossular component, which has a steep gradient between the points B and C on the *P*–*T*–*t* path in Fig. III–9b. This result suggests that almandine–pyrope series garnet originally has a continuous concentration gradient, which does not mark a sharp boundary between core and mantle.

Another problem about diffusion effect is reequirilibrium on garnet–ilmenite thermometry. In the previous discussion, temperature yielded from garnet–ilmenite thermometry is assumed to be the temperature when the ilmenite was included. If later diffusion effect caused a reequilibration between ilmenite and host garnet, the result of thermometry is meaningless. One reason that the obtained temperatures are believed to be original is that their distribution shows a rim-ward increase. This assures for that the *P*–*T* path obtained from the inclusion thermobarometry is quantitatively valid. And if diffusion effect have worked, the temperature for each inclusion tends to homogenised. The obtained tempeatures form inclusion thermometry range over 500–700 °C, which covers almost entire temperature range of garnet stabitlity in a studied rock. Hence it is not realistic to assume they originally have wider temperature variation than present.

Fractional Crystallisation of Garnet

In the previous discussions, equilibrium recrystalisation has been assumed. That is assuming the equilibrium of all phases present in the assemblage at all times. This model assumes chemical homogenenity of every mineral phase, hence compositional zoning is denied in such a situation. A more realistic model is the fractional crystallisation model assuming local equilibrium at rims of the presents phases, and inside of the grain is regarded to be isolated. This model is often used in a situation of crystallisation from melt in igneous petrology. Garnet in this study has very distinctive compositional zonation. This clearly suggests the equilibrium crystallisation model is inappropriate. In the fractional crystallisation model, the bulk chemistry changes associtaed with crystal (in this case, garnet) growth. In the following discussion, crystal growth of garnet is simulated with taking into consideration of its fractionation effect.

In this simulation, the following assumptions are made: 1) garnet core is isolated from the system once they crystalised; 2) all the phases other than garnet is regarded to be homogeneous and chemically active all the times; and 3) equilibrium in the system is maintained at the rim of garnet and the other minerals. Under these assumptions, garnet growth along the model *P*–*T* path estimated in the previous paragraph was simulated in a changing bulk composition by its fractional effect. The simulation was performed using UniEQ computer program of Omori & Ogasawara (1998) and thermodynamic parametres of Berman & Aranovich (1996).

The result is summarised in Table III–4. The mole fraction of newly cystallised garnet in each *P*–*T* section (DGrt) and its composition in terms of X_{Grs} are listed. The column between these shows the integrated molar volume of crystallised garnet. Garnet shows a highly discontinuous reaction. The garnet growth is restricted to three stages. In very low-grade stage, 67 % of garnet is crystallised. Second growth stage corresponds to the staurolite breakdown event, which is labeled as B ~ C on the model *P*–*T*–*t* path (Fig. III–9). In this stage, 23 % of newly crystallised garnet is added to the formerly crystallised core. The last stage of garnet growth occurs beteen 9.5 to 10.5 kbar, 665 to 679 °C. In this stage 9 % of garnet has overgrown. No garnet involving reaction is predicted from the petrogenetic grid. And after that, garnet growth ceased. This cannot explain the growth from the point C to D on the *P*–*T*–*t* path.

A slightly modified model is applied. In the previous model, all the crystallised garnet is assumed to be chemically isolated from the system. However, a certain depth

from the crystal growth surface may be reactive. As this effect is taken into account, 90 % of crystallised garnet is removed from the system in the following model. The result is shows no significant difference from the previous calculation (Table III–5). Growth of garnet becomes slightly more continuous than the complete fractional crystallisation model. And garnet grows continuously between the second and third growth stages of the previous model. However, virtually no growth is calculated after that, as is the case with the previous model.

Assuming the point A is the grain nucleation centre, the radius ratio at the points B, C and D is 3 : 5 : 6. Acoordingly, the volume ratio of newly grown garnet from A to B, B to C and C to D is calculated as 13 %, 45 % and 42 %, respectively. This is highly inconsistent with the numerical simulation of garnet growth. A large amount of growth after the mantle domain of garnet cannot be explained by this model.

P–T–t Path and Metamorphic Field *P–T* Gradient

Thermobarometry using Ti-phase inclusions and a thermodynamic forward modeling of grossular zoning succeeded to reveal a major part of prograde *P–T–t* path for the whiteschist. The obtained *P–T–t* path is a counter-clockwise curve with a clipping point around 700 °C, 12–15 kbar. Above this point, d*P*/d*T* of the path becomes steeper than the lower-grade part. This result is highly different from the traditionally drawn *P–T* path in many collisional metamorphic belt of the world.

Estimation of the *P–T–t* path from zoned garnet has a long history in the study of metamorphic petrology. It has been a major branch in metamorphic petrology since the advent of electron microprobe in 1960's, which enabled a micron-scale *in-situ* chemical analyses. With an influence of electron microprobe, study of chemical zoning in metamorphic minerals has become popular, and estimation of *P–T–t* path from zoned minerals especially from garnet, has culminated in the late 1980's to early 1990's. Figure III–13 is an example of an estimation of *P–T–t* path using the Gibbs method by Spear (1993). Figure III–13a illustrates a hypothetical zoning profile of garnet. From the paired compositions of almandine and grossuar components at eight points from core to rim, *P–T–t* path was estimated as shown in Fig. III–13b. The obtained path is clockwise. It first experienced nearly isothermal pressure increase followed by heating with gently decreasing pressure. Although this is an extreme example as it is hypothetical, many metamorphic studies have obtained more or less similar *P–T–t* path. The largest

problem of the Gibbs method is equilibrium mineral assemblage must be given arbitrary. Therefore, if the given assemblage was wrong, it gives a wrong path. Many previous workers assumed equilibrium of the present matrix assemblage with garnet throughout its growth. This is the largest misassumption in the *P–T–t* path estimation. The most problematical mineral is plagioclase. Plagioclase is one of the commonest metamorphic minerals in low- to medium-grade metapelite. However, its stability field does not exceed *ca*. 12 kbar even for the single phase albite. Maximum pressure limit of the stability field of plagioclase solid-solution in a pelitic system is lower than that. Hence the estimated *P–T* path also does not exceed 12 kbar.

In this study, equilibrium matrix mineral assemblages are thermodynamically calculated and some are confirmed as inclusions in garnet. This is because we know the matrix mineral assemblages have experienced nearly complete recrystallisation during the retrograde hydration stage form the inclusion mineralogy of zircon (Katayama *et al.*, 2000). As a consequence, the obtained prograde *P–T–t* path extended far beyond the higher pressure side than plagioclase stability, and is counter-clockwise.

The estimated *P–T–t* path from this study coincides with the metamorphic facies series of the massif (Fig. III–14). Metamorphic facies seres is defined as a curve connecting the peak metamorphic conditions for each individual rock of various grades, which is approximately regarded as a geothermal gradient of the subduction zone where the metamorphic belt was formed. In traditional understanding of metamorphic petrology, metamorphic facies series and *P–T* trajectory of individual rocks do not coincide in general (Fig. III–15a). Nevertheless, *P–T* path deduced from zoning patterns of garnet porphyroblast in whiteschist exactly traces the metamorphic field *P–T* curve obtained from *P–T* estimations of metabasites (Fig. III–15b).

Indeed this seems quite natural, but is highly different from most of the previous results. Hence, the previous workers had to give an ‘unnatural’ explanation for the discordance between the *P–T–t* path of individual rocks and the metamorphic field gradient of the terrane. A plausible explanation for this problem is the retardation of thermal evolution relative to pressure increase. A ‘doubly-thickened crust’ model of England & Thompson (1984) gave a theoritical support to this explanation. The essence of this model is the relaxation of thermal profile made by overthrusted crusts. Contact of the bottom of the hanging wall of about 500 °C and the top of the footwall of 0 °C makes a thermal gap, which changes to recover normal geotherm with time (*see*

discussion in Chap. IV). However, such an ‘unnatural’ explanation is no more needed if the *P–T–t* path of individual rocks coincide with metamorphic field *P–T* gradient, as is observed in the Kokchetav massif.

The next question is whether this is unique to the Kokchetav massif or a common feature to all collisional terranes. The answer to this question will be provided by the reevaluation of *P–T–t* path of other collisional terranes. In many metamorphic belts, peak metamorphic conditions, particularly pressure, could have been underestimated. Recent discovery of HP–UHP minerals from formerly regarded ‘medium-*P*’ type metamorphic belts (*e.g*. Kaneko *et al*., 2001; O’Bbrien *et al*., 2001; Parkinson *et al*., 2001) suggests such a reevaluation is needed.

REFERENCES

Berman, R. G. & Aranovich, L. Y., 1996. Optimized standard state and solution properties of minerals I. Model calibration for olivine, orthopyroxene, cordierite, garnet and ilmenite in the system FeO–MgO–CaO–Al_2O_3–TiO_2–SiO_2. *Contributions to Mineralogy and Petrology*, **126,** 1–24.

Bohlen, S, R., Wall, V. J. & Boettcher, A. L., 1983. Experimental investigations and geological applications of equilibria in the system FeO–TiO_2–Al_2O_3–SiO_2–H_2O. *American Mineralogist*, **68,** 1049–1058.

Chakraborty, S. & Ganguly, J., 1992. Cation diffusion in alminosilicate garnets: experimental determination in spessartine–almandine diffusion couples, evolution of effective binary coefficients and application. *Contributions Mineralogy and Petrology*, **111,** 74–86.

England, P. C. & Thompson, A. B., 1984. Pressure–Temperature–time paths of regional metamorphism. I. Heat transfer during regions of thickened continental crust. *Journal of Petrology*, **25,** 894–928.

Ellis, D. J., 1987. Origin and evolution of granulites in normal and thickened crusts. *Geology*, **15,** 167–170.

Kaneko, Y., Maruyama, S., Terabayashi, M., Yamamoto, H., Ishikawa, M., Anma, R., Parkinson, C. D., Ota, T., Nakajima, Y., Katayama, I., Yamamoto, J. & Yamauchi, K., 2000. Geology of the Kokchetav UHP–HP massif, Kazakhstan, central Asia. *The Island Arc*, **9,** 264–283.

Kaneko, Y., Yamamoto, H., Katayama, I., Misawa, I., Ishikawa, M., Hafees, R. U. & Shiraishi, K., 2001. Coesite inclusions and prograde compositional zonation of zircons in Himalayan gneisses, NW Himalaya, Pakistan: Evidence from SHRIMP-dating of coesite-bearing zircon. Abstract: *UHPM workshop: Fluid/slab/mantle interactions and ultrahigh-P minerals*. Waseda University, Tokyo, 121–123.

Katayama, I., Zayachkovsky, A. A. & Maruyama, S., 2000. Prograde pressure–temperature records from inclusion in zircons from ultrahigh-pressure–high-pressure rocks of the Kokchetav Massif, northern Kazakhstan. *The Island Arc*, **9,** 417–427.

Katayama, I., Maruyama, S., Parkinson, C. D., Terada, K. & Sano, Y., 2001. Ion micro-probe U–Pb zircon geochemistry of peak and retrograde stages of ultrahigh-pressure metamorphic rocks from the Kokchetav massif, northern Kazakhstan. *Earth and Planetary Science Letters*, **188,** 185–195.

O'Brien, P. J., Zotov, N., Law, R., Kahn, M. A. and Jan, M. -Q., 2001. Coesite in Himalayan eclogite and implications for models of India–Asia collision. *Geology*, **29,** 435–438.

Omori, S. & Ogasawara, Y., 1998. "UniEQ": A computer program package for constructing petrogenetic grids. *EOS transactions, American Geophysical Union*, **79,** F999.

Ota, T., Terabayashi, M., Parkinson, C. D. & Masago, H., 2000. Thermobaric structure of the Kokchetav ultrahigh-pressure–high-pressure massif deduced from a north–south transect in the Kulet and Saldat-Kol regions, northern Kazakhstan. *The Island Arc*, **9,** 328–357.

Parkinson, C. D., 2000. Coesite inclusions and prograde compositional zonation of garnets in whiteschist of the Kokchetav UHP–HP massif, Kazakhstan: a record of

progressive UHP metamorphism. *Lithos*, **52,** 215–233.

Parkinson, C. D., Motoki, A., Onishi, C. T. & Maruyama, S., 2001. Ultrahigh-pressure pyrope-kyanite granulites and associated eclogites in Neoproterozoic nappes of southeast Brazil. Abst: *UHPM workshop: Fluid/slab/mantle interactions and ultrahigh-P minerals*. Waseda University, Tokyo, 87–90.

Pownceby, M. I., Wall, V, J. & O' Neill, H. S. T., 1991. An experimental study of the effect of Ca upon garnet–ilmenite Fe–Mn exchange equilibria. *American Mineralogist*, **76,** 1580–1588.

Schwandt, C. S., Cygan, R. T. & Westrich, H. R., 1996. Ca self-diffusion in grossular garnet. *American Mineralogist*, **81,** 448–451.

Spear, F. S., 1993. *Metamorphic Phase Equilibria and Pressure–Temperature–Time Paths*. Mineralogical Society of America, MONOGRAPH, 575–639, Washington, D. C.

Table III–1. Representative analyses of garnet and inclusion ilmenite. A, B, C and D correspond to the points A–D on the line profile in Fig. III–9, respectively.

Garnet	A	B	C	D	**Ilmenite**	
SiO_2	37.28	36.90	37.42	37.25		0.04
TiO_2	0.00	0.06	0.00	0.07		53.53
Al_2O_3	21.39	21.10	21.48	21.19		0.04
Cr_2O_3	0.00	0.02	0.00	0.00		0.00
FeO*	31.40	30.84	36.64	36.89		44.37
MnO	6.67	5.67	0.43	0.24		1.40
MgO	1.18	1.09	2.18	2.01		0.31
CaO	2.56	3.81	1.76	2.04		0.00
Na_2O	0.03	0.04	0.01	0.04		0.03
K_2O	0.01	0.00	0.00	0.01		0.03
P_2O_5	0.00	0.02	0.00	0.00		0.00
Total	100.52	99.55	99.90	99.74		99.75
Si	3.006	3.000	3.015	3.013		0.001
Ti	0.000	0.004	0.000	0.004		1.011
Al	2.032	2.021	2.039	2.021		0.001
Cr	0.000	0.001	0.000	0.000		0.000
Fe^{2+}	2.118	2.097	2.469	2.495		0.932
Mn	0.456	0.391	0.029	0.016		0.030
Mg	0.142	0.133	0.262	0.242		0.012
Ca	0.221	0.332	0.152	0.176		0.000
Na	0.005	0.006	0.001	0.006		0.001
K	0.001	0.000	0.000	0.001		0.001
P	0.000	0.001	0.000	0.000		0.000
Total	7.981	7.985	7.966	7.975		1.989
X_{Alm}	0.721	0.710	0.848	0.852	$X_{Fe\text{-}Ilm}$	0.957
X_{Prp}	0.048	0.045	0.090	0.083	X_{Php}	0.031
X_{Sps}	0.155	0.132	0.010	0.006	X_{Gei}	0.012
X_{Grs}	0.075	0.113	0.052	0.060		

All iron is calculated as Fe^{2+}.

Table III–2. Results of thermobarometry using garnet–ilmenite geothermometer (Pownceby *et al*., 1991) and garnet–alminosilicate–ilmenite–rutile geobarometer.

inclusion No.	distribution	T (°C)	P (kbar)
N306 Grt1			
inc 2	inner-core	568	7.3
inc 5	inner-core	569	7.8
inc 20	outer-core	680	12.6
inc 6	outer-core	745	13.1
N307 Grt3–3			
inc 7	inner-core	535	8.3
inc 8	inner-core	543	7.3
N307 Grt3–8			
inc 3	inner-core	468	-
inc 4	outer-core	501	11.3
inc 5	inner-core	505	-
inc 23	rim	512	-

Table III–3. Diffusion distance of Fe, Mg and Ca in garnet at 700 °C, 750°C and 1000 °C at various time after the original compositional boundary was formed.

	time (m.y.)	diffusion distance (μm)		
		Fe	Mg	Ca
700° C	1	15	58	10
	5	33	130	23
	10	46	184	33
	20	66	261	47
	30	80	319	57
	50	104	412	74
750° C	1	34	126	17
	5	75	281	37
	10	106	397	53
	20	15	561	74
	30	184	687	91
	50	237	888	118
1000° C	1	794	2356	100
	5	1775	5269	223
	10	2510	7452	315
	20	3550	10538	445
	30	4348	12907	545
	50	5614	16662	704

Table III–4. Results of garnet growth simulation in a fractional crystallisation model.

P (kbar)	T (°C)	ΔGrt (mol)	Grt (%)	X_{Grs}
0.7	459	0.000	0.00	-
1.4	509	0.000	0.00	-
2.0	526	0.011	67.01	0.07
2.6	544	0.000	0.00	-
3.1	562	0.000	0.00	-
3.9	577	0.000	0.00	-
4.9	593	0.000	0.00	-
5.9	609	0.000	0.00	-
7.3	630	0.004	23.76	0.13
8.3	648	0.000	0.20	0.08
9.5	665	0.000	0.00	-
10.5	679	0.001	9.03	0.00
11.8	695	0.000	0.00	-
13.1	710	0.000	0.00	-
14.7	725	0.000	0.00	-
16.9	739	0.000	0.00	-
19.6	752	0.000	0.00	-
24.7	769	0.000	0.00	-
34.3	826	0.000	0.00	-

Table III–5. Results of garnet growth simulation in a 90 % fractional crystallisation model.

P (kbar)	T (° C)	DGrt (mol)	Grt (%)	X_{Grs}
0.7	459	0.000	0.00	-
1.4	509	0.000	0.00	-
2.0	526	0.011	60.56	0.07
2.6	544	0.001	5.74	0.07
3.1	562	0.000	0.57	0.08
3.9	577	0.000	0.11	0.09
4.9	593	0.000	0.00	-
5.9	609	0.000	0.00	-
7.3	630	0.004	21.73	0.13
8.3	648	0.001	3.55	0.08
9.5	665	0.000	2.82	0.01
10.5	679	0.001	4.92	0.00
11.8	695	0.000	0.01	0.00
13.1	710	0.000	0.00	-
14.7	725	0.000	0.00	-
16.9	739	0.000	0.00	-
19.6	752	0.000	0.00	-
24.7	769	0.000	0.00	-
34.3	826	0.000	0.00	-

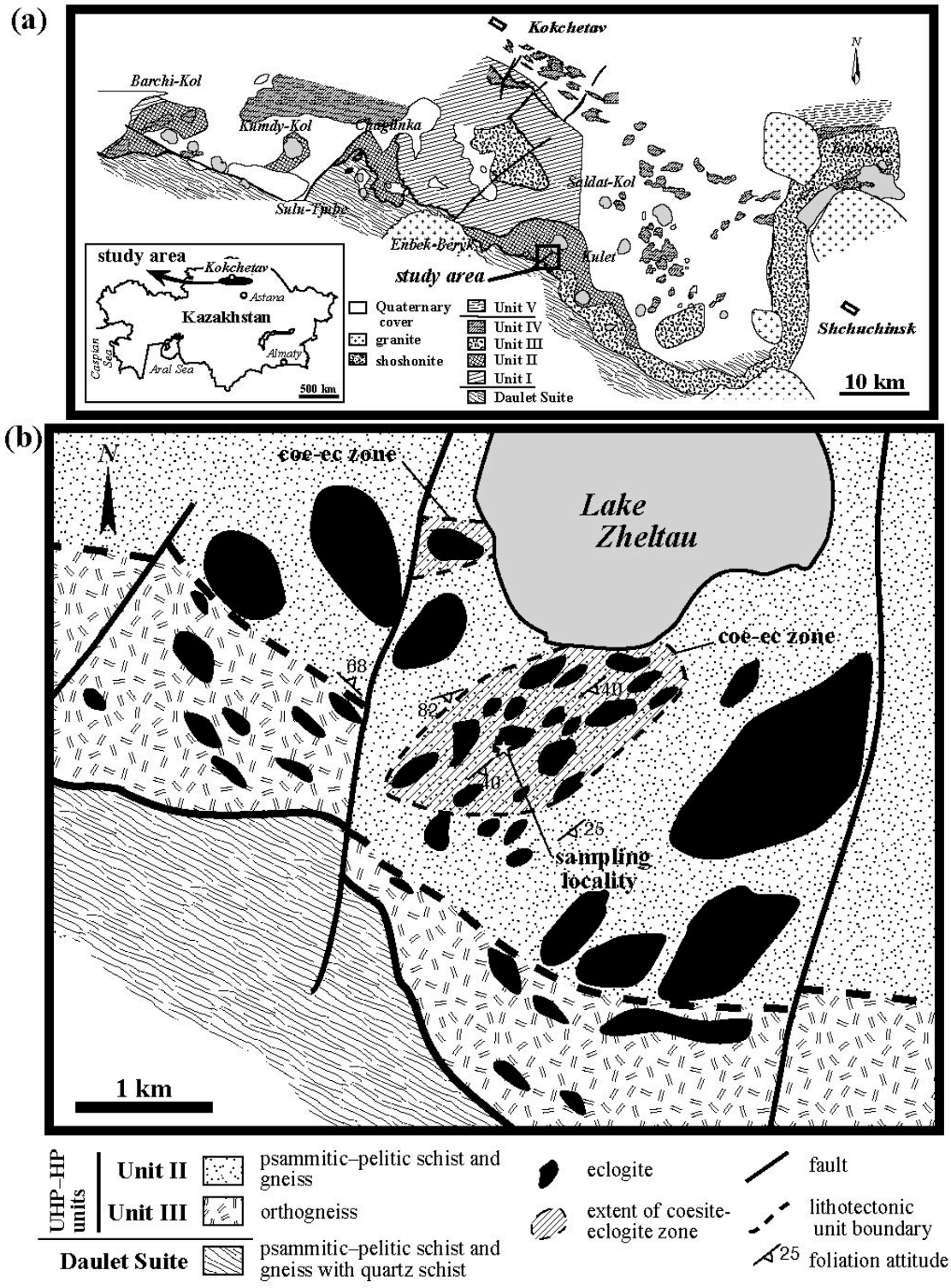

Fig.III–1 a) Simplified geological map of the Kokchetav massif (after Kaneko *et al.*, 2000). Studied area is marked by the square,which is presented in detail in (b). b) Geological map of the Kulet area showing the sampling locality of the studied whiteschists (after Kaneko *et al.*, 2000; Parkinson, 2000). Studied samples are taken from the centre of the coesite-eclogite (coe-ec) zone (Ota *et al.*, 2000).

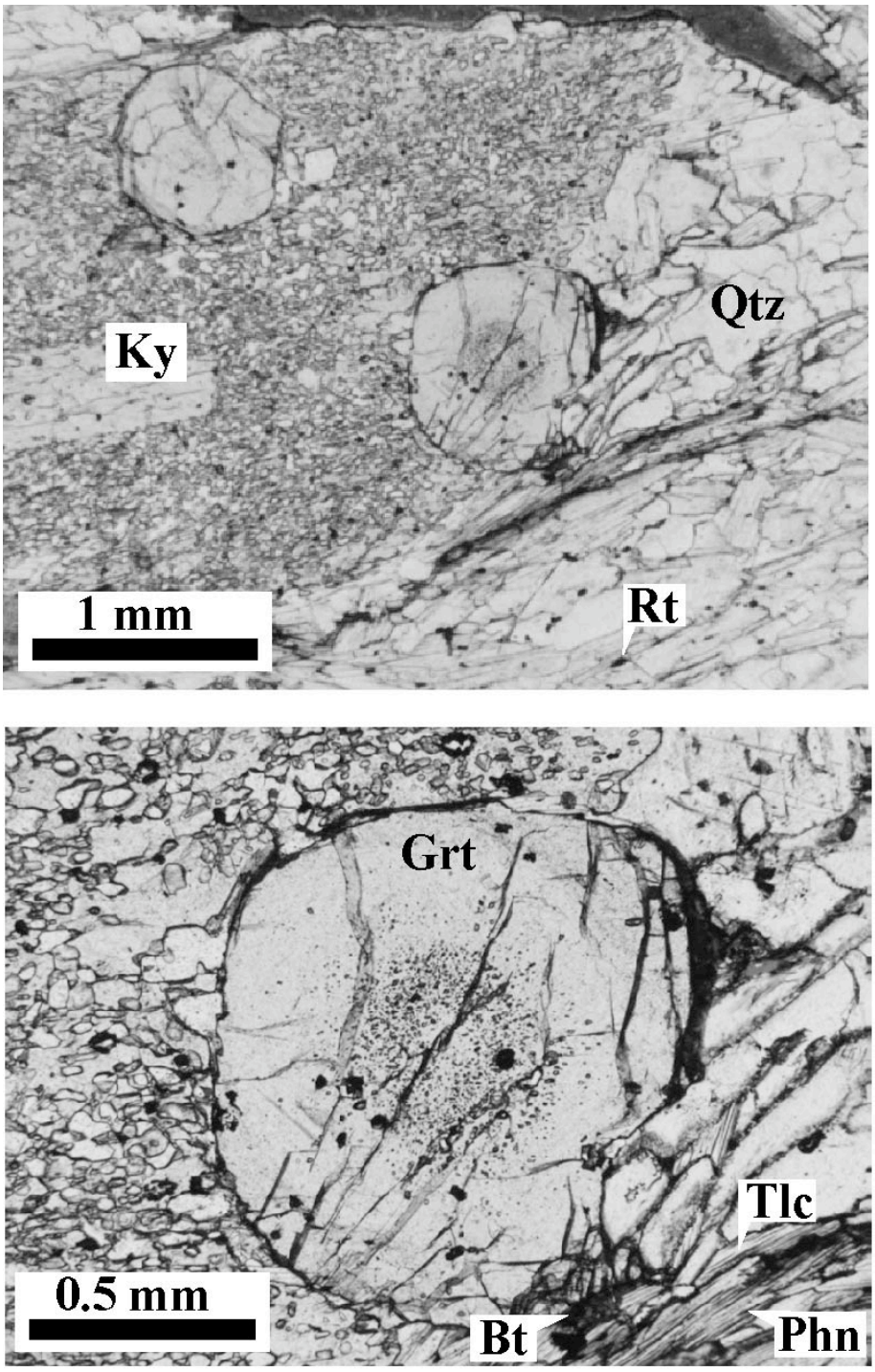

Fig. III–2 Photomicrographs of whiteschist. a) Garnet and kyanite occur as porphyroblasts in a matrix consists of quartz, phengite, talc and rutile; b) Closed view of the central part of (a). Garnet porphyroblast contains abundant inclusions (mostly quartz) particularly in its core part. Secondary biotite, which is partly chloritised, is formed at the boundary between garnet and phengite. Plain polarised light.

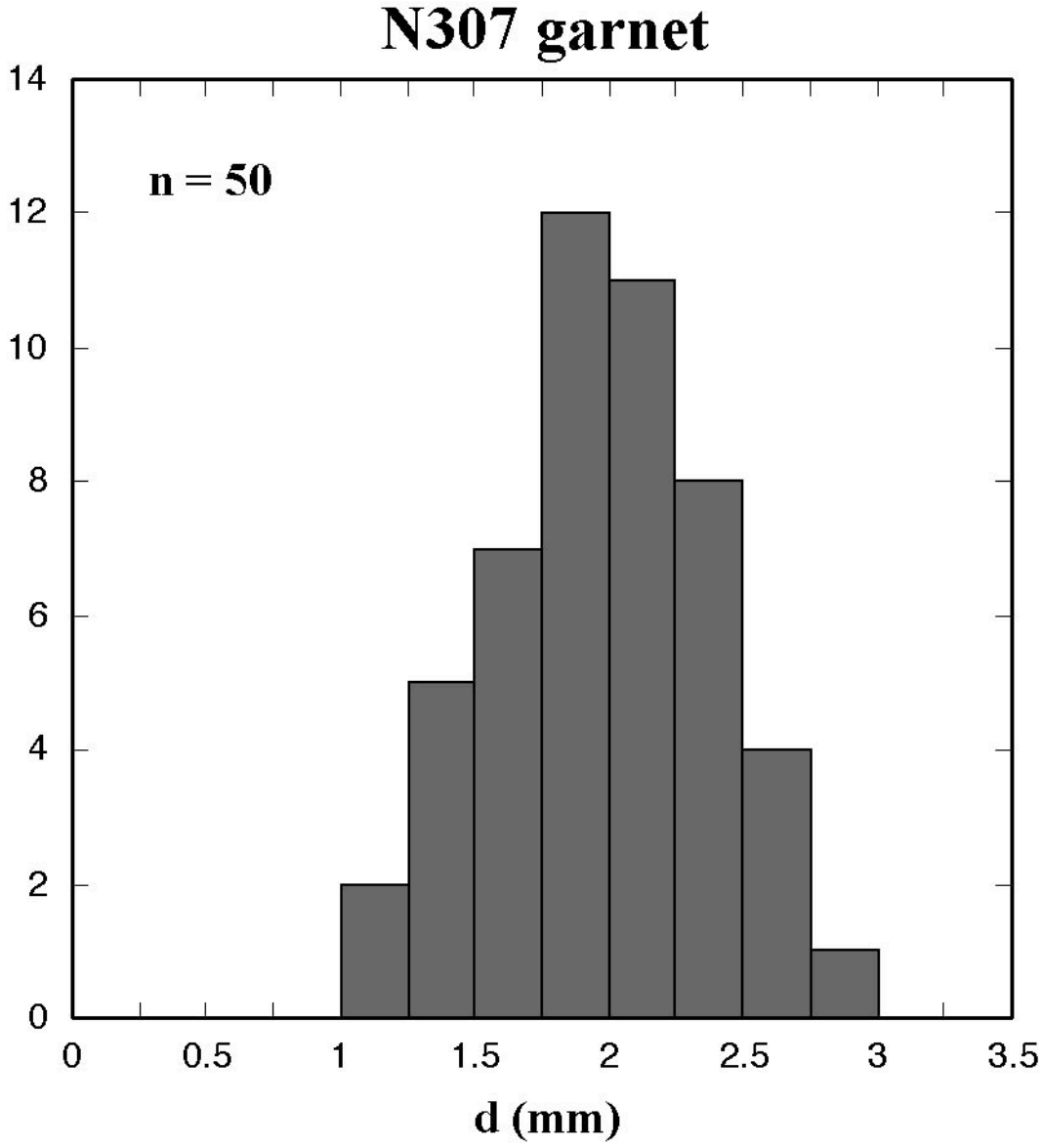

Fig. III–3 Grain diameter distribution of separated garnet grains from N307.

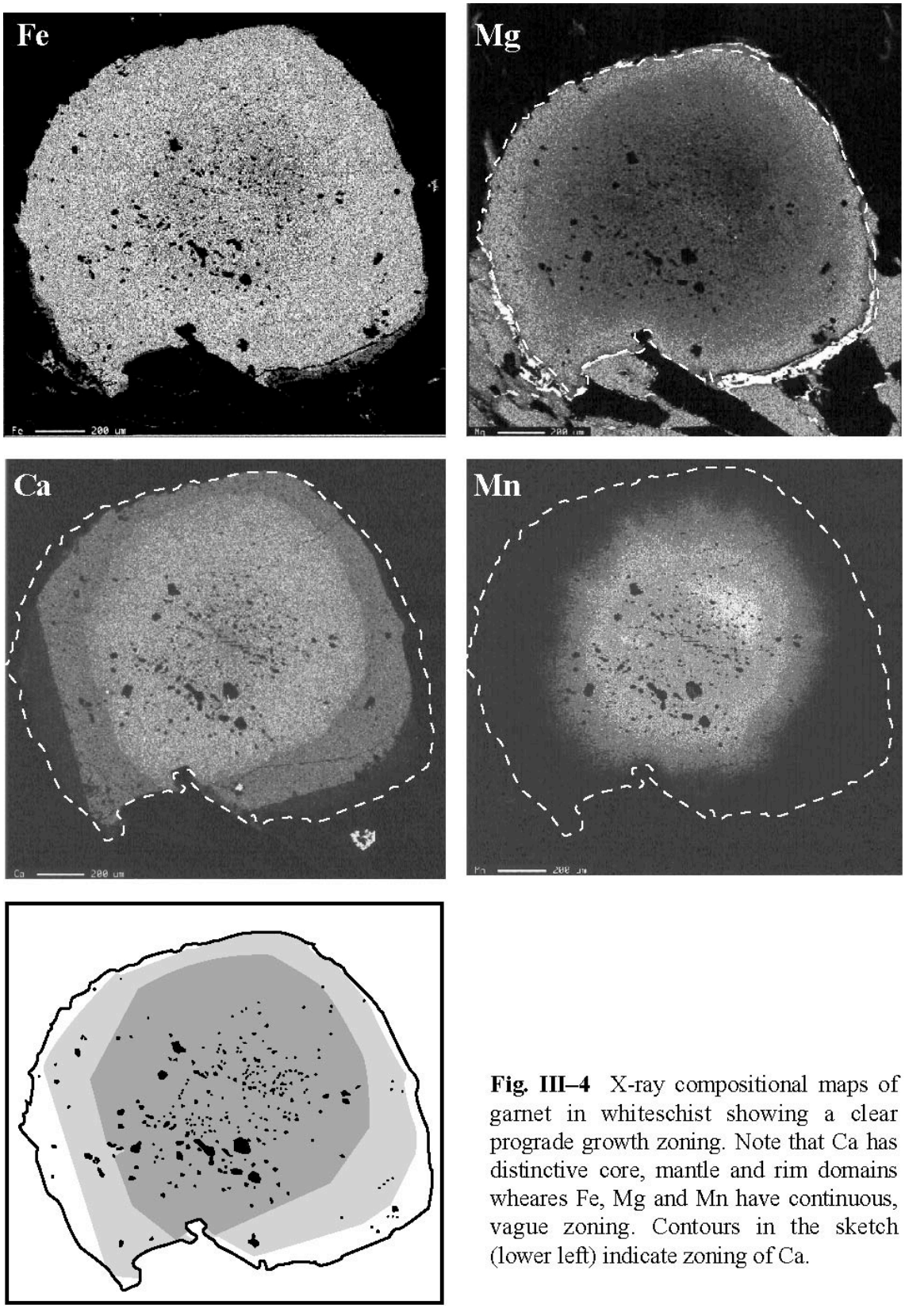

Fig. III–4 X-ray compositional maps of garnet in whiteschist showing a clear prograde growth zoning. Note that Ca has distinctive core, mantle and rim domains wheares Fe, Mg and Mn have continuous, vague zoning. Contours in the sketch (lower left) indicate zoning of Ca.

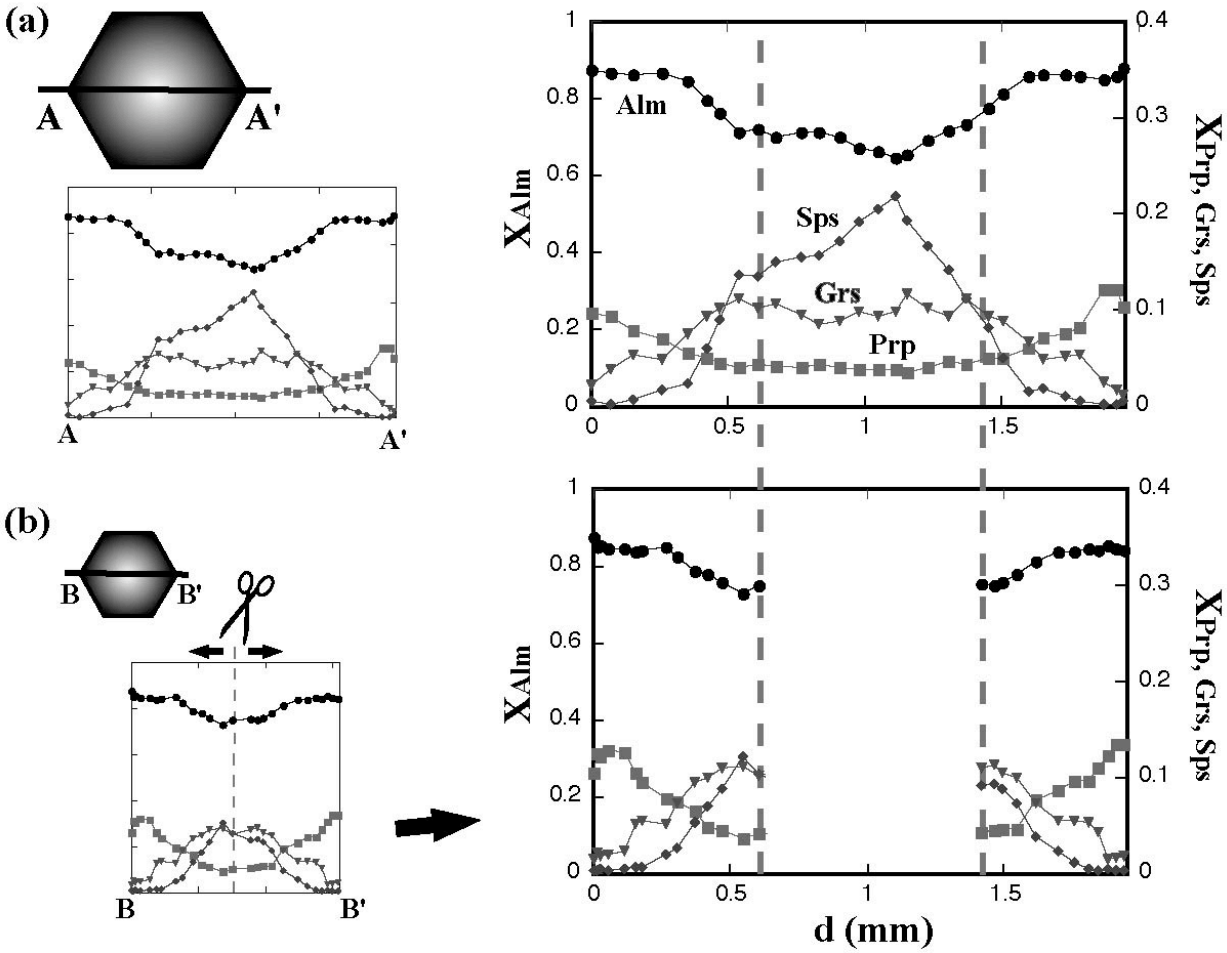

Fig. III–5 Comparison of compositional profiles of a) larger and b) smaller garnet porphyroblasts. The smaller porphyroblast has zoning patterns correspond to the mantle ~ rim part patterns of the larger porphyroblast.

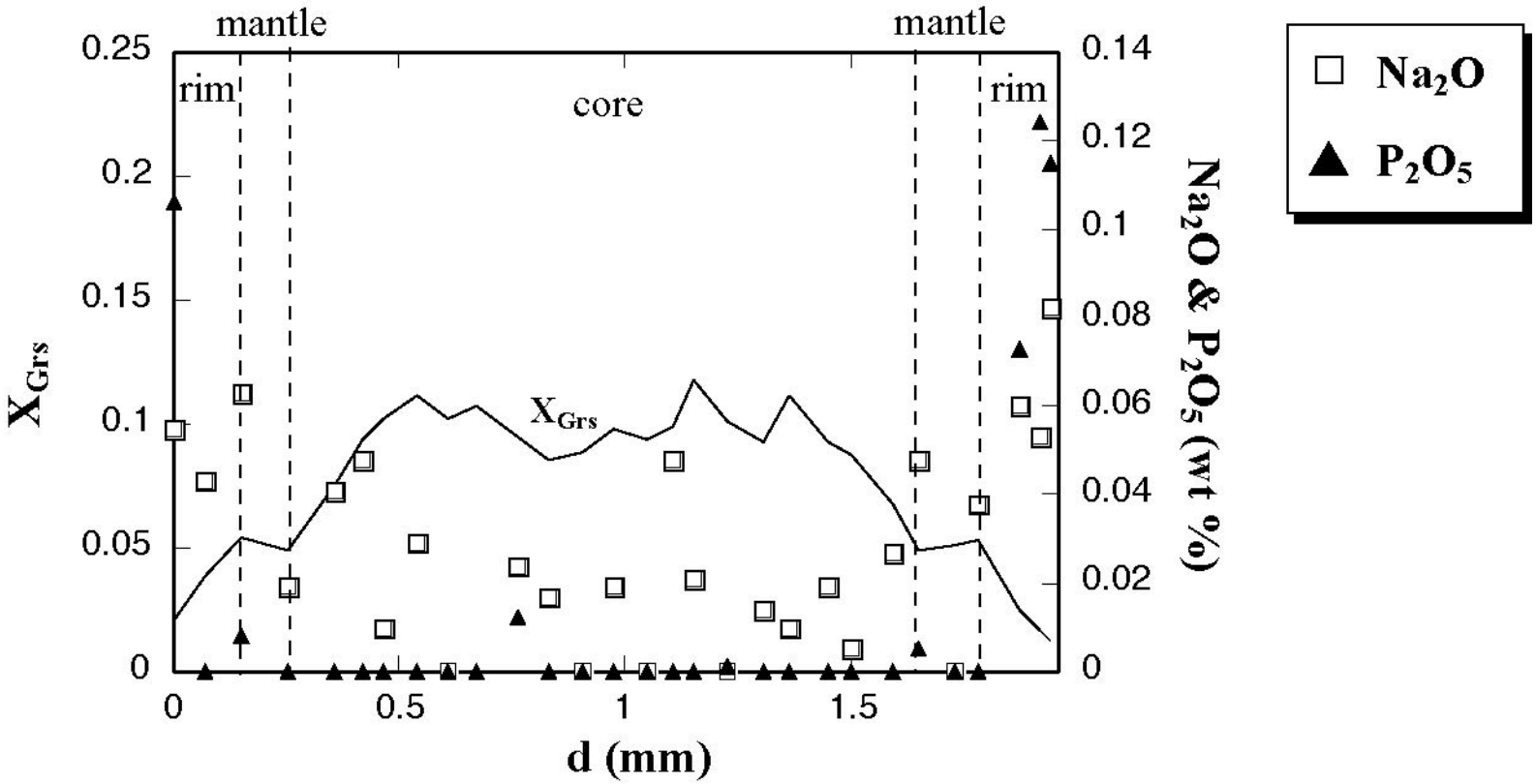

Fig. III–6 Compositional profiles of trace elements in garnet. Core, mantle and rim of garnet is defined by the zoning pattern of grossular component.

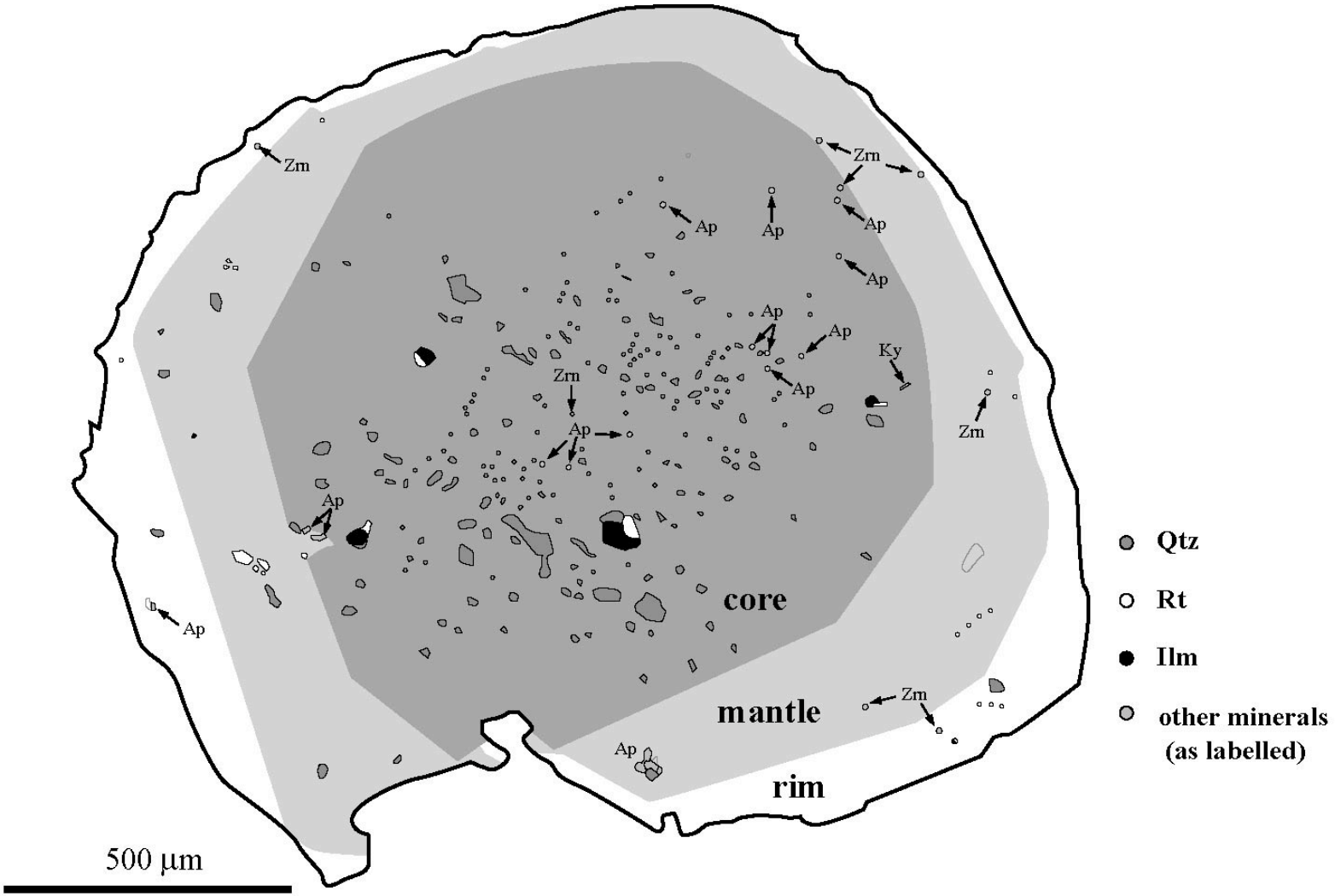

Fig. III–7 Distribution of mineral inclusions in garnet porphyroblast showing the correlation between inclusion assemblages and compositional zonation of garnet. Core, mantle and rim domains of garnet are defined by the difference of grossular component.

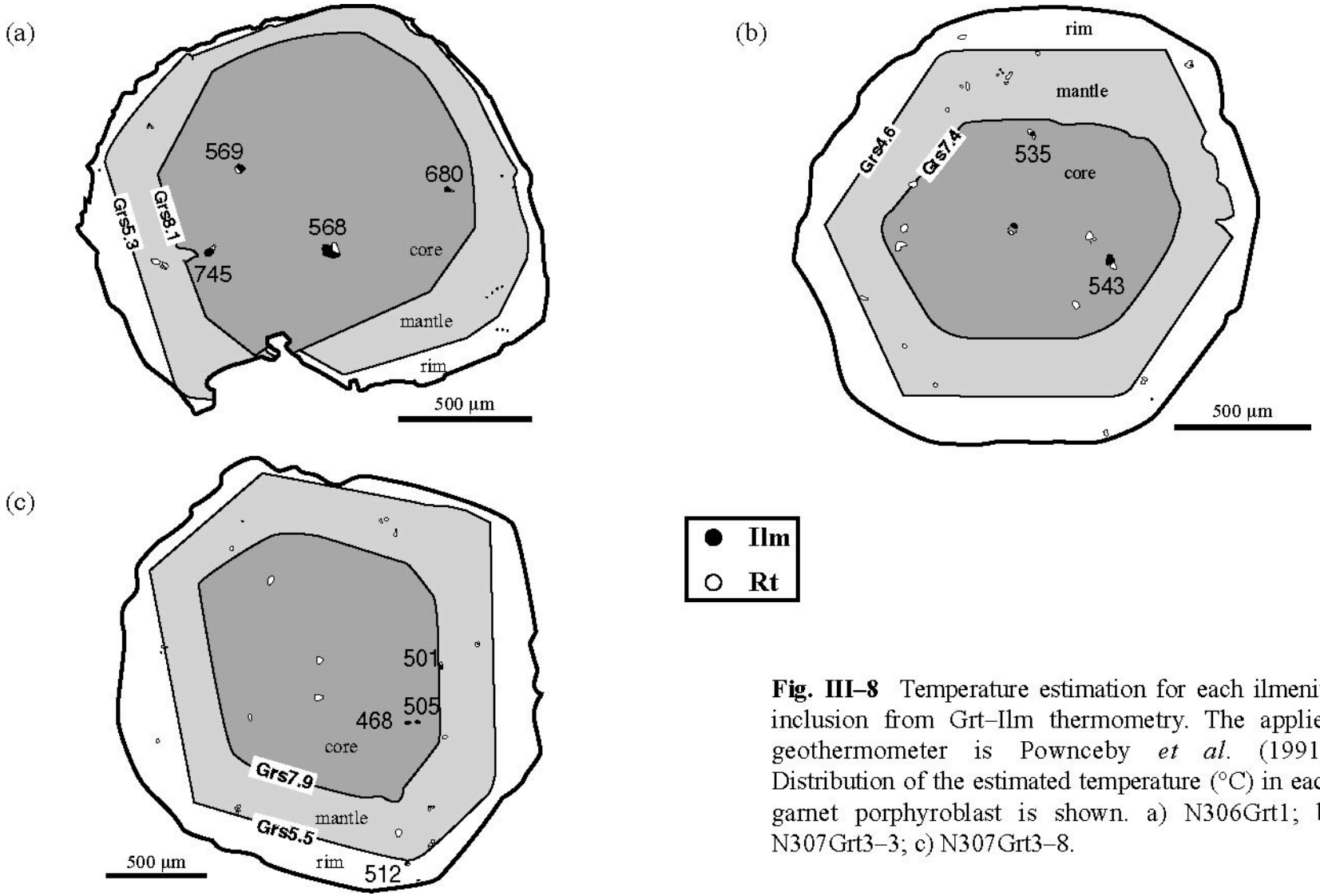

Fig. III–8 Temperature estimation for each ilmenite inclusion from Grt–Ilm thermometry. The applied geothermometer is Pownceby *et al.* (1991). Distribution of the estimated temperature (°C) in each garnet porphyroblast is shown. a) N306Grt1; b) N307Grt3–3; c) N307Grt3–8.

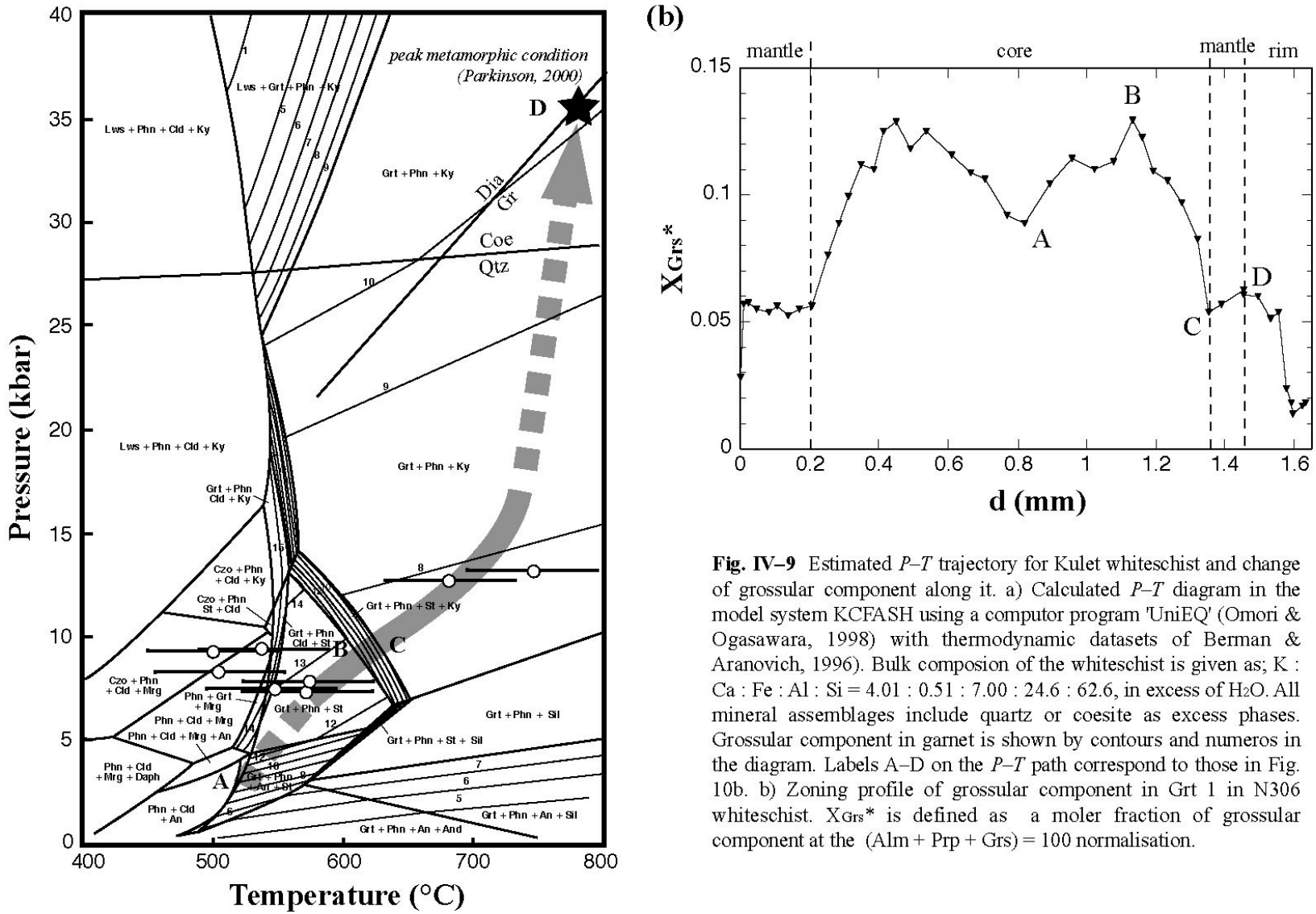

Fig. IV–9 Estimated *P–T* trajectory for Kulet whiteschist and change of grossular component along it. a) Calculated *P–T* diagram in the model system KCFASH using a computor program 'UniEQ' (Omori & Ogasawara, 1998) with thermodynamic datasets of Berman & Aranovich, 1996). Bulk composion of the whiteschist is given as; K : Ca : Fe : Al : Si = 4.01 : 0.51 : 7.00 : 24.6 : 62.6, in excess of H_2O. All mineral assemblages include quartz or coesite as excess phases. Grossular component in garnet is shown by contours and numeros in the diagram. Labels A–D on the *P–T* path correspond to those in Fig. 10b. b) Zoning profile of grossular component in Grt 1 in N306 whiteschist. X_{Grs}* is defined as a moler fraction of grossular component at the (Alm + Prp + Grs) = 100 normalisation.

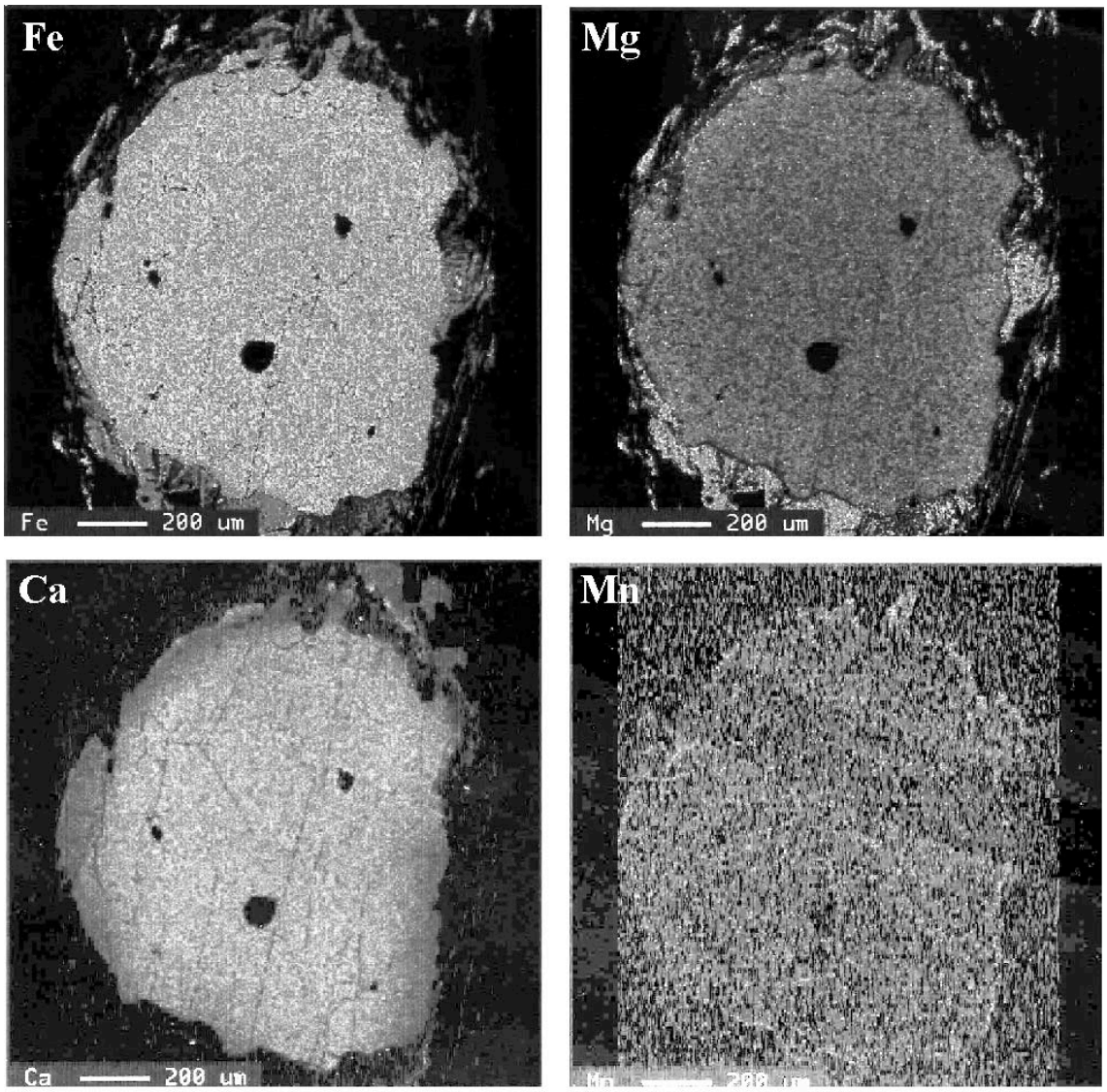

Fig. III–10 X-ray compositional maps of garnet in a diamond-bearing metapelite from the Kumdy-Kol region.

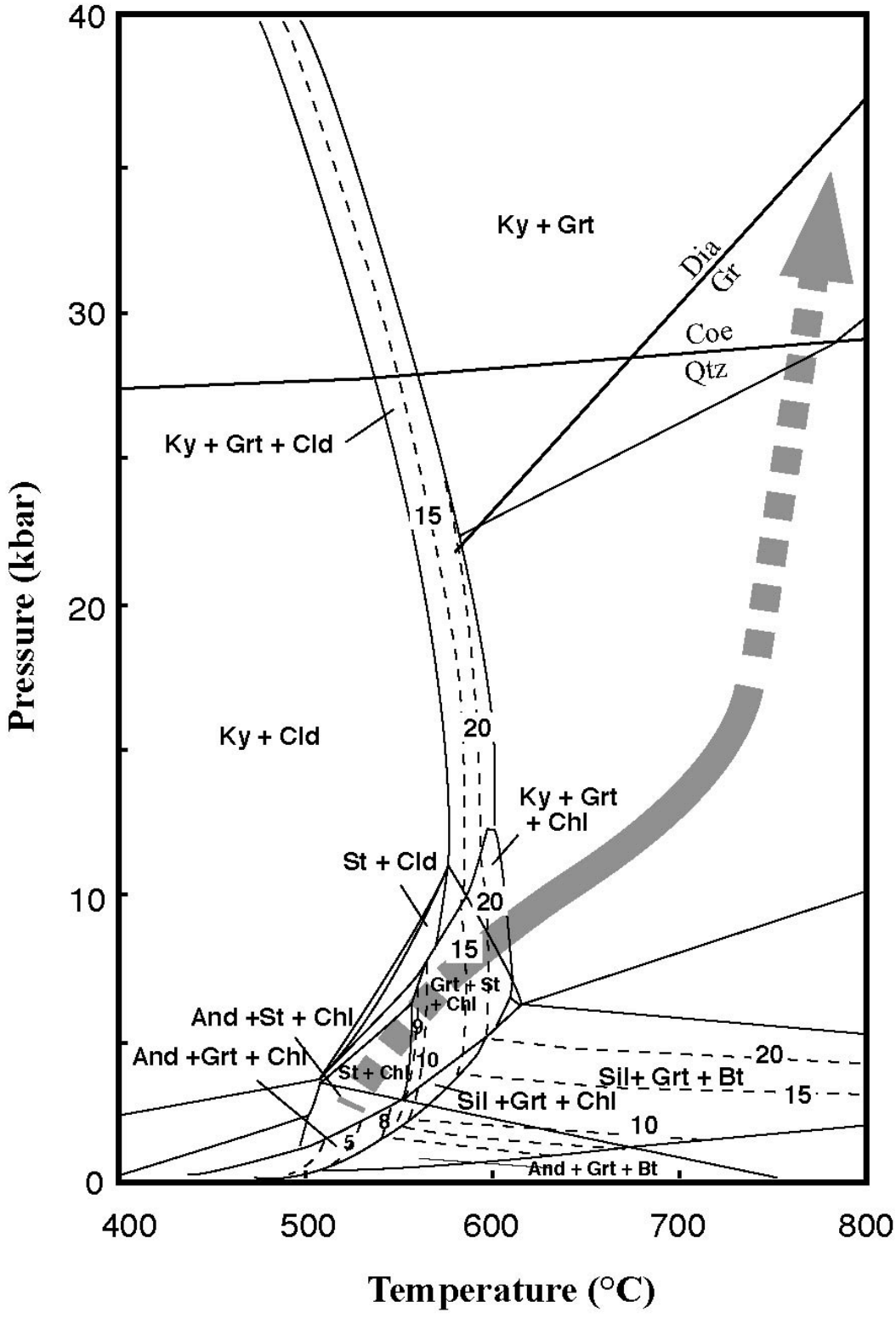

Fig. III–11 Calculated *P–T* diagram in the model system KFMASH. The calculation method and conditions are same as the *P–T* diagram shown in Fig. III–9a. Numeros on the countours (shown in sashed lines) represent pyrope component. A model *P–T* path estimated from the thermobarometry and grossular zoning is also shown as a gray line.

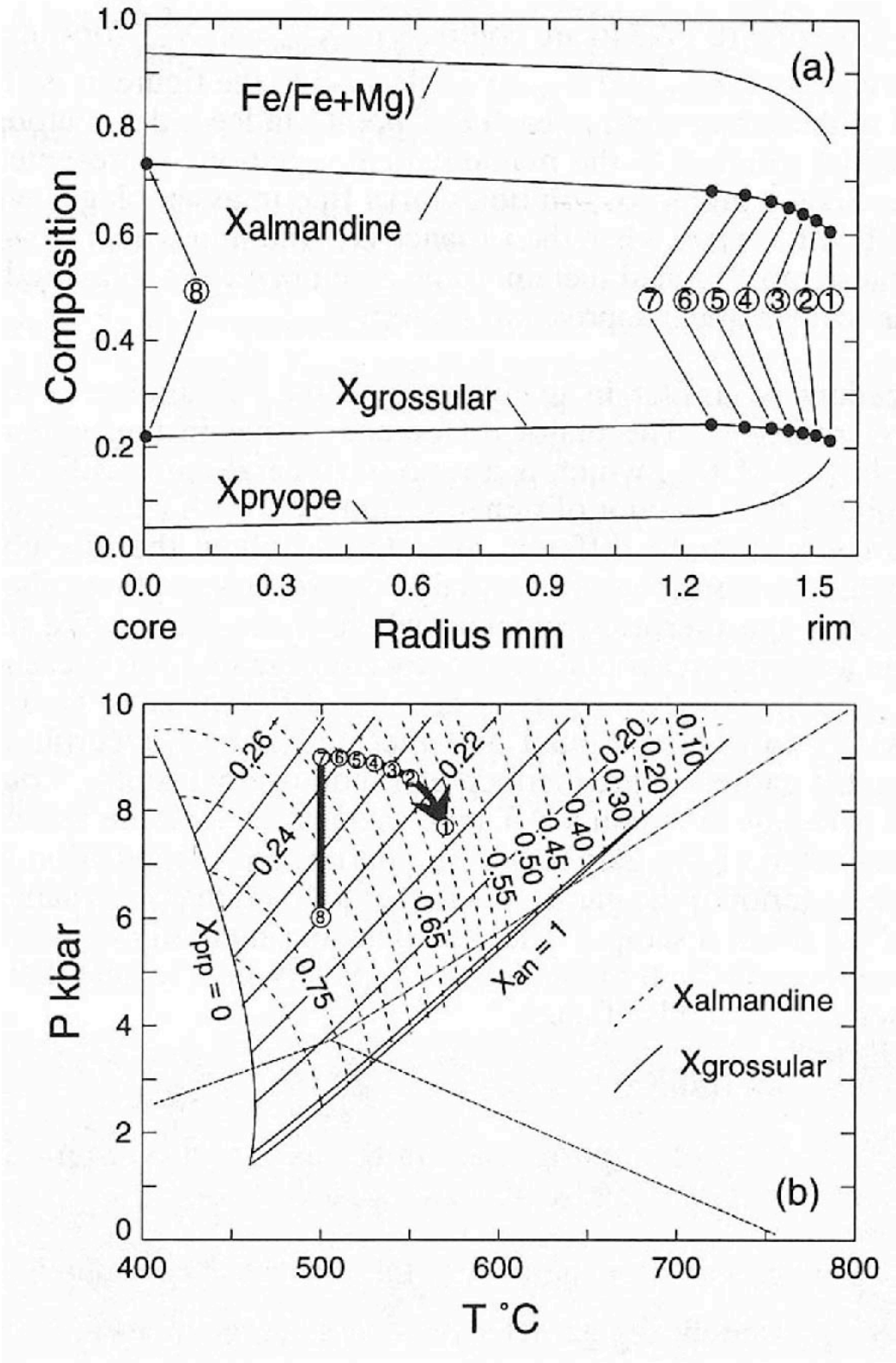

Fig. III–12 An example of *P–T–t* path estimation from compositionally zoned garnet (Spear, 1993). a) A hypothetical zoning profile of garnet. The numeros 1–8 correspond to those in (b). b) *P–T–t* path estimation by Gibb's method from the almandine and grossular zoning patterns of (a).

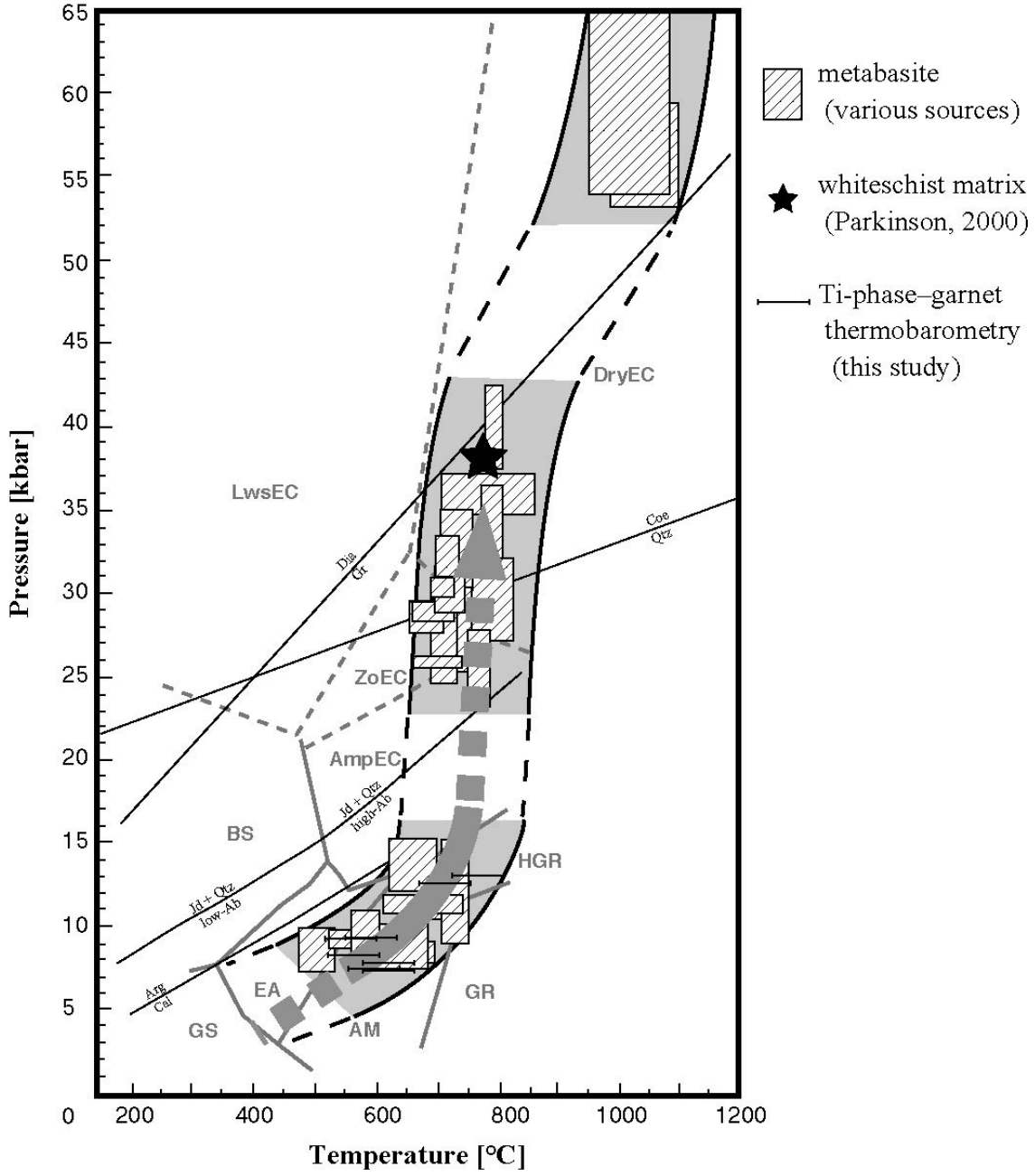

Fig. III–14 Comparison of *P–T* trajectories of whiteschists to metamorphic field geothermal gradient deduced from metabasites, which is shown as a shaded zone. Boxes show estimated *P–T* conditions for metabasites of Barchi-Kol, Kumdy-Kol, Sulu-Tjube, Chaglinka, Kulet, Saldat-Kol and Borovoye regions (Ota *et al.*, 2000; Masago, 2000; Okamoto *et al.*, 2000; Chap. III of this thesis). Star-mark represents the peak *P–T* conditions for whiteschists based on the matrix mineral assemblage assuming the stability of coesite (Parkinson, 2000).

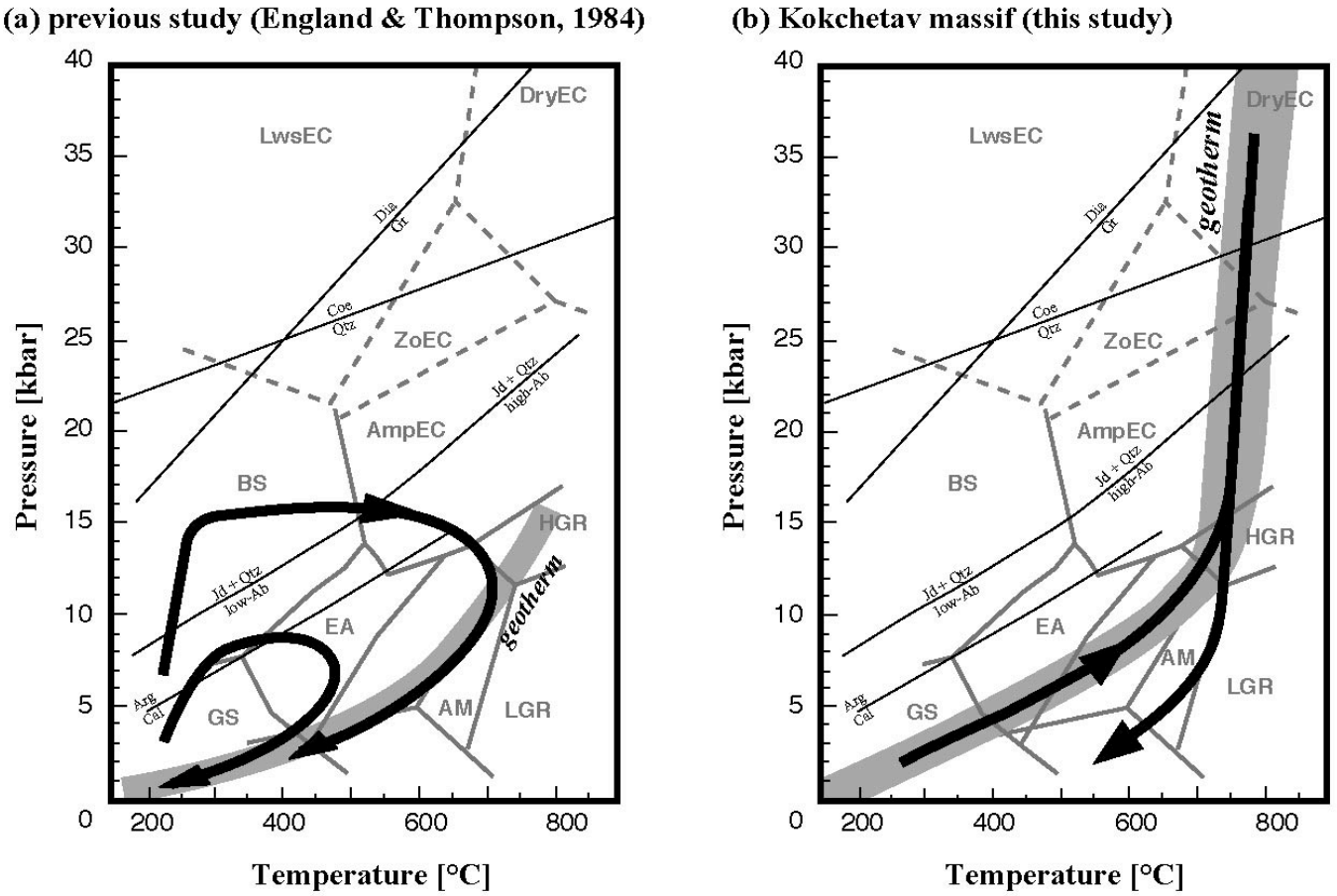

Fig. III–15 Relationships between metamorphic *P–T* paths of individual rocks and geothermal gradient of the collisional metamorphic belt. a) Classical explanation in the model of England & Thompson (1984). Geothermal gradient of the metamorphic belt is defined as a series of *P–T* conditions of the individual rocks at their thermal peak stages. *P–T* paths of individual rocks and the *P–T* gradient of the metamorphic belt do not coincide in general. b) *P–T* path and gradient estimated for the Kokchetav massif. Prograde *P–T* path is counter-clockwise and coincides with the geothermal gradient of the massif.

CHAPTER IV

Summary of the Kokchetav Metamorphism and Future Perspectives of UHPM Study

ABSTRACT

The geological, structural, petrological and isotopic studies described in the foregoing chapters have provided some new insights to the Kokchetav metamorphism. Lithological assemblage of terriginous affinity suggests a passive continental margin environment for the protolith deposition. And low-$\delta^{18}O$ eclogites of MORB-like bulk chemistry infer continental rift to immature oceanic environments for the protolith formation. The orogen-scale structure of the Kokchetav massif is a subhorizontal thin sheet. The whole HP–UHP package is underlain by the low-pressure Daulet Suite, and overlain by the weakly metamorphosed sedimentary rocks (Unit V). The top and the bottom boundaries are also subhorizontal, and the shear senses are top-to-the south and north for the top and the bottom boundaries, respectively. Internal structures are dominated by later-stage high-angle folds of various dimension. However, boundaries between each lithologic unit are subhorizontal. Thermobaric structure estimated by mineral assemblages and conventional thermobarometry of metabasites is subparallel to the geological structure, and the highest metamorphic grade is situated at the structural intermediate portion of the whole HP–UHP unit. Metamorphic facies series is medium-*P* type in the lower-grade parts, which bent steeply towards high-*P* side at around 700 °C, 12–15 kbar. This observation well corresponds to the numerically simulated subduction geothermal gradient. Application of inclusion mineralogy and thermodynamic analysis to the compositionally zoned garnet porphyroblast enabled to delineate the prograde *P*–*T* path. The estimated path is counter-clockwise and coincides with the metamorphic geotherm of the massif. By synthesising above-mentioned evidences, tectonic evolution from the protolith formation, subduction, metamorphism to exhumation is speculated.

The study of the Kokchetav massif has provided three important implications to metamorphic petrology. Firstly, the UHPM is not like an olistolith in the low-grade country rocks but has a regional extent of orogen-scale. Secondly, UHPM is a rather common phenomena to the continental collision zones. This means the classical regimes of orogeny are no more applicable to many of the collisional orogens. Thirdly, the initiation of UHPM is closely related to the cooling history of the earth. The 530 Ma Kokchetav massif, together with two Late Proterozoic UHPM terranes, is a key to solve this problem.

INTRODUCTION

In the foregoing chapters, several aspects of the Kokchetav massif were revealed involving field mapping, structural analyses, metamorphic thermobarometry (Chap. I), *P–T* path determination from inclusion mineralogy and compositional zoning in garnet (Chap. III), and oxygen isotope analyses (Appendix II). In this chapter, concluding remarks of these studies are summarised, and a plausible history of tectonic evolution of the Kokchetav massif is presented.

PROTOLITHS OF THE KOKCHETAV MASSIF

A detailed field mapping revealed the protoliths of the Kokchetav HP–UHPM units include bimodal volcanics, shallow marine/terrestrial sediments and orthogneiss, and are lacking deep-sea sediments. The passive continental margin nature of the protoliths, the lack of an extensive, associated granite belt and the very high pressures of peak metamorphism (*i.e*. $P >> 12$ kbar) define the metamorphic constituents of the Kokchetav massif as an 'A-type' or collisional terrane within the classification of Maruyama *et al*. (1996). Furthermore, extremely light oxygen isotope compositions in eclogites suggest their protoliths are of continental rift origin (Appendix II). In contrast to 'B-type' HP metamorphic terranes, which are predominantly located in the circum-Pacific region (*e.g*. Sanbagawa and Franciscan Belts), and are characterized by remnants of relatively shallow subduction of accretionary complexes, all UHPM terranes belong to the A-type. Final (micro)continental collision and doming following metamorphism and uplift of 'A-type' HP–UHPM terranes ensures dismemberment and tectonic complexity.

RELATIONSHIP TO THE SUB- AND SUPER-JACENT GEOLOGICAL UNITS AND THEIR BOUNDARIES

The HP–UHPM units are structurally underlain by the low-*P* type Daulet Suite (Dobrzhinetskaya *et al*., 1994; Dobretsov *et al*., 1995), with which it is juxtaposed

across a low-angle N-dipping fault against the HP–UHPM rocks in the Chaglinka, and Sulu-Tjube areas, and across a high-angle normal fault in the Kulet region (Appendix I). Rocks of the Daulet Suite are composed chiefly of pelitic-psammitic gneisses or schists and quartz schists with minor metacarbonates and metabasites. The representative assemblages in metapelites are: Chl + Ms ± Grt, And + Bt + Crd + Kfs ± Grt, Sil + Bt + Crd + Kfs ± Grt, with the appearance of the latter, highest grade assemblage restricted to near the contact with the HP–UHPM units. (Terabayashi *et al.*, 2002). Pressure-temperature conditions of the Daulet metamorphism is 600–650 °C at nearly constant pressures of about 2 kbar. The sequential change of mineral assemblage and compositional change of solid-solution minerals of buffered assemblages indicate that the metamorphic grade increases towards the boundary with the overlying HP–UHP units (Terabayashi *et al.*, 2002). The upward increasing metamorphic grade implies contact metamorphism by the tectonic juxtaposition of the hot Kokchetav HP–UHP slab. However, there is a clear tectonic and metamorphic discontinuity between the Daulet Suite and the Kokchetav HP–UHP unit; a pressure gap of several kilometers exists across the boundary thrust (Terabayashi *et al.*, 2002). These data have an important bearing on exhumation models for Kokchetav HP–UHPM rocks.

In the lower part of the HP–UHPM units, near the tectonic contact with the Daulet Suite, the structure is characterized by stretching lineations, and flat-lying foliations (S-planes) defined by alignment of the basal planes of sheet silicates, accompanied by mylonitic shear bands (C-planes), that usually indicate a top-to-the north sense of movement. These indicators and detailed geologic cross-sections indicate that the UHPM unit was emplaced onto the low-pressure Daulet Suite rocks from the south to the north (Appendix A).

The Kokchetav HP–UHPM units are structurally overlain in the north of the massif (notably in the Borovoye region) by another low-pressure sequence of low-grade to feebly metamorphosed rocks (Unit V; Appendix A), and is also known as the Elektin and Borovsk Series (*e.g.* Dobretsov *et al.*, 1995). This low-*P* unit consists mainly of mudstone, shale, slate (in the northern part), quartzite, sandstone, conglomerate, limestone (in the southern part) and minor metabasic schist. Most of them retain sedimentary structures such as graded bedding and cross-laminae. Mineral parageneses in metabasites: Ep + Chl + Ab + Qtz ± Ttn indicates greenschist facies metamorphic condition. In contrast, the Unit IV (the lowermost unit of the HP–UHPM unit)

metabasite is epidote-amphibolite with assemblages of: Ep + Hbl + Pl (Ab–Olg) + Qtz ± Ilm ±Ttn, which notably lacks actinolite. Therefore, a two-amphibole coexisting zone is lacking between Units IV and V, suggesting a small break of metamorphic conditions between them (Chap. III).

The tectonic boundary between this low-*P* unit and the HP–UHPM units is a subhorizontal normal fault, which is locally cut by secondary ENE–WSW striking high-angle normal faults. Shear sense indicators yield consistent top-to-the-south sense of movement (Appendix A).

Hence, in terms of orogen-scale architecture the overall, gross structure of the massif is sandwich-like, with the HP–UHPM nappe group juxtaposed against underlying low-*P* type Daulet rocks on the bottom, and against low-grade to unmetamorphosed clastic and carbonate rocks (Unit V) on the top, across large-scale subhorizontal faults (*cf.* Maruyama *et al.*, 1996).

THERMOBARIC STRUCTURE OF HP–UHPM UNITS

The distribution of metamorphic facies within the HP–UHPM unit has been clarified from mineral assemblages in metabasites, mineral inclusions in zircon and garnet, and conventional geothermobarometric determinations. Metamorphic facies of metabasites in the Kokchetav HP–UHPM unit range from intermediate-high-pressure epidote-amphibolite through high-pressure amphibolite, quartz-eclogite and coesite-eclogite to diamond-eclogite facies. In general, the combined effects of thermal re-equilibration, increased fluid mobility and deformation during uplift ensure that only a few UHPM vestiges are retained in metamorphic rocks returned to the surface. However, zircon is a common phase in Kokchetav UHPM rocks and is an excellent container of relict UHPM phases, since it is mechanically strong, chemically resistant, relatively impermeable to fluids, and extremely stable and resistant over a wide pressure and temperature interval (*e.g.*, Chopin & Sobolev, 1995; Liou *et al.*, 1998). Hence, zircon is the best tool with which to clarify the areal extent of UHP metamorphism in the Kokchetav massif, as demonstrated by the extensive study of inclusions in Kokchetav zircons reported by Katayama *et al.* (2000). Occurrence of the diamond is restricted to the southwest of Kumdy-Kol lake (Sobolev & Shatsky, 1990), and the drilling sample to

the west of Barchi-Kol lake (Lavrova, 1996) of Unit II. Coesite inclusions have been recognised in zircon and garnet in eclogite and pelitic gneiss or whiteschist from Unit II of Kumdy-Kol and Barchi-Kol regions (Zhang *et al*., 1997) and in garnet and kyanite from whiteschists south of Kulet (Shatsky *et al*., 1998). Inclusions of quartz pseudomorphs after coesite in garnet, omphacite and zoisite have been reported from unit II of the Barchi-Kol, Kumdy-Kol, Chaglinka, Sulu-Tjube and Kulet regions. These data indicate that large parts of unit II correspond to the coesite-eclogite facies or higher (*i.e*. UHPM).

Metabasites are another excellent indicators to delineate the original thermobaric conditions at the metamorphic peak stage. They are less permeable than the surrounding metasedimentary rocks, and are widespread throughout the massif although relatively minor in volume. Metabasites in Unit I comprise amphibolite and garnet-amphibolite, in Unit II eclogite, Unit III garnet-amphibolite and eclogite, and in unit IV, epidote-amphibolite. The occurrence of eclogite in unit III is restricted to the base of that unit. Intermediate structural levels of unit III, particularly in the Saldat-Kol region, are characterized by garnet-amphibolite and orthogneiss. No coesite has been identified from unit III, although estimated pressures for some phengite-bearing eclogites of unit III in the Saldat-Kol are within the coesite stability field (Ota *et al*., 2000). However, for the most part unit III corresponds to the quartz-eclogite facies or lower. Consequently, the higher grade diamond- and coesite-eclogite facies rocks are restricted to unit II, the structural intermediate part of the HP–UHPM belt, and the metamorphic grade decreases to amphibolite facies zone toward both the underlying Unit I and the overlying Unit III (the upper part) through the quartz-eclogite facies zone (the lower part of Unit III). The metabasite in Unit IV is widely distributed as intercalations within quartzite in the Borovoye region, and also rarely in the Barchi-Kol region. They are intermediate-high pressure epidote-amphibolites (Chap. I). Subdivision of the HP–UHPM unit I–IV is based on the lithological and structural definitions. It has a good correspondence with independently estimated thermobaric structure. The tectonic boundary between each of the adjacent units is also marking a *P–T* break. Significant pressure breaks of up to 7 kbar also occur across the lower tectonic boundaries of the HP–UHPM unit.

METAMORPHIC FACIES SERIES

One of the most important contributions of this study to the Kokchetav and UHPM studies is to have clarified the nature of the metamorphism of lower-grade portions of UHPM terrane. By the conventional thermobaromeric analyses of metabasites, *P–T* conditions of low- to high-grade were estimated (Fig. IV–1; Chap. I). The known lowest metamorphic facies of the Kokchetav HP–UHPM unit is EA facies in Unit IV. The metamorphic field *P–T* gradient begins from EA facies followed by AM facies in Unit I and III. In the uppermost part of Unit I, it passes from AM to QEC facies, which is also very close to high-pressure granulite (HGR) facies. Transitional reactions from AM to QEC facies are documented in the Barchi-Kol region (Chap. II). Pressure conditions of in Unit II eclogites except for the Kumdy-Kol ones cluster around 23–42 kbar covering QEC, CEC and a lowermost part of DEC facies. On the other hand, temperatures show no significant variation in the range of 650–875 °C. Only Kumdy-Kol eclogites show extremely high pressure as high as 60 kbar (Okamoto *et al*., 2000). Temperature is also higher than the rest of Unit II eclogites as 950–1100 °C (Okamoto *et al*., 2000). Two important features are provided by these thermobarometric results. First is that metamorphic field gradient is not almost straight as traditionally drawn, but bending steeply at around 600–700 °C, 12–15 kbar which corresponds to Moho depth. The geothermal gradient metamorphic belt changes at this depth from approximately 20 °C/km at shallower part to 2 °C/km at deeper part. This metamorphic field gradient, which is approximately able to be regarded as a geothermal gradient of the metamorphic massif is similar to the numerically simulated geotherm along the Benioff-plane (Peacock, 1996). It is now obvious that geothermal gradient of the metamorphic belt is not uniform but changes with depth, hence traditionally defined *P–T* type of metamorphic belts (*i.e*. low-*P* type, medium-*P* type and high-*P* type) no more makes any sense. The second feature is the existence of large *P–T* break among and even within each unit. There is a pressure break of *ca*. 7 kbar between Unit III and the lower-grade part of the Unit II. Such a *P–T* (chiefly pressure) break of *ca*. 10 kbar also exists between the Kumdy-Kol and other regions of the Unit II. The missing parts are probably lost during reconstruction associated with the exhumation. The pressure range of the Unit II is over 40 kbar, which corresponds to 120 km of slab thickness. Whereas, the total pressure range for the Unit I, III & IV is only 8 kbar, *i.e*. 24 km of slab

thickness. These facts suggest that the reconstruction during exhumation occurs more effectively at the deeper parts of the slab.

PRESSURE–TEMPERATURE–TIME PATH

As is the case with other UHPM terranes, vestiges of the early, prograde stage of metamorphism are rare in Kokchetav UHPM rocks. However, whiteschists from the Kulet region contain large porphyroblastic garnets which preserve prograde compositional zonation and inclusion fabrics. Some mineral species have characteristic zonal distribution. For SiO_2 polymorphs, quartz occurs mainly in the cores and rarely at rims, whereas coesite occurs mantles of the garnet porphyroblast. Titanium-phase minerals also have similar distribution: Ilmenite + rutile composite in cores, mono-phase rutile in mantles, and either rutile, ilmenite and their composite in the rims. These rocks enables to delineate the prograde *P–T* trajectory of the Kokchetav massif (Chap. III). Garnet displays normal, prograde zoning with decreasing spessartine and increasing almandine and pyrope components, from core to rim. Grossular component shows a complex repetition of increase and decrease from core to rim. Composite inclusions of Ilm + Rt in garnet cores enables to calculate *P–T* conditions of crystallisation. The calculated *P–T* conditions show a systematic increase from core to rim in the range of 470–745 °C and 7.4–13.3 kbar (Chap. III). On the other hand, peak *P–T* conditions were estimated for the mantle part of the garnet porphyroblast as 36 kbar at 750 °C (Parkinson, 2000). A model petrogenetic grid was made for the system K_2O–CaO–FeO–Al_2O_3–SiO_2 in excess of H_2O. Forward modeling of grossular component along the estimated prograde *P–T* path shows a good correspondence to the observed compositional profile of the garnet (Chap. III).

The estimated prograde *P–T* path from garnet porphyroblasts is counter-clockwise and is similar to the metamorphic *P–T* gradient. Traditionally, *P–T* path for each individual rock has been drawn as a clockwise curve in general, and do not coincide with the *P–T* gradient of the metamorphic belt.

TECTONIC SYSNTHESIS OF THE KOKCHETAV MASSIF

Based on the foregoing geologic, structural, petrological, geochemical and geochronological data, a possible tectonic evolution of the Kokchetav HP–UHPM rocks is proposed as below. Schmatic diagrams of Fig. IV–2 will help readers to understand this speculative model.

Protolith Formation

In the Late Proterozoic, an ocean existed between the Siberian craton and the Kokchetav microcontinent. Most of the Kokchetav metamorphic terrane consists of protoliths of a microcontinent rifted from the Siberian craton; bimodal volcanics, shallow marine/terrestrial sediments and quartzo-feldspathic rocks in the HP–UHPM belt supports the rifting origin. Furthermore, low $\delta^{18}O$ in eclogites of MORB-like origin strongly suggests the continental rift to early ocean environments for their formation, where oceanic basalt interacts with negative-$\delta^{18}O$ meteoric water preferably under cold climate (Appendix B). The protolith ages are provided by Sm–Nd model age method as 2.2–2.3 Ga (Jagoutz *et al*., 1990), as well as by zircon U–Pb method as 1.2–2.0 Ga (Claoué-Long *et al*., 1991; Katayama *et al*., 2001). From the oxygen isotope study, the 'Snowball Earth' period is very preferable for the timing of formation of low-$\delta^{18}O$ eclogite protolith, which occurred several times during the Late Proterozoic time, immediately before the Kokchetav metamorphism (Hoffman *et al*., 1998).

Subduction and Metamorphism

In the Latest Proterozoic, southward subduction of an oceanic plate beneath the Kazakhstan microcontinents and formation of Proterozoic accretionary complex took place. Paleogeographic reconstructions and REE pattern of the metasediments in this massif support passive margin origin (Mossakovsky & Dergunov, 1985).

In the Early Cambrian, the Kokchetav microcontinent and its overlying Proterozoic sequence were subducted to depths of about 200 km, and formed HP–UHP metamorphic rocks. Detail geochronological studies reveal that the peak metamorphism was taken place around 530–540 Ma (Claoué-Long *et al*., 1991; Shatsky *et al*., 1999; Katayama *et al*., 2001). During this stage, a few amounts of Alpine-type peridotites were incorporated in the subducted slab.

Exhumation and Later-Stage Structural and Petrological Modification

The subducted supracrustal rocks returned to mid-crustal levels in the Late Cambrian. The Kokchetav HP–UHPM unit was extruded as a thin sheet, from a root zone in the south toward the foreland in the north by a wedge extrusion mechanism, based on following evidences: 1) dimensions — very thin (approximately 2 km), but very wide sheet-like aspect, 2) subhorizontal internal structural fabrics and metamorphic zonation, 3) opposing senses of shear at the bottom (top-to-the-north) and top (top-to-the-south sense) of the pile, 4) paired, subhorizontal bounding structures juxtaposing the nappe against lower grade or unmetamorphosed rock above and below, 5) the underlying low-*P* type Daulet Suite exhibits provides fluids and 6) the thermobaric structure, with highest grade, highest pressure (UHPM) components occupying a medial position. The thermal structure within the HP–UHPM unit implies substantial differential movement, with more ductile, higher grade material being extruded from much greater depths, and being juxtaposed, in the nappe core, against progressively cooler rocks at shallower levels. Choking of the Kokchetav subduction zone by collision of a continental fragment (crustal and supra-crustal components of which represent protoliths of most Kokchetav HP–UHPM rocks), resulting in slab break-off and buoyancy of the stranded, recrystallised sialic material is a possible driving force for extrusion.

The exhumed UHP rocks were juxtaposed against lower grade rocks of the Daulet Suite, which represents the footwall to the HP–UHPM slab. This relatively ‘wet’ low-grade metasedimentary package is considered to be necessary for the source of fluids which caused hydration of the UHPM rocks at mid-crustal levels. The tectonic juxtaposition of the dry HP–UHP rocks underlying the low-grade Daulet Suite rocks would allow infiltration of fluids and effectively obliterate the HP–UHP matrix mineral assemblages and formed Barrovian-type assemblages. During emplacement, the Daulet was extensively thermally recrystallised at the contact with the overlying HP–UHPM unit. Zircon separates from sillimanite grade pelitic gneiss at the contact have SHRIMP ages of 520 ± 4 Ma, consistent with the ages obtained from the rims of UHP mineral-bearing zircons, for Barrovian hydration metamorphism (Katayama *et al.*, 2001). Thus, the source of fluid for hydration may have been dehydration and thermal

recrystallisation of the much lower grade Daulet sedimentary package during subhorizontal emplacement of the HP–UHPM slab (Terabayashi *et al*., 2002).

After the collisional event, widespread island-arc volcanism with subjacent, synkinematic and later anorogenic granitoid plutonism intruded in this massif during Ordovician and Silurian times.

DISCUSSION

Regional Extent of UHPM

Since the first discovery of metamorphic coesite in Dora Maira of Western Alps (Chopin, 1984) and Western Gneiss Region of Norway (Smith, 1984), there has been a long debate about whether UHPM is a detrital gravel in conglomerate in oliststrome, a tectonic block in a mélange unit, or a regional coherent nature. In the former opinion, UHPM is regarded just like as an olistolith whose origin is uncertain, incorporated to the low-grade country rocks. What this theory is based on is rarity of UHPM minerals or rocks in whole metamorphic terrane. In fact, in many UHP terranes, UHP rocks or minerals are commonly surrounded by low pressure rocks (< 10 kbar). Also in the Kokchetav massif, mélange-like model regarding HP–UHP rocks as blocks in the low pressure matrix (‘mega-mélange’ model: Dobretsov *et al*., 1995) was dominant before our TITech research team project. Kokchetav study has given an answer to this problem. In the Kokchetav massif, coesite and its pseudomorph were found as inclusions in zircon, garnet or other rigid minerals from numbers of rocks including eclogite, gneiss and whiteschist in addition to eclogitic metabasite (*e.g*. Zhang *et al*., 1997; Katayama *et al*., 2000; Parkinson, 2000). More importantly, their distribution has a regional extent covering the Barchi-Kol, Kumdy-Kol and Kulet regions. Moreover, all of these coesite localities are not randomly distributed but restricted to Unit II, the structural intermediate nappe of the Kokchetav nappe system. Now it is obvious that UHPM has a regional extent and structural relationship in the whole massif in Kokchetav. The next question is whether the regional extent of UHP is characteristic to Kokchetav massif or a common nature to all UHPM terranes over the world. What caused the largest confusion to the former researchers of UHPM is a low pressure rocks occupying overwhelmingly large volume of the massif as mentioned above. The study of the

Kokchetav massif has revealed that these Barrovian-type mineral assemblages are formed at the later-stage recrystallisation and give no information about peak metamorphism. Application of the methodology established in the Kokchetav study: an extensive inclusion mineralogy in zircon and garnet, will give the answer to this question. In Sulu belt, numbers of coesite inclusions were found from ortho- and paragneisses in drilled core samples (Liu *et al*., 2001; 2002). Further application of this method will delineate the regional extent of UHPM in other UHP terranes of the world.

Generality of UHPM in the Collisional Orogens

During several years after the first discovery of metamorphic coesite by Chopin (1984) and Smith (1984), UHPM has been regarded as a peculiar phenomena restricted to a few very limited geological environments. However, the following report of coesite or its pseudomorph came out first from Dabie, China (Wang *et al*., 1989), then from the Bohemian massif (Schmedicke, 1991), and many other thereafter. Metamorphic microdiamond is also reported from several regions such as Kokchetav massif (Sobolev & Sahatsky, 1990) and Western Gneiss Region (Dobrzhinetskaya *et al*., 1995), although not as much as coesite.

In Table IV–1, age, traditionally defined baric type and presence/absence of UHPM indices of continental collision zones of the world are summarised. In addition to the basic three baric types: low-*P*, medium-*P* and high-*P* types, two more types are also introduced: intermediate high-*P* and intermediate low-*P*. The former is distinguished from medium-*P* type by the lack of sillimanite, and from high-*P* type by the lack of lawsonite. The characteristic metamorphic facies series for this baric type is BS–(GS)–EA–EC facies. The latter is introduced to distinguish from contact metamorphism which is characterized by pyroxene hornfels and/or sanidinite facies, although it also has andalusite–sillimanite series alminosilicates as low-*P* type has.

Among 21 collisional orogens recognised in the world, 17 have indices of UHPM. Now UHPM is reported from Europe, Asia, Africa, and recently from South America and Antarctica (Fig. IV–3), and is recognised as a rather common feature to the collisional orogens. Notably, all UHPM were reported from orogens which formerly regarded as ‘medium-*P*’ type characterized by kyanite–sillimanite series metamorphic facies. Many metamorphic petrologists have tried to explain metamorphism in the scheme of tectonics or geodynamics. The first important contribution in this field is the

finding of ‘paired metamorphic belt’ by Miyashiro (1961). This is far before the appearance of the plate tectonic concept, and its foresightedness is worthy of admiration. Since then, this field was energetically studied by numbers of researchers especially in the late 1970’s to 1980’s, accelerated by the appearance of the plate tectonic concept. This culminated in mid to late 1980’s by the formation of the paradigm of collisional orogeny (*e.g*. England & Thompson, 1984; Thompson & England, 1984). In these paradigms, metamorphism associated by continental collision is explained by the duplication of continental crusts.

This model explained well about features of collision type metamorphism until UHP was discovered. Doubly-thickened continental crusts cause an immediate increase of pressure at the top of the footwall. On the other hand, temperature does not show an instant response to the depth of burial, and discontinuous thermal profile is formed along the contact depth of the overlapping continental crusts. The process of recovering normal geotherm accompanied by the isostatic elevation coupled by surface erosion forms a clockwise *P–T* path (Fig. IV–4). And it also explains that collision-type metamorphism has medium-*P* (Barrovian) type metamorphic facies series of which maximum pressure never exceed the Moho depth. Discovery of UHPM drastically changed this concept. Pressure for coesite stability (at least 25 kbar under normal geothermal gradient) cannot be attained by this duplicated crusts model. Furthermore, *P–T* path deduced by UHPM rocks is counter-clockwise (Chap. III), which cannot be explained by this model. These findings in the Kokchetav study concludes that the former orogenic model is no more applicable as a standard of the continental collision tectonics.

What caused these confusions to traditional metamorphic petrology is an intense retrograde metamorphism accompanied by large amount of hydration at mid-crustal depth. As is mentioned in the previous paragraph, most of rocks have experienced nearly complete recrystallisation during exhumation, obliterating all evidences of the former stages. The Barrovian type metamorphism, which traditionally has been a standard of the collision type metamorphism is actually a production of the retrograde hydrated recrystallisation. Reevaluation of metamorphic belts by present-day insights in application of methods used in this thesis and related studies will provide highly different results from the traditional ones.

Recently, coesite was reported from the Himalaya (O' Brien, 2001; Sachan *et al*., 2001; Kaneko *et al*., 2001), which used to be regarded as a type locality of the 'medium-*P*' type collisional orogen. Then, the Dalradian, Appalachian or other 'medium-*P*' type collisional orogens are the next targets. When the reexamination of these classic metamorphic belts has been done, the textbook of metamorphic petrology will need to be rewritten under the new paradigm of metamorphic petrology. And the Kokchetav massif will be come a new standard of the collision orogeny.

Initiation of UHPM and the Cooling History of the Earth

The first appearance of UHPM on the earth is the Late Proterozoic related to the Pan-African orogeny. Two UHPM localities belonging to this orogeny are known in Mali (Caby, 1994) and Brazil (Parkinson *et al*., 2001). Occurrence of UHPM is clustered in several orogenic periods (Fig. IV–5). The first group is those of Late Proterozoic ~ Early Cambrian. Kokchetav massif and above-mentioned two terranes are included. The other groups correspond to the Caledonian, Pangean and Alpine-Himalayan orogenic periods, respectively. No UHPM was found before the Late Proterozoic. The subduction zone geotherms recorded in regional metamorphic belts have changed with time from Archaean to present (Fig. IV–6). In the Archaean time, metamorphic belts generally have much higher geotherms than present. The geotherms suddenly have shifted towards higher-*P*/*T* side during the Middle Proterozoic time (1000–750 Ma), and the first UHP occurred at the end of the Proterozoic. It is key to the occurrence of UHPM whether the subduction geotherm crosses the wet solidus. If the subduction geotherm is rather high, it crosses the wet solidus which results in slab melting. Estimated *P–T* gradient of the Kokchetav massif passes slightly lower-*T* side of the wet solidus. Consequently, the subducting slab attained to the depth of coesite and diamond stability field without being melted. At present, the Kokchetav massif is the only example to examine the relationship between the cooling earth's gotherm and the appearance of UHPM at the transitional period from the Proterozoic to the Phanerozoic. In Mali and Brazil UHPM terranes, their *P–T* gradient and path are not certain. Further evidences will be provided by examining *P–T* gradient and path of the two Proterozoic UHPM. From the Brazilian UHPM, coesite inclusion was found in a compositionally zoned garnet in whiteschist (A. Motoki, *pers. comm*.), which is very similar to those of the Kokchetav massif (Chap. III).

REFERENCES

Beane, R. J., Liou, J. -G., Coleman, R. G. and Leech, M. L., 1995. Petrology and retrograde P–T path for eclogites of the Maksyutov Complex, Southern Ural Mountains, Russia. *The Island Arc*, **4,** 254–266.

Bohlen, S. R. & Boettcher, A. L., 1982. The quartz–coesite transformation: A pressure determination and the effect of other components. *Journal of Geophysical Research*, **87**, 7073–7078.

Bundy, F. P., 1980. The P, T phaseand reaction diagram for elemental carbon. *Journal of Geophysical Research*, **85**, 6930–6936.

Caby, R., 1994. Precambrian coesite from northern Mali: first record and implications for plate tectonics in the trans-Saharan segment of the Pan-African belt. *European Journal of Mineralogy*, **6,** 235–244.

Campos Neto, M. & Caby, R., 1999. Neoproterozoic high-pressure metamorphism and tectonic constraint from nappe system south of the São Francisco Craton, southeast Brazil. *Precambrian Research*, **97,** 3–26.

Carlson, W. D., 1983. The polymorphs of $CaCO_3$ and the argonite–calcite transformation. *Reviews in mineralogy*, **11**, 191–225.

Chopin, C., 1984. Coesite and pure pyrope in high-grade pelitic blueschists of the Western Alps: A first record and some sequences. *Contributions to Mineralogy and Petrology*, **86,** 107–118.

Chopin, C. & Sobolev, N. V., 1995. Principal mineralogic indicators of UHP in crustal rocks. In: Coleman, R. G. & Wang, X. (Eds.), *Ultrahigh-pressure Metamorphism*, pp. 96–133. *Cambridge University Press*. London.

Claoué-Long, J. C., Sobolev, N. V., Shatsky, V. S. and Sobolev, A. V., 1991.Zircon response to diamond pressure metamorphism in Kokchetav massif, USSR. *Geology*, **19,** 710–713.

Dobretsov, N. L., Sobolev, N. V., Shatsky, V. S., Coleman, R. G. & Ernst, W. G., 1995. Geotectonic evolution of diamondiferous paragneisses, Kokchetav complex, northern Kazakhstan: the geologic enigma of ultrahigh-pressure crustal rocks within a Paleozoic foldbelt. *The Island Arc*, **4**, 267–279.

Dobrzhinetskaya, L. F., Braun, T. V., Sheshkel, G. G. & Podkuiko, Y. A., 1994. Geology and structure of diamond-bearing rocks of the Kokchetav massif, Kazakhstan. *Tectonophysics*, **233,** 293–313.

England, P. C. & Thompson, A. B., 1984. Pressure–temperature–time path of regional metamorphism, Part I: Heat transfer during the evolution of regions of thickened continental crust. *Journal of Petrology*, **25,** 894–928.

Ghiribelli, B., Ferezzotti, M. L. & Palmeri, R., 2002. Coesite in eclogites of Lanterman Range (Antarctica): Evidence from textural and Raman studies. *European Journal of Mineralogy,* **14,** 355–360.

Gilotti, J. A. & Ravna, E. J. Krogh, 2001. Textural and thermobarometric evidence for ultrahigh-pressure metamorphism in the north-east Greenland Caledonides. Abstract: *UHPM workshop: Fluid/slab/mantle interactions and ultrahigh-P minerals*. Waseda University, Tokyo, 208–212.

Hoffman, P. F., 1987. Continental transform tectonics: Great Slave Lake shear zone (1.9 Ga), northwest Canada. *Geology*, **15,** 785–788.

Hoffman, P. F., 1988. United plates of America, the birth of a craton: early Proterozoic assembly and growth of Laurentia. *Annual Review of Earth and Planetary Sciences*, **16,** 543–603.

Hoffman, P. F., 1991. Does the breakout of the Laurentia turn Gondwanaland inside-out? *Science*, **252,** 1409–1412.

Hoffman, P. F., Kaufman, A. J., Halverson, G. P. & Schrag, D. P., 1998. A Neoproterozoic snowball Earth, *Science*, **281,** 1342–1346.

Holland, T. J. B., 1980. The reaction albite = jadeite + quartz determined experimentally in the range 600–1200°C. *American Mineralogist*, **65**, 125–134.

Jagoutz, E., Shatsky, V. S. & Sobolev. N. V., 1990. Sr–Nd–Pb isotopic study of ultrahigh *PT* rocks from Kokchetav massif. *EOS Transactions, American Geophysical Union*, **71,** 1707.

Kaneko, Y., Yamamoto, H., Katayama, I., Misawa, I., Ishikawa, M., Hafees, R. U. & Shiraishi, K., 2001. Coesite inclusions and prograde compositional zonation of zircons in Himalayan gneisses, NW Himalaya, Pakistan: Evidence from SHRIMP-dating of coesite-bearing zircon. Abstract: *UHPM workshop: Fluid/slab/mantle interactions and ultrahigh-P minerals*. Waseda University, Tokyo, 121–123.

Katayama, I., Zayachkovsky, A. A. & Maruyama, S., 2000. Prograde pressure–temperature records from inclusion in zircons from ultrahigh-pressure–high-pressure rocks of the Kokchetav Massif, northern Kazakhstan. *The Island Arc*, **9,** 417–427.

Katayama, I., Maruyama, S., Parkinson, C. D., Terada, K. & Sano, Y., 2001. Ion micro-probe U–Pb zircon geochemistry of peak and retrograde stages of ultrahigh-pressure metamorphic rocks from the Kokchetav massif, northern Kazakhstan. *Earth and Planetary Science Letters*, **188,** 185–195.

Lavrova, L. D., Pechinikov, V. A., Petrova, M. A., Zayachkovsky, A. A., 1996. Geology of Barchi-Kol diamondiferous area. *Otechestvennaia Geologia*, **12**, 20–27. (*in Russian*)

Liou, J. G., Zhang, R. Y., Ernst, W. G., Rumble, D. & Maruyama, S. 1998. High-pressure minerals from deeply subducted metamorphic rocks. In: Hemley, R. J. (Ed.), *Ultrahigh-pressure Mineralogy: Physics and Chemistry of the Earth's Interior Mineralogical Society of America, Reviews in Mineralogy,* **37,** 33–96.

Liu, F. -L., Xu, Z. –Q., Yang, J. –S., Maruyama, S., Liou, J. -G., Katayama, I. & Masago, H., 2001. Mineral inclusions of zircon and UHP metamorphic evidence from paragneiss and orthogneiss of pre-pilot drillhole CCSD-PP2 in north Jiansu Province, China. *Chinese Science Bulletin*, **46,** 1037–1042.

Liu, F. -L., Xu, Z. –Q., Liou, J. -G., Katayama, I., Masago, H., Maruyama, S. & Yang, J. –S., 2002. Ultrahigh-pressure mineral inclusions in zircons from gneissic core

samples of the Chinese Continental Scientific Drilling Site in eastern China. *European Journal of Mineralogy*, **14,** 499–512.

Maruyama, S., Liou, J. G. & Terabayashi, M., 1996. Blueschists and eclogites of the world and their exhumation. *International Geology Review*, **38,** 485–594.

Maruyama, S., Parkinson, C. D. & Liou, J. G., 2002. Overview of the tectonic evolution of the Kokchetav massif and the role of fluid in subduction and exhumation. In: Parkinson, C. D., Katayama, I., Liou, J. G. & Marruyama, S. (Eds.), *The Diamond-Bearing Kokchetav Massif, Kazkahstan*. 427–442. Universal Academy Press, Tokyo.

Masago, H., 1998. Tectonics of the northwestern Capricorn orogen, the Early-Proterozoic continental collision zone. *M. Sc. thesis*, Tokyo Institute of Technology.

Masago, H., 2000. Metamorphic petrology of the Barchi-Kol metabasites, western Kokchetav ultrahigh-pressure–high-pressure massif, northern Kazakhstan. *The Island Arc*, **9,** 358–378.

Miyashiro, A., 1961. Evolution of metamorphic belts. *Journal of Petrology*, **2,** 277–311.

Mossakovsky, A. A. & Dergunov, A. V., 1985. The Caledonides of Kazakhstan, Siberia and Mongolia: a review of structure, development history and paleo-tectonic environments. In: Gee, D. G. & Sturt, B. A. (Eds.), *The Caledonide Orogens — Scandinavia and related areas*. pp. 1201–1215. John Wiley & Sons, New York.

Mposkos, E. D. & Kostopoulos, D. K., 2001. Diamond, former coesite and supersilicic garnet in metasedimentary rocks from the Greek Rhodope: a new ultrahigh-pressure metamorphic province established. *Earth Planetary Science Leters*, **192,** 497–506.

Newton, R. C. & Smith, J. V., 1967. Investigations concerning breakedown of albite at depth in the earth. *Journal of Geology*, **45,** 268–286.

Novgorodtsev, O., Takasu, A. and Bakirov, A., 2001. UHP metamorphic rocks from eclogite-bearing metamorphic complex of the Atbashy ridge, Southern Tien-Shan, Kyrghyzstan. Abstract: *6th International Eclogite Conf*erence, Niihama, pp. 101.

O'Brien, P. J., 1993. Partially retrograded eclogites of the Müchberg Massif, Germany: Record of a multi-stage Variscan uplift history in the Bohemian Massif. *Journal of*

*Metamorphic Geol*ogy, **11,** 241–260.

O'Brien, P. J., Zotov, N., Law, R., Kahn, M. A. and Jan, M. -Q., 2001. Coesite in Himalayan eclogite and implications for models of India–Asia collision. *Geology,* **29,** 435–438.

Oh, C. W. & Liou, J. G., 1998. A petrogenetic grid for eclogite and related facies under high-pressure metamorphism. *The Island Arc*, **7**, 36–51.

Okamoto, K. & Maruyama, S., 1998. Multi-anvil re-equilibration experiments of a Dabie Shan ultrahigh-pressure eclogite within the diamond-stability fields. *The Island Arc*, **7**, 52–69.

Okamoto, K., Liou, J. G. & Ogasawara, Y., 2000. Petrology of the diamond-grade eclogite in the Kokchetav Massif, northern Kazakhstan. *The Island Arc*, **9,** 379–399.

Ota, T., Terabayashi, M., Parkinson, C. D. & Masago, H., 2000. Thermobaric structure of the Kokchetav ultrahigh-pressure–high-pressure massif deduced from a north–south transect in the Kulet and Saldat-Kol regions, northern Kazakhstan. *The Island Arc*, **9,** 328–357.

Parkinson, C. D. & Katayama, I., 1999. Present-day ultrahigh-pressure conditions of coesite inclusions in zircon and garnet: Evidence from laser Raman microspectorometry. Geology, 27, 979–982.

Parkinson, C. D., 2000. Coesite inclusions and prograde compositional zonation of garnets in whiteschist of the Kokchetav UHP–HP massif, Kazakhstan: a record of progressive UHP metamorphism. *Lithos,* **52,** 215–233.

Parkinson, C. D., Motoki, A., Onishi, C. T. & Maruyama, S., 2001. Ultrahigh-pressure pyrope-kyanite granulites and associated eclogites in Neoproterozoic nappes of southeast Brazil. Abst: *UHPM workshop: Fluid/slab/mantle interactions and ultrahigh-P minerals*. Waseda University, Tokyo, 87–90.

Peacock, S. M., 1996. Thermal and petrologic structure of subduction zone. In: Bebout, G. E., Scholl, D.W., Kirby, S. H. & Platt, J. P. (Eds.), *Subduction: Top to Bottom*, Geophysical Monograph, **96,** 119–133. American Geophysical Union. Washington

D. C.

Sachan, H. K., Mukherjee, B. K., Ogasawara, Y., Maruyama, S., Pandey, A. K., Muko, A., Yoshioka, N. and Ishida, H., 2001. Discovery of coesite from Indian Himalaya: consequence on Himalayan tectonics. Abstract: *UHPM workshop: Fluid/slab/mantle interactions and ultrahigh-P minerals*. Waseda University, Tokyo, 124–128.

Schmedicke, E., 1991. Quartz pseudomorphs after coesite in eclogites from the Saxonian Erzgebirge. *European Journal of Mineralogy*, **1,** 231–238.

Shatsky, V. S., Theunissen, K., Dobretsov, N. L. & Sobolev, N. V., 1998. New indication of ultrahigh-pressure metamorphism in the mica schist of the Kulet site of the Kokchetav massif. *Russian Geology and Geophysics*, **39,** 1041–1046.

Smith, D. C., 1984. Coesite in clinopyroxene in the Caledonides and its implications for geodynamics. *Nature*, **310**, 641–644.

Sobolev, N. V. & Shatsky V. S., 1990. Diamond inclusions in garnets from metamorphic rocks. *Nature*, **343,** 742–746.

Song, S. -G., Yang, J. -S., Wu, C. -L., Liou, J. -G. & Xu, Z. -Q., 2001. Petrology, geochemistry and isotopic ages of eclogites in the Dulan UHPM terrane, the North Qaidam, NW China. Abstract: *6th International Eclogite Conf*erence, Niihama, pp. 150.

Tagiri, M., Yano, T., Bakirov, A., Nakajima, T. and Uchiumi, S., 1995. Mineral parageneses and metamorphic P–T path of ultrahigh-pressure eclogites from Kyrghyzstan Tien–Shan. *The Island Arc*, **4,** 280–292.

Terabayashi, M., Ota, T., Yamamoto, H. & Kaneko, Y., 2002. Contact metamorphism of the Daulet Suite by solid-state emplacement of the Kokchetav UHP–HP metamorphic slab. *International Geology Review*, **44,** 819–830.

Thompson, A. B. & England, P. C., 1984. Pressure–temperature–time path of regional metamorphism, Part II: Their influence and interpretation using mineral assemblages in metamorphic rocks. *Journal of Petrology*, **25,** 929–955.

Van Reenen, D. D., Barton, J. M., Roering, C. A., Smith, C. A. & Van Schalkwyk, J. F.,

1987. Deep crustal response to continental collision: the Limpopo belt of southern Africa. *Geology*, **15,** 11–14.

Wang, X., Liou, J. -G. & Mao, H. -K., 1989. Coesite-bearing eclogite from Dabie mountains, central China. *Geology,* **17,** 1085–1088.

Zhang, R. –Y. & Liou, J. –G., 1994. Coesite-bearing eclogite in Henan Province, China: detailed petrography glaucophane stability and PT-path. *European Journal of Mineralogy*, **6,** 217–233.

Zhang, R, -Y., Liou, J. -G., Coleman, R. G., Ernst, W. G., Sobolev, N. V. & Shatsky. N. S., 1997. Metamorphic evolution of diamond-bearing and associated rocks from the Kokchetav massif, northern Kazakhstan. *Journal of Metamorphic Geology*, **15,** 479–496.

Table IV–1. Summary of the metamorphic features of collisional orogens of the world.

Orogens	Age (Ma)	UHP index	baric type	Representative papers
Limpopo	2870–2650?	-	intermediate-low	Van Reenen et al. (1987)
Thelon	2020–1960	-	intermediate-low	Hoffman (1987; 1988)
Wopmay	1890–1880	-	intermediate-low	Hoffman (1988)
Capricorn	1880–1850	-	intermediate-low	Masago (1998)
Grenville	1150–1100	-	intermediate-low	Hoffman (1991)
Brazil (Pan-African)	604	Coe	medium	Campos Neto & Caby (1999); Parkinson et al. (2001)
Mali (Pan-African)	620	Coe	?	Caby (1994)
Makshutov	590?	Coe-ps	?	Beane et al. (1995)
Kokchetav	540	Coe , Dia	medium	this volume
Lanterman Range	500	Coe-ps		Ghiribelli et al. (2001)
Makbal	480	Coe		Tagiri et al. (1995)
N. Qaidam	475	Coe	?	Song et al. (2001)
E. Greenland (Caledonian)	450	Coe	medium	Gilloti & Ravna (2001)
WGR (Caledonian)	415	Coe, Dia	medium	Smith (1984)
Ertzgebirge (Variscan)	340	Dia	medium	Schmedicke (1991); O'Brien (1993)
Atbashy (Variscan)	300	Coe	intermediate-high	Novgorodtsev et al. (2001)
Qinling–Dabie–Sulu (Pangean)	220–230	Coe, Dia?	intermediate-high	Zhang & Liou (1994)
Sulawesi	140	Coe	intermediate-high	Parkinson. & Katayama (1999)
Himalaya	50	Coe	medium	O'Brien (2001)
Dora Maira (Eo-Alpine)	35	Coe	intermediate-high	Chopin (1984)
Greek Rhodope (Eo-Alpine)	35	Dia-ps	intermediate-high	Mposkos & Kostopoulos (2001)

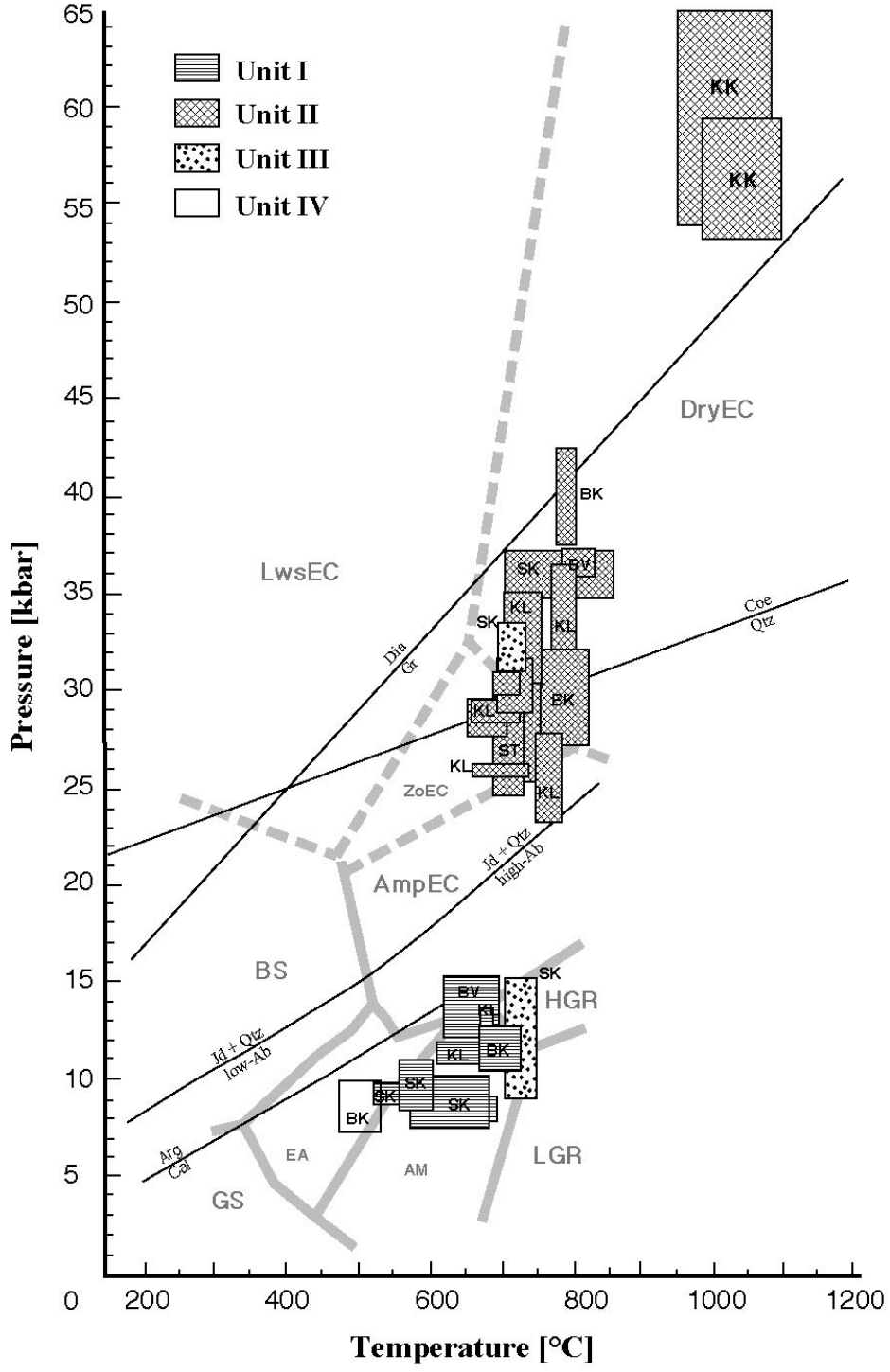

Fig. IV–1 Compilation of *P–T* data for HP–UHPM rocks from all units and regions of the Kokchetav massif. BK: Barchi-Kol (Chap. I; Masago, 2000); KK: Kumdy–Kol (Okamoto *et al*., 2000); ST: Sulu-Tjube (Okamoto unpub. data in Maruyama & Parkinson, 2000); SK: Saldat–Kol (Ota *et al*., 2000); KL: Kulet (Zhang *et al*., 1997; Ota *et al*., 2000; Parkinson, 2000); BV: Borovoye (Chap. I). The *P–T* regimes are after the petrogenetic grid of Oh & Liou (1998) and Okamoto & Maruyama (1998) together with the experimenatally determined stability fields for Dia/Gr (Bundy, 1980), Coe/Qtz (Bohlen & Boettcher, 1982), Jd + Qtz = high-Ab (Holland, 1980), Jd + Qtz = low-Ab (Newton & Smith, 1967) and Arg/Cal (Carlson, 1983).

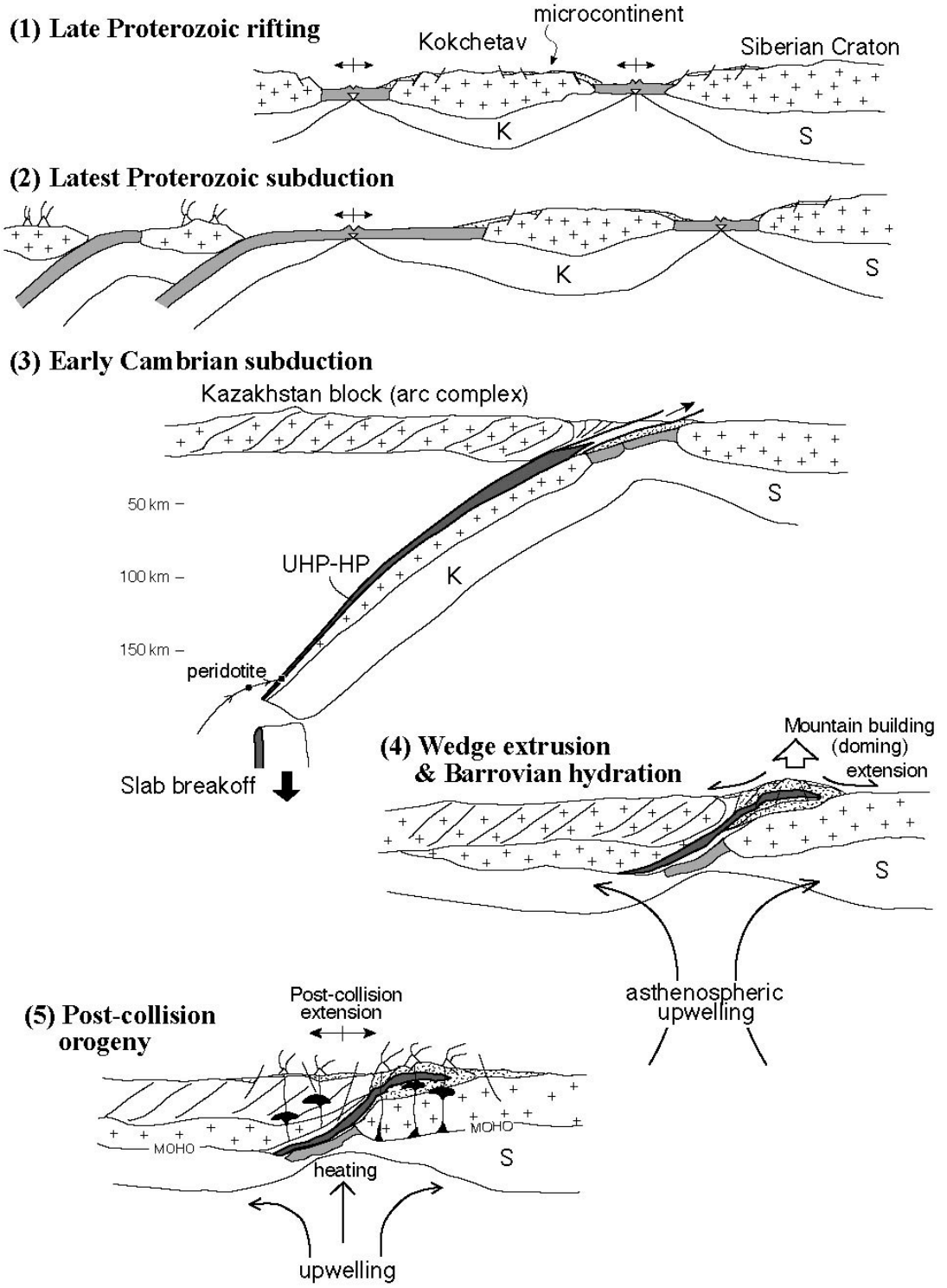

Fig. IV–2 Schematic diagrams showing the tectonic evolution of the Kokchetav massif (Maruyama *et al.*, 2002). 1) Rifting of the Kokchetav microcontinent in Late Proterozoic; 2) Subduction of small ocean and formation of Proterozoic accretionary complex in Latest Proterozoic; 3) Subduction of the Kokchetav microcontinent formation of HP–UHPM unis in Early Cambrian; 4) Exhumation of the HP–UHPM units and Barrovian overprint due to hydration from the underlying Daulet Suite; 5) Post-collision orogenic events involving extensional collapse and magmatism in Ordovician.

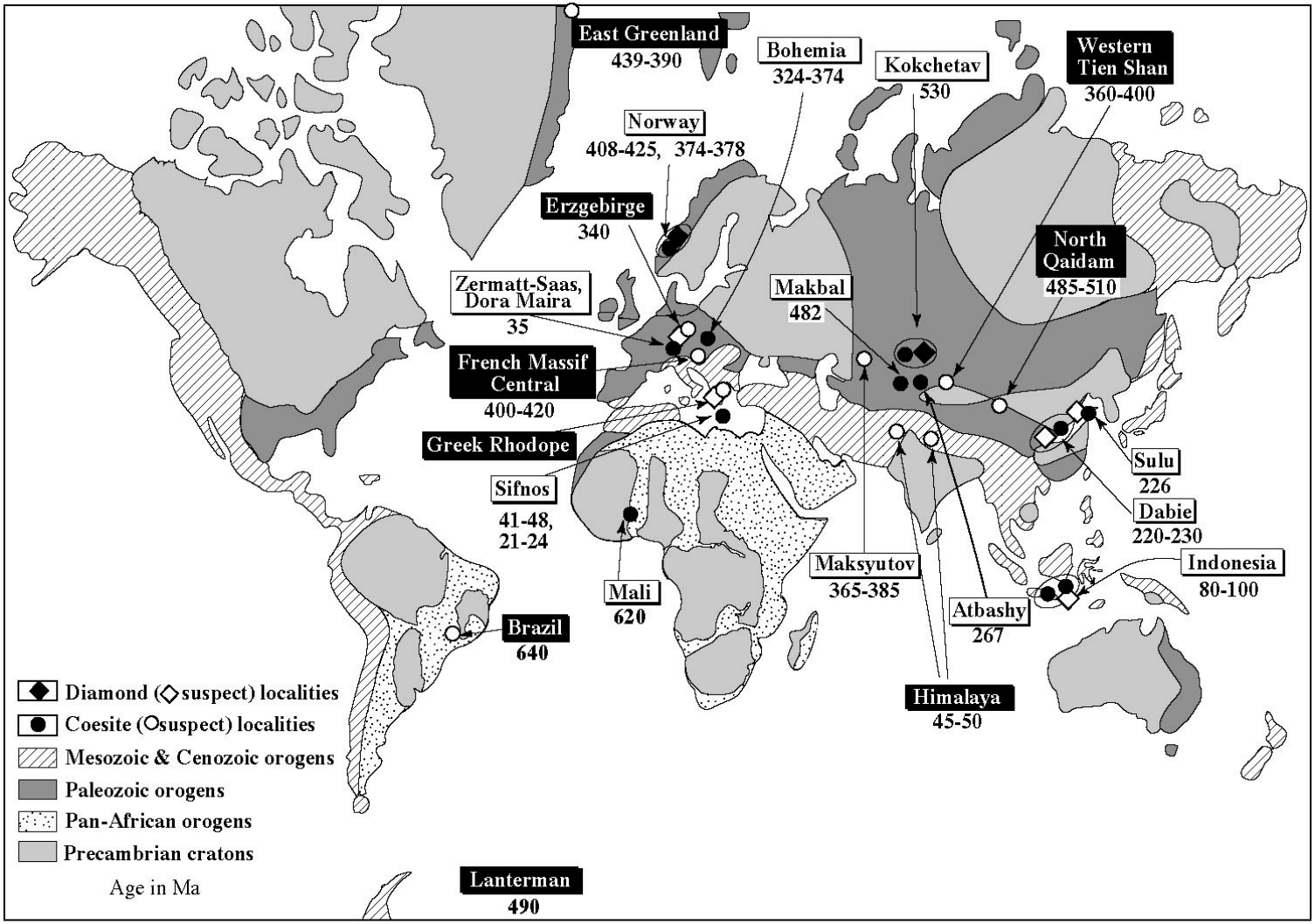

Fig. IV–3 Distribution of UHPM of the world (partly modified after Liou *et al*, 2002). Numeros beneath localities represent ages in Ma. Localities shown in reversed colour are newly discovered UHPM terranes after 2000.

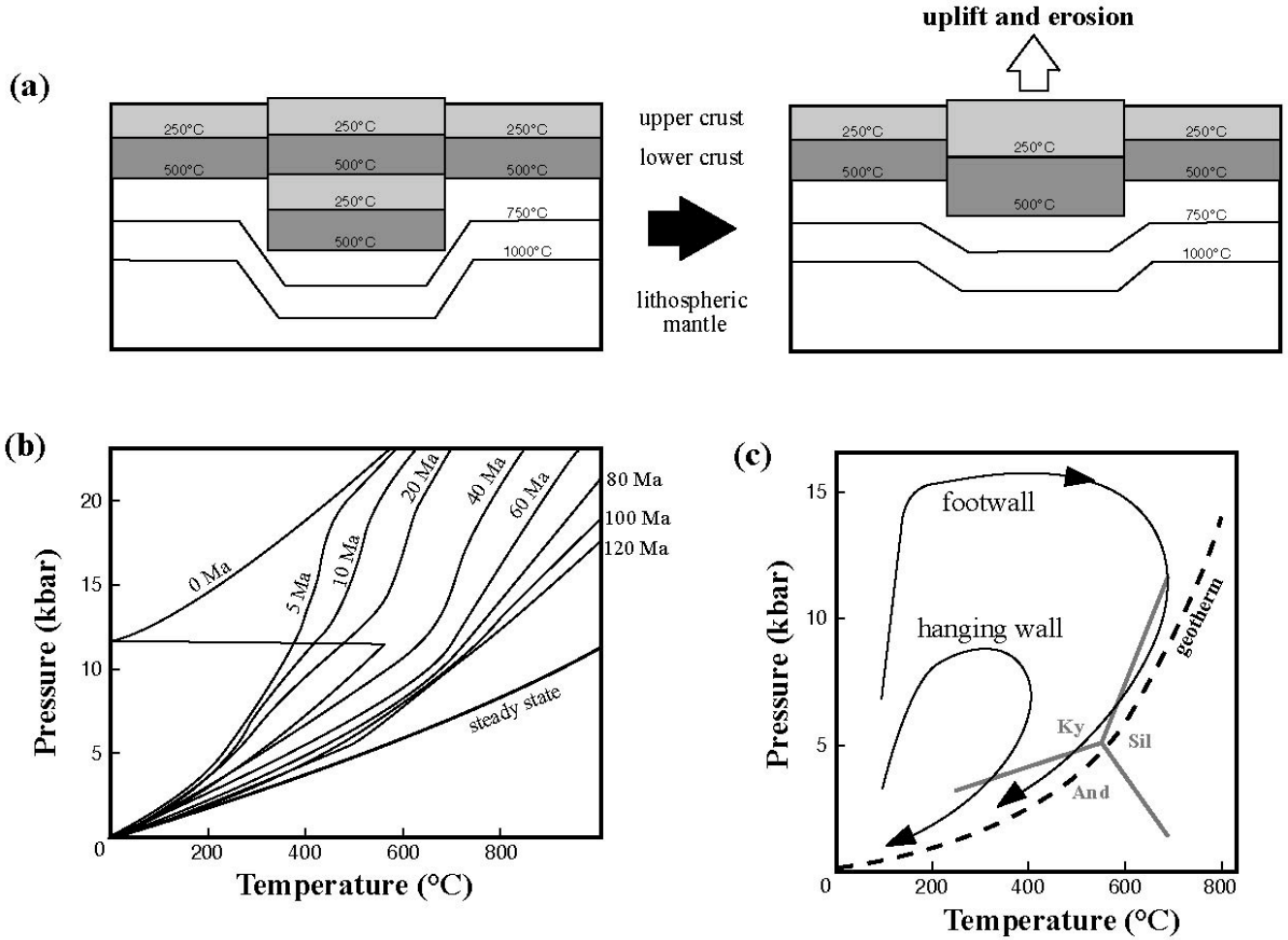

Fig. IV–4 Classical model for continetal collision orogeny of England & Thompson (1984) and Thompson & England (1984). a) Schematic cross-sections of the collisional orogen showing the crustal thickening by collision (left) and the sebsequent uplift and erosion (right). b) Thermal profiles along depth of the collision zone at various time after collision. Discontinuous thermal profile formed by doubly-thickened crusts (0 Ma) changes to recover the steady state geotherm with time. c) Pressure–temperature paths for the hanging wall and the footwall of the orogen.

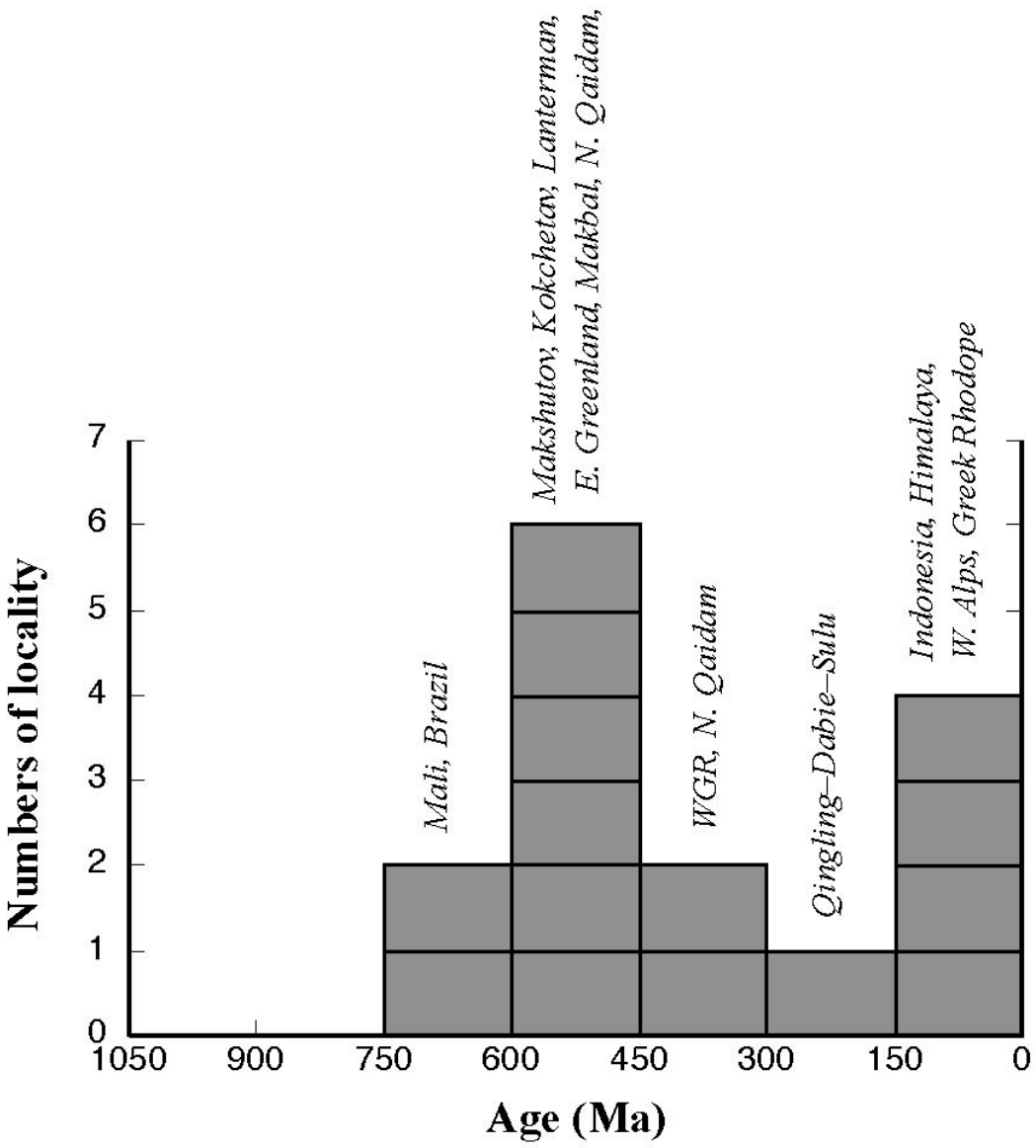

Fig. IV–5 Age distribution of UHPM occurrence of the world. Note no UHPM occurs before Late Proterozoic (>750 Ma), and 40 % of world UHPM terranes were formed at Caledonian age.

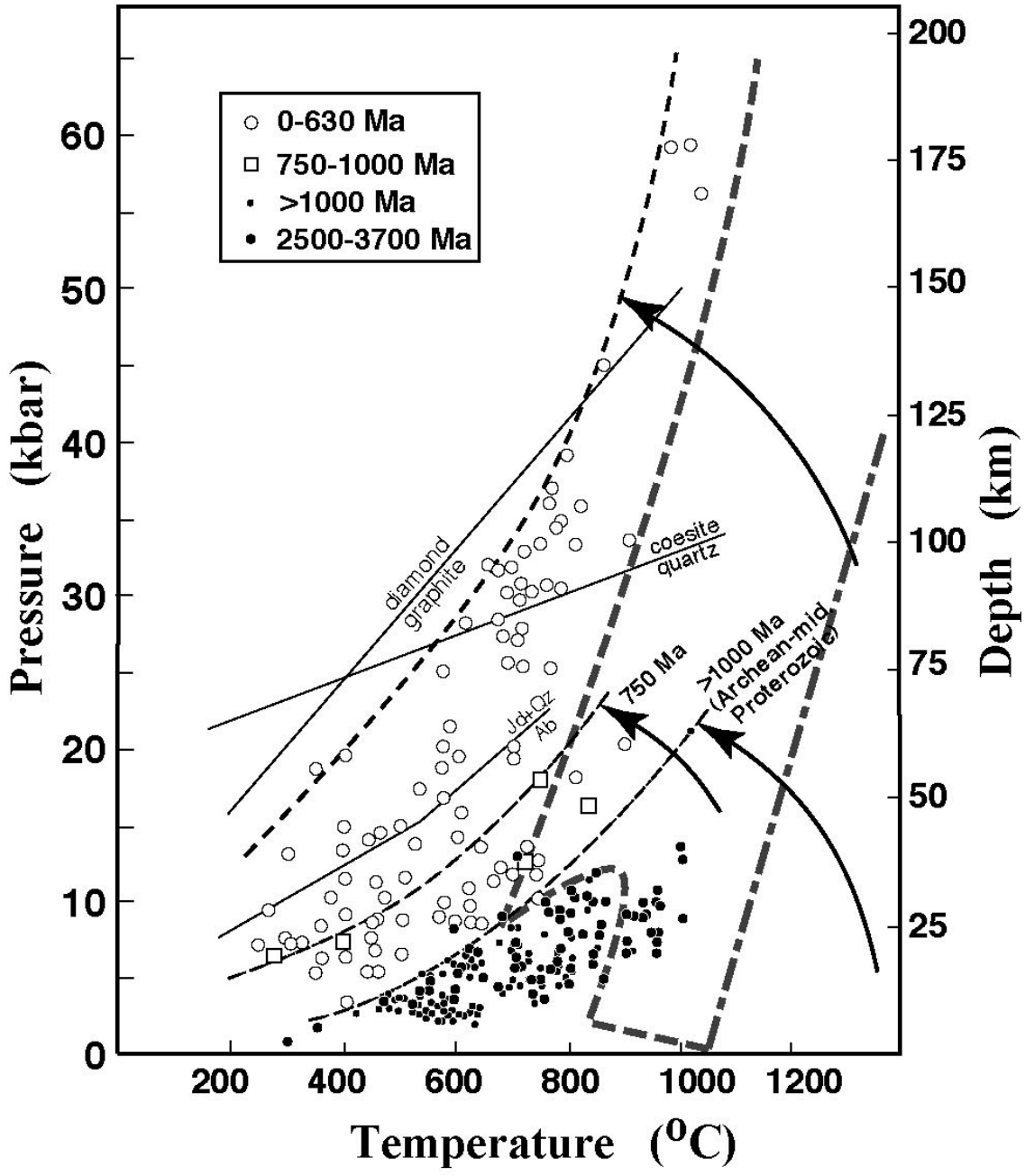

Fig. IV–6 Secular variation of *P–T* conditions recorded in regional metamorphic belts of the world (Maruyama *et al.*, 2002). The subduction geothermal gradient has cooled gradually wih time. The occurrence of UHPM is restricted to the periods after Late Proterozoic.

Appendix

APPENDIX A

Geology of the Kokchetav Massif

ABSTRACT

Detailed mapping of the Kokchetav massif has revealed the lithological, structural, and thermobaric features of the Kokchetav massif. In the Kokchetav massif, apparently subvertical structures are dominant. However, the field mapping and structural analyses have revealed that these structures are of later folding origin, which has no connection to the formation and denudation of the HP–UHPM massif. The HP–UHPM unit primarily has a flat-lying structure and its total thickness is estimated to be around 2 km. The first order structure is sandwich-like; *i.e*. the HP–UHPM units are separated from underlying low-*P* metamorphic rocks of the Daulet Suite and from overlying feebly metamorphosed to unmetamorphosed sedimentary strata by subhorizontal faults. Kinematic indicators show top-to-the south and top-to-the north displacements along the top and the bottom boundaries, respectively. These shear senses, together with the observed metamorphic gradient suggests the northward extrusion of the UHPM unit as a thin sheet. These geological and structural features of the Kokchetav massif seems to be best explained by the wedge extrusion model.

INTRODUCTION

The Kokchetav massif is situated within the central Asian foldbelt, a major late-Paleozoic collision zone including the North China, Tarim, Tadzhik, Karakorum and Kazakhstan–North Tienshan cratons and the Siberian shield (Zonenshain *et al*. 1990). The HP–UHPM rocks of the Kokchetav massif are overlain by Cambro–Ordovician volcanic and sedimentary strata of island arc origin, Devonian volcanic molasse, and Carboniferous and Triassic shallow water and lacustrine deposits. The HP–UHPM rocks have undergone several orogenic processes, and were intruded by Silurian to Early Devonian syn-tectonic granites, and by Late Devonian to Carboniferous post-collisional granites, syenites and granite porphyries (Dobretsov *et al*., 1995).

Because of the low topographic relief, it is difficult to determine structural contacts of the various units in the field. However, numerous drill-holes, trenches and marmot holes provide us with a good opportunity to collect fresh samples. The HP–UHPM package is structurally overlain by a low-grade metamorphic unit on the top, and is underlain by the low pressure (low-*P*) facies series of the Daulet Suite. These two major tectonic boundaries are subhorizontal, and locally modified by secondary high-angle normal faults (Maruyama *et al*., 1996; Ishikawa *et al*., 2000; Kaneko *et al*., 2000). Post-metamorphic and post-orogenic Devonian granitoid intrusions occupy the southern part of the study area. A set of NE–SW and NW–SE trending high-angle strike-slip faults indicates post-orogenic deformation. The age of UHPM is Middle Cambrian, as indicated by Sm–Nd and U–Pb ages between 520 and 540 Ma (Jagoutz *et al*., 1990; Claoué-Long *et al*., 1991). SHRIMP analyses of metamorphic zircons yielded 530 ± 7 Ma (Claoué-Long *et al*., 1991) for the UHPM, which is consistent with a Sm–Nd isochron ages of 533 ± 7 and 505 ± 43 Ma for eclogite, biotite gneiss and diamondiferous rocks (Shatsky *et al*., 1993). Age of retrograde metamorphism is determined by $^{40}Ar/^{39}Ar$ method for mica from diamond-bearing garnet-biotite gneiss as ~515 to 517 Ma (Troesch & Jagoutz, 1993). The most reliable age constraints are SHRIMP U–Pb dating of zoned zircon, which yielded 537 ± 9 Ma for UHP mineral-bearing cores and 507 ± 8 Ma for retrograde rims (Katayama *et al*., 2001).

OUTLINE OF GEOLOGY

The Kokchetav massif is ~150 km long and 20 km wide and strikes NW–SE in the west and bends to NE–SW in the east. The Kokchetav HP–UHPM rocks, also known as the Zerenda Series (Dobretsov *et al*. 1995) is underlain by Low-*P* type metasedimentary rocks of the Daulet Suite, and overlain by low to weakly metamorphosed units bounded by a normal fault (Kaneko *et al*. 2000). The HP–UHPM rocks have been subdivided into four units by Kaneko *et al*. (2000) on the basis of the differences in lithofacies in the field (Fig. A–1), and termed as Unit I–IV from structural bottom to top. Unit I is composed mainly of alternation of siliceous schist (leptite) and amphibolite. Unit II is composed mainly of pelitic/psammitic gneiss with locally abundant eclogite boudins and minor whiteschist and ultramafic rocks. Unit III is characterized by alternation of orthogneiss and amphibolite, with minor amount of eclogite blocks. Unit IV consists mainly of quartzite and siliceous schist with a small amount of epidote-amphibolite. Detailed descriptions of each lithological unit are in the following sections.

LITHOLOGYICAL AND STRUCTURAL FEATURES OF EACH LITHOTECTONIC UNIT

HP–UHPM units

Unit I

Unit I is predominantly composed of leptite (fine-grained acidic gneiss) and amphibolite involved as a massive block and/or intercalated as a thin layer, and with a small amount of pelitic schist and orthogneiss, as lenses or layers of various sizes (Fig. A–2). This structurally lowermost metamorphic unit is exposed mainly in a middle region as a tectonic window (25 km x 10 km) along the WNW–ESE axis of an antiformal fold (Figs. A–1b & c), and is tectonically overlain by the UHPM rocks of Unit II. Unit I also exposed in the northern Barchi-Kol region, however structural relationship is uncertain in this region. Foliations are axial planar. Outcrop scale upright folds with axial plane parallel to WNW–ESE orientation are observed in the Unit I rocks. The earliest structures are intrafolial isoclinal folds with a well-developed

foliation. This foliation and the isoclinal folds have been highly deformed by a later generation of NW-trending close to open folds, to form steep-dipping fold axial planes observed throughout the region. Detailed geologic cross-sections of this unit indicate that the enveloping surface is subhorizontal (Fig. A–1b). Mineral lineations defined by preferred orientation of amphibole and/or mica dip moderately to the ENE or SE. Sigmoidal polycrystalline aggregates, asymmetric pressure shadows, drag folds, and shear bands, clearly indicate top-to-the-north sense of shear (Yamamoto *et al*. 2000; Fig. A–1b).

The representative mineral parageneses of amphibolite are: Hbl + Pl + Qtz + Ep/Czo + Ilm ± Rt ± Grt. In a part of Barchi-Kol region, clinopyroxene-bearing amphibolite occurs. These clinopyroxenes have sodic-augite to omphacite compositions, suggesting transitional conditions to eclogite facies (Masago, 2000). Actually, some ‘amphibolite’ with omphacitic clinopyroxene lack plagioclase and should be termed as eclogite. Acidic schist has a compositional layering defined by quartzo-feldspathic layers (several mm to 1 m thick) and thin mica-rich layers (~ a few mm thick), and often includes porphyroclastic quartz, plagioclase and K-feldspar. The characteristic mineral assemblages are: Qtz + Pl + Ms + Bt + Grt + Kfs + Sil ± Tur ± Ap ± Ilm, Qtz + Pl + Ms + Bt + Grt + Kfs ± Tur ± Ap ± Ilm, Qtz + Pl + Ms + Bt + Grt + St ± Tur ± Ap ± Ilm , and Qtz + Pl + Ms + Kfs ± Tur ± Ap ± Ilm. Pelitic schist is highly foliated and often microfolded. The representative assemblage is: Bt + Qtz + Pl + Ms ± Grt ± Sil ± Tur ± Ap ± Ep. Orthogneiss is coarse-grained and characteristically includes porphyroblastic K-feldspar, that often exhibits an augen texture. The mineral assemblages are: Pl + Qtz + Kfs + Ms + Bt + Sil ± Rt ± Ilm ± Tur and Pl + Qtz + Kfs + Ms + Bt ± Rt ± Ilm ± Tur.

Unit II

Unit II is composed mainly of pelitic–psammitic gneiss and subordinate whiteschist that contain abundant eclogite blocks (Fig. A–1c). Minor amounts of metacarbonate, ultramafic rocks (peridotite and pyroxenite) and orthogneiss are present. The pelitic–psammitic gneiss commonly contains muscovite (phengite), biotite, quartz and plagioclase with variable amounts of garnet, kyanite, sillimanite and K-feldspar. Apatite, rutile and tourmaline occur as common accessory minerals. Whiteschist has somewhat different mineral parageneses. Matrix is composed of quartz, phengite, talc and rutile with large porphyroblasts of garnet and kyanite up to a few millimetre. Garnet

porphyroblast contains inclusions of coesite and/or quartz surrounded by radial fractures, which are probable pseudomorphs after coesite. Petrological features of whiteschists are described in detail in Chap. III. Diamonds occur as inclusions in garnet and zircon in pelitic gneiss, and marble in the Kumdy-Kol region and whiteschist in the Kulet region. Diamondiferous lithologies are garnet–biotite, garnet–zoisite and garnet–chlorite gneisses and garnet–pyroxene–quartz rock (Zhang *et al*., 1997). Coesite inclusions are found in zircon from pelitic rocks (Sobolev *et al*., 1991; Katayama *et al*., 2000), in garnet from whiteschist (Zhang *et al*., 1997, Parkinson, 2000) and from eclogite (Korsakov *et al*, 1998) with or without associated microdiamond.

Lenticular eclogite blocks, usually a few hundreds metres across, are enclosed in the whiteschist and pelitic gneiss. Occurrence of the eclogite is localised in several regions in Unit II; Barchi-Kol (Fig. A–4), Kumdy-Kol (Fig. A–5), Chaglinka (Fig. A–6), Sulu-Tjube (Fig. A–7), Kulet (Fig. A–8), Saldat-Kol (Fig. A–9) and Borovoye (Fig. A–10) areas from the west to the east. These eclogites are classified into three types in terms of their primary mineral assemblages: amphibole–eclogite (dark-coloured eclogite; Fig. A–3a), zoisite–eclogite (pale-coloured eclogite; Fig. A–3a) and dry–eclogite (without hydrous minerals; Fig. A–3a). Phengite is another hydrous mineral which is contained in all these types of eclogite. However, it occupies only minor modal proportion compared to other hydrous minerals, thus no specific category as phengite–eclogite is made here. Kyanite-bearing eclogite was not found throughout the Unit II. All types of eclogites are more or less retrogressed to amphibolite.

Unit III

Unit III is predominantly composed of orthogneiss, migmatite and amphibolite, with minor amount of eclogites. Neither coesite nor diamond was reported in eclogite and country rocks. As in Unit II, eclogites occur as lenses enveloped in country rocks, and have variably amphibolitised margins around the pods. Eclogite has mineral assemblages of: Grt + Cpx (sodic-augite to omphacite composition) + Qtz + Rt ± Prg ± Zo ± Phn. Apatite and zircon are relatively common accessory minerals. Amphibole-bearing eclogites are relatively common in the Saldat-Kol (Fig. A–9) and Kulet (Fig. A–8) regions. Foliations in eclogite lenses are defined by preferred orientation of elongate omphacite and pargasite grains, which is usually discordant to the elongation direction of the pod. In most eclogite bodies, intense amphibolitisation has obliterated

the primary texture and mineralogy. Mineral assemblages in orthogneiss are muscovite, biotite, quartz, plagioclase and K-feldspar with minor amount of garnet and sillimanite. Amphibolite is composed of Hbl + Pl + Qtz + Ilm/Rt ± Grt ± Ep ± Ap.

The rocks of Unit III occupy large areas to the north of Borovoye around a central antiformal axis trending ENE–WSW (Fig. A–10). In contrast, to the west of Saldat-Kol, the rocks of Unit III are situated in an axial part of a synform trending NW–SE (Fig. A–9). The NW-plunging synformal axis occupies the central portion of Unit III. Further, separate occurrences of Unit III rocks are situated to the south and southwest of Lake Zheltau (Fig. A–8). They are folded about the same axis with wavelengths ranging between tens of centimetres to several kilometres. In this unit, asymmetric structures such as sigmoidal polycrystalline aggregates of quartz, pressure shadows, drag folds and shear bands, clearly indicate top-to-the-south sense of movement (Fig. A–10; Yamamoto *et al*., 2000). Asymmetric augen and S–C fabrics observed in some orthogneiss were formed during sinistral strike-slip deformation postdates the exhumation of the HP–UHPM units (Fig. A–11). The upper border is covered by rocks of Unit IV. However, their contact relation is unclear because of the lack of the exposure.

Unit IV

This structural uppermost HP–UHPM unit is tectonically overlain by a low-pressure unit (Unit V), and occupies the southern and northern parts of the mapped area (Fig. A–1). It consists chiefly of quartzite and siliceous schist, but locally includes epidote-amphibolite (Fig. A–12). Quartzite is in fault contact with the underlying rocks of Unit III. The constituent minerals in the amphibolite are: Hbl + Pl + Qtz + Ep ± Ilm ± Ttn. Garnet also is very rarely present. The presence of isoclinal to tight folds in quartzite and marble indicates that Unit IV underwent the same deformation phase as other HP–UHP units. Sigmoidal polycrystalline aggregates of quartz, asymmetric pressure shadows, drag folds, and shear bands clearly indicate top-to-the-south sense of movement (Fig. A–10).

Geological units other than HP–UHPM units

Unit V

The rocks of Unit IV are overlain by weakly metamorphosed rocks of Unit V, which is widely distributed in the northernmost part of the Borovoye area (Fig. A–10). Unit V consists mainly of slate, shale, quartzite, sandstone, marble/limestone and conglomerate with highly elongate/flattened pebbles 2–5 mm in diameter. Sandstone exhibits graded bedding and cross-laminae. Bedding planes are truncated by a slaty cleavage. Very minor amount of greenschist occurs close to the boundary to Unit IV. Quartzite of Unit V is in fault contact with underlying rocks of the HP unit (Unit IV). This major sharp tectonic boundary is subhorizontal, and locally modified by secondary high-angle normal faults. Asymmetric textures such as porphyroclast systems, preferred orientation of quartz aggregates, drag folds and shear bands indicate a top-to-the south sense of movement (Fig. A–10).

Daulet Suite

The Daulet Suite is a unit which occupies the lowest structural level in the whole of the Kokchetav massif, and is underlying Unit I. However, it has a direct fault-contact with Units II & III at some localities in Chaglinka, Sulu-Tjube and Kulet areas (Figs. A–1, 7 & 8, respectively). In every observed location, the primary sense of shear of the boundary fault is thrusting of the HP–UHPM units onto the Daulet Suite. The Daulet Suite is composed chiefly of quartzite, pelitic and psammitic schist/gneiss with minor metacarbonate (Dobretsov *et al*., 1995). These rocks commonly have andalusite and/or sillimanite, suggesting high-*T*/low-*P* metamorphic facies series. Metamorphic zonation of the Daulet Suite has been done in the Kulet area based on the mineral assemblages in metapelite (Terabayashi *et al*., 2002). Isograds do not display a concentric distribution around the adjacent granitoid plutons, but are distributed parallel to the thrust between the Daulet Suite and the HP–UHPM units. This clearly indicates that the Daulet metamorphism is not caused by contact metamorphism of the granitoid plutons, but by contact with HP–UHPM rocks.

STRUCTURAL RELATIONSHIP BETWEEN HP–UHPM UNITS AND SOURROUNDING UNITS

Folds in the mapped area represented in Fig. A–13 are predominantly shallow

plunging, open-to-close, upright folds that trend WNW–ESE (Figs. A–13 & 14), except for some NE–SW trends in the western part of the studied area. They are mainly recognised on a scale of hundreds of metres, deforming the lithological boundaries, and often have outcrop-scale fold expressions. The wide distribution of the upright folds indicate that the enveloping surface of the folds is not subvertical, but subhorizontal. This implies that each HP–UHP unit is a subhorizontal sheet, and that the unit boundaries also are not subvertical, but subhorizontal. Furthermore, the kilometre-scale structural features clearly indicate that the subhorizontal HP–UHP units and Daulet suite were juxtaposed across subhorizontal fault and/or shear zones.

Based on fold analysis, structural relationships between each unit are illustrated in Fig. 1b. The lowermost Unit I forms the core of an antiform in the central part of the study area (Fig. A–1c) and is tectonically overlain by the UHPM rocks of Unit II. To the west of the Saldat–Kol and to the south of the Kulet regions, Unit II is cut by a low-angle fault dipping < 30° to the north or south along its upper boundary, where it is juxtaposed with overlying rocks of Unit III. To the west of Saldat–Kol, Unit III occurs in an axial part of the NW–SE trending synform. The NW-plunging synformal axis occurs in the central portion of Unit III. The rocks of Unit III are also situated to the south and southwest of the Kulet region. Rocks of Unit IV are distributed in the northern part of the mapped area (Fig. A–1). Unit IV is the structural top of the Kokchetav metamorphic belt in the studied area.

The low-pressure Daulet Suite is disposed along the southern margin of the HP–UHP units, and consists mainly of pelitic schist. The Daulet Suite is in fault contact with Units I & II, and the boundary between the HP–UHP units and Daulet Suite can be observed around Sulu-Tjube hill. The structure and general geology of Sulu-Tjube and adjacent areas has been described by Kushev & Vinogradov (1978) and Dobrzhinetskaya *et al*. (1994) as comprising distinct HP and LP metamorphic units. *P–T* estimates for metabasites and metapelites in the area (Shatsky *et al*., 1989) suggest that a distinct pressure gap of around 10 kbar exists between the UHP unit and the Daulet Suite.

HP metamorphic rocks in the Sulu-Tjube area correspond to Unit II of Kaneko *et al*. (2000), and comprise eclogite, amphibolitised eclogite and pelitic gneiss. Sulu-Tjube hill is composed of a large eclogite body of *ca*. 1 km in diameter. Amphibolitised eclogite displays a strong foliation trending NNE and dips moderately to NW. Pelitic

gneiss in Unit II is also characterized by a consistent, gentle W-dipping gneissosity, and a N–S and NE–SW trending mineral lineation of micas. The fold axes of upright folds in the pelitic gneiss plunge to the west. Foliation and associated isoclinal folds have been strongly deformed by a later generation NW-trending tight to open fold with steep-dipping fold axial planes and W-plunging fold axes, to form the steep-dipping foliations observed throughout the studied area. The enveloping surface of upright fold is subhorizontal.

All large-scale internal structures in both the HP–UHP and LP units are generally subhorizontal or gently-dipping. This implies that the boundary between the units is also a subhorizontal or gently-dipping fault or shear zone. Indeed, the irregular surface trace of the boundary between Unit II and the Daulet Suite rocks in the Sulu-Tjube and adjacent areas also indicates that the unit boundary is subhorizontal (Fig. A–15). The HP–UHPM foliation (S_0) of the eclogite is oriented slightly oblique to a later gneissosity (S_1) in amphibolitized eclogite. It is difficult to identify the S_0 foliation in the HP–UHP pelitic gneisses because they underwent strong recrystallisation during the formation of S_1.

The boundary between the HP–UHP and LP units is generally subparallel to the regional metamorphic foliation (S_1), which is defined by the preferred orientation of biotite and hornblende. Orientation of S_1 is highly variable, due to small-scale folding during a later phase of deformation.

REFERENCES

Claoué-Long, J. C., Sobolev, N. V., Shatsky V. S. & Sobolev, A. V., 1991. Zircon response to diamond pressure metamorphism in Kokchetav massif, USSR. *Geology*, **19**, 710–713.

Dobretsov, N. L., Sobolev, N. V., Shatsky, V. S., Coleman, R. G. & Ernst, W. G., 1995. Geotectonic evolution of diamondiferous paragneisses, Kokchetav complex, northern Kazakhstan: the geologic enigma of ultrahigh-pressure crustal rocks within a Paleozoic foldbelt. *The Island Arc*, **4**, 267–279.

Dobrzhinetskaya, L. F., Braun, T. V., Sheshkel, G. G. & Podkuiko, Y. A., 1994. Geology

and structure of diamond-bearing rocks of the Kokchetav massif, Kazakhstan. *Tectonophysics*, **233,** 293–313.

Ishikawa, M., Kaneko, Y., Anma, R. & Yamamoto, H., 2000. Subhorizontal boundary between ultrahigh-pressure and low-pressure metamorphic units in the Sulu–Tjube area of the Kokchetav Massif, Kazakhstan. *The Island Arc*, **9,** 317–327

Jagoutz, E., Shatsky, V. S. & Sobolev. N. V., 1990. Sr–Nd–Pb isotopic study of ultrahigh *PT* rocks from Kokchetav massif. *EOS Transactions, American Geophysical Union*, **71,** 1707.

Kaneko, Y., Maruyama, S., Terabayashi, M., Yamamoto, H., Ishikawa, M., Anma, R., Parkinson, C. D., Ota, T., Nakajima, Y., Katayama, I., Yamamoto, J. & Yamauchi, K., 2000. Geology of the Kokchetav UHP–HP massif, Kazakhstan, central Asia. *The Island Arc*, **9,** 264–283.

Kaneko, Y., Maruyama, S., Terabayashi, M., Yamamoto, H., Ishikawa, M., Anma, R., Parkinson, C. D., Ota, T., Nakajima, Y., Katayama, I., Yamamoto, J. & Yamauchi, K., 2002. Geology of the Kokchetav UHP–HP massif. In: Parkinson, C. D., Katayama, I., Liou, J. G. & Marruyama, S. (Eds.), *The Diamond-Bearing Kokchetav Massif, Kazkahstan*. 47–70. Universal Academy Press, Tokyo.

Katayama, I., Maruyama, S., Keneko, Y. & Liou, J. G., 1998. Mineral inclusions in zircon — a window to prograde metamorphism of the Kokchetav UHP rocks. *EOS transactions, American Geophysical Union*, **79,** W126.

Katayama, I., Zayachkovsky, A. A. & Maruyama, S., 2000. Prograde pressure–temperature records from inclusion in zircons from ultrahigh-pressure–high-pressure rocks of the Kokchetav Massif, northern Kazakhstan. *The Island Arc*, **9,** 417–427.

Katayama, I., Maruyama, S., Parkinson, C. D., Terada, K. & Sano, Y., 2001. Ion micro-probe U–Pb zircon geochemistry of peak and retrograde stages of ultrahigh-pressure metamorphic rocks from the Kokchetav massif, northern Kazakhstan. *Earth and Planetary Science Letters*, **188,** 185–195.

Korsakov A. V., Shatsky, V. S. & Sobolev, N. V., 1998. First occurrence of coesite in

eclogites from the Kokchetav massif, Northern Kazakhstan. *Russian Geology and Geophysics*, **34,** 40–50.

Kushev, V. G. & Vinogradov, D. P., 1978. *Metamorphic Eclogites*. Nauka Press, Novosibirsk (*in Russian*).

Maruyama, S., Liou, J. G. & Terabayashi, M., 1996. Blueschists and eclogites of the world and their exhumation. *International Geology Review*, **38,** 485–594.

Masago, H., 2000. Metamorphic petrology of the Barchi-Kol metabasites, western Kokchetav ultrahigh-pressure–high-pressure massif, northern Kazakhstan. *The Island Arc*, **9,** 358–378.

Parkinson, C. D., 2000. Coesite inclusions and prograde compositional zonation of garnets in whiteschist of the Kokchetav UHP–HP massif, Kazakhstan: a record of progressive UHP metamorphism. *Lithos*, **52,** 215–233.

Shatsky V. S., Sobolev, N. V. & Gilbert, A. E., 1989. Eclogites of the Kokchetav massif. In: Sobolev, N. V. (Ed.) *Eclogites and Glaucophane Schists in Folded Belts*. pp. 54–83. Nauka Press, Novosibirsk (*in Russian*).

Shatsky, V. S., Jagoutz, E., Kozmenko, O. A, Blinchic, T. M. & Sobolev, N. V., 1993. Age and genesis of eclogites from the Kokchetav massif, northern Kazakhstan. *Russian Geology and Geophysics*, **34,** 40–50.

Sobolev, N. V., Shatsky, V. S., Vavilov, M. A. & Goryainov, S. V., 1991. Coesite inclusion in zircon from diamondiferous gneiss of Kokchetav massif — first find of coesite in metamorphic rocks in the USSR territory. *Doklady Academy Nauk SSSR*, **321,** 184–188 (*in Russian*).

Terabayashi, M., Ota, T., Yamamoto, H. & Kaneko, Y., 2002. Contact metamorphism of the Daulet Suite by solid intrusion of the Kokchetav Massif. In: Parkinson, C. D., Katayama, I., Liou, J. G. & Marruyama, S. (Eds.), *The Diamond-Bearing Kokchetav Massif, Kazkahstan*. 413–424. Universal Academy Press, Tokyo.

Troesch, M. & Jagoutz, E., 1993. Mica cooling ages of a diamond-bearing gneiss from Kokchetav Massif, Kazakhstan. *Terra Abstracts*, **7,** 396.

Yamamoto, H., Ishikawa, M., Anma, R. & Kaneko, Y., 2000. Subhorizontal boundary between ultrahigh-pressure and low-pressure metamorphic units in the Sulu-Tjube area of the Kokchetav massif, Kazakhstan. *The Island Arc,* **9,** 304–316.

Yamamoto, H., Ishikawa, M., Anma, R. & Kaneko, Y., 2002. Subhorizontal structure and kinematic evolution of HP–UHP metamorphic rocks in the central Kokchetav massif. In: Parkinson, C. D., Katayama, I., Liou, J. G. & Marruyama, S. (Eds.), *The Diamond-Bearing Kokchetav Massif, Kazkahstan*. 71–89. Universal Academy Press, Tokyo.

Zhang, R. Y., Liou, J. G., Coleman, R., Ernst, W. G., Sobolev, N. V. & Shatsky, V. S., 1997. Metamorphic evolution of diamond-bearing and associated rocks from the Kokchetav massif, northern Kazakhstan. *Journal of Metamorphic Geology,* **15,** 479–496.

Zonenshain, L. P., Kuzmin, M. I. & Natapov, D. C., 1990. Geology of the USSR: A plate-tectonic systhesis. Page, B. M. (Ed.), American Geophysical Union, Geodynamic Series 21, Washington D. C.

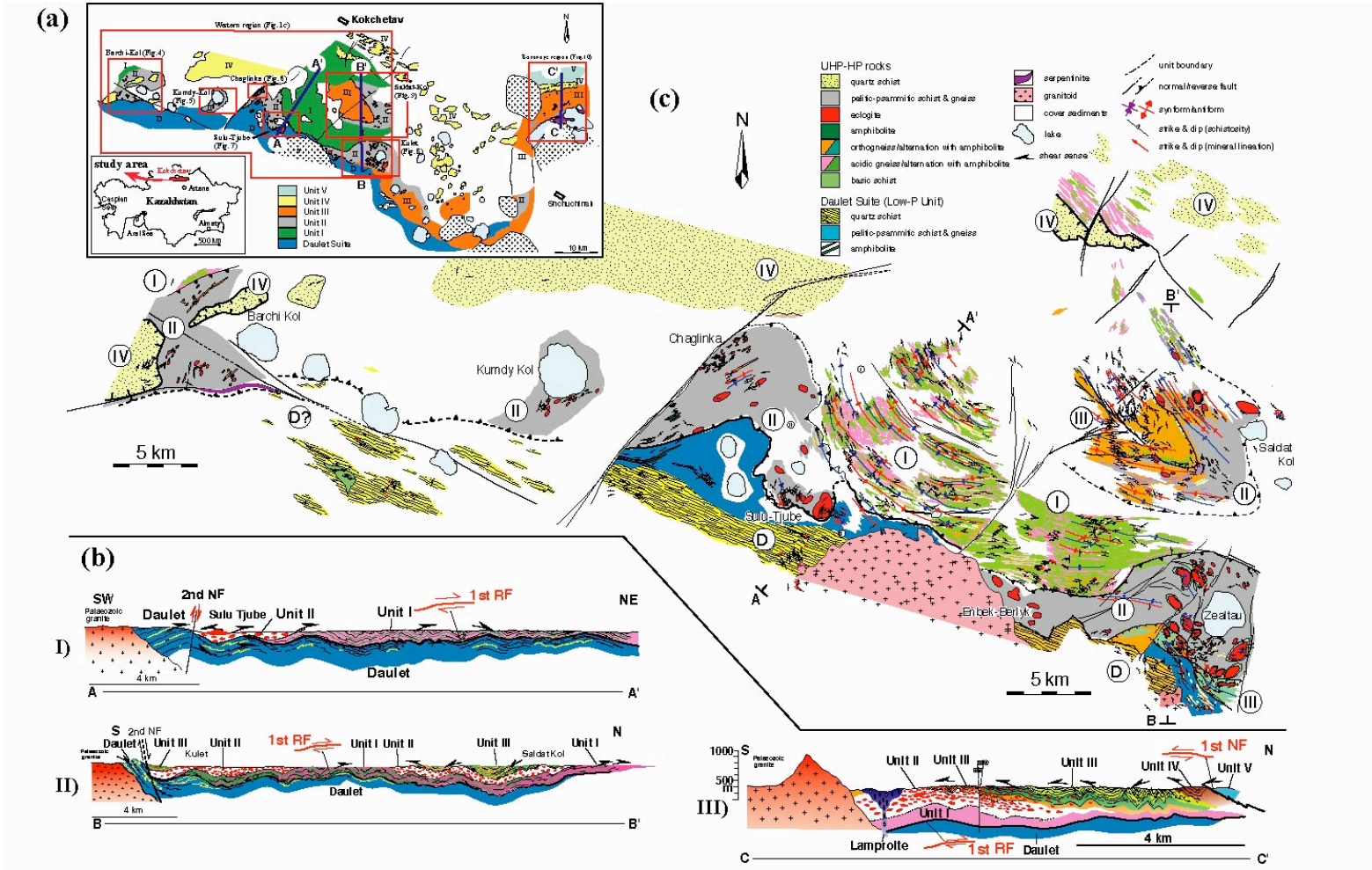

Fig. A–1 Geological maps of the Kokchetav massif (Kaneko *et al.*, 2000). a) Geological sketch map of the whole Kokchetav massif.A–A', B–B' and C–C' represent the locations for the cross-sections shown in (b). Detailed map of the marked areas are shown in (c) and Figs. A–4 – A–10. b) Geologic cross-sections for three representative profiles shown in (a). NF: normal fault; RF: reverse fault. c) detailed geological map of the western half of the Kokchetav massif. Roman numbers I–V and D in circle reprsent Unit I–V and the Daulet Suite, respectively.

Fig. A–2 Field photograph showing the alternation of amphibolite (thin dark layers) and acidic gneiss (pale coloured layers). Unit I. (Kaneko *et al.*, 2002).

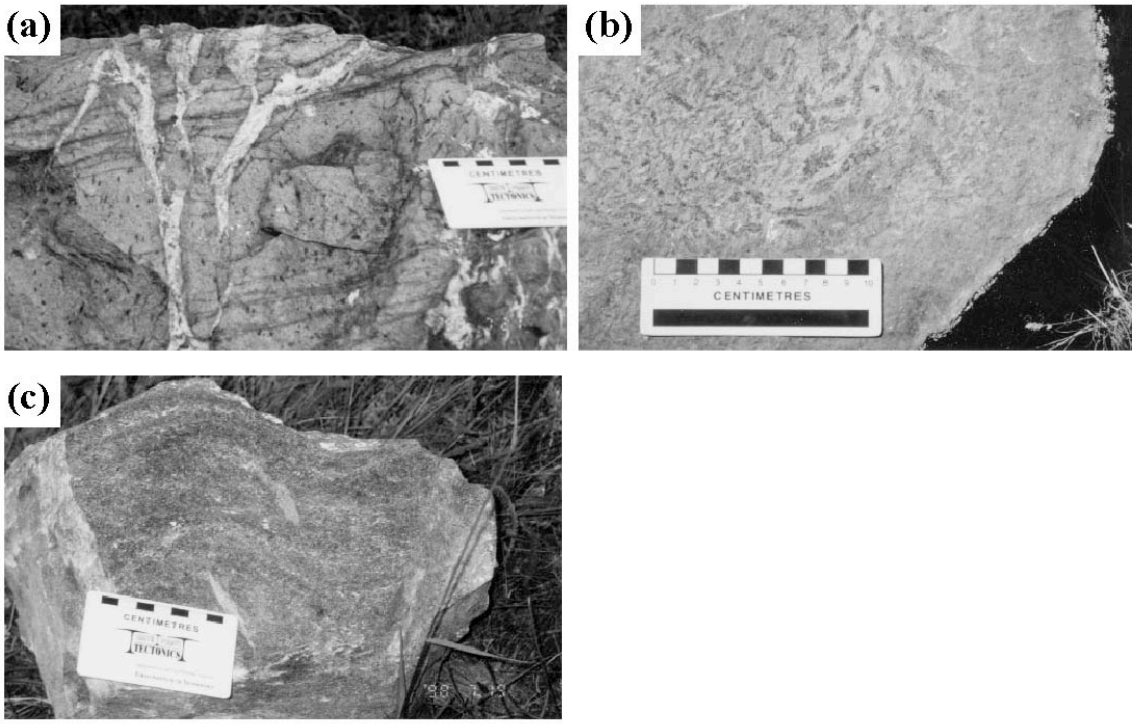

Fig. A–3 Field photographs of three eclogite types (Kaneko *et al.*, 2002). a) Amphibole-eclogite. dark spots are primary amphibole. Late-stage amphiboles make bands which in turn are trancated by quartz veins. Unit II, Kulet. b) Zoisite-eclogite. Primary zoisite appears as dark elongated minerals. Unit II, Sulu-Tjube. c) Dry-eclogite. Unit II, Kumdy-Kol. Garnet-rich (dark coloured) and omphacite-rich (pale coloured) layers are forming compositional banding.

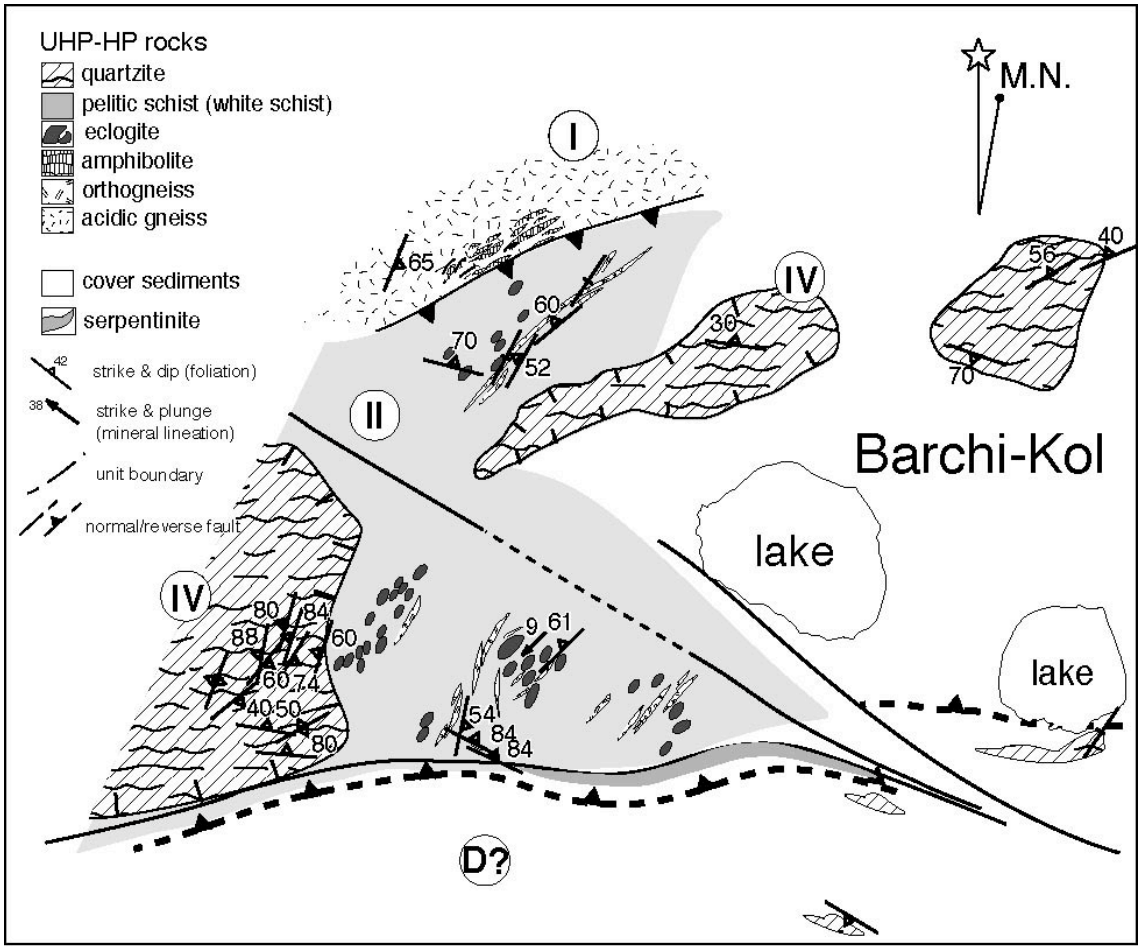

Fig. A–4 Geologic map of the Barchi-Kol region (Kaneko *et al.*, 2000).

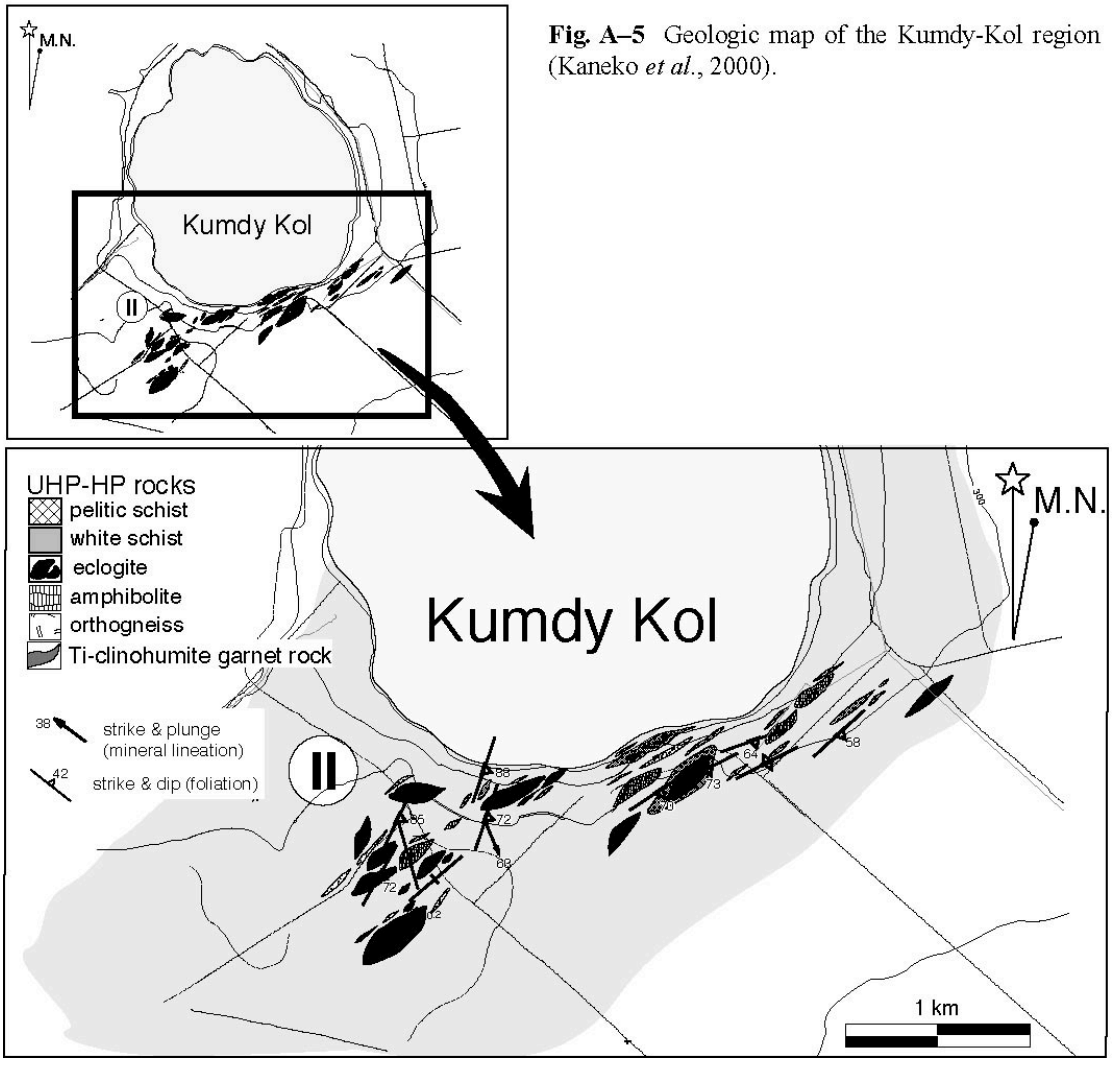

Fig. A–5 Geologic map of the Kumdy-Kol region (Kaneko *et al.*, 2000).

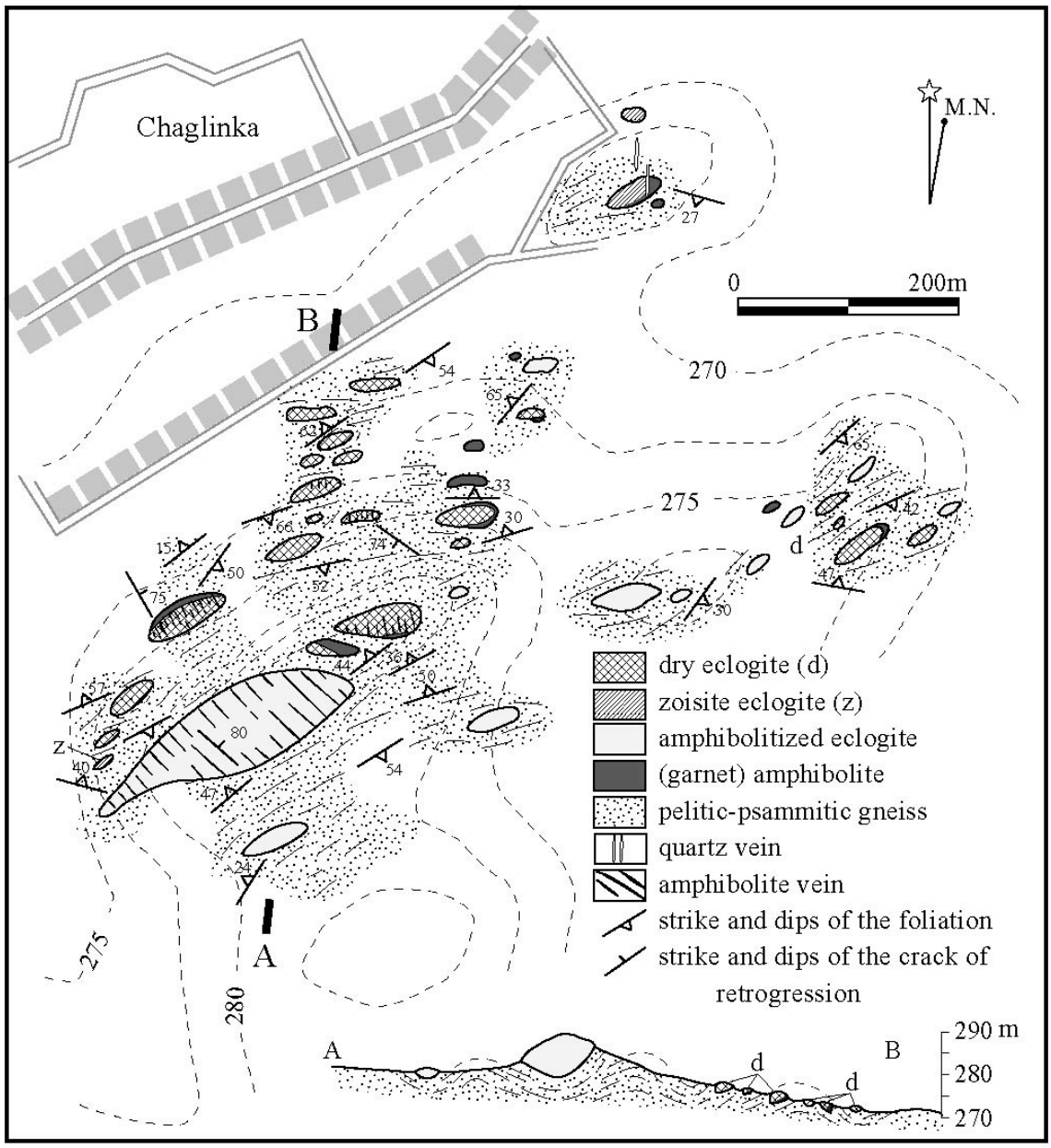

Fig. A–6 Geologic map and cross-section of the Chaglinka region (Kaneko *et al*., 2000).

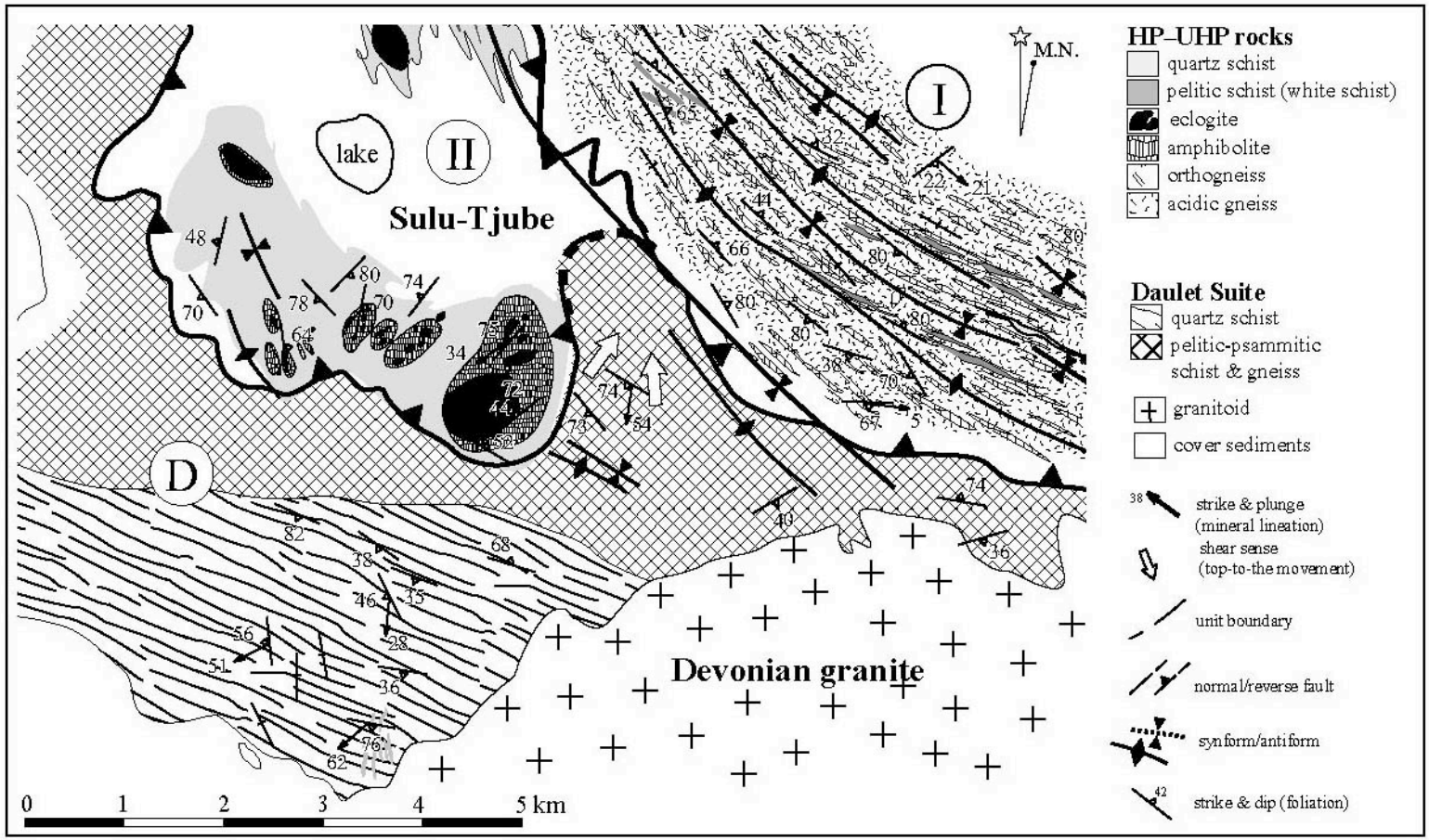

Fig. A–7 Geologic map and cross-section of the Sulu-Tjube region (Kaneko *et al*., 2000).

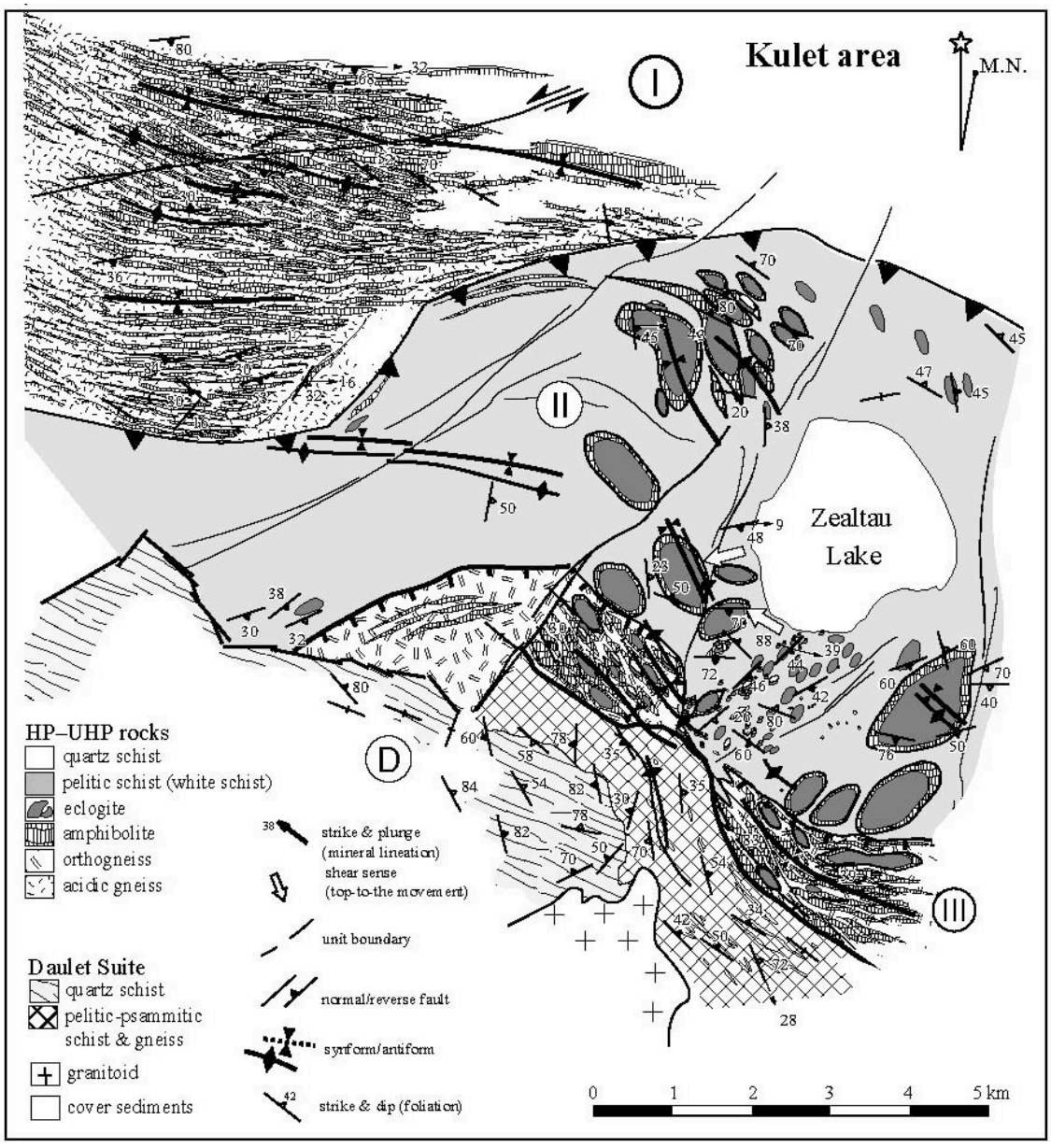

Fig. A–8 Geologic map of the Kulet region (Kaneko *et al.*, 2000).

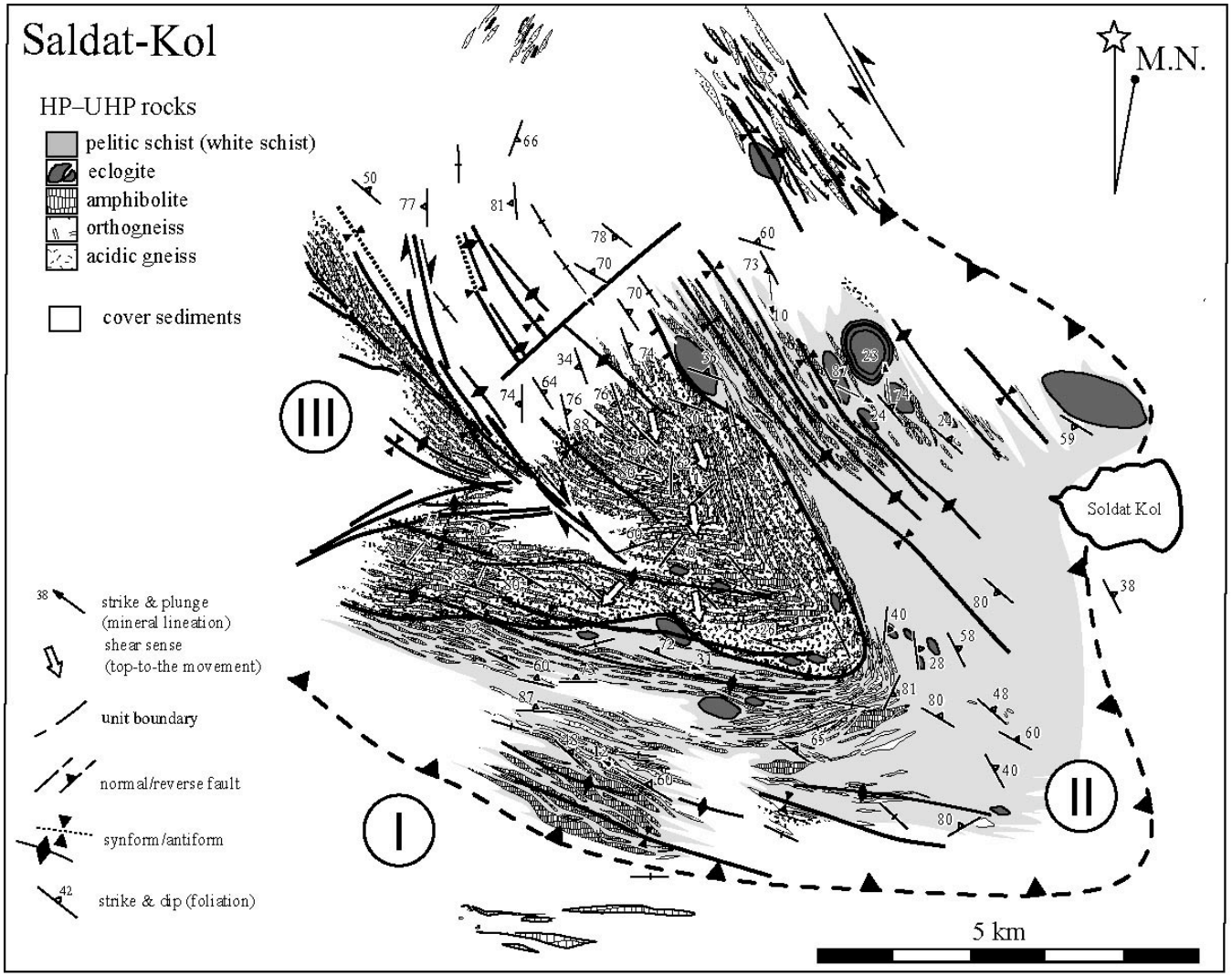

Fig. A–9 Geologic map of the Saldat-Kol region (Kaneko *et al.*, 2000).

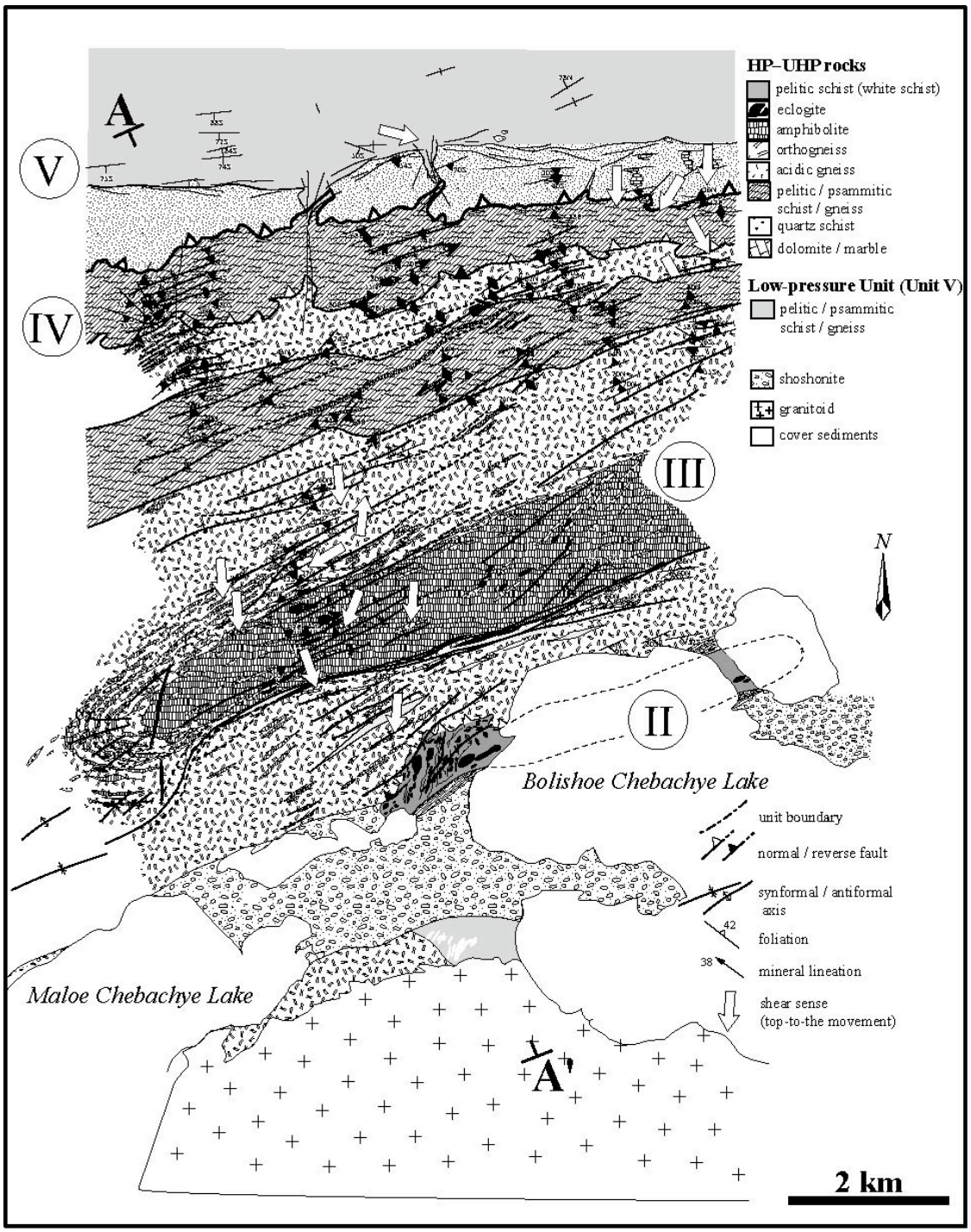

Fig. A–10 Geologic map of the Borovoye region (modified after Kaneko *et al.*, 2000).

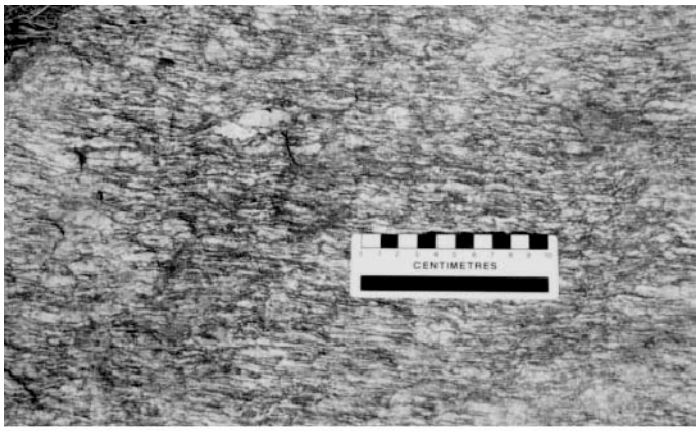

Fig. A–11 Outcrop of orthogneiss of Unit III. Augen and S–C structures are developped (Kaneko *et al*., 2002).

Fig. A–12 Outcrop of alternation of epidote-amphibolite and siliceous schist of Unit IV. (Kaneko *et al*., 2002).

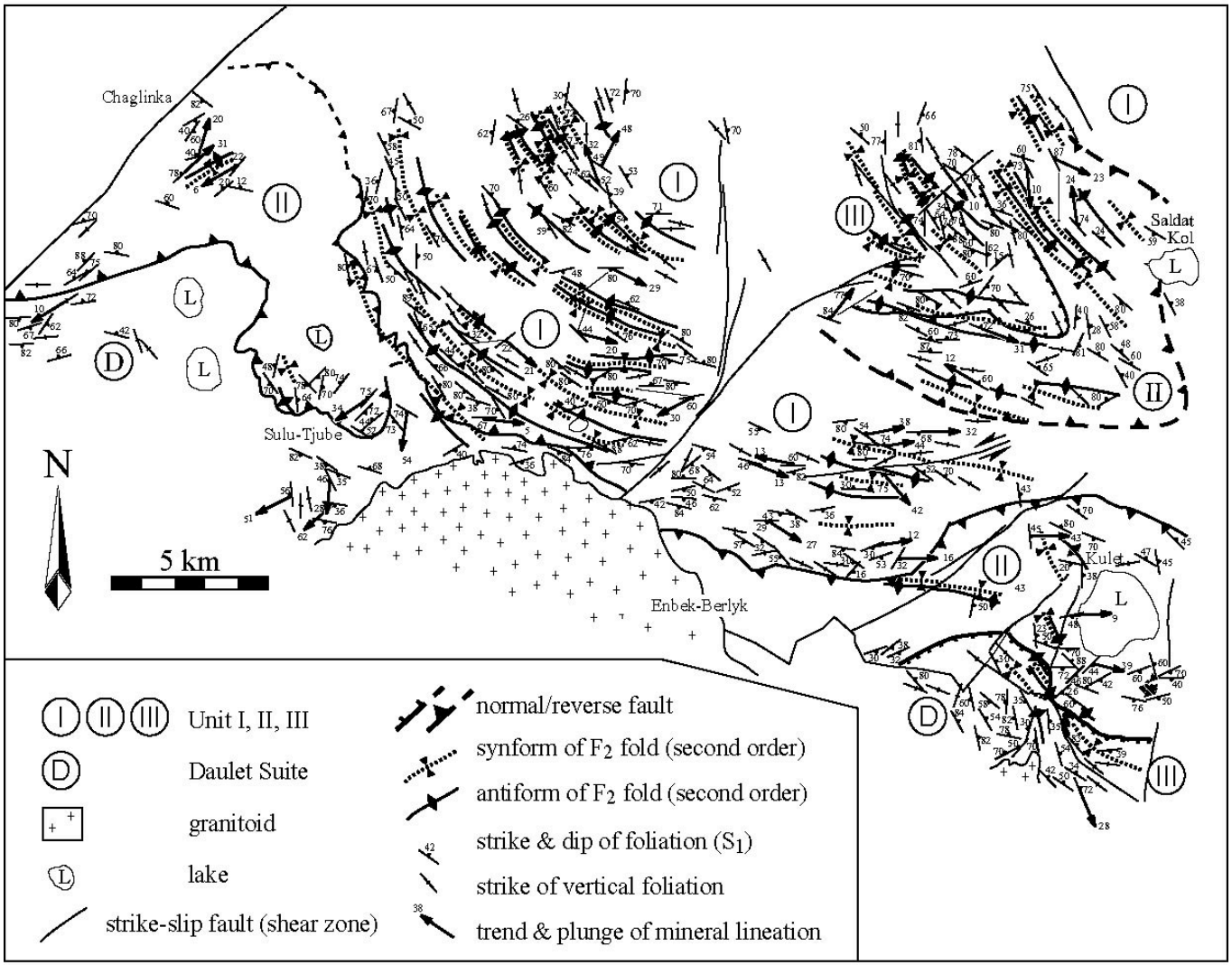

Fig. A–13 Structural map of the Chaglinka–Kulet regions (Yamamoto et al., 2000).

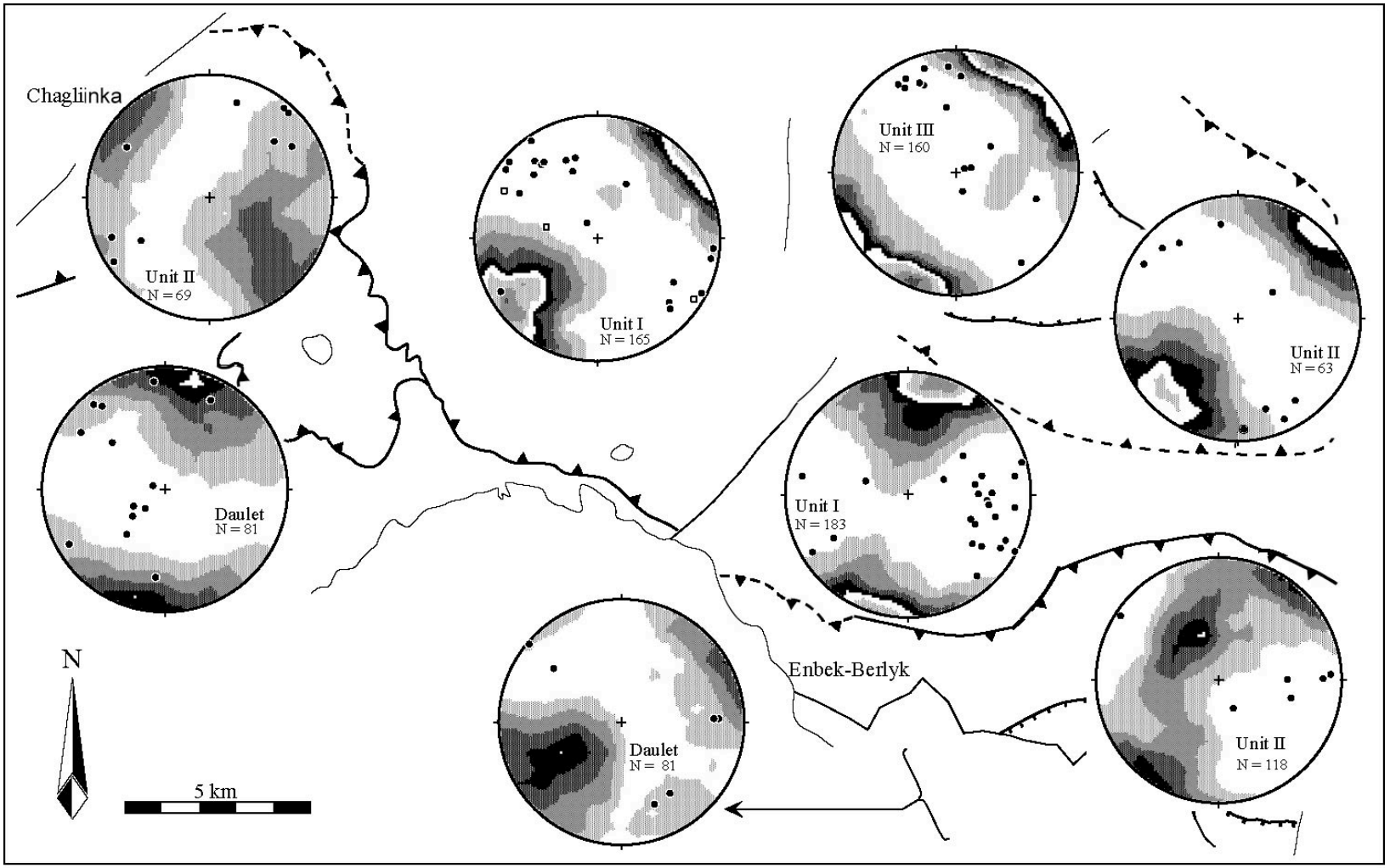

Fig. A–14 Lower hemisphere equal-area projections of the attitudes of planer and linear structures (Yamamoto *et al.*, 2002). Contour: pole of S_1 foliation. The numbers of data for each projection are indicated as 'N' in each diagram. Contour interval is 2.0 σ; Dot: mineral lineation on S_1 foliation; +: fold axis of F_2 fold.

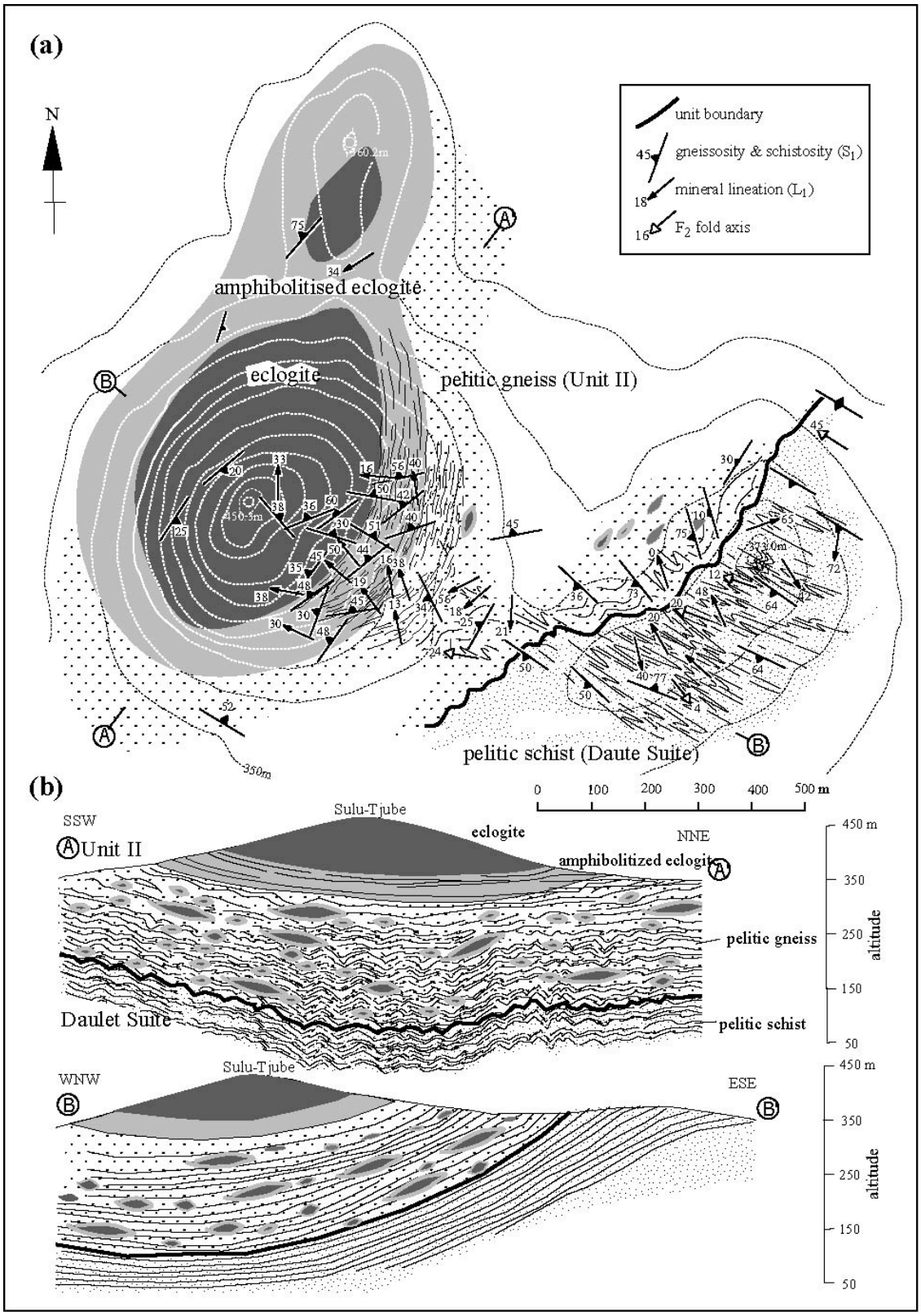

Fig. A–15 a) Structural map around the boundary between the HP–UHP units and the Daulet Suite in the Sulu-Tjube region. b) Geologic cross-sections along A–A' and B–B' shown in (a) (Yamamoto *et al*., 2002).

APPENDIX B

Low $\delta^{18}O$ Eclogites from the Kulet Region

—A Pre-Subduction Record of Fluid–Rock Interaction

ABSTRACT

Oxygen isotopic compositions of silicates in eclogites and whiteschists of the Kokchetav massif were analyzed by whole-grain CO_2-laser fluorination methods. Systematic analyses by CO_2-laser fluorination yielded extremely low $\delta^{18}O$ for eclogites, as low as –3.9‰ for garnet; these values are comparable with those previously reported for Dabie-Sulu UHP eclogites. Oxygen isotope compositions are heterogeneous in samples of eclogite, even on an outcrop scale. Schists have rather uniform oxygen isotope values compared to eclogites, and no $\delta^{18}O$ depletion was observed. Isotope thermometry indicated that both eclogites and schists achieved high-temperature isotopic equilibration at around 500–800 °C. This implies that both prograde and retrograde metamorphic recrystallization barely modified the pre-metamorphic oxygen isotopic signatures. A possible geologic environment to account for the low-$\delta^{18}O$ basaltic protolith is a continental rift subjected to the conditions of a cold climate; only the basalt interacted with low-$\delta^{18}O$ meteoric water, then was tectonically inserted into the surrounding sedimentary units prior to- or during- subduction and ultrahigh-pressure metamorphism.

INTRODUCTION

Since the first report of metamorphic diamonds over a decade ago (Sobolev & Shatsky, 1990), the Kokchetav massif has attracted the interest of geoscientists worldwide. Kokchetav metamorphic rocks represent the deepest recovered relics of subduction so far identified on Earth. In contrast to previously described and relatively well-known ultrahigh-pressure metamorphic (UHPM) terranes, the remarkable abundance of microdiamonds and other mineralogic indicators of burial to depths as much as 200 km (*e.g.* Maruyama & Parkinson, 2000) are unique features of the compex.

The significance of the Kokchetav massif and the much greater depths of burial indicated by microdiamond and other phases, is that UHPM rocks are not just mineralogic curiosities, and the sole preserve of metamorphic petrologists. Study of UHPM rocks, especially those of the Kokchetav massif, challenges the conventional understanding of a wide range of geodynamic and petrochemical processes, and impinges on much more general fields of experimental mantle mineralogy, genesis of arc magmas, fluid transport, and geochemical recycling between crust and deep upper mantle, and the tectonic processes responsible for growth and destruction of continents. The 30 to 200 km vertical sequence represented by Kokchetav HP–UHPM rocks provides an excellent natural laboratory for direct study of these processes.

Considerable attention was focused initially on the mineralogy and petrology of the highest grade, diamond-bearing rocks of the massif. The recent, integrated structural and petrochemical studies of the entire complex have produced a substantial database essential for the quantitative investigation of devolatilization processes in the upper mantle. One fertile, but so far neglected avenue of research, concerns the role of fluids in ultradeep subduction, and the information that can be gleaned from relics exhumed from diamond-stable depths. Specifically, the investigation of Kokchetav rocks, along with previous stable isotope studies of UHPM rocks in the Western Alps and the Dabie–Sulu terrane of China, may clarify the source and nature of fluids involved in UHP and retrograde metamorphism.

The recognition of UHP rocks derived from depths appropriate for magmatic arc generation provides a unique opportunity to investigate the nature and source of deep fluids, and the extent of rock–fluid interaction. The most negative $\delta^{18}O$ values ever recorded for high-T silicates have been reported from coesite-bearing eclogites and

quartzites from China (Yui *et al*., 1995; Zheng *et al*., 1996; Baker *et al*., 1997; Rumble, 1998). Isotopic equilibrium between minerals and host rocks suggests that these Dabie-Sulu rocks acquired negative $\delta^{18}O$ compositions during meteoric water–rock interactions prior to UHPM. They were then isolated from fluid interaction during descent to and return from mantle depths. This hypothesis, which evokes a unique set of conditions, can be tested with isotopic characterization of UHP minerals from microdiamond-bearing rocks from the Kokchetav massif. Important conclusions derived from the stable isotope work in east-central China are: 1) an oxygen-bearing fluid did not attend UHPM or the subsequent exhumation; and 2), a large tract of UHP rocks (about 40 x 50 km in lateral dimensions) retained its isotopic integrity during return to the surface.

The aims of the present reconnaissance study are: 1) to determine oxygen isotopic compositions of Kokchetav silicate minerals in both retrograded and unretrograded UHP (diamond- and coesite-grade) rocks; and 2) to provide constraints on fluid–rock interactions related to the Kokchetav metamorphism.

GEOLOGICAL BACKGROUND AND SAMPLE DESCRIPTION

The Kokchetav massif is situated in the Central Asian Fold Belt, a major Late-Proterozoic–Early-Cambrian tectonic zone. The massif strikes roughly NW–SE, and extends for over 150 km, and is ca. 20 km wide. The massif is composed of several fault-bound lithotectonic units termed Unit I, II, III and IV on the basis of lithology (Kaneko *et al*., 2000; Maruyama & Parkinson, 2000; Fig. B–1a). All four units underwent HP–UHPM, and metamorphic grade increases towards the structurally intermediate Unit II, from epidote-amphibolite facies (Unit IV) through amphibolite (Unit I and III), quartz-eclogite (Unit III) and coesite-eclogite facies to diamond eclogite facies. All these HP–UHPM units are underlain by rocks of the low-pressure Daulet metamorphic suite. This unit is characterized by sillimanite–cordierite series metapelites, probab ly due to contact metamorphism by the overlying HP–UHPM rocks (Terabayashi *et al*., 2002).

Twenty-seven samples, including representative, relatively unretrograded eclogite, amphibolitized eclogite, whiteschist/metapelite and quartz vein material, were selected

for oxygen isotope analyses from Unit II of the Kulet, Barchi-Kol and Kumdy-Kol areas. Mineral compositions were analyzed by JEOL8800 electron microprobe analyzer in the Department of Earth and Planetary Science of Tokyo Institute of Technology.

Samples from the Kulet area

The Kulet region contains the largest and most complete exposures of Unit II. Eclogites and associated metasedimentary schists are mainly exposed around Lake Zheltau. As is many other parts of Unit II, the geology of this region is characterized by block-in-matrix relationships involving abundant lensoidal eclogite bodies enclosed in the enveloping metapelite. The elongation direction of the eclogite lenses is roughly NE–SW in the eastern half of the region, and NW–SE in the western half; they are roughly concordant with the strike of the foliation of the enveloping schists. The length of the eclogite bodies (long axis) varies from a few meters to approximately 1 km. Relatively small blocks of eclogite are concentrated in the central part on the south side of the lake. The highest metamorphic grades occur in this central part, where coesite inclusions in garnet of whiteschist are common (Parkinson, 2000). Coesite-bearing rocks are limited to a narrow fault-bounded zone in which adjacent eclogites also yield coesite-grade *P–T* conditions up to 31 kbar, 760 °C (Ota *et al*., 2000). Eclogite samples for this study were taken from the largest eclogite body which has dimensions of about 1 km x 350 m, and an adjacent smaller body, located on the southeast side of the lake (Fig. B–1b). These rocks are within the quartz-eclogite (Qtz-EC) facies zone of Ota *et al*. (2000). However, thermobarometric results using the Grt–Cpx–Phn geobarometer of Waters & Martin (1993), coupled with the Grt–Cpx cation exchange thermometer of Krogh (1988), are close to the quartz–coesite transformation curve, at 27–29 kbar, 650–730 °C.

Ten eclogite samples of quartz-eclogite from two adjacent bodies, and six mica schist samples were analyzed (Fig. B–1b). Fresh eclogite (ZZ32, ZZ50, ZZ62, ZZ82, ZM52, ZM57) and amphibolitized eclogite (ZZ73 & ZZ78) were sampled from the larger eclogite body (EC body 2). Eclogites are medium to fine-grained and contain the mineral assemblage: Grt + Omp + Qtz + Rt ± Zo ± Phn. Garnets are typically almandine-rich ($Alm_{43–59}Prp_{14–29}Grs_{21–30}Sps_{01–02}$). Clinopyroenes are omphacite, with compositions of $Jd_{33–36}Di_{46–53}Hd_{12–18}$, the acmite component being generally negligible. Phengites have Si contents in the range 3.4–3.5 p.f.u. Peak equilibrium eclogitic mineral

assemblages are relatively well preserved. However most samples display Hbl + Pl symplectites around omphacite grain boundaries. Samples ZZ78 and ZZ73 are well foliated garnet- and epidote-amphibolite, respectively. They are amphibolitized eclogites, and eclogitic minerals and textures have been almost completely obliterated. Minute relict omphacite blebs are preserved in ZZ78. The composition of garnets in ZZ78 shows a slight decrease in Fe/Mg ratio towards the rim, and the compositional range overlaps those of garnet in fresh eclogites; they may, therefore, retain relics of the peak metamorphic stage. Amphiboles are compositionally zoned: ZZ78 amphibole has barroisite cores and hornblende rims; ZZ73 amphibole is more irregular, and compositions varies from hornblende to actinolite.

The smaller eclogite body (EC body 1) is composed of two petrographically and compositionally distinct types of eclogite. The body appears to be a composite of two smaller components, separated by a thin metapelite intercalation. The first type (ZM25 & ZM27), occupying the southwestern half of the body, is composed of very coarse-grained Hbl + Zo with interlocking textures, and has a gabbroic (or at least, coarse-grained igneous precursor) appearance. Fine-grained eclogitic phases (Grt + Omp + Rt + Qtz) are present in the interstices between hornblende and zoisite. Both garnet and omphacite are rich in Mg, with compositions of $Alm_{43–50}Prp_{25–32}Grs_{21–27}Sps_{01}$ for garnet and $Jd_{32–35}Di_{54–55}Hd_{11}$ for omphacite (the acmite component is negligible). Phengite is also present, but texturally appears to be a retrograde product. The second eclogite type (ZM34 & ZM42), which occupies the northeastern half of the body, is medium-grained and contains Grt + Omp + Rt + Qtz and large porphyroblasts of retrograde amphibole. Garnet and omphacite are more Fe-rich than in ZM25 and ZM27; they are in the respective ranges: $Alm_{54–62}Prp_{13–17}Grs_{20–32}Sps_{01}$, and $Jd_{31–35}Di_{44–48}Hd_{21–22}$.

Sample ZM46 is a medium-grained amphibolitized eclogite composed of Amp + Grt + Qtz + Pl. ZM30 is also an amphibolitized eclogite, with very coarse-grained Amp + Grt + Pl. Apatite and titanite are common accessories. Amphibole is compositionally zoned, with barroisitic cores and hornblende rims. Garnet compositions are similar to those of the fresh eclogites.

Sample N306 is a whiteschist that contains Grt + Ky +Phn + Tlc + Rt + Qtz/Coe. Coesite inclusions are abundant in the mantles of large garnet porphyroblasts, and peak *P–T* condition have been estimated as 34–37 kbar, 720–760 °C (Parkinson, 2000). Garnet cores also include prograde micro-assemblages of quartz, zoisite, margarite,

chlorite and graphite. ZZ25 is a fine-grained psammitic schist composed of Qtz + Phn + Grt. The modal abundances of mica and garnet are rather low. Four pelitic schists (ZM40, ZM58, ZL2, ZM69) contain the assemblage: Qtz + Phn ± Grt ± Ky ± Bt. Sample ZM40 is a metapelite derived from the intercalated layer between the northern and southern eclogite components of EC body 2. ZM58 was sampled from the matrix near EC body 1. Sample ZM69 was taken from a shallow trench, and contains coarse-grained garnet and kyanite blades up to 1 cm long. ZL2 is an unusual kyanite-rich schist with a very distinctive bluish color, and contains high-Cr_2O_3 kyanite (up to 1.9 wt%). Garnet and biotite in this rock also have abnormally high Cr_2O_3 contents. Vein quartz (ZM37) was sampled from a 1 m wide quartz vein cutting EC body 2. The sample is almost monomineralic, and has a coarse-grained, interlocking texture.

Samples from the Barchi-Kol Area

Three eclogite samples were taken from a single body defined by a distinctive hummocky topography, reflecting a number of widely dispersed eclogite outcrops (Fig. B–1c). Samples F430 and F431 were collected from the same exposure. F413 was collected from an outcrop 100 m from the other two. The rocks are all medium-grained, and contain Grt + Omp + Rt + Qtz ± Phn ± Ap. Polycrystalline quartz pseudomorphs after coesite are present in omphacite grains. Eclogitic minerals have sharp grain boundaries; retrograde alteration is generally minor. Thin films of retrograde hornblende and/or Hbl + Pl symplectites occur at the rims of some omphacite grains. Retrograde biotite fringes some phengite grains. Peak *P–T* conditions were estimated to be 35–40 kbar, 770–825 °C (Masago, 2000).

Samples from the Kumdy-Kol Area

Kumdy-Kol is the highest grade, highly diamondiferous part of the Kokchetav massif (Fig. B–1d). To the south of Kumdy-Kol, diamond-grade eclogites crop out as numerous small lensoidal blocks within metapelitic schist together with minor amounts of garnet-clinopyroxenite, garnet-titanoclinohumite rock, garnet-biotite-gneiss and diopside-dolomite marble. *P–T* estimates for rocks of the Kumdy-Kol area include 60 kbar, 950–1050 °C for eclogite (Okamoto *et al*., 2000), and up to 70 kbar at 980 °C for diopside-dolomite marble (Ogasawara *et al*., 2000).

Three eclogite samples and one metapelitic schist sample were selected for analysis. Eclogites were derived from two adjacent bodies. The schist was taken from an outcrop close to eclogite A21 (Fig. B–1d). Eclogite samples A15, A21, and A34 are medium- to coarse-grained rocks and dominantly bimineralic (Grt + Omp), with minor amounts of quartz and rutile. The metapelitic rock (A12) is a diamondiferous garnet–phengite schist composed of Grt + Phn + Qtz + Ky + Pl. Rutile, ilmenite, zircon and apatite occur as accessory minerals. Microdiamonds were identified as inclusions in zircon, garnet and kyanite (Katayama *et al.*, 2001).

ANALYTICAL METHODS

Oxygen isotope analyses were made by laser-ablation fluorination at the Geophysical Laboratory of the Carnegie Institution of Washington. Samples were prepared as mineral separates by a combination of sieving, panning, magnetic separation, heavy liquid separation, acid dissolution and hand picking. Approximately 2 mg of mineral separates were heated to incandescence and melted by CO_2-laser with 10.5 micron wavelength (Sharp, 1990) in the presence of BrF_5 to extract oxygen. Oxygen isotopes were analyzed using a Finningan MAT 252 mass spectrometer. Comparison materials UWG-2 garnet and NBS-28 quartz were utilized as standards for interlaboratory normalization. The precision of analyses is better than 0.2 ‰.

RESULTS

Results of analyses for Kulet samples are listed in Table B–1. Samples from the smaller eclogite body (body 1 in Fig. B–2) have rather uniform $\delta^{18}O$ compositions from +3.5 to +4.7 ‰ for garnet, +4.6 ‰ for omphacite (one sample), +7.4 to +8.8‰ for quartz and +1.6‰ for rutile (one sample). In contrast, samples from the larger eclogite body (body 2 in Fig. B–2) have a rather wide variation of $\delta^{18}O$ values, ranging from –3.9 to +1.1 ‰ for garnet, from –3.5 to –0.5 ‰ for omphacite, from +0.1 to +5.1‰ for quartz and –5.4 ‰ for rutile. The whiteschists and other metapelitic schists have rather uniform $\delta^{18}O$ values throughout the area: from +6.1 to +7.5 ‰ for garnet, from +9.9 to

+10.7 ‰ for quartz, and +6.7 to +6.8 ‰ for phengite (Fig. B–2). ZM37 vein quartz has $\delta^{18}O$ of +8.7 ‰.

Figure B–3 illustrates the spatial variation of $\delta^{18}O$ values in the Kulet region. $\delta^{18}O$ values from eclogite body 2 display a rather heterogeneous distribution. The lowest $\delta^{18}O$ eclogite sample (–3.9 ‰ for garnet) is located in the central part, at the top of the eclogite hill; the highest $\delta^{18}O$ eclogite sample (+1.1 ‰ for garnet) is located on the outermost margin of the body. However, the distribution of intermediate $\delta^{18}O$ eclogite samples appears to be random.

The results of analyses of Barch-Kol samples are listed in Table 2. Two eclogite samples (F430 and F431) exhibit nearly identical $\delta^{18}O$ values: from –0.4 to –0.1 ‰ for garnet, from +0.5 to +1.2 ‰ for omphacite, from +2.5 to +3.2 ‰ for quartz, and from –2.6 to –2.4 ‰ for rutile. The other sample (F413 —100 m distant, but from the same eclogite body) has very different $\delta^{18}O$ values of +5.1‰ for garnet, +5.0‰ for omphacite, +9.0 ‰ for quartz and +2.2 ‰ for rutile.

Eclogite samples from the Kumdy-Kol region (Table B–3; Fig. B–2) display considerable variation, ranging from +7.0 to +12.5 ‰ for quartz, and from +4.3 to +7.9 ‰ for garnet. They can be subdivided into two groups. Samples A15 and A21 have rather similar $\delta^{18}O$ values, and A34 possesses values about 4 ‰ lower. The diamondiferous schist, A12, has $\delta^{18}O$ values about 3 ‰ heavier than the Kulet schists: +13.5 ‰ for quartz, +10.5 ‰ for garnet, +10.3 ‰ for phengite and +11.6 ‰ for kyanite. The $\delta^{18}O$ values of garnet and phengite display a reverse fractionation and are clearly out of isotopic equilibrium.

ISOTOPE THERMOMETRY

Figure B–4 shows oxygen isotopic fractionations between garnet and co-existing minerals. Garnet is compositionally and isotopically resistant to late-stage alteration. It is, therefore, one of the most reliable phases preserving isotopic compositions of peak metamorphism. Isopleths in Fig. B–4 show isotopic equilibration at given temperatures. The calibrations of Sharp (1995), Matthews (1994), and Javoy (1977) were used.

For eclogites, omphacite–garnet pairs generally yielded petrologically unrealistically high temperatures > 1000°C. In some samples, omphacite has a lower

$\delta^{18}O$ value than that of garnet, and is clearly out of equilibrium. Most of temperatures deduced from the quartz–garnet and garnet–rutile pairs are within the range of 600–700 °C. Garnet–amphibole pairs generally yielded petrologically unrealistically low temperatures < 200°C, suggesting isotopic disequilibrium. Temperatures estimated from garnet–zoisite pairs scatter over a wide range from 550 to 900 °C. The isotopic fractionation between garnet and zoisite is small, thus analytical uncertainties may have caused the apparent variation in temperatures.

The thermometric results of the whiteschist show very good correspondence. Garnet–kyanite and garnet–phengite pairs yielded equilibrium temperatures of 750–800 °C. Quartz–garnet pairs yielded temperatures of about 600°C. For the other schists, garnet–kyanite and quartz–garnet pairs yielded about 800 °C and 600 °C, respectively. Garnet–phengite pairs scatter and yielded unrealistically high temperatures.

DISCUSSION

Origin of Low $\delta^{18}O$ in Kokchetav Eclogites

Eclogites of the Kokchetav massif yielded very low $\delta^{18}O$ values, with the most negative being –3.9´‰ for garnet in eclogite ZM52, from eclogite body 2 in the Kulet area. This is an unusually low value for eclogites. Oxygen isotope compositions of various metamorphic rocks are summarized in Figure B–5. Typical eclogites have values from +2 to +5 ‰ for garnet. Note that low $\delta^{18}O$ eclogites have been reported from the Dabie–Sulu UHPM terrane (Yui *et al*., 1995; 1997; Zheng *et al*., 1996; 1998; 1999; Baker *et al*. 1997; Rumble & Yui, 1998). This study reports a second UHPM terrane with abnormally low $\delta^{18}O$ eclogite.

Low $\delta^{18}O$ eclogites were found in both the Kulet and Barchi-Kol areas. These two areas are separated by about 60 km, and are of different metamorphic grades; the former is Qtz-EC facies and the latter is Coe-EC facies. Low $\delta^{18}O$ signatures were not detected in diamond-grade Kumdy-Kol eclogites, but that may simply reflect the limited number of samples analyzed.

Kokchetav eclogite bodies appear to be isotopically heterogeneous. Eclogite body 2 in Kulet shows a wide variation, ranging from –3.9 to +1.1 ‰ for garnet. Even the

much smaller Barchi-Kol eclogite body has an isotopic variation from –0.4 to +5.1 ‰ (for garnet). Similar local but widespread heterogeneities have been reported from other HP and UHPM terranes, including Sulu and Dabie areas (Philippot & Rumble, 2000), as well as mafic blueschists and eclogites of the Western Alps (Barnicoat & Cartwright, 1997).

It is generally regarded that dehydration during subduction does not significantly change a slab's oxygen isotopic composition. Fractionation of oxygen isotopes during dehydration under the temperatures of interest is less than 1 ‰ (Valley, 1986). Numerical simulation of oxygen isotope fractionation by dehydration from amphibolite resulted in a change of less than 0.2 ‰ (Barnicoat & Cartwright, 1997). The only possible way to effectively and substantially lower the $\delta^{18}O$ of a rock is interaction with markedly negative $\delta^{18}O$ fluid. The only source of negative $\delta^{18}O$ is meteoric water, especially in a cold climate (high latitude and/or high altitude). Thus, the low $\delta^{18}O$ Kokchetav protoliths must have interacted with meteoric water at some time after initial magmatic crystallization. The opportunity for eclogitic rocks to interact with meteoric water is limited to either during a pre-subduction episode (protolith) or after exhumation of the UHPM belt to the surface. Thermometric results show high temperature (> 500°C) oxygen isotope equilibrations for eclogitic minerals. This appears to preclude near-surface alteration subsequent to UHP metamorphism and exhumation.

Major, trace and rare earth element abundances of Kokchetav metabasites are generally comparable with MORB (Yamamoto *et al*., 2002). One possible geologic setting whereby newly erupted basalts could interact with meteoric water is a transition from a continental rift to an oceanic environment, analogous to present-day Afar, but, in contrast, under cold climate conditions. The Earth experienced extreme global climatic conditions at all latitudes during the Neoproterozoic (*i.e*. immediately prior to the Kokchetav UHPM orogenic event). Hoffman *et al*. (1998) proposed that global icehouse conditions alternated with greenhouse conditions several times during this time span, based on widespread glacial deposits and the correlation of associated carbonate sediments by isotopic stratigraphy. It is interesting to speculate that the parental basalts of Kokchetav eclogites, presumably erupted some time during the Neoproterozoic (although we have no independent confirmation of protolith ages), may preserve the isotopic signature of extremely cold climatic conditions related to 'Snowball Earth'.

Speculative Tectonic Model

Basaltic protoliths of the Kokchetav eclogite were erupted in a continental rift, and underwent extensive but heterogeneous infiltration by very cold meteoric water during 'Snowball Earth' climatic conditions. As a result, heterogeneous, low $\delta^{18}O$ compositions were recorded in eclogite protoliths (Fig. B–6a). The abundance of orthogneiss, impure marble and whiteschist (possibly of evaporitic origin resulting from conditions analogous to modern polar deserts as in the Antarctic dry valleys), with which the eclogites are presently intercalated, probably originated in a passive continental margin sedimentary basin, and interacted with normal $\delta^{18}O$ seawater (Fig. B–6b).

The parental basalt and passive margin sediments were tectonically juxtaposed prior to- or during- subduction to depths up to 200 km and recrystallized under coesite- to diamond-grade eclogite-facies conditions (Fig. B–6c). Isotopic fractionation due to progressive dehydration was negligible. Oxygen isotopes were re-equilibrated among coexisting minerals, essentially in a closed system; the rocks were isolated from fluid interaction during their descent to mantle depths.

During exhumation, HP–UHPM rocks underwent extensive hydration at mid-crustal depths, resulting in amphibolite-facies recrystallization (Fig. B–6d), and probable minor modifications in isotopic equilibration. Grain boundary diffusion-induced isotopic exchange might also have played a role in producing limited isotopic disequilibrium.

In conclusion, Kokchetav eclogites have low negative $\delta^{18}O$ values, and are directly comparable with similar negative $\delta^{18}O$ values for coesite-bearing eclogites and quartzites, schists, and gneisses from east-central China. In both UHPM terranes, these compositions were acquired during meteoric water–rock interactions prior to UHP metamorphism.

REFERENCES

Agrinier, P., Javoy, M., Smith, D. C. & Pineau, F., 1985. Carbon and oxygen isotopes in eclogites, amphibolites, veins and marbles from Western Gneiss region, Norway. *Chemical Geology*, **52,** 145–162.

Baker, J., Matthews, A., Mattey, D., Rowley, D. B. & Xue, F., 1997. Fluid–rock interaction during ultra-high pressure metamorphism, Dabie Shan, China. *Geochimica et Cosmochimica Acta*, **61,** 1685–1696.

Barnicoat, A. C. & Cartwright, I., 1997. Focused fluid flow during subduction: Oxygen isotope data from high-pressure ophiolites of the western Alps. *Earth and Planetary Science Letters*, **132,** 53–61.

Hoffman, P. F., Kaufman, A. J., Halverson, G. P. & Schrag, D. P., 1998. A Neoproterozoic snowball Earth, *Science*, **281,** 1342–1346.

Javoy, M., 1977. Stable isotopes and geothermometry. *Journal of Geological Society of London,* **133,** 609–636.

Kaneko, Y., Maruyama, S., Terabayashi, M., Yamamoto, H., Ishikawa, M., Anma, R., Parkinson, C. D., Ota, T., Nakajima, Y., Katayama, I., Yamamoto, J. & Yamauchi, K., 2000. Geology of the Kokchetav UHP–HP metamorphic belt, northern Kazakhstan. *The Island Arc*, **9,** 264–283.

Katayama, I., Maruyama, S., Parkinson, C. D., Terada, K. & Sano, Y., 2001. Ion micro-probe U–Pb zircon geochronology of peak and retrograde stages of ultrahigh-pressure metamorphic rocks from the Kokchetav massif, northern Kazakhstan. *Earth and Planetary Science Letters*,**188,** 185–198.

Krogh, E. J., 1988. The garnet–clinopyroxene Fe-Mg geothermometer – a reinterpretation of existing experimental data. *Contributions to Mineralogy and Petrology*, **99,** 44–48.

Maruyama, S. & Parkinson, C. D., 2000. Overview of the geology, petrology and tectonic framework of the high-pressure–ultrahigh-pressure metamorphic belt of the Kokchetav Massif, Kazakhstan. *The Island Arc*, **9,** 439–455.

Masago, H., 2000. Metamorphic petrology of the Barchi-Kol metabasites, western Kokchetav UHP–HP massif, northern Kazakhstan. *The Island Arc*, **9,** 358–378.

Matthews, A., 1994. Oxygen isotope geothermometers for metamorphic rocks. *Journal of Metamorphic* Geology, **12,** 211–219.

Ogasawara, Y., Ohta, M., Fukasawa, K., Katayama, I. & Maruyama, S., 2000. Diamond-bearing and diamond-free metacarbonate rocks from Kumdy-Kol in the Kokchetav Massif, northern Kazakhstan. *The Island Arc*, **9,** 400–416.

Okamoto, K., Liou, J. G. & Ogasawara, Y., 2000. Petrology of the diamond-grade eclogite in the Kokchetav Massif, northern Kazakhstan. *The Island Arc*, **9,** 379–399.

Ota, T., Terabayashi, M., Parkinson, C. D. & Masago, H., 2000. Thermobaric structure of the Kokchetav ultrahigh-pressure massif deduced from a north–south transect in the Kulet and Saldat-kol regions, northern Kazakhstan. *The Island Arc*, **9,** 328–357.

Parkinson, C. D., 2000. Coesite inclusions and prograde compositional zonation of garnets in whiteschist of the Kokchetav UHP–HP massif, Kazakhstan: a record of progressive UHP metamorphism. *Lithos*, **52,** 215–233.

Philippot, P. & Rumble, D. III., 2000. Fluid–rock interactions during high-pressure and ultrahigh-pressure metamorphism. *International Geological Revew*, **42,** 312–327.

Rumble, D., 1998. Stable isotope geochemistry of ultrahigh-pressure rocks. In: *When Continents Collide: Geodynamics and Geochemistry of Ultrahigh-Pressure Rocks* (eds. B. R. Hacker & J. G. Liou), 241–259. Kluwer Academic Publishers, Dordrecht.

Rumble, D. & Yui, T. F., 1998. The Qinglongshan oxygen and hydrogen isotope anomaly near Donghai in Jiangsu province, China. *Geochimica et Cosmochimica Acta*, **62,** 3307–3321.

Sharp, Z. D., 1990. A laser-based microanalytical method for the in-situ determination of oxygen isotope ratios of silicates and oxides. *Geochimica et Cosmochimica Acta*, **54,** 1353–1357.

Sharp, Z. D., Essene, E. J. & Hunziker, J. C., 1993. Stable isotope geochemistry and phase equilibria of coesite-bearing whiteschists, Dora Maira Massif, western Alps. *Contrbutions to Mineralogy and Petrology*, **114,** 1–12.

Sharp, Z. D., 1995. Oxygen isotope geochemistry of the Al_2SiO_5 polymorphs. *American Journal of Science*, **295,** 1058–1076.

Sobolev, N. V. & Shatsky, V. S., 1990. Diamond inclusion in garnets from metamorphic rocks: a new environment for diamond formation. *Nature*, **343**, 742–746.

Terabayashi, M., Ota, T., Yamamoto, H. & Kaneko, Y., 2002. Contact metamorphism of the Daulet Suite by solid-state emplacement of the Kokchetav UHP–HP metamorphic slab. *International Geology Review,* **44,** 819–830.

Valley, J. W., 1986. Stable isotope geochemistry of metamorphic rocks. In: *Stable Isotopes in High Temperature Geological Processes* (Eds. J. W. Valley, H. P. Taylor, J. R. O' Neil), 445–489. Mineralogical Society of America. Washington, D. C.

Waters, D. J. & Martin, H. N., 1993. Geobarometry in phengite-bearing eclogites. *Terra Abstract,* **5,** 410–411.

Yamamoto, J., Maruyama, S., Parkinson, C. D. & Katayama, I., 2002. Geochemical characteristics of metabasites from the Kokchetav massif: Subduction zone metasomatism along an intermediate geotherm. In: Parkinson, C. D., Katayama, I., Liou, J. G. & Marruyama, S. (Eds.), *The Diamond-Bearing Kokchetav Massif, Kazkahstan*. 71–89. Universal Academy Press, Tokyo.

Yui T. F., Rumble D. & Lo C. H., 1995. Unusually low $d^{18}O$ ultrahigh-pressure metamorphic rocks from the Sulu terrain, eastern China. *Geochimica et Cosmochimica Acta*, **59,** 259–2864.

Yui, T. F., Rumble, D., Chen, C. H. & Lo, C. H., 1997. Stable isotope characteristics of eclogites from the ultra-high-pressure metamorphic terrain, east-central China. *Chemical Geology,* **137,** 135–147.

Zheng, Y-. F., Fu, B., Gong, B. & Li, S., 1996. Extreme ^{18}O depletion in eclogite from the Su-Lu terrane in East China. *European Journal of Mineralogy,* **8,** 317–323.

Zheng, Y-. F., Fu, B., Li, Y., Xiao, Y. & Li, S., 1998. Oxygen and hydrogen isotope geochemistry of ultrahigh-pressure eclogites from the Dabie Mountains and Sulu

terrane. *Earth and Planetary Science Letters*, **155,** 113–129.

Zheng, Y. F., Fu, B., Xiao, Y., Li, Y. & Gong, B., 1999. Hydrogen and oxygen isotope evidence for fluid–rock interactions in the stages of pre- and post-UHP metamorphism in the Dabie Mountains. *Lithos*, **46,** 677–693.

Table B–1. Oxygen isotope compositions in the Kulet samples. Numbers are presented as $\delta^{18}O$ (‰).

sample No.	lithology	Qtz	Grt	Omp	Amp	Rt	Zo/Ep	Pl	Phn	Ky	Bt
ec body 1											
ZM52	ec	0.1	-3.9	-4.3	-4.1	-6.9	-2.5				
ZM57	ec	1.2	-2.4	-2.5	-2.4						
ZZ32	ec	5.1	1.1	0.5	1.2	-2.2	2.0				
ZZ50	ec	1.2	-3.5	-3.4							
ZZ62	ec	1.8	-3.4	-3.9	-3.2		-2.6				
ZZ82	ec	3.9	-1.1	-0.5	-0.5						
ZZ78	am (retro-ec)	3.0	-2.4		-1.4	-5.4					
ZZ73	am (retro-ec)				-0.2		1.5				
ec body 2											
ZM25	ec	8.9	4.7		5.1	1.6	6.2				
ZM27	ec	8.4	4.2		4.5		4.9				
ZM34	ec	7.4	4.4	4.6		1.6					
ZM42	ec	7.4	3.9	3.7	4.3						
ZM46	am (retro-ec)		3.5		4.1						
ZM30	am (retro-ec)		5.2		5.6			9.7			
schist											
ZZ25	psam sch	10.7	6.8								
ZM40	pel sch	10.9	6.7						7.5		
ZM58	pel sch	9.9							6.6		
ZM64	pel sch		6.8						7.5	7.6	
ZL2	pel sch		7.5						7.4	8.1	6.0
N306	whiteschist	10.1	6.1						7.2	6.9	
Qtz vein											
ZM37		8.7									

ec: eclogite; am (retro-ec): amphibolite (retrograded from eclogite); psam sch: psammitic schist; pel sch: pelitic schist.

Table B–2. Oxygen isotope compositions in Barchi-Kol samples. Numbers are presented as $\delta^{18}O$ (‰).

sample No.	lithology	Qtz	Grt	Omp	Rt
F413	ec	9.0	5.1	5.0	2.2
F430	ec	3.2	-0.1	1.2	-2.4
F431	ec	2.5	-0.4	0.5	-2.6

Abbreviations for minerals are same as those used in Table B–1.

Table B–3. Oxygen isotope compositions in Kumdy-Kol samples. Numbers are presented as $\delta^{18}O$ (‰).

sample No.	lithology	Qtz	Grt	Omp	Rt	Phn	Ky
A15	ec	12.5	7.9		6.7		
A21	ec	11.3	7.8	7.5	6.1		
A34	ec	7.0	4.3	4.1	2.1		
A12	pel sch	13.5	10.5			10.3	11.6

Abbreviations for minerals and rocks are same as those used in Table B–1.

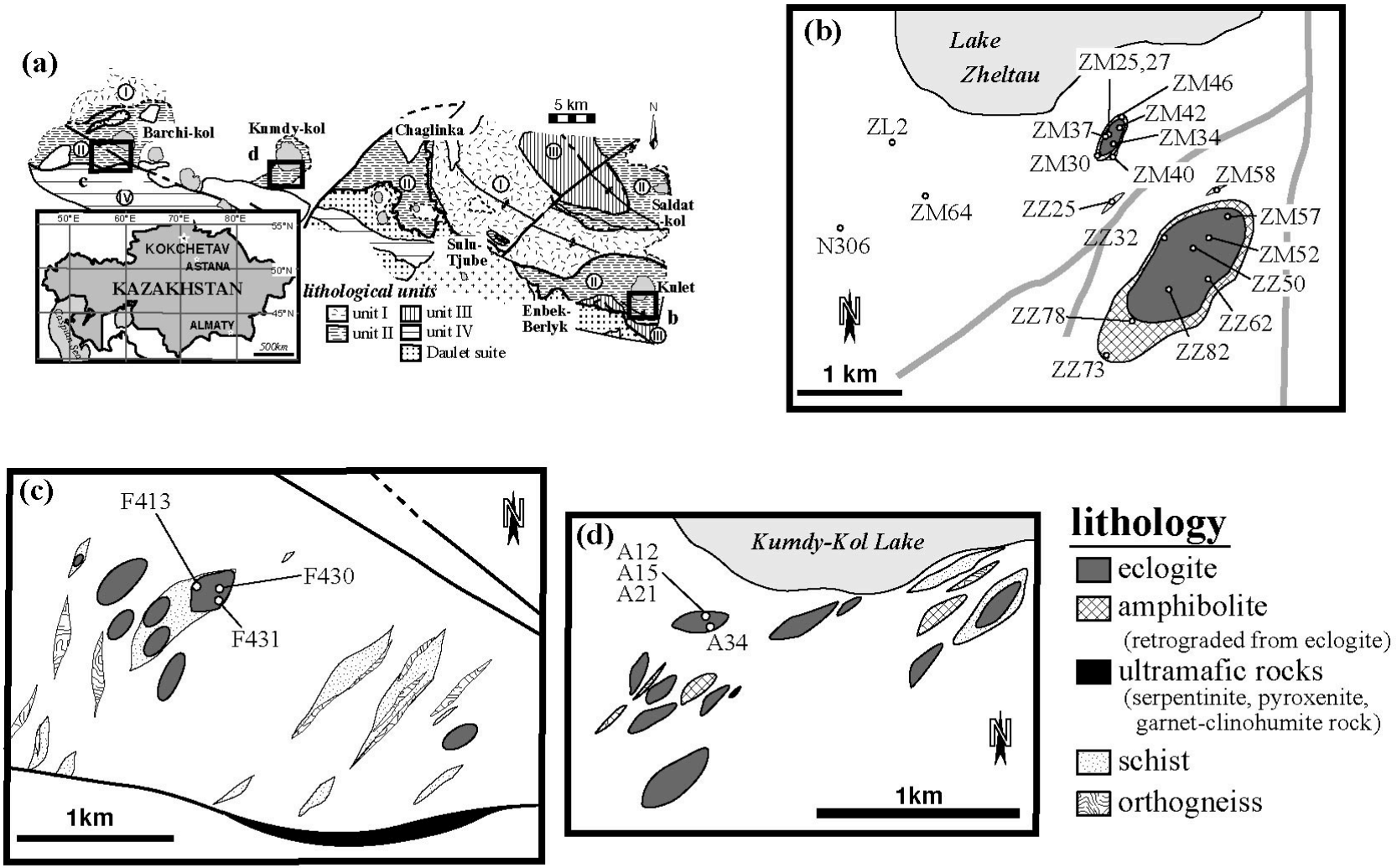

Fig. B–1 a) Geologic map of the Kokchetav massif (simplified after Kaneko *et al.*, 2000). (b)–(d) Geologic maps and sample locations in b) Kulet; c) Barchi-Kol; and d) Kumdy-Kol regions.

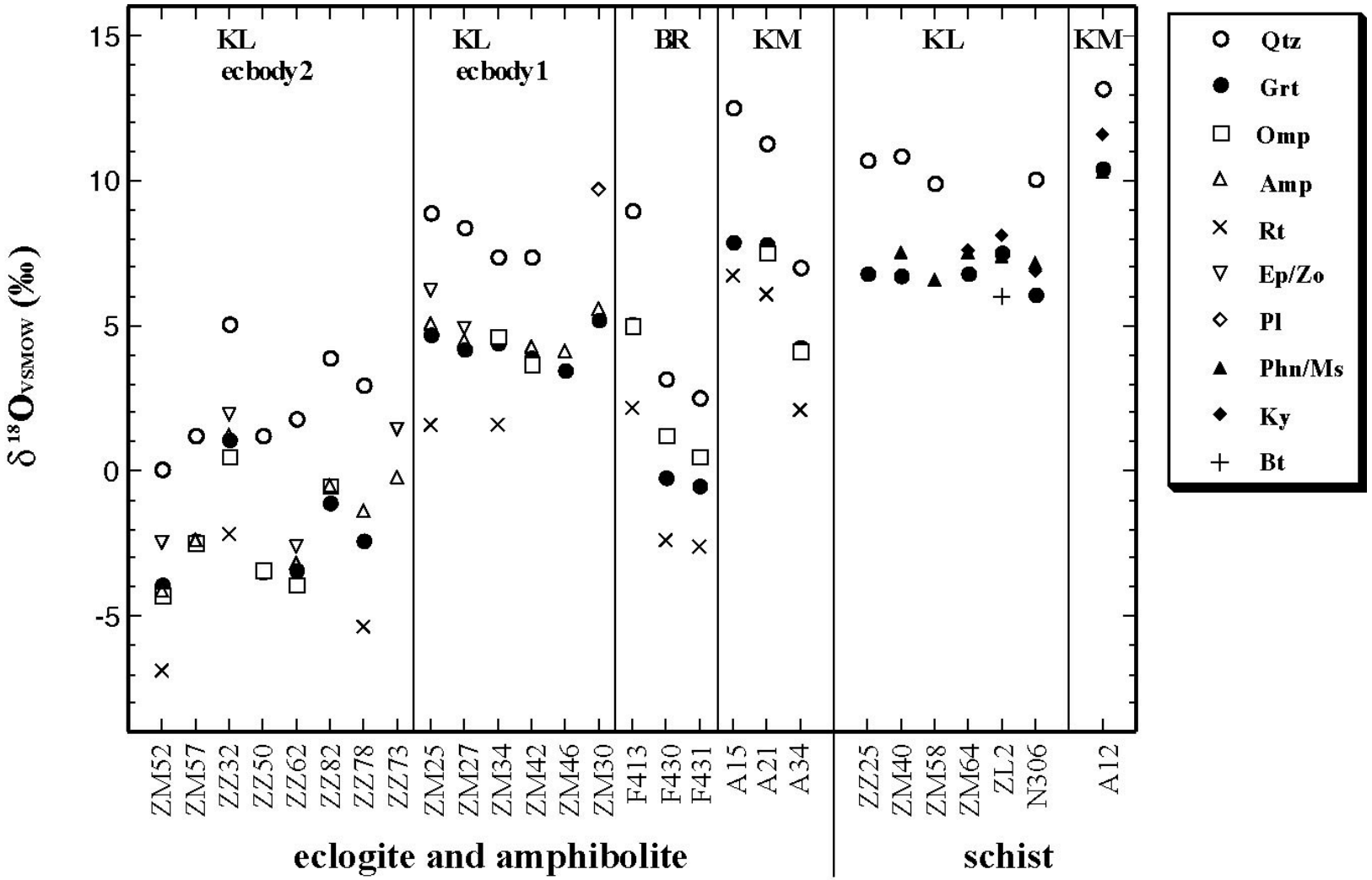

Fig. B–2 $\delta^{18}O$ values of eclogites, amphibolites and schists. KL: Kulet; BR: Barchi-Kol; KM: Kumdy-Kol.

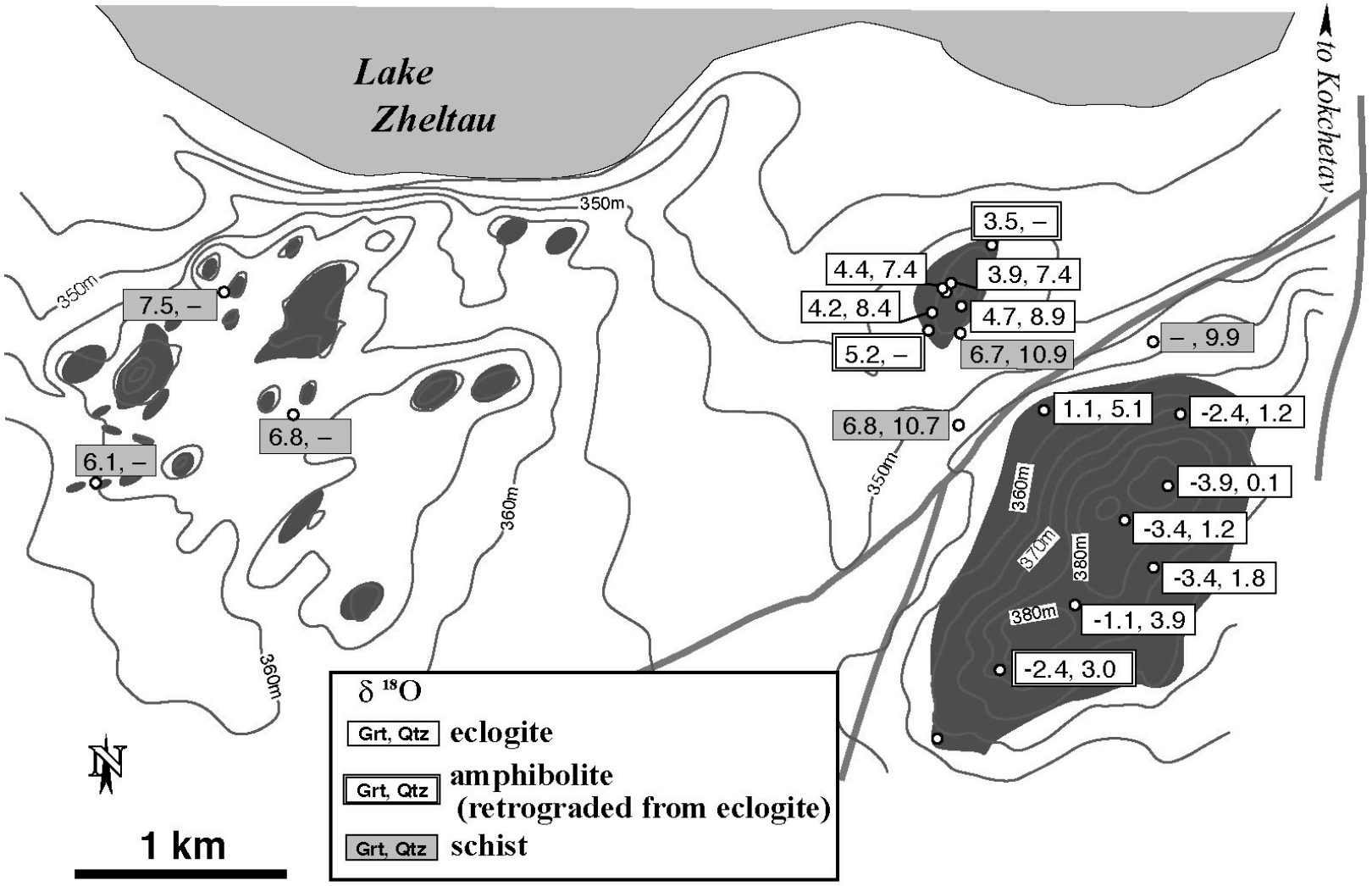

Fig. B–3 Distribution of $\delta^{18}O$ values in the Kulet region.

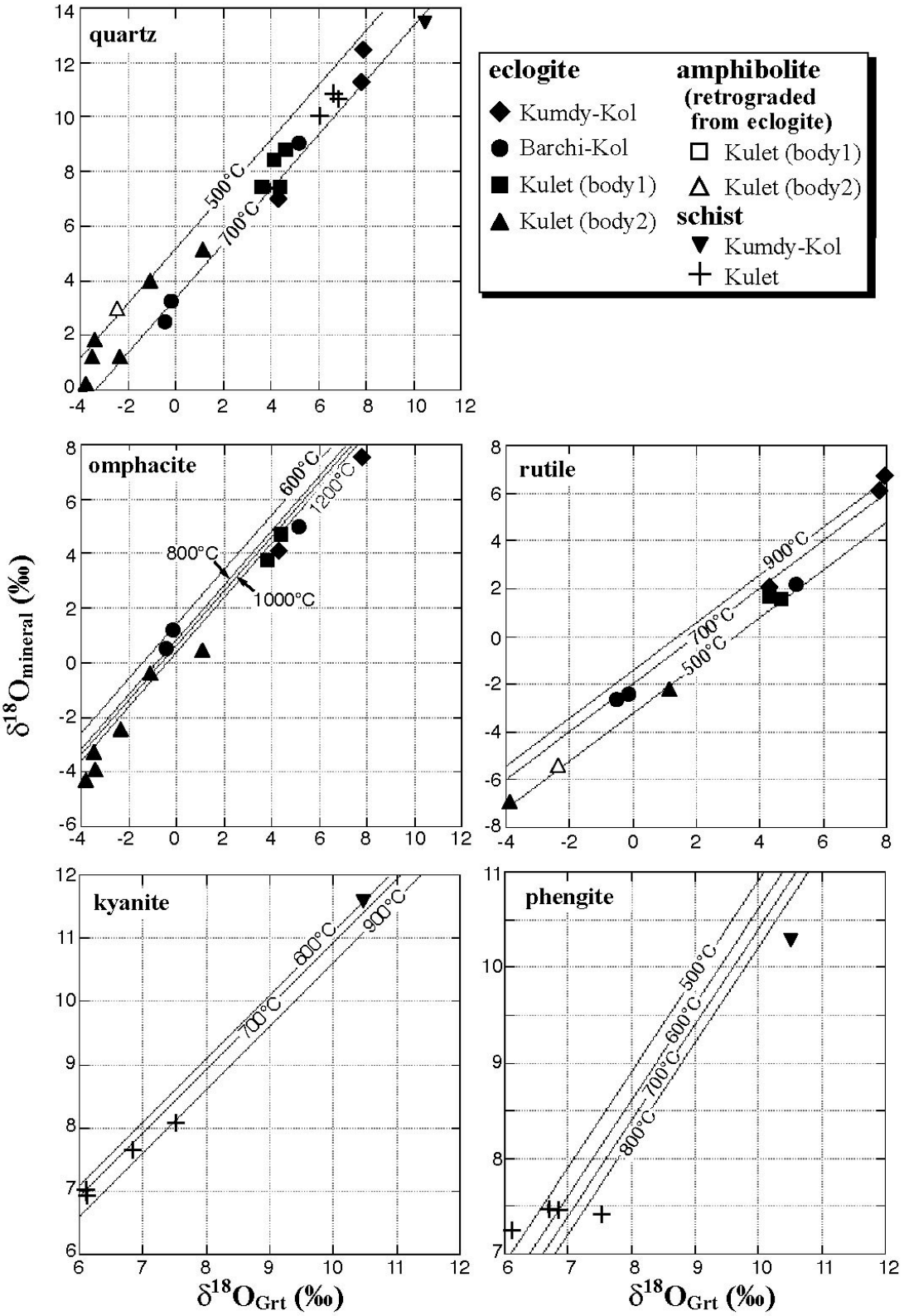

Fig. B–4 Oxygen isotope fractionations between garnet and other minerals from eclogites, amphibolites and schists.

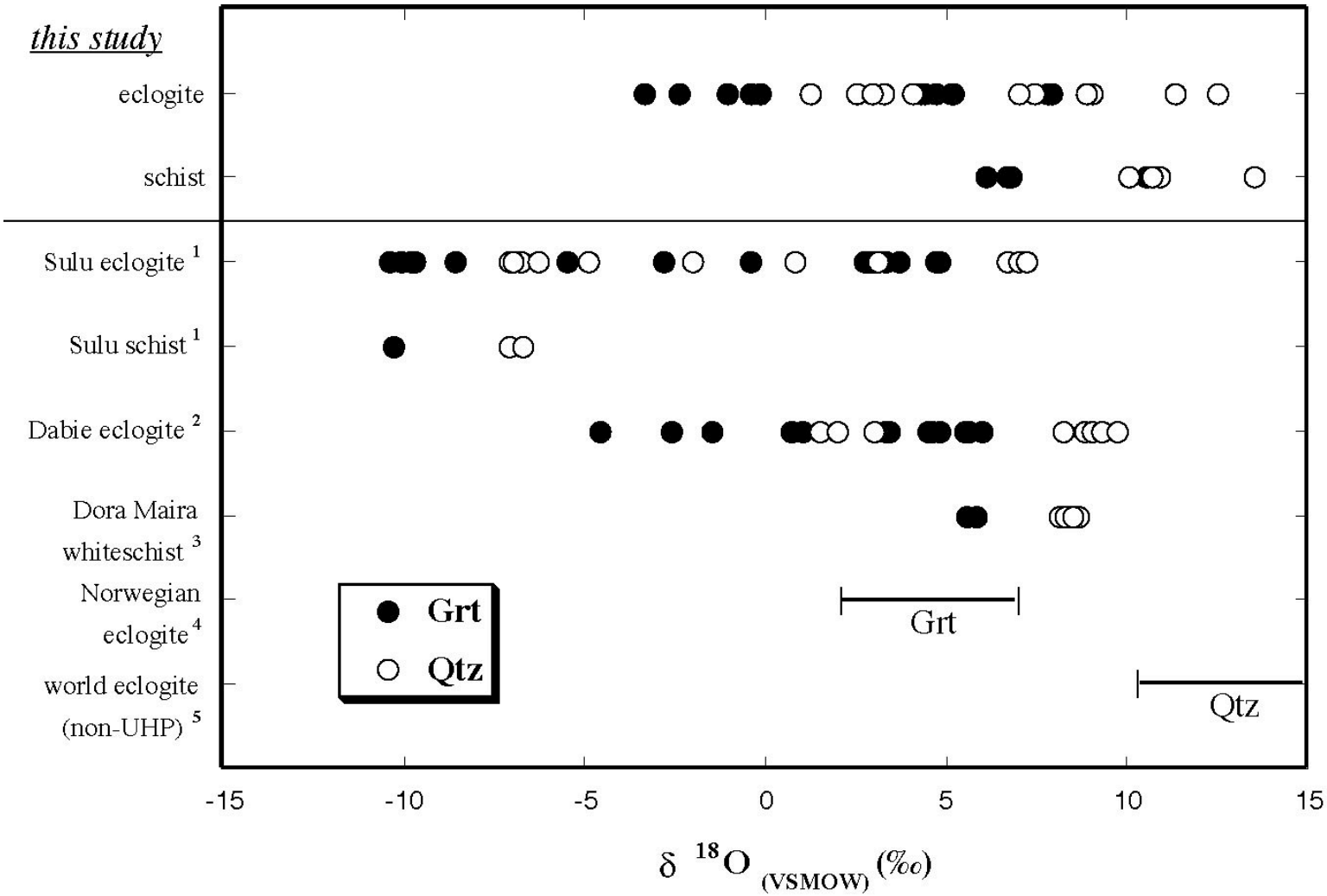

Fig. B–5 Comparison of Kokchetav oxygen isotope mineral analyses with published data. 1: Zheng *et al.* (1996; 1998); Yui *et al.* (1997); Rumble & Yui (1998); 2: Baker *et al.* (1997); 3: Sharp *et al.* (1993); 4: Agrinier *et al.* (1985); 5: Sharp *et al.* (1993).

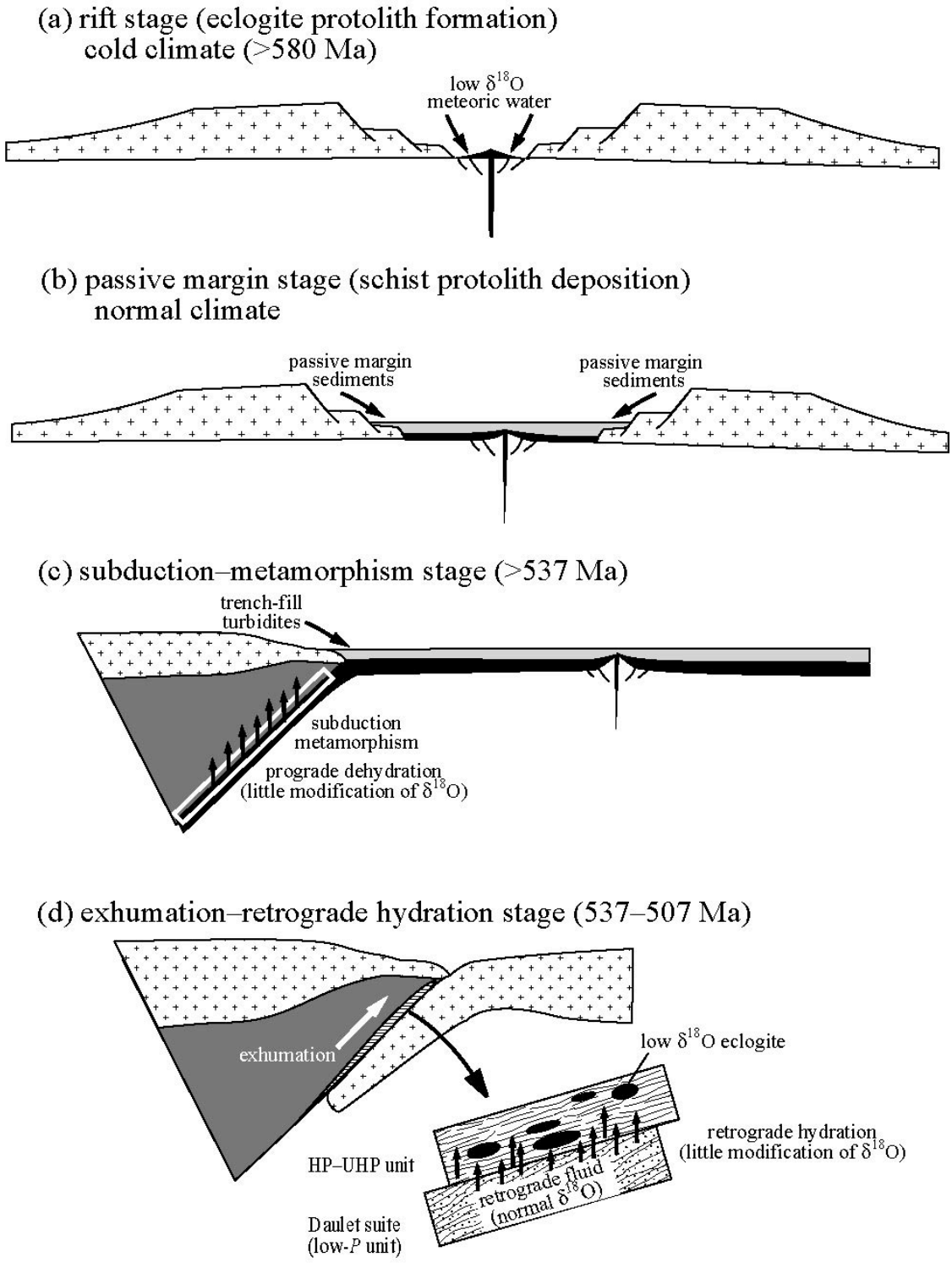

Fig. B–6 Tectonic model of evolution of the Kokchetav massif and the origin of low $\delta^{18}O$ values in eclogites.

Appendix C

Exhumation Tectonics of the High-*P/T* Sanbagawa Metamorphic Belt, SW Japan —Constraints from the Top and Bottom Boundary Faults

ABSTRACT

The exhumation process of the Sanbagawa Belt has long been controversial because the deformation structures related to the exhumation were obscured by later penetrative E–W orogen-parallel extension. The Sanbagawa Belt is tectonically intercalated as a thin subhorizontal sheet (about 2 km) with an overlying weakly metamorphosed Jurassic accretionary complex and an underlying weakly metamorphosed Cretaceous accretionary complex (*e.g.* Maruyama *et al.*, 1996). We investigated kinematic indicators at the top and bottom boundaries in central Shikoku and Kii Peninsula, respectively. On the bottom boundary, pumpellyite–actinolite facies metabasites have undergone semi-brittle thrust deformation indicating top-to-the south sense of shear, and a regionally EW-directed stretching lineation swings to N–S direction just above the boundary controlled by the fault movement. The top boundary observed in central Shikoku is north-vergent and indicates top-to-the north sense of shear; this suggests that the original normal fault on the boundary was warped by subsequent doming. These results support a model of selective exhumation of the Sanbagawa Belt from 30 km depth, and its juxtaposition against the over- and underlying accretionary complexes by orogen-orthogonal movements.

INTRODUCTION

Exhumation tectonics of high *P/T* rocks is a key to the understanding of orogenic process at oceanic plate subduction zones and continental collision zones. A number of models have been proposed to explain the exhumation processes of high *P/T* metamorphic belts: buoyancy uplift (Ernst, 1971; Ernst & Liou, 1995); a two-way-street model combining underplating of newly accreted materials and surface erosion (Ernst, 1970; Suppe, 1972; Platt, 1975); a mélange or diapir model, uplift by net buoyancy owing to the relatively low density matrix (Cloos, 1982; England & Holland, 1979; Carlson & Rosenfeld, 1981; Moore, 1984); extension tectonics (Lister *et al*., 1984; Lister & Davis, 1989; Blake & Jayko, 1990; Jolivet *et al*., 1994), and their combinations. Maruyama *et al*. (1996) reviewed 41 blueschist belts of the world in terms of their geological, thermobaric structure and chronology, and proposed a 'wedge extrusion' model to explain their exhumation. Similar tectonic models were proposed by Meissner (1989), Maruyama (1990), Wheeler (1991), Michard *et al*. (1993), Henry *et al*. (1993), Caby (1994), Wakabayashi & Unruh (1995) and Terabayashi *et al*. (1996). The essence of these models is a selective denudation of a thin slice of a high *P/T* belt with normal and reverse faults on its top and bottom boundaries, respectively. All the other models involve different combinations of the fault kinematics hence, the determination of the kinematic sense of the boundary faults is of fundamental importance.

The Cretaceous high *P/T* Sanbagawa metamorphic belt in SW-Japan is regarded as a product of ancient subduction along the continental margin of Asia. The belt runs from the Kanto Mountains near Tokyo to Kyushu Island along the SW-Japan arc (Fig. C–1). It extends for over 1,000 km along strike, but its width across the strike is less than 30 km, and its thickness is less than 2 km. This means that the Sanbagawa Belt is a fault-bound, thin, subhorizontal tectonic slice (Fig. C–2). There have been a number of studies regarding the internal geologic and thermobaric structure of the Sanbagawa Belt. However, few studies were concerned with the top and bottom boundaries of this high *P/T* belt; a few exceptions are Kawato *et al*. (1990), Sasaki & Isozaki (1992), Isozaki & Maruyama (1991) and Maruyama *et al*. (1996). The first two determined the structural relationships between the Sanbagawa Belt and the overlying and underlying accretionary complexes, but did not mention the fault kinematics. The last two outlined the possible tectonic models for exhumation of the fault-bound high *P/T* belt. However,

they did not provide structural evidence for the fault kinematics to verify their models.

In general, subduction zone-related large tectonic boundary faults are commonly reactivated numerous times during subduction and subsequent exhumation processes. Hence, it is particularly difficult to distinguish kinematic features related to the individual events. Moreover, we have discovered outcrops that preserve evidence for shear deformation during exhumation of the Sanbagawa Belt. This paper presents new structural data on the fault kinematics at the top and bottom boundaries of the Sanbagawa Belt.

Mineral abbreviations used in this paper are after Kretz (1983).

DESCRIPTION OF UPPER BOUNDARY FAULT (TOSAYAMA AREA, CENTRAL SHIKOKU)

General Geology of the Tosayama Area

The Mesozoic accretionary complex in the Tosayama area, central Shikoku, consists of two distinct geologic units: the Akaragi and Takakawa units as defined by Kawato *et al*. (1991). These two units are bounded by the E–W striking and southward-dipping Sasagatani fault. The Akaragi unit is composed of basic and pelitic phyllites with allochthonous blocks of chert, greenstones, limestone and dolomite, and possesses metamorphic mineral parageneses of glaucophane schist facies overprinted by pumpellyite–actinolite facies. The Takakawa unit is composed of pebbly mudstone with allochthonous blocks of chert, greenstones, sandstone and limestone, and is characterized by metamorphic mineral parageneses of pumpellyite + chlorite.

Microfossil ages indicate that the Takakawa and Akaragi units formed as accretionary complexes probably in the middle Jurassic and the early Cretaceous, respectively. K–Ar ages deduced from white micas of the Akaragi unit concentrate around 115 Ma, and those of the Takakawa unit around 140 Ma (Kawato *et al*., 1991). On the basis of the microfossil and K–Ar ages, the Akaragi unit corresponds to the Sanbagawa high-*P/T* metamorphic rocks, and the Takakawa unit to the Jurassic accretionary complex of the Chichibu Belt. There is a large break in metamorphic age and peak metamorphic mineral parageneses across the Sasagatani fault between these two units. Thus, in central Shikoku, the Sasagatani fault defines the geotectonic

boundary between the Sanbagawa high-*P/T* metamorphic belt and the overlying, Jurassic, accretionary Chichibu Belt.

The Akaragi unit (Sanbagawa schist) has a general strike of ENE–WSW and it dips 40°–70° to the south. However, the strike swings from ENE–WSW to NE–SW and dips gently to the north in the Akaragi path area, the western part of the study area. The maximum thickness of the unit reaches ca. 1,500 m around the Sasagatani area.

The Takakawa unit (Jurassic accretionary complex) generally strikes from E–W to ENE–WSW and dips 40°–80° both to the north and south. The Takakawa unit dips to the south in the northern part, and to the north in the southern part. The maximum apparent thickness of this unit is *ca*. 3,500 m.

The Upper Boundary Fault Zone

The boundary fault was traced by Kawato *et al*. (1991) based on outcrops of fault breccia and fault gauge. At Loc. 7 of Kawato *et al*. (1991), a dominant 10 m-wide fault gauge is evident (Fig. C–3). At this locality altered metabasites of the Jurassic accretionary complex overlie the massive Sanbagawa chert. The boundary fault strikes N83°E and dips 46° to the south, and the fault zone is comprised of alternating green and black clay layers which represent altered and highly sheared metabasites.

Towards the centre of the fault gouge is a 50 cm-wide shear zone, where fragmented black material is dominant. Kink-like recumbent folds are developed just above the shear zone. Well-developed axial plane cleavages are parallel to the fault plane and shear zone, and another set of cleavages intersects them (Fig. C–4). From their geometrical relationship, these cleavages are interpreted as Riedel shear planes R_1 and P. The sense of shear deduced from the asymmetry of the kink fold and the Riedel shear planes is top-to-the N35°E thrust sense.

DESCRIPTION OF LOWER BOUNDARY FAULT (HIGASHI-YOSHINO AREA, CENTRAL KII PENINSULA)

General Geology of the Higashi-Yoshino Area, Central Kii Peninsula

In SW-Japan, the lower boundary of the Sanbagawa Belt is generally obscured as the overlying Jurassic accretionary belt (Chichibu Belt) is in direct contact with the

underlying Shimanto Belt. However, in central Kii Peninsula (Figs. C–5), however, the structural relationships between these three geologic units are clearly observed, and the lower boundary of the Sanbagawa Belt is well exposed in the Higashi-Yoshino area (Yamato–Omine research group, 1981; 1987; Takeuchi & Yamato–Omine research group, 1984).

The Higashi-Yoshino area is located in the middle of the Kii Peninsula, just to the south of the Median Tectonic Line, where the Sanbagawa Belt fades out towards the east and the Shimanto Belt is in direct contact with the Median Tectonic Line (Fig. C–5). Sasaki & Isozaki. (1992) described the geology of this area, and divided into two distinctive units: the northern and southern.

The northern unit is predominantly composed of pelitic schist with well-developed planar and deformation structures involving sheets and lenses of basic and psammitic schists of metre to kilometre scale. The black or dark grayish pelitic schist exhibits a distinctive foliation and/or micro-folding. The basic schist occurs as sheets or lenses of various sizes within the pelitic schist. Epidote, chlorite, actinolite, and white mica are common metamorphic minerals with alkali amphibole occurring in some samples. The medium- to coarse-grained psammitic schist occurs as blocks within the pelitic schist similar to the basic schist.

The southern unit mainly consists of pelitic phyllite and lensoid blocks of basic rocks and/or sandstones. The blocks range in length from a centimetre to a kilometre. Planar structures that are well-developed in the northern part of the unit, decreases in intensity southward. The degree of recrystallisation of the pelitic phyllite is generally low and therefore many detrital quartz and plagioclase grains are preserved. The basic schist occurs within the pelites either as massive blocks of centimetre to decimetre scale, is foliated and contains epidote, chlorite, actinolite and white micas. Sandstones form lenses or blocks a few centimetres to hundreds of metre long, which are massive or display weak elongation lineations.

The northern and southern units are bounded by an E–W striking fault. Sasaki & Isozaki. (1992) reported three outcrops of this boundary fault and described two of them in detail. At one outcrop (Loc. 2 of Sasaki & Isozaki., 1992), basic schist of the northern unit is separated from pelitic phyllite of the southern unit by a 1 m-wide fault fracture zone. The contact and the foliation of the underlying southern unit strike N70°E and dip 40°N. Some 1 m wide subhorizontal fracture zones propagate from the main fault into

the southern unit. At another outcrop (Loc. 3 of Sasaki & Isozaki., 1992), pelitic schist of the northern unit is separated from the pelitic phyllite of the southern unit by a 1.5 m wide fracture zone. The fault zone strikes N80°E, although the surface is not clearly observed. Sasaki & Isozaki. (1992) also reported 11 other locations where the southernmost part of the northern unit and northernmost part of the southern unit are well exposed. The very contact between the units can be observed at these outcrops providing a supportive information about the surface trace of the fault. The estimated strike of the fault plane is N90°E to N80°E, and the dip is 20° to 30°N; this is consistent with the observed fault attitude at exposure.

The Lower Boundary Fault Zone

A new outcrop of the lower boundary was identified by the present study. Foliations defined by mica minerals in the Shimanto pelitic schists are subparallel to the boundary fault, whereas those in the Sanbagawa metabasites are slightly oblique to the fault. Mineral lineation in the matrix metabasites generally has an E–W azimuth and a gentle plunge to the west, but near the boundary fault it has different attitudes. Figure C–6 shows the change in attitude of the mineral lineation approaching the boundary fault. The azimuth of the lineation swings from E–W to SE–NW in a narrow zone less than 30 cm from the boundary fault. The plunge of the lineation also changes to NW.

As shown in Fig. C–6b, the fault has a rough surface, suggesting the faulting occurred in a semi-brittle manner. Figure C–7 is a close-up view showing anastomosing, sigmoidal shear planes, and the boundary itself is oscilated. A metabasite layer has been dislocated and some fragments are included in the footwall metapelite. The host metapelites and metabasites blocks are well recrystallised, and contain a foliation which is parallel to the main fault plane. A sheared metabasite sample has the following mineral assemblage: Chl + Ab + Qtz + Cal + Hem ± Pmp ± Act ± Ep ± Ttn ± white mica. The three-phase paragenesis Pmp + Act + Ep was not observed, indicating pumpellyite–actinolite facies metamorphic condition. Epidote and albite occur as porphyroclasts set within a chloritic matrix. A relict igneous augite porphyroclast is surrounded by actinolite pressure fringes. Epidote porphyroclasts have asymmetric tails mostly of quartz and/or albite, and albite porphyroclasts have asymmetric tails of chlorite. In albite porphyroclasts, abundant inclusion trails mostly consist of epidote and are generally oblique to the external foliation defined by chlorite. Thrust shear sense

was deduced from these porphyroclasts as top-to-the south.

DISCUSSION AND CONCLUSIONS

Shear Sense of the Upper and Lower Boundary Faults and Exhumation Tectonics of B-type Orogens

Our study has revealed the shear sense of both boundary faults. The lower boundary fault, in the Higashi-Yoshino area, has a thrust-sense indicating top-to-the south movement of the Sanbagawa Belt onto the Shimanto Belt. This is consistent with the fact that deeply subducted high *P/T* rocks overly the feebly metamorphosed accretionary material.

The observed shear sense on the upper boundary in the Tosayama area is top-to-the N35°E. At this locality, the boundary fault plane dips moderately to the south where it forms the southern limb of a regional scale antiform. This sense implies thrusting of the overlying Chichibu Belt onto the Sanbagawa Belt. However, regionally this fault plane is north-dipping with local re-orientation occurring during later antiformal doming. and was changed in attitude due to later doming. In such a case, the movement sense of this upper boundary is thus normal and not reverse. In either case, the top-to-the north movement relationship between the Chichibu and the Sanbagawa Belts is the same. The same top-to-the north sense of shear on the upper boundary of the Sanbgawa Belt is reported in the Shimonita area, Kanto Mountains (Wallis *et al*., 1990). In this region, the boundary fault plane dips gently to the north and the top boundary of the Sanbagawa Belt is a low-angle normal fault. Our results support the model that the fault-bound Sanbagawa Belt was selectively denuded as a wedge between the Chichibu and the Shimanto accretionary complexes. The deduced kinematics of the boundary faults are also consistent with the internal ductile deformation of the Sanbagawa Belt. In the Iratsu and Higashi-Akaishi areas, central Shikoku, selective southward exhumation of the core part of the Sanbagawa Belt is reported (Yamamoto *et al*., 2003).

Many models have been proposed to explain the exhumation of regional metamorphic belts. They are classified into the following five groups. The first model is buoyancy uplift (Ernst, 1971; Ernst & Liou, 1995). This model simply explains that the exhumation force is related to the buoyancy of the relatively less dense metamorphic

rocks themselves. The second is a mélange or diapir model (Cloos, 1982; England & Holland, 1979; Carlson & Rosenfeld, 1981; Moore, 1984). This is essentially similar to the first model, buoyancy-driven uplift. The difference is that buoyancy is driven not by the metamorphic rocks themselves but by significantly less dense matrix materials. This model assumes a corner flow in a serpentinised mantle wedge, and metamorphic rocks are incorporated as a tectonic block and transported to the surface (Fig. C–8a). The third is the two-way-street model (Ernst, 1970; Suppe, 1972; Platt, 1975). This model is a combination of 'jack-up' by underplating of newly accreted materials and surface erosion of the overburden materials (Fig. C–8b). The fourth is extension tectonics (Lister *et al*., 1984; Lister & Davis, 1989; Blake & Jayko, 1990; Jolivet *et al*., 1994). This model is unique for assuming an extensional regime in a plate convergent zone. The continental crust is thinned in an extensional stress field forming a listric normal fault system, and deep metamorphic rocks are exposed at the surface (Fig. C–8c). The fifth is the wedge extrusion model (Maruyama, 1990; Maruyama *et al*., 1996). The essence of this model is a selective uplift of the fault-bound metamorphic belt by squeezing of the mantle wedge due to change in subduction angle (Fig. C–8d).

A major criticism at the first three models is a lack of a large sedimentary basin to account for the voluminous eroded materials by uplift of the metamorphic belt. Since these models require erosion of the overburden of the metamorphic belt, voluminous amounts of eroded materials should have been supplied to the foreland basin of the exhumed metamorphic belt. However, the amount of the sediments in the foreland basins of high-*P/T* belts is too small to account for the erosion of the overlying materials of > 30 km thick. A further criticism is that these models cannot explain the episodic uplift of metamorphic rocks which occurs *ca*. every 100 m.y. Therefore the exhumation process of these metamorphic belts requires selective extrusion. The fourth model is acceptable on these points; however, both upper and lower boundary faults are normal, *i.e*. extensional (Fig. C–8c). This is inconsistent with our observation in the Sanbagawa Belt where the lower boundary fault is a thrust. In addition, mantle materials should be present below the metamorphic belt in this model. However, at present no drilling research has identified mantle materials beneath high-*P/T* metamorphic belts. The wedge extrusion model is currently applied to many regional metamorphic belts of both A-type (collision type) and B-type (circum-Pacific, cordilleran type) plate convergent margins. Crocodile-type extrusion (Meissner, 1989; Wheeler, 1991; Michard *et al*.,

1993; Henry *et al*., 1993; Caby ,1994) and tectonic wedging (Wakabayashi & Unruh, 1995) are essentially similar. The features of these models are characterized by a tectonic insertion of a regional metamorphic belt amongst non- or feebly metamorphosed units. The following three features are essential to the application of this model: 1) a subhorizontal structure of the metamorphic belt, 2) normal and reverse fault at the top and bottom boundaries of the metamorphic belt, respectively, and 3) gap of metamorphic grade (chiefly pressure) across boundary faults. These features are relatively well documented in A-type orogens. Pressure breaks across the boundaries are relatively significant in the case of A-type orogens, which enables them to be easily recognised. In addition, kinematics of the paired faults are also clarified in many orogens such as Alps (Michard *et al*. 1993), Himalaya (*e.g*. Grujic *et al*., 1996; Kaneko, 1997), and Kokchetav Massif (Kaneko *et al*., 2000; Yamamoto *et al*. 2000), as well as their subhorizontal structures. Compared to A-type orogens, applications of the model to B-type orogens are inadequately confirmed. Although the subhorizontal, sandwitched structure of metamorphic belts is recognised in many orogens (*see* review of Maruyama *et al*., 1996), kinematics of the boundary faults and the gap in metamorphic grade are poorly recognised in these orogens. In the case of the Sanbagawa Belt, a subhorizontal structure has long been recognised (*e.g*. Higashino, 1990), and gaps of metamorphic grade between the overlying Jurassic Chichibu and the underlying Upper Cretaceous Shimanto accretionary belts has also beeen demonstrated (Isozaki & Maruyama, 1991). Therefore, our kinematic results combined with the above mentioned features clearly suggest that the wedge extrusion model can be applied to the Sanbagawa Belt.

Contrasting Nature at the Faulting Conditions of the Upper and Lower Boundaries

The conditions and nature of faulting at the upper and lower boundaries are significantly different. The upper fault zone is composed of fault breccia and gouge, without the recrystallisation of metamorphic minerals. This infers the faulting took place in a brittle manner at low temperature conditions. However, a 50 cm-wide fracture zone around the boundary has experienced extensive argillisation, suggesting the presence and interaction of fluid during this faulting event. Kink folds are developed just above this boundary. In general, kink folds are formed in relatively competent layers under dry and high inter-layer friction conditions (Honea & Johnson, 1976; Reches & Johnson, 1976). Considering the features mentioned above, the faulting

condition on the upper boundary was generally dry and brittle at low temperature with localised fluid flow playing an important role as a hydrosoftening agent.

Contrastingly, the lower boundary is coherent and recrystallized at pumpellyite–actinolite facies conditions. The absence of fault gauge suggests that faulting occurred at higher temperature than the upper boundary, and under fluid-rich conditions. This may imply abundant fluid supply from the descending slab beneath the ascending Sanbagawa Belt, in contrast to the A-type plate convergent margins where subduction ceases after the collision of two continents.

We emphasize that the mineral lineation changes its azimuth from E–W to NW–SE just above the boundary fault. This implies the syn-deformational recrystallisation of the lower boundary occurred under pumpellyite–actinolite facies condition when the Sanbagawa Belt was thrusted onto the Shimanto Belt. The Sanbgawa belt has a regional EW-striking mineral lineation. However, the general sense of shear is complex; top-to-the east (Faure, 1985), top-to-the west (Wallis, 1990; Wallis *et al*., 1992), inversion of top-to-the E and top-to-the W in the outcrop to mappable scales (Hara *et al*., 1992), and top-to-the east in the Kanto Mountains (Guidi *et al*., 1984; Otoh & Yanai, 1989; Abe *et al*., 2001). The N–S directed movement is not dominant throughout the belt except highest grade zones aound the eclogite bodies (Okamoto, 1998; Yamamoto *et al*., 2003) suggesting SW-ward-extrusional exhumaiton of eclogite into the lower grade schists. The E–W directed shear deformation of low non-coaxiality is interpreted to have been taken place during formation of the foliation during extensional flow. Oblique plate subduction along an E–W trench axis was the principal cause of the constriction-dominant stress regime (Faure, 1985; Toriumi, 1985; Abe *et al*., 2001). Also, the general trend of the mineral lineation on the boundary fault is E–W. However, the N–S trending mineral lineation developed only in the vicinity of the lower boundary fault thus indicating that exhumation of the Sanbagawa Belt was orthogonal to the orogen.

REFERENCES

Abe, T., K. Shimada, H. Takagi, S. Kimura, K. Ikeyama, & A. Miyashita, 2001. Ductile shear deformation of the Sanbagawa metamorphic rocks in the Kanto Mountains. *Journal of Geological Society Japan,* **107,** 337–353 (*in Japanese with English*

abstract).

Blake, M. C. Jr. & A. S. Jayko, 1990. Uplift of the very high pressure rocks in the western Alps: Evidence for structural attenuation along low-angle faults. *Mémoir de Societé Géologique de France, N. S.*, **156,** 237–246.

Caby, R., 1994. Precambrian coesite from northern Mali: First record and implications for plate tectonics in the trans-Saharan segment of Pan-African belt. *European Journal of Mineralogy*, **6,** 235–244.

Carlson, W. D. & J. L. Rosenfeld, 1981. Optical determination of topotactic aragonite–calcite growth kinetics: Metamorphic implications. *Journal of Geology*, **89,** 615–638.

Cloos, M., 1982. Flow mélange: Numerical modeling and geologic constraints on their origin in the Franciscan subduction complex, California. *Geological Society America Bulletin*, **93,** 330–345.

England, P. C. & T. J. B. Holland, 1979. Archimedes and the Tauern eclogites: The role of buoyancy in the preservation of exotic eclogite blocks. *Earth and Planetary Science Letters*, **53,** 63–68.

Ernst, W. G., 1970. Tectonic contact between the Franciscan mélange and the Great Valley Sequence —crustal expression of a late Mesozoic Benioff zone. *Journal of Geophysical Research*, **75,** 886–901.

Ernst, W. G., 1971. Do mineral parageneses reflect unusually high-pressure conditions of Franciscan metamorphism? *American Journal of Science*, **270,** 81–108.

Ernst, W. G. & J. G. Liou, 1995. Contrasting plate-tectonic styles of Qinling–Dabie–Sulu (Alpine-type) and Franciscan (Pacific-type) metamorphic belts. *Geology*, **23,** 353–356.

Faure, M., 1985. Eastward ductile shear during the early tectonic phase in the Sanbagawa Belt. *Journal of Geological Society of Japan,* **89,** 319–329.

Guidi, A., J. Charvet & T. Sato, 1984. Finding of granitic olistoliths and pre-Cretaceous radioralians in the northwestern Kanto Mountains, Gunma Prefecture, Central

Japan. *Journal of Geological Society of Japan,* **90,** 853–856.

Grujic, D., M. Casey, C. Davidson, L.S. Hollister, R. Kündig, T. Pavlis & S. Schmid, 1996. Ductile extrusion of the Higher Himalayan Crystalline in Bhutan: evidence from quartz microfabrics. *Tectonophysics,* **260,** 21–43.

Hara, I., T. Shiota, K. Hide, K. Kanai, M. Goto, S. Seki, K. Kaikiri, K. Takeda, Y. Hayasaka, T. Miyamoto, Y. Sakurai, & Y. Ohtomo, 1992. Tectonic evolution of the Sambagawa schists and its implications in convergent margin processes. *Journal of Science of Hiroshima University, Series C,* **9,** 495–595.

Henry, C., A. Michard & C. Chopin, 1993. Geometry and structural evolution of the high-pressure rocks from the Dora-Maira massif, western Alps, Italy. *Journal of Structural Geology,* **15,** 965–981.

Higashino, T., 1990. Metamorphic zones of the Sambagawa metamorphic belt in central Shikoku, Japan. *Journal of Geological Society of Japan,* **96,** 703–718 (*in Japanese with English abstract*).

Honea, E. & A. M. Johnson, 1976. A theory of concentric, kink, and sinusoidal folding and of monoclinical flexuring of compressible, elastic multilayers. Part IV: development of sinusoidal and kink folds in multilayers confined by rigid boundaries. *Tectonophysics,* **30,** 197–239.

Isozaki, Y. & S. Maruyama, 1991. Studies on orogeny based on plate tectonics in Japan and new geotectonic subdivision of the Japanese islands. *Journal of Geology of Japan*, **100,** 697–761 (*in Japanese with English abstract*).

Jollivet, L., J. M. Daniel, C. Truffert & B. Goffé, 1994. Exhumation of the deep crustal metamorphic rocks and crustal extension in arc and back-arc regions. *Lithos,* **33,** 3–30.

Kaneko, Y., 1997. Two-step exhumation model of the Himalayan Metamorphic Belt, central Nepal. *Journal of Geological Society of Japan,* **103,** 203–226.

Kawato, K., Y. Isozaki & T. Itaya, 1990. Geotectonic boundary between the Sanbagawa and Chichibu Belts in central Shikoku, Southwest Japan. *Journal of Geological*

Society of Japan, **97,** 959–975 (*in Japanese with English abstract*).

Kretz, R., 1983. Symbols for rock-forming minerals. *American Mineralogist,* **68,** 277–279.

Lister, G. S., G. Banga & A. Feenstra, 1984. Metamorphic core complexes of Cordilleran type in the Cyclades, Aegean Sea, Greece. *Geology,* **12,** 221–225.

Lister, G. S. & G. A. Davis, 1989. The origin of metamorphic core complexes and detachments faults forming during Tertiary continental extension in the northern Colorado River region, U. S. A. *Journal of Structural Geology,* **11,** 65–94.

Maruyama, S., 1990. Denudation process of high-pressure metamorphic belt. *Geological Society of Japan, Abstract,* **97,** 484.

Maruyama, S., J. G. Liou & M. Terabayashi, 1996. Blueschists and eclogites of the world and their exhumation. *International Geology Rev*iew, **38,** 485–594.

Meissner, R., 1989. Rupture, creep, lamellae and crocodiles: Happenings in the continental crust. *Terra Nova*, **1,** 17–28.

Michard, A., C. Chopin & C. Henry, 1993. Compression versus extension in the exhumation of the Dora-Maira coesite-bearing unit, Western Alps, Italy. *Tectonophysics,* **221,** 173–193.

Moore, D. E., 1984. Metamorphic history of a high-grade blueschist exotic block from the Franciscan Complex, California. *Journal of Petrology,* **25,** 126–150.

Otoh, H. & S. Yanai, 1989. Evidence of eastward ductile overthrust shear in the Mikabu and Chishibu Belts, Kanto Mountains. *Journal of Geological Society of Japan,* **95,** 711–714.

Okamoto, K., 1998. Inclusion-trail geometry of albite porphyroblasts in a fold structure in the Sanbagawa belt, central Shikoku, Japan. *The Island Arc,* **7,** 283–294.

Platt, J. P., 1975. Metamorphic and deformational processes in the Franciscan Complex, California: Some insights from the Catalina Schist terrane. *Geological Society of America Bulletin*, **86,** 1337–1347.

Reches, Z. & A. M. Johnson, 1976. A theory of concentric, kink, and sinusoidal folding and of monoclinical flexuring of compressible, elastic multilayers. Part VI: aymmetric folding and monoclinical kinking. *Tectonophysics,* **35,** 295–334.

Sasaki, H. & Y. Isozaki, 1992. Low-angle thrust between the Sanbagawa and Shimanto Belts in central Kii Peninsula, Southwest Japan. *Journal of Geological Society of Japan*, **98,** 57–60 *(in Japanese with English abstract)*.

Suppe, J., 1972. Interrelationships of high-pressure metamorphism, deformation and sedimentation in Franciscan tectonics, U.S.A. *24th International Geological Congress*, **3,** 552–559.

Takeuchi, Y. & Yamato-Omine Research Group, 1984. Chichibu and Shimanto belts in the Central Kii Mountains 11, Otaki region, *Geological Society of Japan Abstract,* **91,** p. 172 *(in Japanese)*.

Terabayashi, M., Maruyama, S. & J. G. Liou, 1996. Thermobaric structure of the Franciscan complex in the Pacheco Pass region, Diablo Range, California. *Journal of Geology,* **104,** 617–636.

Toriumi, M., 1985. Two types of ductile deformation / regional metamorphic belt. *Tectonophysics*, **113,** 1307–1326.

Wakabayashi, J. & J. R. Unruh, 1995. Tectonic wedging, blueschist metamorphism, and exposure of blueschists: Are they compatible? *Geology,* **100,** 19–40.

Wallis, S. R., 1990. The timing of folding and stretching in the Sanbagawa Belt, the Asemigawa region, Centarl Shikoku. *Journal of Geological Society of Japan*, **96,** 345–552.

Wallis, S. R., S. Banno & M. Radvanec, 1992. Kinematics, structure and relationship to metamorphism of the east-west flow in the Sanbagawa Belt, southwest Japan. *The Island Arc*, **1,** 176–185.

Wallis, S. R., T. Hirajima & S. Yanai, 1990. Sense and direction of movement along the Atokura Fault at Shimonita, Kanto Mountains, central Japan. *Journal of Geological Society of Japan*, **96,** 977–980 (*in Japanese*).

Wheeler, J., 1991. Structural evolusion of a subducted continental sliver: The northern Dora Maira massif, Italian Alps. *Journal of Geological Society of London*, **148,** 1101–1113.

Yamamoto, H., M. Ishikawa, R. Anma & Y. Kaneko, 2000. Kinematic analysis of ultrahigh-pressure-high-pressure metamorphic rocks in the Chaglinka–Kulet area of the Kokechetav Massif, Kazakhstan. *The Island Arc*, **9,** 304–316.

Yamamoto, H., K. Okamoto, Y. Kaneko & M. Terabayashi, 2003. Southward extrusion of the eclogite-bearing mafic–ultramafic bodies in the Sanbagawa belt, central Shikoku, Japan. *Lihots, (in press)*.

Yamato-Omine Research Group, 1981. Paleozoic and Mesozoic units in central Kii Mountains. *Association of Geological Collaboration Excurtion Guidebook*, **35,** p 88 (*in Japanese*).

Yamato-Omine Research Group, 1987. Regional Geology of Japan Part 6, KINKI; K. Nakazawa, K. Ichikawa & M. Ichihara (Eds.), Kyoritsu Shuppan, Tokyo, 87–90, (*in Japanese*).

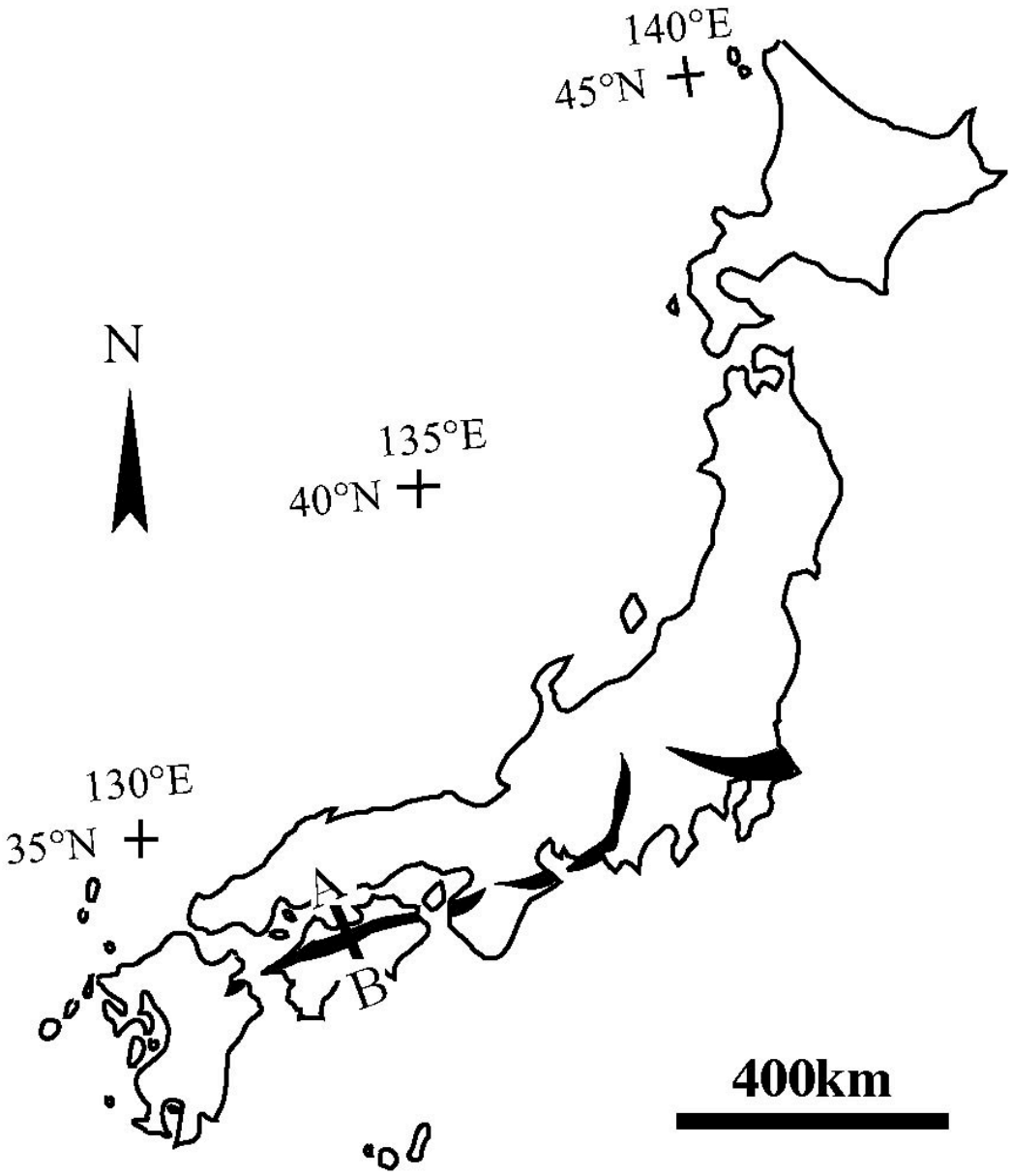

Fig. C–1 Index map showing the distribution of the Sanbagawa Belt (shaded black) in Japan. Study areas of the upper and lower boundaries are also shown.

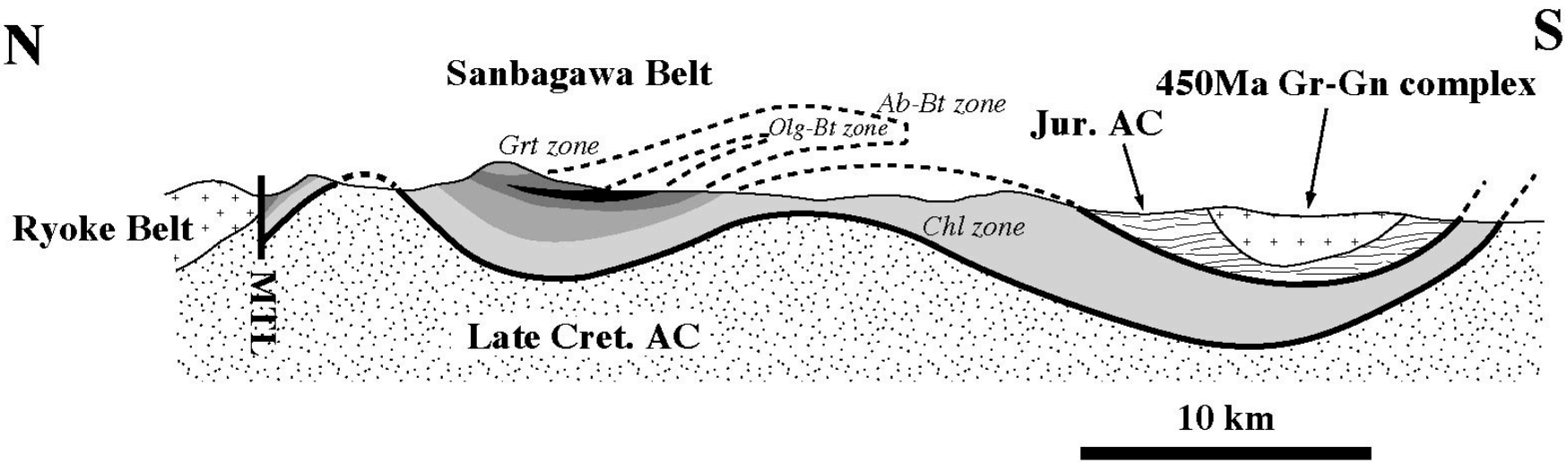

Fig. C–2 Schematic cross-section showing the relationship between the Sanbagawa Belt and the overlying and underlying accretionary complexes in southwestern Japan. MTL: Median Tectonic Line.

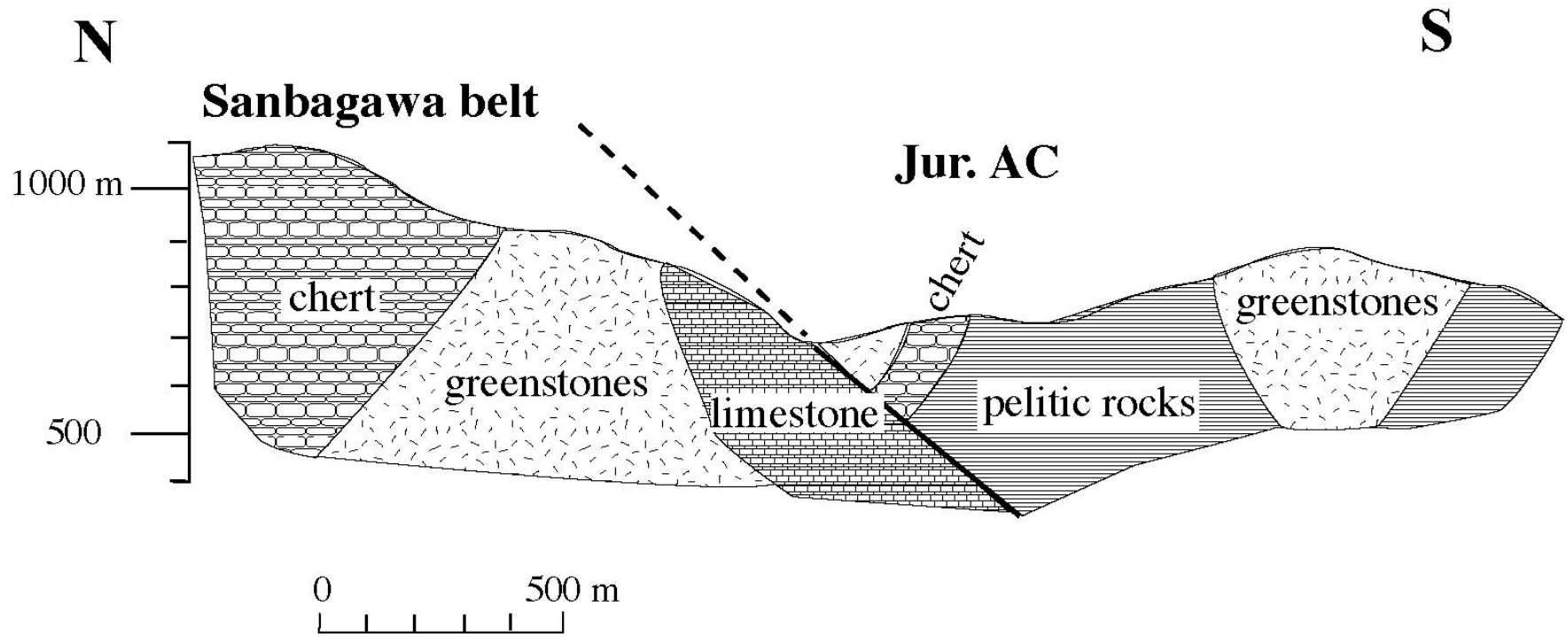

Fig. C–3 Geologic profile of the Tosayama area in central Shikoku (Kawato et al. 1991). Jurassic accretionary complex overlies the Sanbagawa Belt across a south-dipping fault (Sasagatani fault).

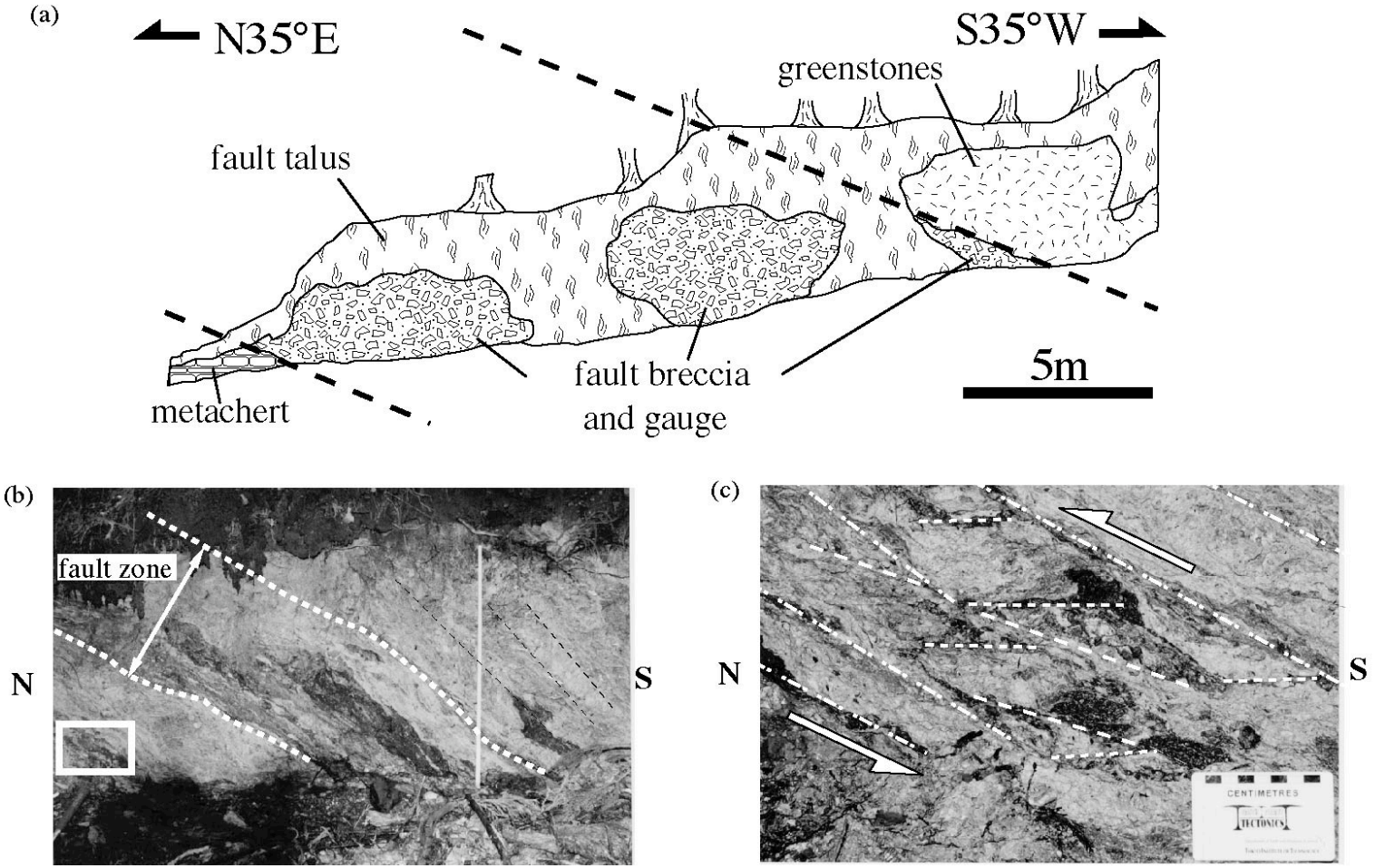

Fig. C–4 Upper boundary of the Sanbagawa Belt in the Tosayama area, central Shikoku. a) A sketch of the outcrop of the fault zone. b) Field photograph of the fault zone. Metabasites suffered alteration related to the faulting. A 50 cm-wide shear zone is in the centre. Kink folds with well-developed axial plane cleavages are formed on the both sides of the shear zone. The scale bar indicates 1 m. Focused view of the open box on the left side is shown in c). c) Riedel shear planes indicating top-to-the north movement are prominent in the fault gouge.

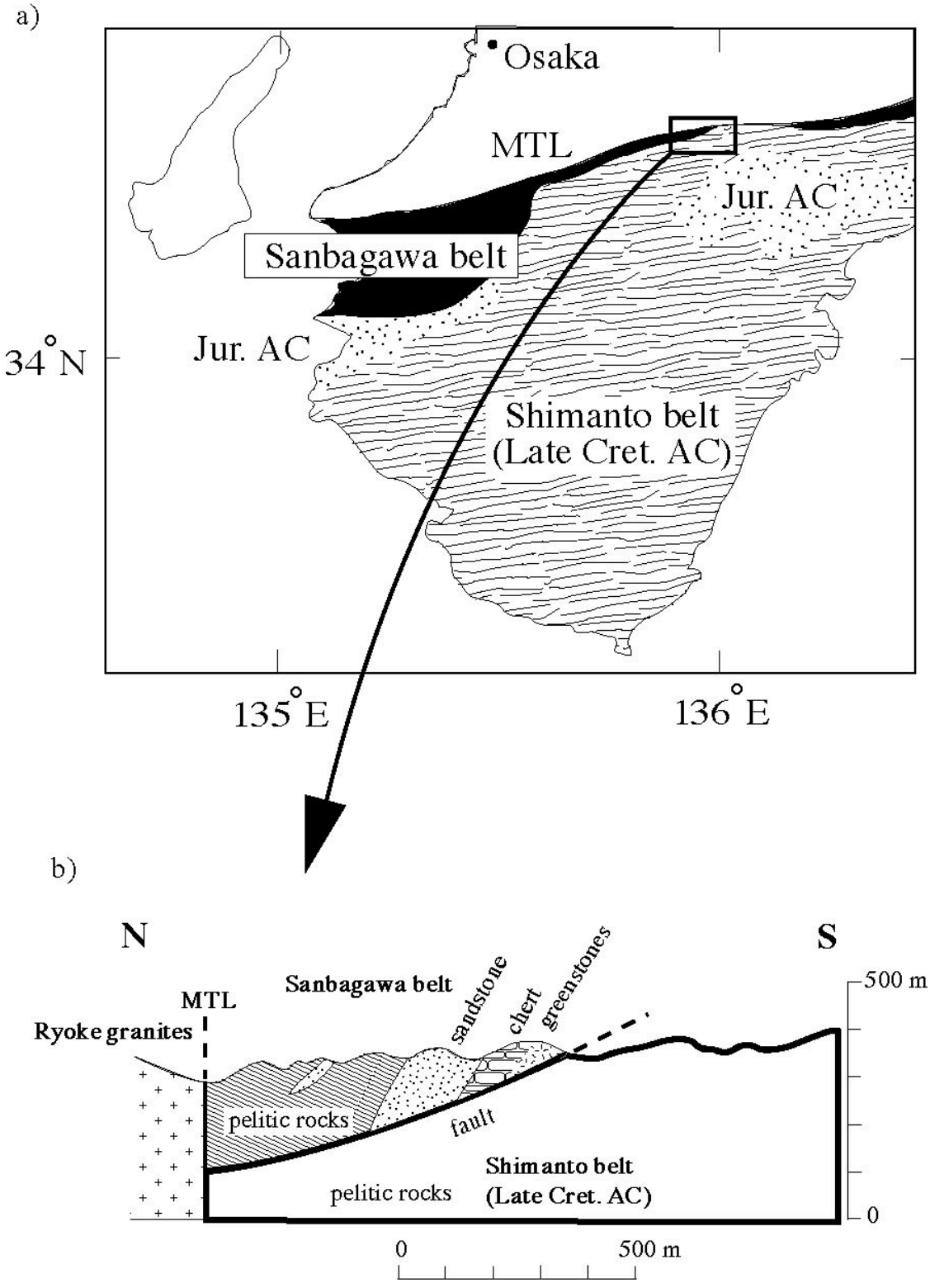

Fig. C–5 Simplified geological map and profile in the Kii Peninsula (mdified after Sasaki & Isozaki, 1992). MTL: Median Tectonic Line; Jur. AC: Jurassic accretionary complex..

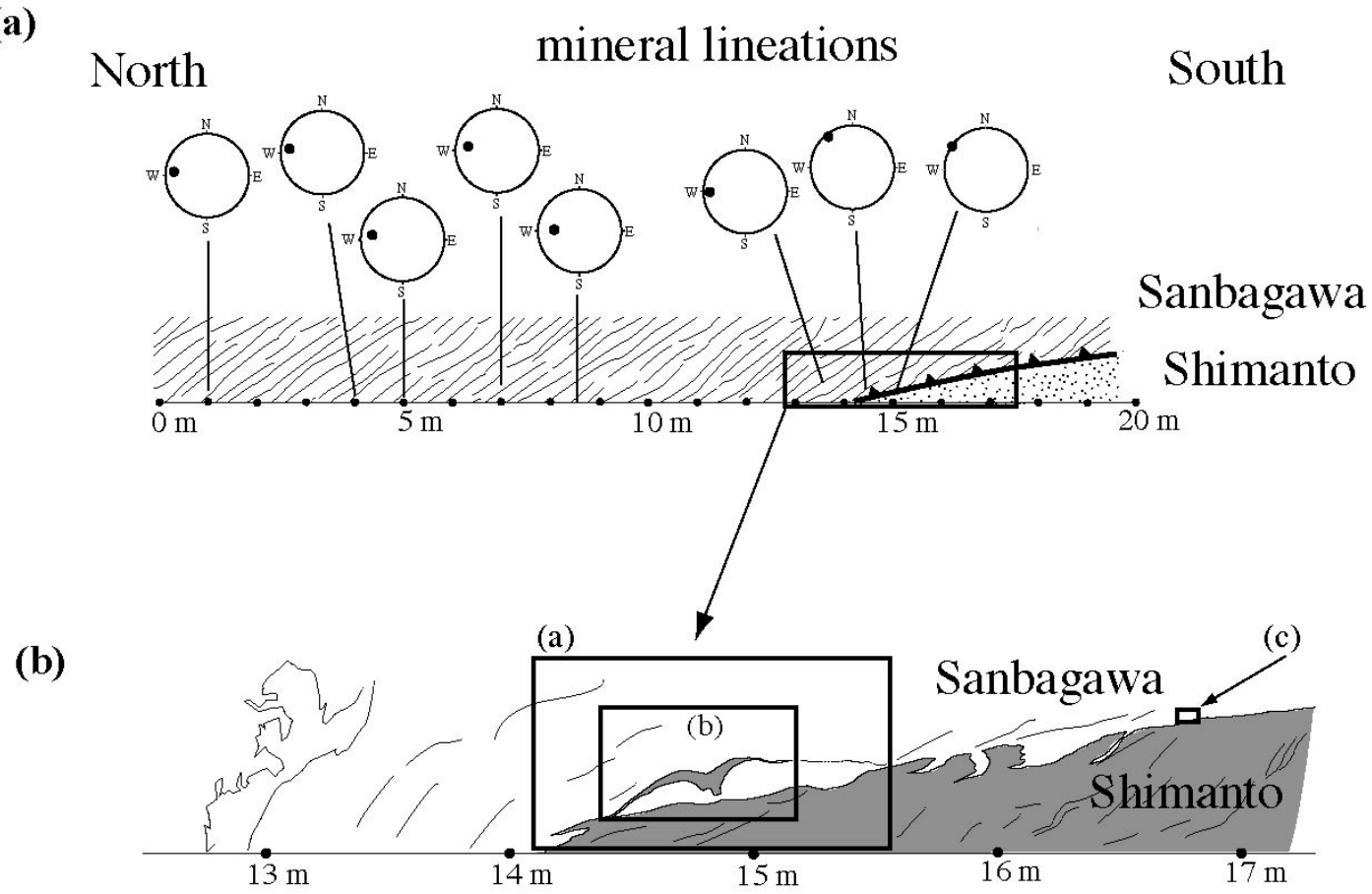

Fig. C–6 a) Schematic diagram of the bottom boundary of the Sanbagawa Belt. The E–W trending mineral lineation in the Sanbagawa schist abruptly changes to the NW–SE trend just above the boundary fault. b) Sketch of the fault zone. The bottom of the Sanbagawa Belt is dislocated and phyllite of the Shimanto Belt is included in the overlying Sanbagawa schist as a lensoid block. Open squares (a) – (c) indicate the field of view of the photographs shown in Fig. C–7.

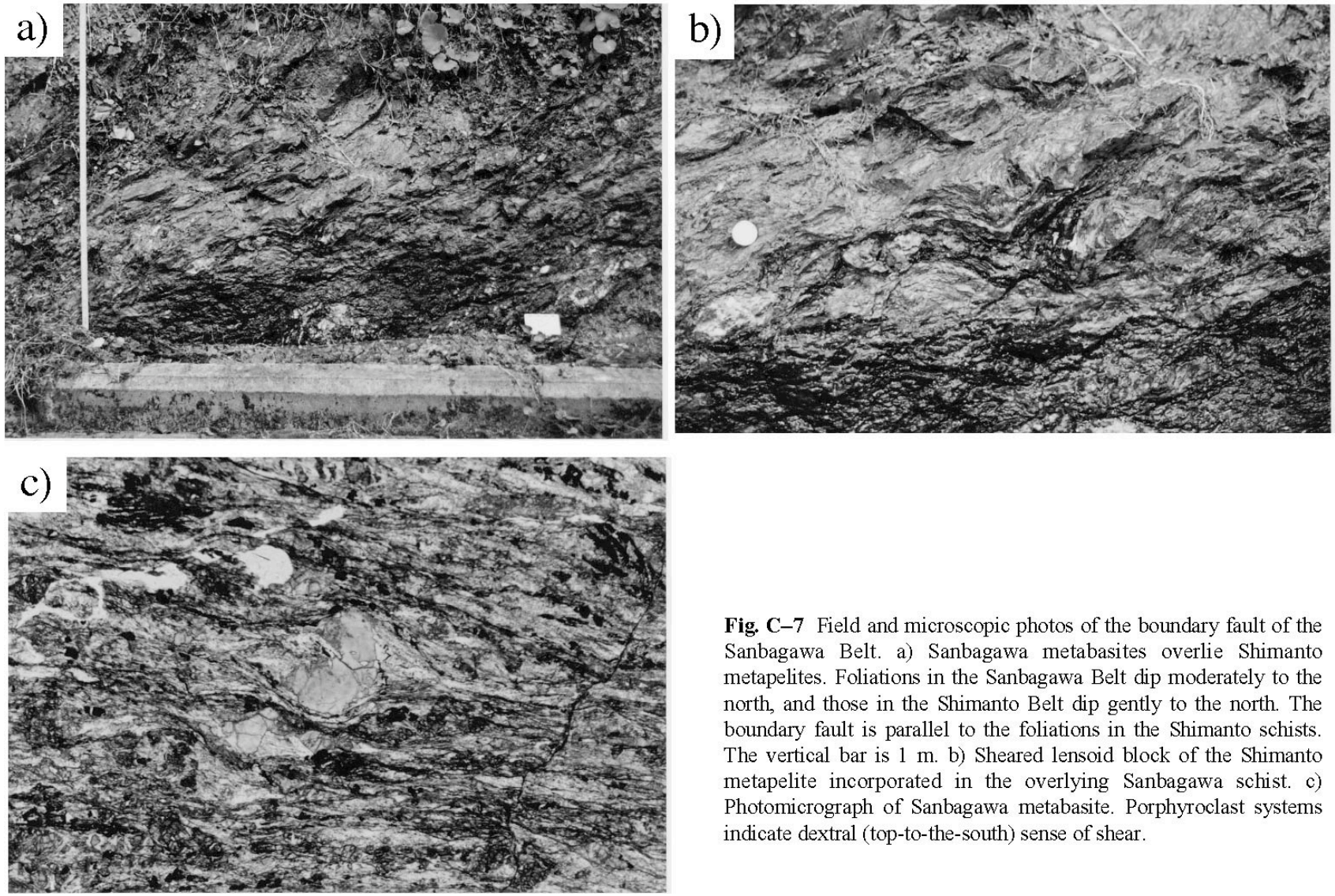

Fig. C–7 Field and microscopic photos of the boundary fault of the Sanbagawa Belt. a) Sanbagawa metabasites overlie Shimanto metapelites. Foliations in the Sanbagawa Belt dip moderately to the north, and those in the Shimanto Belt dip gently to the north. The boundary fault is parallel to the foliations in the Shimanto schists. The vertical bar is 1 m. b) Sheared lensoid block of the Shimanto metapelite incorporated in the overlying Sanbagawa schist. c) Photomicrograph of Sanbagawa metabasite. Porphyroclast systems indicate dextral (top-to-the-south) sense of shear.

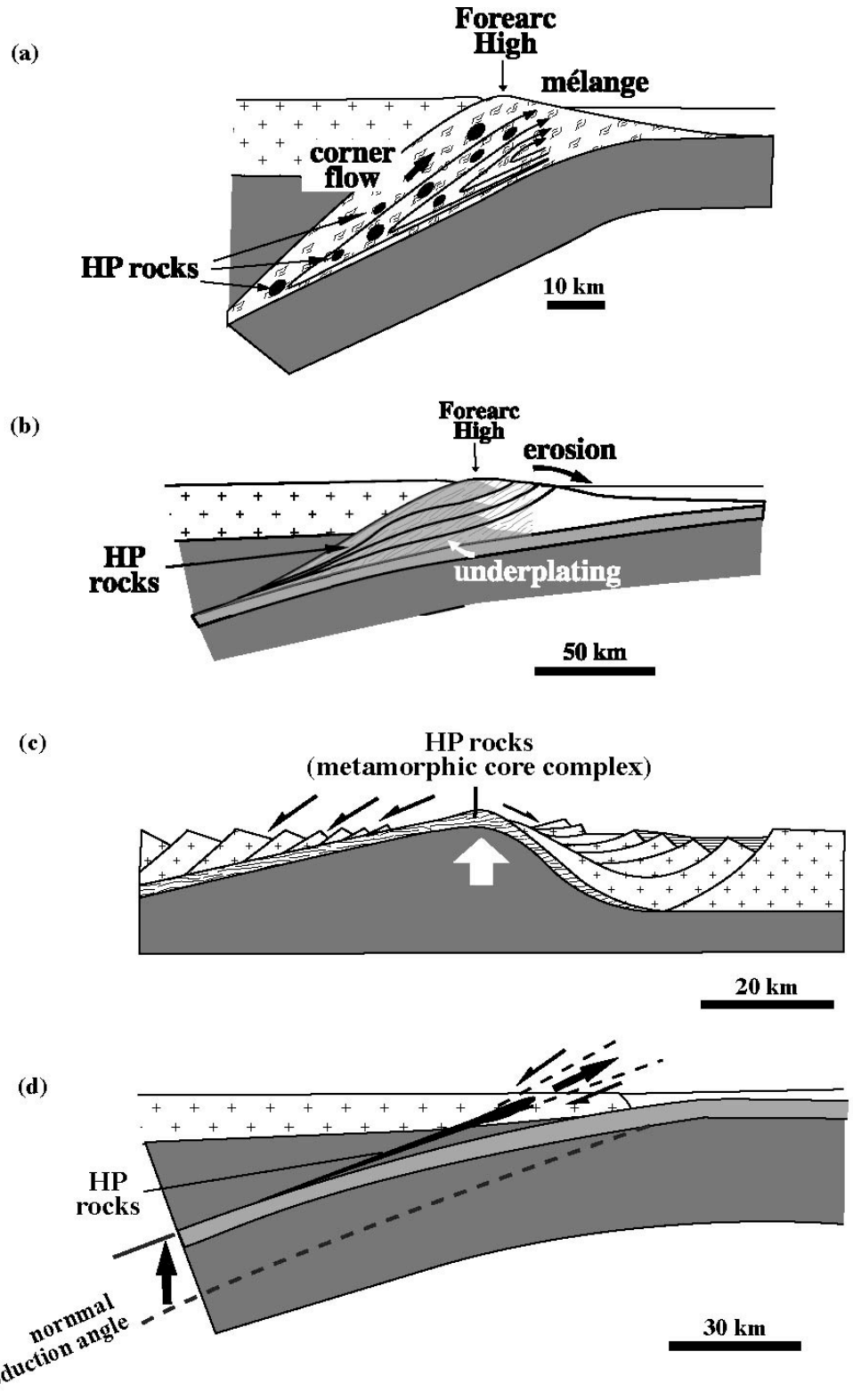

Fig. C–8 Representative exhumation tectonic models of high-P/T metamorphic belt. a) mélange model (simplified after Cloos, 1982), b) two-way-street model (simplified after Platt *et al.*, 1975), c) extension model (simplified after Lister & Davis, 1989), d) wedge extrusion model (simplified after Maruyama *et al.*, 1997). See main text for detailed explanation.